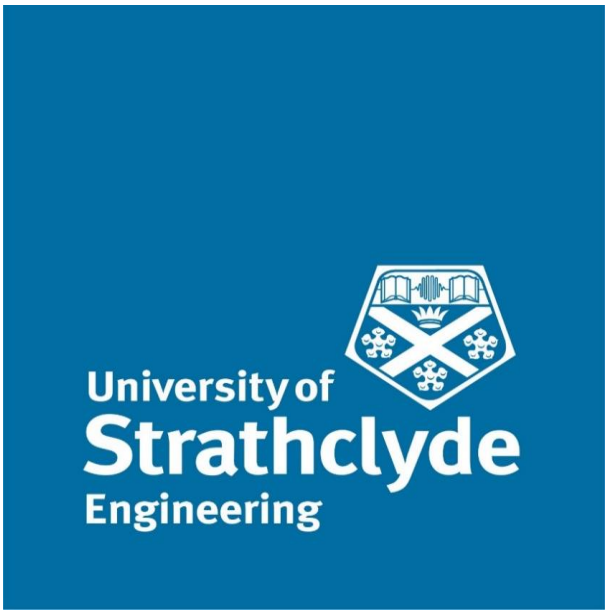

The environmental resistance of glass fibre vinyl ester composites and their interface for use in structural applications

A thesis in fulfilment of the requirements for the degree of
Doctor of Philosophy

By

Georgios Xypolias

Department of Mechanical and Aerospace Engineering
University of Strathclyde
Glasgow, Scotland
UK
2022

DECLARATION OF AUTHENTICITY AND AUTHOR'S RIGHTS

This thesis is the result of the author's original research. It has been composed by the author and has not been previously submitted for examination which has led to the award of a degree.

Signed:

Date: 1/8/2022

ACKNOWLEDGMENTS

This thesis is dedicated to my beloved pappou who sadly passed away during the latter stages of the project. Firstly, I would like to express my sincere gratitude to my supervisor Professor James Thomason for his invaluable advice, guidance and support throughout the course of my studies, and without which this thesis would not have been possible. I greatly appreciate being given the opportunity to undertake a challenging project in the field of composite materials, which I have been deeply interested in since my undergraduate studies. The challenges faced throughout this project not only helped me develop my skills as a researcher in the field, but also contributed to the strengthening of my character and personal attributes. I am also very grateful for the time and assistance of my second supervisor Dr. Liu Yang. Special thanks go to all past and present Advanced Composites Group (ACG) members – ACG is more than a research group, it is a continuously evolving community with a great sense of collaboration and friendship. I am sincerely grateful to all MAE technicians for their excellent co-operation throughout the project. In addition, I would like to extend my gratitude Dr. Pik Leung Tang and Nick Hawkins for their insight into FTIR and thermal analysis data interpretation and experimental method recommendations, respectively. I gratefully acknowledge DACOMAT for the financial support, knowledge and collaboration throughout my project. Last but not least, special gratitude goes to my beloved family, friends and partner for their support and love, which gave me extra strength to overcome any obstacles faced during the course of the project.

PUBLICATIONS

A number of findings in this thesis have been published over the course of the PhD project in the form of journal articles and conference contributions:

Xypolias G, Thomason JL, Yang L. The effect of environmental ageing in the interphase of a glass fibre/vinyl ester composite designed for wind turbine applications. IOP Conference Series: Materials Science and Engineering 2020;942.

Jenkins PG, Bryce D, Xypolias G, Thomason JL. Micro-mechanical investigation of glass fibre/resin interface failure in mode I and mode II. IOP Conference Series: Materials Science and Engineering 2020;942.

Thomason JL, Jenkins PG, Xypolias G. Microbond testing of the interface in glass fibre vinylester composites. Composite Interfaces 2021;29:695-709

Thomason JL, Xypolias G. The effect of environmental ageing on the interphase in glass fibre - vinyl ester composites. Composite Interfaces 2022:1-15

ABSTRACT

The use of fibre reinforced polymers (FRPs) in large infrastructure applications, such as the renewable energy sector has notably increased over the past decade. During their lifetime FRP composites can undergo significant changes upon their inevitable contact with environmental degradation agents, such as moisture. Such interactions may trigger irreversible degradation mechanisms in FRPs and in turn impair their properties. The state of the fibre/matrix interface is a crucial region in defining the reliability, and therefore the durability, of composite materials, or structures, during their service life. Previous reports suggest that potential improvements in the interfacial properties of FRPs do often correlate with improvements in composite macroscale properties. FRP interface can be particularly affected by environmental degradation, as it forms a passageway for moisture ingress into the material. This thesis is part of the larger EU Horizon 2020 funded DACOMAT (Damaged Controlled Composite Materials) project. The scope of this work is to produce an accelerated ageing study which allows the examination of two different DACOMAT glass fibre/vinyl ester systems in wet environments.

A major part of this thesis involves the use of vinyl ester specimens on the microscale. Although information is available on the cure kinetics of vinyl ester matrices on a bulk scale, arising scalability effects when employing microscopic matrix volumes remains an area in need of significantly improved understanding. The use of thermal analysis techniques revealed that microscopic vinyl ester specimens may exhibit a dual glass transition temperature (Tg), indicative of the diphasic nature of the resin. Polymerisation kinetics of microscopic scale samples of vinyl esters were found to be impeded by excess styrene loss promoted by the high surface-to-volume ratio of the employed specimens. Oxygen inhibition was also identified and deemed critical for the curing of vinyl esters. Methods to counteract such effects are proposed.

The microbond test was utilised for the characterisation of the glass fibre/vinyl ester interface. Several vinyl ester matrix systems and vinyl ester-compatible fibres have been examined. Scanning Electron Microscopy (SEM) was also utilised for the study of two DACOMAT vinyl ester micro-composite systems. A novel discovery of the interaction of the cyanoacrylate adhesive often used in the microbond test to “fix” single fibre micro-composites on a mounting card with vinyl ester-compatible sizings and (or) vinyl ester resins is presented.

A macroscale characterisation of the water uptake kinetics, mechanical and thermal properties of two DACOMAT composite systems and their matrix constituents as a function of their environmental history is enabled. The studied reinforcing fibres were two vinyl ester-

compatible glass fibres coated with the same sizing but of a different glass formulation (HiPertex vs Advantex). The studied matrices were a commercially available bisphenol-epoxy-based vinyl ester resin, and a newly developed methyl methacrylate (MMA), styrene-based modified vinyl ester resin. An interesting observation was made; the latter was found to be more hydrophilic than the former, but it formed more moisture-resilient interfacial bonds and showed greater mechanical property retention than the former, when these were used as a composite reinforcement in wet environments.

The stress transfer capability at the glass fibre/vinyl ester interface of the aforementioned composite systems as a function of their environmental history was also assessed by means of microbond testing of IFSS. An epoxy micro-composite system was also employed for comparative purposes. A correlation between the moisture uptake of a microbond vinyl ester droplet and its effect on the resulting IFSS was attempted. Since the monitoring of the moisture gain of microbond droplets was deemed impractical, experimental thin film models, as well as simple mathematical diffusion models were employed. Fourier-transform Infrared Spectroscopy (FTIR) was utilised for the evaluation of hydrolytic changes in vinyl ester films, while an attempt of the estimation of the moisture uptake of films using two different FTIR interfaces is also presented. Micro-mechanical testing was found to be useful for the coupling of the hydrothermal response of the bulk vinyl ester-based composites. Ageing-induced degradation in single fibre micro-composite structures was identified by SEM in the forms of micro-cracking and moisture wicking along the fibre/matrix droplet interface, matrix blistering, as well as the appearance of a two-phase structure, which was made visible by ageing in a wet environment.

TABLE OF CONTENTS

NOMENCLATURE

Abbreviations

a	Degree of cure by Differential Scanning Calorimetry
$\alpha_{ST}(t)$	Fractional conversion of styrene
a_t	Total fractional conversion
$\alpha_{VE}(t)$	Fractional conversion of vinyl ester
$\frac{\Delta V(t)}{V_0}$	Volume changes determined by Fourier-transform Infrared Spectroscopy
$\frac{\Delta w_t}{W_0}$	Fractional absorbed water
ρ	Specimen density
ρ_c	Measured composite density
ρ_f	Fibre density
ρ_m	Matrix density
$\rho_{theoretical}$	Theoretical composite density
σ_f	Flexural strength
φ	Angle of the fibre orientation relative to the surface of a composite laminate
A	Peak area used in Fourier-transform Infrared Spectroscopy calculations
A_e	Embedded area of a microbond droplet
b	Specimen width
c	Weight correction factor used for voume calculation
D	Diffusion coefficient
d	Depth of a beam specimen
D_c	Diffusion coefficient of composite
D_f	Fibre diameter
D_m	Diffusion coefficient of matrix
D_0	Pre-exponential factor
$\frac{dC}{dt}$	Change in moisture concentration of an aged sample as a function of time
E_D	Activation energy

F_{max}	Mximum load applied on a microbond specimen
F_{SBS}	Short-beam shear strength or apparent interlaminar shear stress
H	Heat of reaction
h	Specimen thickness
HI	Hydrolysis index
k	Boltzmann constant
L	Support span
L_e	Embedded length of a microbond droplet
$M, \%$	Mass gain
M_A	Mass of a specimen in air used for a density measurement
M_L	Mass of a specimen in an auxiliary liquid used for a density measurement
M_i	Mass gain of aged specimen
M_m	Effective moisture equilibrium content
M_o	Mass of oven dry specimen
$M(t)$	Time dependent water uptake
P_m	Maximum load observed during a short-beam shear test
T	Temperature
t	Time
t_m	Time to equilibrium for an aged specimen
V	Volume
v_f	Fibre volume fraction
$Void$	Composite void content
w_f	Fibre weight fraction
w_m	Matrix weight fraction
ATR	Attenuated Total Reflectance
CF	Carbon Fibre
CFRP	Carbon Fibre Reinforced Polymer
DACOMAT	Damage Controlled Composite Materials
DI	Deionized

DMA	Dynamic Mechanical Analysis
DSC	Differential Scanning Calorimetry
FEA	Finite Element Analysis
FRP	Fibre Reinforced Polymer
FTIR	Fourier-transform Infrared Spectroscopy
GF	Glass Fibre
GFRP	Glass Fibre Reinforced Polymer
IFSS	Interfacial Shear Strength
ILSS	Interlaminar Shear Strength
IR	Infrared
ISO	Isophtalic Polyester or Isopolyester
LHS	Left Hand Side
Log.	Logarithm
MDSC	Modulated Differential Scanning Calorimetry
PE	Polyester
PMMA	Poly(methyl methacrylate)
RHS	Right Hand Side
RT	Room Temperature
RTM	Resin Transfer Moulding
SCRIPM	Seemann Composites Resin Infusion Moulding Process
SEM	Scanning Electron Microscopy
TBA	Torsional Braid Analysis
TGA	Thermogravimetric Analysis
UD	Unidirectional
UP	Unsaturated Polyester

UTS	Ultimate Tensile Strength
VARTM	Vacuum Assisted Resin Transfer Moulding
VE	Vinyl Ester

LIST OF FIGURES

LIST OF TABLES

CHAPTER 1: INTRODUCTION

1.1 PROJECT BACKGROUND

This project was a part of DACOMAT. DACOMAT was a consortium of industrial and academic partners with an aim to produce more low-cost, damage tolerant and damage predictable FRPs with high environmental durability for use in large load-carrying infrastructure applications. The key to achieving this was the development of materials and condition monitoring solutions, which can allow for manufacturing imperfections and will possess a high capacity to damage. The demonstration of material performance was conducted in two applications: wind turbine blades and bridges. The main goals of DACOMAT included:

- Improvement of wind turbine blade durability by 30 %, and the achievement of a significant reduction of blade-related cost (offshore).
- Improvement of durability and reduced lifetime costs of bridges by 30 %.

The popularity of FRPs in structural applications has significantly increased over the last decade. During their service life, their exposure to environmental degradation agents, such as moisture and thermal cycling is inevitable. Regardless of the close attention to details and the employment of optimum design methods, the long-term exposure of FRPs to their use environment will likely shorten the durability of the materials and eventually trigger irreversible degradation mechanisms which will affect their properties. A method of accurately determining the effect of the in-service environmental conditions on the exposed material is yet to be established. This creates a level of uncertainty about the durability of composites for infrastructure applications, where clients and stakeholders need to "know" how the material will perform over a timescale of many decades. A real-time assessment of in-service composite structures is a time-consuming process and involves high costs. However, these parameters can be lowered by employing laboratory accelerated ageing conditions or by obtaining information directly at the composite fibre-matrix interface.

It has been suggested in previous studies that the fibre-matrix interface is a crucial part of FRPs [1,2]. In fact, the condition of the interface can define the reliability and therefore the durability of composite materials or structures during their service life. Even though the transferability of the properties of the fibre-matrix interface to the bulk laminate is complex, it has been established that a strong interface can potentially contribute to an FRP with high mechanical and chemical properties, and an interfacial failure is likely to compromise the performance of the bulk material and even lead to its failure [1–3]. Studies have also shown

that whenever there was any improvement in the micro-mechanical properties of a composite, there was also a corresponding improvement in the macroscopic properties of the system [2,4]. Although the integrity and properties of the interface are particularly sensitive to hydrothermal ageing, most research to date has been focused on the moisture uptake kinetics and failure of bulk laminate FRPs. Knowledge of the effectiveness of studying interface performance in wet environments as a means of accelerated ageing and, to accurately determine the hydrothermal response of a bulk laminate is yet limited.

The GFRP constituents developed by DACOMAT and deployed throughout this project were a vinyl ester matrix and a glass fibre reinforcement. Vinyl ester resins are widely used in structural components in a broad range of applications, usually in the marine, offshore, and civil infrastructure sectors. Although a typical vinyl ester system may possess inferior properties to a high-performance epoxy system, its fast fabrication cycles and ease of processability, as well as its low cost and high environmental durability often make it a more potent candidate than epoxies in these sectors [5,6]. Glass fibres are the dominant reinforcement in FRPs used in large infrastructures and offer great inherent properties, such as high strength-to-weight ratio, low cost and exceptional resistance to hydrothermal attack.

1.2 AIMS AND OBJECTIVES

The investigation of the durability of the glass fibre/vinyl ester system in wet environments required the establishment of an effective accelerated ageing study. The effect of the matrix constituent and the fibre/matrix interface on composite performance in wet environments was studied in detail, as these were considered particularly sensitive to moisture-induced degradation. The objectives of this thesis can be briefly summarised as follows:

- The thermal characterisation and understanding of vinyl ester chemistry, and the study of scalability effects from a bulk matrix scale to a microscale.
- The investigation of the environmental durability and uptake kinetics of a glass fibre/vinyl ester composite in a real-life, bulk laminate scale, and the influence of manufacturing voids.
- The direct characterisation of the glass fibre/vinyl ester interface and the assessment of its environmental durability, by means of micro-mechanical testing.

1.3 OUTLINE OF THESIS

Chapter 1 presents a brief introduction of the background and objectives of this thesis as well as an outline of the content of each chapter contained.

Chapter 2 entails a thorough discussion of the literature, relevant to the studies undertaken in this thesis. The literature review was divided into 5 main sections: *Introduction to Fibre Reinforced Polymer Composites and Their Constituents, Thermal Characterisation and Understanding of the Chemistry of Vinyl Ester Resin, Mechanical and Micro-mechanical Testing of Fibre Reinforced Polymers* and *Moisture Diffusion Kinetics* and *Moisture Ageing Of Fibre Reinforced Polymer Composites*.

Chapter 3 involves the investigation of the effects of scale and cure environment on the physical and chemical properties of the vinyl ester resins under study. Thermal analysis (TA) techniques, such as Dynamic Mechanical Analysis (DMA) and Differential Scanning Calorimetry (DSC) were used for the thermal characterisation and assessment of resin performance as a function of cured matrix thickness. An ATR-FTIR analysis was carried out for the coupling of the thermal analysis and to provide an insight into the chemistry of the resin. Part of this work was presented via an oral presentation at the 41st Risø International Symposium and subsequently published in the IOP conference proceedings with the title "*The effect of environmental ageing in the interphase of a glass fibre/vinyl ester composite designed for wind turbine applications*."

Chapter 4 allows an assessment of the glass fibre/vinyl ester interface by means of the microbond test, as a measure of IFSS. Different fibre/matrix combinations were examined. Furthermore, the influence of the employed fibre fixing adhesive on the micro-mechanical performance of single fibre microbond specimens was investigated. A significant portion of this study was presented by an article with the title "*Microbond testing of the interface in glass fibre vinylester composites*" published in the *Composite Interfaces* journal and another title with the title "*Micro-mechanical investigation of glass fibre/resin interface failure in mode I and mode II*" published in the IOP conference proceedings of the 41st Risø International Symposium.

Chapter 5 is a presentation of a macroscale characterisation of the water uptake kinetics and thermal properties of two glass fibre/vinyl ester composites and their matrix constituents. The retention in mechanical properties of the composites as a function of environmental history and void content is also enabled. Mechanical properties were evaluated as a measure of Interlaminar Shear Strength (ILSS), flexural strength and Young's modulus, and thermal properties were measured by DMA.

Chapter 6 reports on the study of the moisture uptake of glass fibre/vinyl ester micro-droplets and its direct translation into the micro-mechanical performance of the system. Micro-mechanical performance as a function of environmental history was evaluated by the

microbond test, as a measure of IFSS using single fibre micro-composites. The moisture uptake of micro-droplets was assessed by the employment of experimental thin film models of a similar surface-to-volume ratio to the droplets, while fundamental mathematic diffusion models were also utilised. In addition, DMA and FTIR were employed for the evaluation of the ageing effect on vinyl ester films, and SEM was used for the study of ageing-induced structural and morphology changes in the glass fibre/vinyl ester interface of single micro-composites. This work is an expansion of the conference presentation given in *MECHCOMP7* in *Porto* in *September 2021* and the article published in the IOP conference proceedings of the 41st Risø International Symposium on Materials Science with the title "*The effect of environmental ageing in the interphase of a glass fibre/vinyl ester composite designed for wind turbine applications*."

Chapter 7 contains a summary of the conclusions of this thesis complemented by future work recommendations.

CHAPTER 2: LITERATURE REVIEW

This literature review introduces the background of fibre-reinforced polymer composites (FRPs) and their applications. It also includes a discussion of the chemistry of vinyl ester resins, which were the main studied matrix in this thesis. In addition, it entails an introduction to macro-mechanical and micro-mechanical testing of FRPs. Lastly, it is aimed at providing insight into the moisture diffusion kinetics theory and the behaviour of FRPs under hydrothermal environments, with an emphasis on vinyl ester/glass fibre systems.

2.1. INTRODUCTION TO FIBRE REINFORCED POLYMER COMPOSITES AND THEIR CONSTITUENTS

A composite is a material or structure, which comprises of two or more dissimilar components. The constituents of composites can be classified as:

1) A selected filler or reinforcing agent.
2) A compatible resin matrix, which is used to infuse the reinforcement and remains continuous throughout the composite structure.

Composite constituents do not dissolve or entirely merge into each other, but are tailored in such a manner to act in harmony. The design of composites provides the ability to select and combine constituent materials to achieve a final component which allows for the desired performance and meets certain desired characteristics. The development of composites and their introduction in a large variety of applications, such as transport, aerospace, automotive, structural infrastructure, marine and wind energy has increased significantly from the beginning of the 1940s onwards replacing conventional materials. The “key” benefits of composites, when compared to conventional materials, include high modulus-to-weight and strength-to-weight ratios, electromagnetic neutrality, exceptional fatigue behaviour and excellent durability in hydrothermal and corrosive environments.

Composites can be classified based on the form of their structural components in fibrous, laminar and particulate composites. The reinforcing agent can be either fibrous, powdered, spherical, crystalline, or whiskered and either organic, inorganic, metallic or ceramic. Matrix materials can be classified into thermoplastics and thermosets according to their behaviour when they are heated. Thermoplastics refer to polymers that become pliable or mouldable when they are heated beyond a particular temperature. Common types of thermoplastics include acetal, acrylic, nylon, polypropylene, polyethylene, polystyrene, polyamide, polyvinyl chloride (PVC) and polytetrafluoroethylene (PTFE) polymers. On the other hand, thermosets

refer to highly infusible and insoluble materials in soft solid or viscous liquid forms, which are hardened either by curing under an elevated temperature or by chemical means. Common types of thermosets include polyester, vinyl ester, epoxy and phenolic resins. This work is particularly focused on thermoset-based glass fibre reinforced polymers (GFRPs). GFRPs are the most widely used composite in the commercial sector and refer to polymer composites in which glass fibre is used as the reinforcing agent [7–12].

Glass fibres are one of the most commonly used reinforcing elements in FRP applications accounting for more than 95 % of fibre reinforcements used in the composites industry [12]. They are used in a wide variety of applications including wind energy, civil and marine sectors, where resilience to moist environments is of high importance. Glass fibres exhibit exceptional inherent properties, such as high strength-to-weight ratio, stiffness, hardness and durability which make them desirable candidates for such applications [12,13]. Carbon fibres are also widely used reinforcements, although glass fibres are generally preferred in the composite industry due to their lower cost and higher achievable ultimate strain [6].

The fibre/matrix interphase is a critical region of the FRP since it governs composite structural integrity and lifetime performance. The integrity of the interface/interphase region can define the reliability and durability of composites in their service life. A clear distinction between the terms “interface” and “interphase” must be made. The term “interface” refers to the two-dimensional boundary between two surfaces of distinct chemistry and (or) microstructure in a multiphase material in which the required composite properties are as good, or better than the least constituent. Conceptually, the “interphase” can be defined as a 3-D region surrounding the fibre, where the properties differ from but gradually converge to those of the bulk matrix. The interphase is a result of cross-linking between the fibre and the thermoset matrix and has its own morphology and chemistry. The strength of the interphase is a measure of the stress transfer capability to the load-bearing fibres, whereby the strength is determined by the level of adhesion between the fibre and the matrix [2,9,14–16]. *Figure 2-1* shows a schematic representation of the fibre/matrix interface [2].

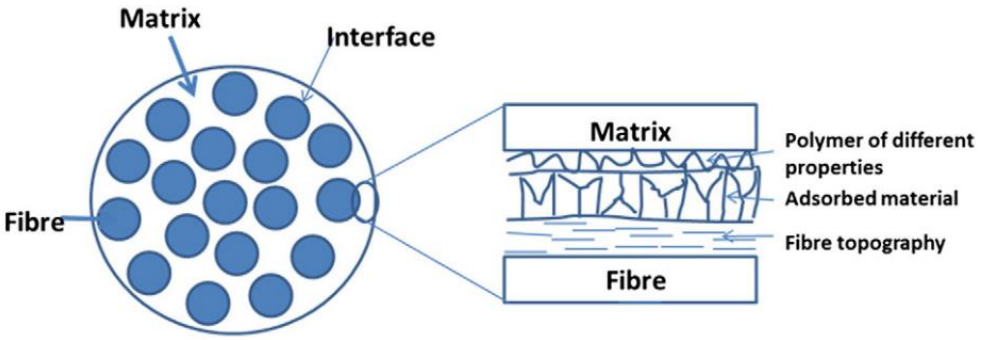

Figure 2-1: *Schematic representation of the fibre/matrix composite interface* [2].

Throughout this study, the concept of a two-dimensional boundary between the fibre and matrix constituents was used and was referred to as "interface". Interfacial adhesion in FRPs reinforced with inorganic fibres, such as glass fibres can be divided into three main categories:

- Chemical adhesion: This refers to the formation of chemical bonds across the interface, which are either formed by direct reaction of the matrix and reinforcement or by chemical bridging between the two, facilitated by fibre surface modifications-coupling agents, such as silanes. In particular, silanes are used on glass fibres, as they are known to enhance the IFSS and the moisture resistance of GFRPs significantly [9].
- Physical adhesion: This is caused by the decrease in surface energy as a result of two contacting surfaces. The wettability of a fibre, which is governing factor for the structural integrity of a laminate, and more specifically for the appearance of areas of air entrapment/voids, is significantly influenced by the surface and the interfacial contact. Voids are likely to occur when the two surfaces are not in contact [9].
- Mechanical adhesion: This refers to microscopic mechanical interlocking over substantial portions of the interface. Mechanical adhesion can be affected by the surface roughness of the fibre and the wettability of the matrix [9].

2.2. THE THERMAL CHARACTERISATION AND UNDERSTANDING OF THE CHEMISTRY OF THE VINYL ESTER RESIN

2.2.1. The Chemistry of Vinyl Ester

Curing in vinyl esters is achieved through free radical polymerisation. An understanding of the fundamentals of the free radical polymerisation process was essential for the study of the

chemistry and thermal behaviour of the resin. This section entails a brief introduction to free radical polymerisation.

According to Stone et al [17], free radical polymerisation can be divided into four stages:

1. The initiation stage, which involves the formation of the initiator radical
2. The addition of the initiator radical to a monomer
3. The propagation of a monomer radical to another monomer molecule, and
4. The termination of all growing chains due to lack of mobility to unreacted monomers.

Vinyl ester resins were introduced in the early 1960s for use in GFRP applications [18,19]. Nowadays they are widely used in structural components in a broad range of applications, usually in the marine, offshore, and civil infrastructure sectors. Although a typical vinyl ester system possesses inferior properties to a high-performance epoxy system, its fast fabrication cycles and ease of processability, as well as its low cost, high environmental durability and the fact that it can still perform adequately, often make it a more potent candidate than epoxies in these sectors [5,6].

Despite the increasing commercial use of vinyl esters, the interrelationship between the chemistry, cure kinetics, morphology and final material properties is not yet well understood. [20]. Vinyl ester curing has been characterised as producing a diphasic structure resulting from the formation of densely cross-linked microgel structures. More specifically, polymerised vinyl ester resins consist of highly cross-linked methacrylate epoxy compounds surrounded by a lightly cross-linked, styrene-rich region. The vinyl ester monomer performs as a cross-linking agent and contributes to major polymer properties, such as modulus, Tg, toughness and durability. Styrene in the monomeric form is used as a diluent in the resin and its role is to control the viscosity of the resin, improve wetting behaviour and reduce the overall cost. Styrene has been associated with increased hydrophobicity and decreased homogeneity in the final polymer. A typical vinyl ester contains 30 – 60 wt % styrene [6,17,20–24]. The chemical structures of the vinyl ester and styrene monomers are shown in *Figure 2-2*.

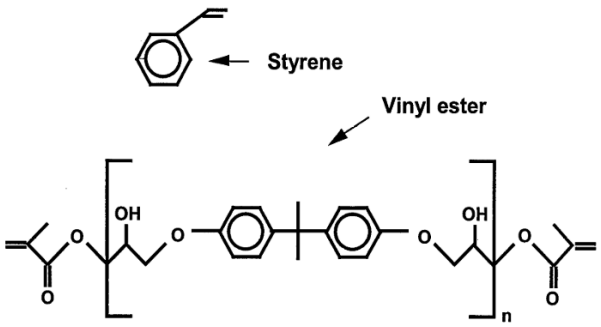

Figure 2-2: *Chemical structures of styrene and vinyl ester monomers [17].*

As previously discussed, curing in vinyl esters is achieved by free-radical polymerisation. Karbhari et al [23] have outlined the main reactions between the vinyl ester and styrene monomers involved in the network formation process of vinyl ester resins. These contribute to the heterogeneity of the resin and can be described, as follows:

- $VE + VE^* \rightarrow (VE - VE)^*$ *(1)*
- $ST + ST^* \rightarrow (ST - ST)^*$ *(2)*
- $\begin{matrix} VE^* + ST \\ ST^* + VE \end{matrix} \rightarrow (VE - ST)^*$ *(3)*

Reactions (1) and (2) represent the homopolymerisation of vinyl ester and styrene monomers, respectively. Reaction (3) represents the copolymerisation of the two monomers. The styrene reaction rate is initially lower than that of vinyl ester, but styrene possesses the ability to continue to react after the vinyl ester monomer reaction is complete. The variation in monomer reaction rates is known to result in microgel formation and therefore heterogeneity in the polymer network [23].

2.2.2. Thermal Behaviour and Cure Kinetics of Vinyl Ester

The Heterogeneity of Vinyl Ester Resins – Microgel Formation

As previously discussed, vinyl ester curing has been associated with the formation of microgel structures, which have been found to significantly affect the cure kinetics of the polymer. Microgels have been characterised as small clusters, gel particles or tightly packed spheres

(high cross-link density), which exhibit a diameter of 0.3 and 1 mm and can be suspended in solvents. They appear mainly in the early stages of the cure and at low temperatures and are produced by the reactions of the vinyl ester and styrene monomers. More specifically, microgels are generated through styrene swelling of the polymer; microgels contain some styrene monomer but the majority of the styrene is present in the surrounding area. An image featuring microgel formation at the early stages of isothermal vinyl ester curing at 70 °C recorded by atomic force microscopy (AFM) is shown in *Figure 2-3* [17,25,26].

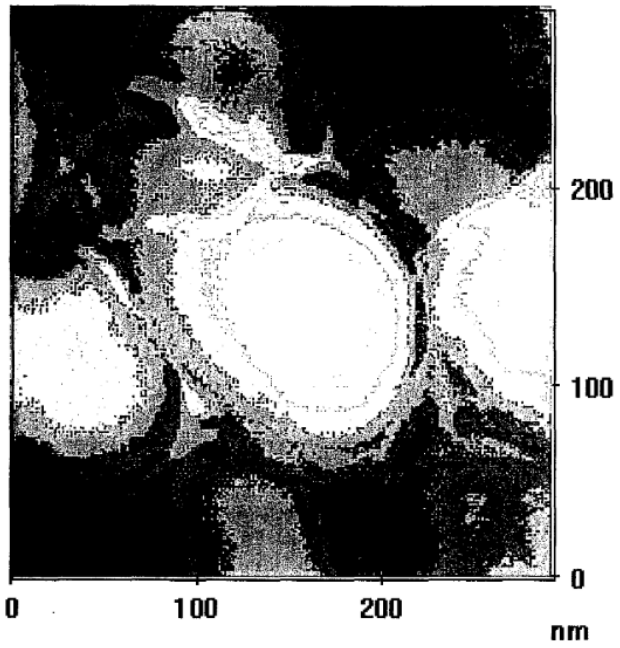

Figure 2-3: *Image featuring an early-stage microgel formation and recorded by atomic force microscopy (AFM) for vinyl ester cured at 70°C* [17].

Ziaee and Palmese [25] studied the effect of temperature on cure kinetics of vinyl ester and observed that at low temperatures, in the early stages of the cure the homopolymerisation reaction rate of the vinyl ester monomer was higher than that of styrene. Stone et al [17] suggested that for every styrene monomer attaching there is more than one vinyl ester monomer attaching when vinyl ester dominates the reaction. After the initial microgel formation, vinyl ester microgels collapse and the mobility of vinyl ester monomers is reduced. This restricts their ability to reach free chain radicals. Besides, the tight structure of microgels hinders styrene diffusion, also stopping it from reaching free chain radicals. Consequently, until microgels are completely collapsed, the reaction rate is reduced. The reaction rate is then increased again until the polymer reaches final conversion. Several workers have reported that styrene has the ability to keep reacting, even after the vinyl ester has reached maximum

conversion [17,24,27]. The difference in monomer reaction rates is the main reason for microgel formation and the assessment of heterogeneity in the polymer (diphasic structure).

The thermal behaviour of these radically polymerised polymers is greatly dependent on several parameters involved in the polymer preparation process. These include reaction conditions, such as solvent, conversion, styrene content, cure environment and temperature employed as well as the initiator used [28,29]. A thorough review of the literature on the cure kinetics and thermal behaviour of vinyl ester resins is presented in the following sections.

An Introduction in the Thermal Behaviour and Cure Kinetics of Vinyl Ester: Conversion, Tg and Cure Temperature Dependency

The degree of cure in thermoset polymers can be assessed by the determination of conversion and the degree of cross-linking [30]. Maximum conversion in thermoset polymers is achieved when diffusional limitation curtails the ability of the system to react. During thermoset curing the number of cross-links increases resulting in an increase in the fractional conversion and Tg of the polymer. Hence, the determination of polymer Tg can also be indicative of the thermal behaviour and performance of the material. Most to-date studies focused on cure kinetics of vinyl ester matrices involve fractional conversion evaluation through thermal analysis techniques, such as DSC or spectroscopic methods, such as FTIR. Fractional conversion through DSC is measured when the material starts to vitrify/solidify. The assessment of morphological states of heterogeneous matrices, such as vinyl esters can be assessed by evaluating the Tg of the polymer, through thermal analysis techniques with DSC and DMA being the most prominent [21,24]. Generally, DSC is capable of detecting material property changes as a function of temperature, while DMA measures the thermal behaviour of a material in terms of its stiffness (storage and loss modulus) and damping (tan δ) as a function of temperature. FTIR allows the monitoring of the curing process by the determination of the reduction of the concentration of reacting material species. These are reflected in the signal of certain absorption bands featured by FTIR. FTIR is capable of identifying the conversion over the entire curing process, despite the curing thermoset undergoing different state transitions during polymerisation [27].

Stone et al [17] suggested that vinyl esters exhibit a lower maximum degree of cure as opposed to high-temperature cure thermosets, such as epoxies. This is due to diffusional limitation being reached at lower conversions, as the monomer molecules possess low thermal energy to begin with. The authors found that for a typical vinyl ester resin, the Tg increased at a high rate prior to vitrification reaching the cure temperature. Nonetheless, Tg increase was found

to be rather slower beyond vitrification. Generally, it has been reported that the Tg of high-temperature thermosets, such as epoxy systems stops increasing when vitrification is achieved. On the contrary, cure in vinyl ester resins is known to progress slowly after vitrification or post-cure due to the ability of the styrene to find reactive sites within the final polymer [17].

Gillham [31] reported that Tg can be correlated to the conversion of thermosets. However, Stone et al [17] noted that this relationship is only direct for vinyl ester for isothermal curing, due to the complexity of the reactions of the styrene and vinyl ester monomers. In fact, the relationship between Tg and degree of conversion in vinyl ester resins has been found to be greatly dependent on temperature history. Ziaee and Palmese [25] examined the effect of initial isothermal cure temperature (30 °C and 90 °C) on the cure kinetics of vinyl ester. They found that regardless of the initial cure temperature, the Tg and degree of conversion were mainly governed by the post-cure temperature (Tg =118 – 122 °C). Cook et al [20] investigated the cure kinetics and thermal properties of a bisphenol A vinyl ester resin with a styrene content of 45 wt % through isothermal curing in DSC at different temperatures. First of all, they found that vinyl ester exhibited varying reaction rates during cure, which is commonly observed in free radical polymerisation of divinyl monomers. The polymerisation rate and fractional conversion were found to increase as a function of increasing cure temperature until maximum conversion was reached. Maximum conversion was achieved at moderate temperature regimes below 100 °C. However, at cure temperatures of 100 °C and 120 °C conversion was reduced due to the depolymerisation of the dimethacrylate phase or due to premature initiator loss. Visco et al [32] detected slight peaks in the DSC thermograms of a vinyl ester matrix at 115 – 120 °C. These peaks were attributed to unreacted oligomer species, which move with difficulty into the thermoset network. The authors highlighted that high temperatures are required for these species to diffuse into the network, especially at higher conversions.

A series of studies identified a Tg or conversion increase in vinyl esters as a function of room temperature exposure or ageing. Karbhari and Wang [33] found a notable Tg increase for cured vinyl GFRPs exposed to an ambient room temperature environment for 6 months. Ghorbel and Valentin [34] reported increased conversion as a function of hydrothermal ageing for cured vinyl ester, which, however, was not reflected in the Tg of the polymer due to the opposing effects of post-curing and moisture-induced degradation.

Although vinyl esters are known to exhibit a diphasic structure, most workers have reported a single Tg. Zhang and Richardson [21] suggested that this may be due to the insensitivity of conventional thermal analysis methods, such as DSC and DMA, to deconvolute the two transitions. Literature search results manifesting a single transition are summarised in *Table*

2-1, from which it can be concluded that Tg values can vary even for the same resin. As previously discussed, the thermal behaviour and Tg of vinyl ester are greatly dependent on cure conditions and manufacturing parameters as well as the polymer network of the resin, and thus such variation can be expected. It is also established that different Tg detection techniques may exhibit a different sensitivity and therefore different output.

Vinyl Ester Type	Styrene Content (wt %)	Detection Method	Tg (°C)	Reference
Derakane 411C-50	44	DSC	111	[24]
	44	DMA	138	[24]
	45	DMA	118	[25]
	50	TBA	125	[17]
Derakane 470-300	28	DSC	174	[24]
	33	DSC	110	[35]
	28	DMA	183	[24]
Dow Derakane 411-350	45%*	DSC	101	[36]
	45	DMA	109 - 115	[33]
	33	DMA	120	[35]
	45%*	DMA	111	[36]
bisGMA	30	DSC	156	[24]
	30	DMA	169	[24]
Diglycidyl Bisphenol-A	N/A	DSC	114	[34]
AME 6000 T 35	35	DSC	142	[37]
Grade HPR 8711 by Bakelite Hylam	N/A	DMA	101	[38]

*thickness = 0.23 – 0.26 mm

Table 2-1: *Tg of vinyl ester resins and detection method.*

Several studies suggest a dual Tg, which nonetheless can only be detected in certain cases. Garay et al [35] studied the thermal and viscoelastic properties of vinyl ester resin and its composites with glass fibre. A DMA analysis was carried out for cured and post-cured (following initial cure) neat vinyl ester specimens with a thickness of 4 mm. Matrix plates were manufactured in silicone moulds and were cured at room temperature for 24 h. The post-cure cycle was at 90 °C for 6 h in an air-circulation oven. *Figure 2-4* features a comparison of the tan δ curves for the cured and post-cured matrix, generated by DMA. Two distinct transitions – tan δ peaks – at 65 °C and 120 °C are shown for the cured matrix. The first peak nearly disappeared upon post-cure and a slight shoulder was remnant. The second peak shifted to a slightly lower value of 115 °C. The authors attributed the double Tg to partial curing of the matrix. However, a detailed explanation of the appearance and the cause of the appearance of a double peak in the tan δ curve was not provided. Fraga et al [39] detected two tan δ peaks in a neat vinyl ester matrix and its composites within the same temperature region of 100 °C and 120 °C, which they attributed to "thermal instability". The authors produced a comparative study with an unsaturated polyester resin, which despite containing styrene, showed only one distinct tan δ peak. A comparison of the neat vinyl ester and unsaturated polyester thermal curves is presented in *Figure 2-5*.

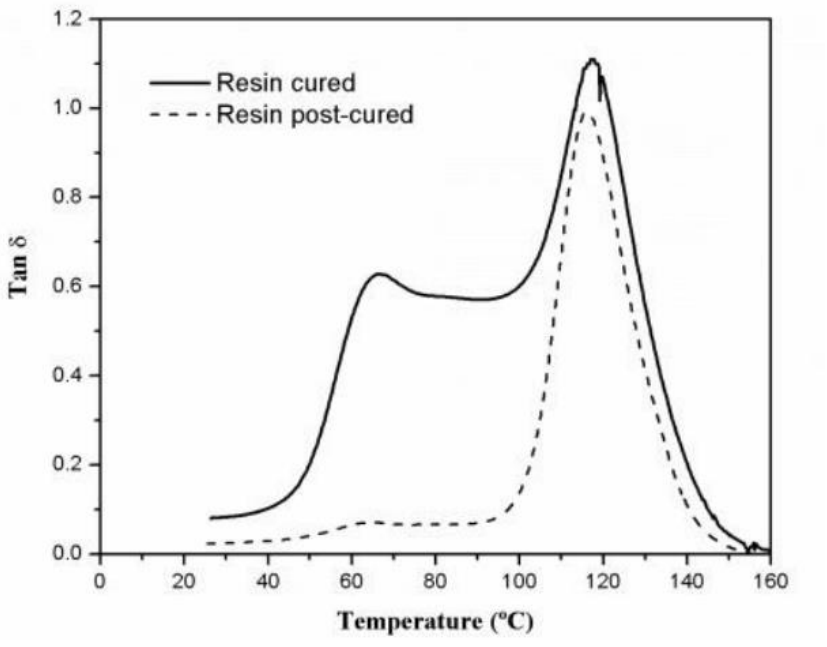

Figure 2-4: *A comparison of cured and post-cured vinyl ester tan δ curves, generated by DMA. Evidence of diphasic nature for the vinyl ester matrix upon initial cure (appearance of a shoulder) – shoulder becomes less prominent upon post-cure* [35].

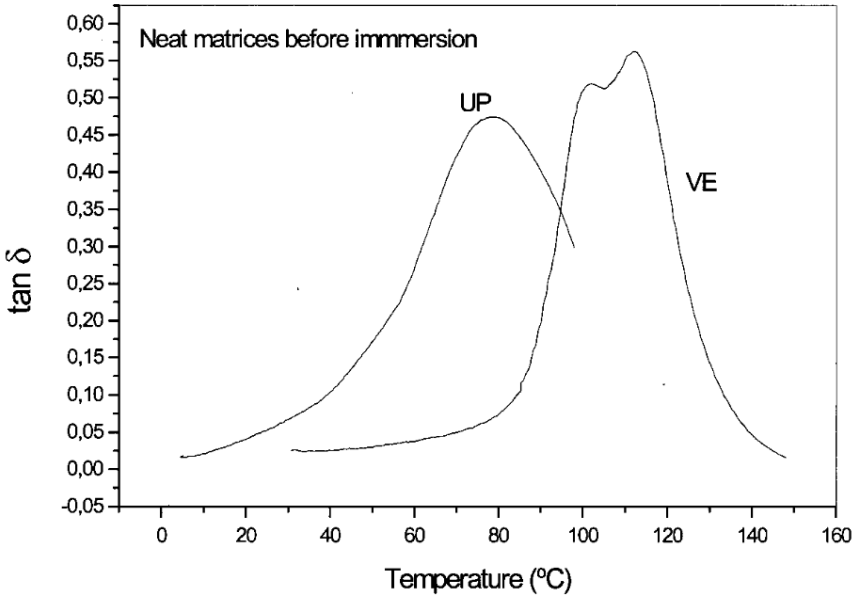

Figure 2-5: *A comparison of neat vinyl ester and unsaturated polyester tan δ curves. Evidence of diphasic nature for the vinyl ester matrix – double peak* [39].

A diphasic vinyl ester structure was also found by Zhang and Richardson [21], who investigated the micro-heterogeneity of urethane vinyl ester resin networks using modulated differential scanning calorimetry (MDSC). The matrix was initially cured overnight at room temperature in a glass mould and after extracting entrapped air by vacuum. It was then post-cured at 100 °C for 3 h and 150 °C for 1 h in an air-circulating oven. The authors reported two overlapping Tgs for the vinyl ester resin assessed by MDSC, which were found to be 10 °C apart. It was suggested that the double transition was a feature of the two phases of the resin; the styrene-rich and the vinyl ester-rich phase. The lower temperature Tg was attributed to the styrene-rich phase, whereas the higher temperature Tg was attributed to the vinyl ester-rich phase. This was due to the lower and higher cross-link densities possessed by the styrene-rich and vinyl ester-rich phases, respectively. This assignment was in accordance with the assumption that matrix Tg is proportional to cross-link density. It is noteworthy that conventional DSC and DMA thermal analysis techniques were incapable of detecting the two overlapping transitions, due to reduced sensitivity as opposed to MDSC.

Li et al [26] reported a diphasic vinyl ester structure by studying the cure kinetics of a commercial dimethacrylated epoxy-based vinyl ester resin mixed with a high-temperature-

decomposing initiator and a low-temperature-decomposing initiator. The authors carried out an isothermal cure experiment through DSC for various cure temperatures. They found that only a single transition was shown during the isothermal cure scan. However, the diphasic nature of the already isothermally cured vinyl ester samples was revealed upon re-scanning the samples through DSC to 250 °C.

FTIR can be used to monitor the concentration of various reacting components within a thermoset system. Each vibrational mode absorbs energy at a characteristic wavelength. Depletion of different reacting components is measured given that the absorption peaks can be distinguished from the non-reacting and product peaks. The conversion of vinyl ester matrices can be determined by monitoring the depletion of C=C double bonds of both vinyl ester and styrene monomers at 945 cm^{-1} and 910 cm^{-1}, respectively. 945 cm^{-1} corresponds to the act of plane bending of carbon-hydrogen (C-H) in the vinyl group of the vinyl ester monomer and, 910 cm^{-1} corresponds to wagging CH_2 in the vinyl group of the styrene monomer. A decrease in absorbance intensity can be observed independently from the polymerisation degree, due to physical changes, such as changes in the thickness of the sample film and (or) evaporation of a component. A correction for such effects can be carried out using absorption intensities corresponding to the bending of aromatic C-H at 830 cm^{-1} in vinyl ester monomer and 700 cm^{-1} in styrene. Fractional conversion (degree of cure) through FTIR absorption for vinyl ester and styrene double bonds can be calculated by *Equations 2-1* and *2-2*, respectively, derived from the Beer-Lambert law [27].

$$\alpha_{VE}(t) = 1 - \left(\frac{ABS\ (t)945\ cm^{-1}}{ABS\ (t=0)945\ cm^{-1}}\right) * \left(\frac{ABS\ (t=0)830\ cm^{-1}}{ABS\ (t)830\ cm^{-1}}\right)$$

2-1

$$\alpha_{ST}(t) = 1 - \left(\frac{ABS\ (t)910\ cm^{-1}}{ABS\ (t=0)910\ cm^{-1}}\right) * \left(\frac{ABS\ (t=0)700\ cm^{-1}}{ABS\ (t)700\ cm^{-1}}\right)$$

2-2

where: α is the fractional conversion of double bonds corresponding to each monomer at time t and ABS is the peak absorption intensity at time t. Brill and Palmese [27] suggested that during the reaction the location of peaks may change. They found that the absorbance peak at 945 cm^{-1} may shift to slightly lower absorbance values of 941 cm^{-1}.

Brill and Palmese [27] assessed the fractional conversion of a vinyl ester resin as a function of increasing cure temperature and for various styrene contents through FTIR. Indicative conversion values obtained through FTIR after isothermal cure at 100 °C were 0.74 and 0.89 for the vinyl ester monomer and the styrene monomer, respectively and, for a resin with 47%, wt styrene. The conversion calculation suggested that the reaction of the vinyl ester monomer commenced before the reaction of styrene. Results also confirmed that the reaction of styrene continues after the vinyl ester monomer reaction was terminated. Furthermore, the authors found that an increase in cure temperature resulted in higher reaction rates and higher final conversion for both monomers vinyl ester and styrene monomers. Similar results were reported by Scott et al [24], who found that the conversion rate of vinyl ester monomer was initially higher than that of styrene. However, styrene kept reacting after the vinyl ester monomer had reached final conversion.

Mousa et al [40] monitored the absorbance of 1641 cm^{-1} and 1612 cm^{-1} corresponding to vinyl ester and styrene, respectively. The absorbance of 830 cm^{-1} was used to account for physical changes. Presumming that no styrene evaporation takes places, the authors determined the total fractional conversion of the polymer by using conversion values for the vinyl ester and styrene monomers, through *Equation 2-3*, as follows:

$$a_t = \left(\frac{\alpha_{ST} + I * \alpha_{VE}}{1 + I}\right)$$

2-3

In conclusion, it has been established that the degree of conversion and Tg of thermoset resins can dictate their thermal behaviour. It was found that cure temperature can be decisive for the conversion and Tg of vinyl ester resins. Reports show that the reaction kinetics of vinyl ester resin can be rather complex. FTIR can be a useful tool for the determination of cure kinetics of vinyl ester matrices over the entire conversion, despite the curing thermoset undergoing different state transitions during polymerisation. Since one of the primary focuses of this study is to obtain information directly on the fibre/matrix interface, the assessment of the degree of cure of vinyl ester on the microscale has been deemed critical. Nonetheless, the bulk of the information available on diffusion kinetics of vinyl ester has been obtained on the bulk polymer scale and a property transferability to a microscale remains ambiguous.

Effect of Initiator and Inhibitors on Vinyl Ester Curing

The nature of the initiator employed in vinyl ester curing is critical for the polymerisation rate, molecular weight, structure and final material properties of the polymer. A few types of initiators widely used in free radical polymerisation reactions include:

- Peroxides
- Hydroperoxides
- Azo compounds
- Redox initiators
- Photoinitiators

The initiator should be relatively stable at room temperature but to ensure practical reaction rates should decompose rapidly at polymer processing temperatures. Free radicals produced by initiation are generated by the thermal decomposition of the initiator. The polymerisation reaction propagates through the addition of the monomer to the growing polymer chain and continues the propagation of the radical to the new monomer site. Initiation at low temperatures can be accelerated by the addition of accelerators/promoters, such as T (dimethylamino) benzene, cobalt naphthenate, or dimethyl aniline. The rate of initiation is directly linked to the decomposition rate of the initiator [17,41].

Varying amounts of initiators can produce different heats of reaction, cross-link density and degrees of microgel formation and/or phase separation in the vinyl ester matrix [42]. Cook et al [20] studied the effect of varying amounts of initiator for a bisphenol A vinyl ester resin with a styrene content of 45 wt %. Samples of vinyl ester resin were cured at room temperature for 16 h with or without a post-cure. The addition of two different systems were employed: a methyl ethyl ketone peroxide (MEKP) initiator – amounts varied from 0 to 2.4 wt % (1.2% was the "standard" level, equivalent to 0.48 wt % of pure MEKP) and, a cobalt II octoate metal – amounts varied from 0 to 3.2 wt % (0.2 wt % was the "standard level", equivalent to 0.012 wt % Co-II). The authors reported that the exotherm peak (maximum reaction rate), as shown by DSC, was shifted to a lower tempeature as a function of increasing MEKP. In some cases, a shoulder was observed prior to the main exotherm. This was attributed to probable presence of H_2O_2 in the mixture, as it is a common MEKP contaminant. On the other hand, cobalt II was found to be a polymerisation inhibitor; it was observed that increasing the amount of cobalt II lowered the reaction rate. Induction periods in the polymerisation process were found for vinyl ester systems containing cobalt. This was attributed to oxygen traces within the resin

mixture or to cobalt ions themselves. Increasing concentrations of both MEKP and cobalt II were found to reduce the overall gel time of the resin. However, in theory, gel time is inversely related to the reaction rate of the polymer and thus reduced gel time with an increasing cobalt II concentration was an unexpected result. The authors suggested that in this case cobalt II accelerated the reaction at its early stages but acted as an inhibitor thereafter at higher conversion levels.

Li et al [26] investigated the effect of initiators on the cure kinetics and mechanical properties of a commercial dimethacrylated epoxy-based vinyl ester resin. The workers suggested that in bulk scale pultrusion-based manufacturing it is common to use two or three initiators that decompose in low, moderate and high-temperature regimes. The use of a single, high-temperature-decomposing initiator may result in lower production efficiency and quality due to rapid decomposition at high temperatures. On the other hand, for a vinyl ester cured with a single low-temperature-decomposing initiator, decomposition will occur at the early polymerisation stages resulting in a lower cross-link density and in turn poorer mechanical properties. Li et al [26] characterised the cure kinetics of the resin for varying amounts of two types of initiators: a high-temperature-decomposing initiator and a low-temperature-decomposing initiator, by isothermal cure in DSC. DSC results suggested an induction time prior to the main exotherm, which was attributed to inhibitor depletion at a low temperature. The combination of initiators reduced the induction and exotherm peak times, especially for samples cured at low temperatures. An increase of the high-temperature-decomposing initiator in the dual initiator system accelerated the reaction and reduced the induction time, whereas an increase of the low-temperature-decomposing initiator had no decisive effect. Mechanical properties were found to be independent of initiator concentration but were strongly dependent on the cure temperature.

An increase in polymerisation rate with an increased initiator concentration was observed by Scott et al [24] for a commercial vinyl ester resin, which nonetheless did not affect fractional conversion. Xu and Drzal [42] confirmed that changes in the initiator concentration can influence the polymerisation of vinyl esters. Additionally, they proposed that for a carbon fibre/vinyl ester composite, absorption of a very small amount of the resin initiator by the fibre can have a severe impact on the integrity of the interface.

It has been suggested that for ideal free radical chain growth polymerisation, the rate of inhibitor consumption and the rate of polymerisation should increase as a function of initiator concentration [24,26]. Inhibitors are added in vinyl ester processing to increase shelf life. It has been established that the addition of an inhibitor in the resin can change the kinetics of the

reactions. Inhibitors introduced an induction time in vinyl ester curing, i.e. delayed curing, followed by microgel formation [17,24–26,43]. Stone et al [17] have found that the addition or removal of inhibitors increased and reduced reaction rates, respectively, despite delaying curing.

Effect of Styrene Content on Vinyl Ester Curing

As previously discussed, vinyl ester resin properties are highly dependent on the performance of both the vinyl ester and the styrene phase of the resin, with styrene having a crucial role in the overall performance and cost of the material. Styrene serves as a cross-linking agent in vinyl ester polymerisation, whereby the initiator activates the double-carbon bonds between the vinyl ester and styrene molecules allowing them to cross-link [35]. A high styrene content can result in reduced cross-link density in the short term but can produce volumetric shrinkage and enhanced performance of the matrix over time. Thus a higher styrene content can contribute to higher maximum conversion through long-term reaction; this is because when the vinyl ester monomer has completed homopolymerisation, styrene keeps reacting [24]. Furthermore, an increase in styrene content is known to enhance the hydrophobicity of the resin and decrease the total moisture gain of the matrix. On the other hand, in vinyl ester-based FRPs volumetric shrinkage caused by styrene increase is a common initiator of micro-cracking in resin-rich regions and a residual stress generator for regions of high fibre volume fractions. High styrene content matrices and FRPs are associated with a high degree of heterogeneity through microgel formation and therefore incomplete polymerisation. Incomplete polymerisation makes the final polymer or FRP more susceptible to change of properties and cure over time, and induces lower heat stability and resistance to hydrolysis [44].

Scott et al [24] investigated the effect of varying styrene content in the cure kinetics of vinyl ester resins through DSC and FTIR. They reported slower polymerisation rates for increased styrene vinyl ester resins, but better ultimate conversion due to reduced cross-link density and the ability of styrene to react after the final polymer is formed. Similar observations were made by Brill and Palmese [27], who reported increased ultimate conversion of the vinyl ester monomer with increased styrene content. Nevertheless, increased styrene did not affect the conversion of the styrene monomer itself.

Studies on the thermal behaviour of vinyl ester resin with varying styrene content suggest that Tg is loosely dependent on the styrene content of the matrix. Scott et al [24] confirmed that despite the poorer cross-linking of increased styrene specimens, Tg variation between different styrene concentrations was insignificant. However, a small Tg decrease was consistently

apparent for high styrene content specimens. Similar results were recorded by Ghorbel and Valentin [34], who reported styrene loss through hydrothermal exposure of a glass fibre/polyester composite, which nonetheless did not affect its Tg.

Varying styrene content in vinyl ester resins can affect the thermal properties of vinyl ester, reflected in the output of DMA analysis. The breadth of the tan δ curve has been found to increase in the Tg region, while the tan δ maximum is known to decrease, with decreasing styrene concentration [24,45]. Moreover, the rubbery modulus underwent an increase as a function of increasing cross-link density promoted by a reduction in styrene content [24].

Styrene-based polymers have been associated with styrene vaporisation effects, especially in the case of specimens of a high surface-to-volume ratio. It is therefore useful to be able to identify when such effects take place for a more thorough understanding of vinyl ester matrices. Hernández et al [46] presented ATR-FTIR spectra styrene copolymers as a function of styrene content. It was shown that the bending of aromatic C-H in styrene at 695 cm^{-1} increased with styrene concentration, while the peak was not apparent when styrene was not present in the material. A comparative plot comparison for varying styrene content co-polymers is shown in *Figure 2-6.*

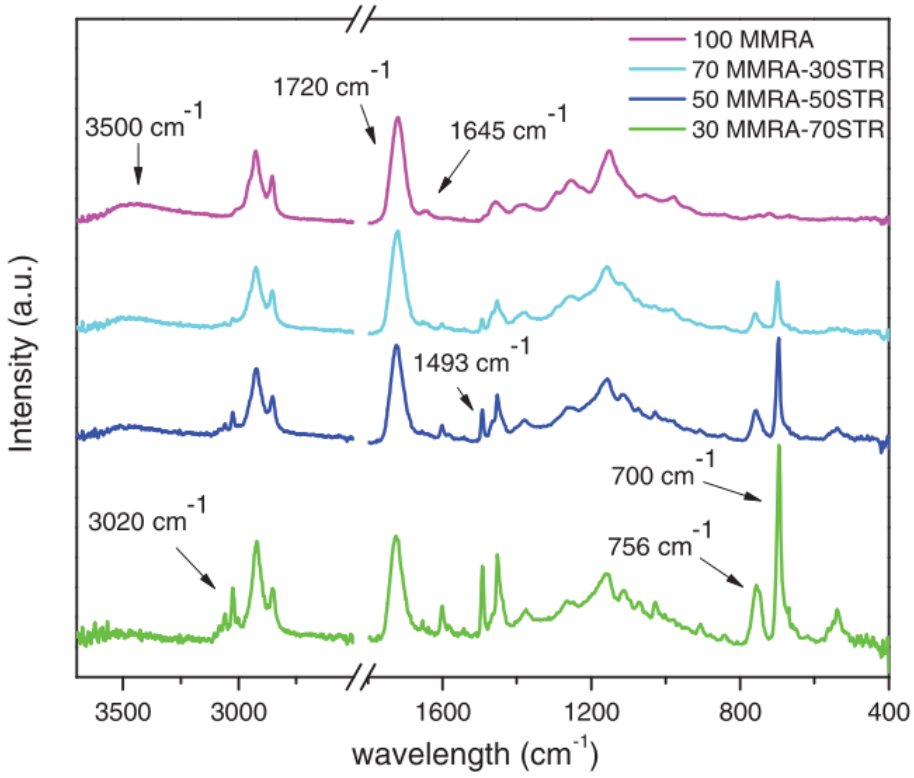

Figure 2-6: *ATR-FTIR spectra of highly functionalised a biobased derivative of ricinoleic acid (MMRA) with varying styrene concentrations of 0 %, 30 %, 50 % and 70 %* [46].

The Effect of Ambient Oxygen on Vinyl Ester Curing

A significant parameter in the cure kinetics of vinyl ester polymers and their composites is the influence of ambient oxygen on the polymerisation process. Although polymerisation may be achieved under an ambient environment, oxygen interaction with the pre-polymer has been identified as an "efficient scavenger" in radical polymerisation. Therefore, rigorous attention needs to be paid into excluding oxygen from the polymerisation medium. Oxygen interaction with the pre-polymer mix may result in the formation of additional radicals which may complicate the polymerisation and compromise the final properties of the polymer. Oxygen intrusion can be minimised by conducting the experiment under vacuum or inert atmosphere conditions (e.g. nitrogen) [28]. However, Albertin et al [47] found that the use of a nitrogen environment may not be adequate for complete oxygen removal from the polymer mix. Polymerisation inhibition of vinyl ester by the presence of oxygen during curing in DSC has been reported by Scott et al [24]; induction times were apparent in DSC thermograms prior to the main exotherm, attributed to entrapped oxygen in the DSC pan. Oxygen presence within polymer links has been associated with thermal instability along with other parameters involved in the polymer preparation process, as previously discussed [28].

Nouranian et al [48] reported on the effects of moulding and curing atmosphere on the flexural properties of vinyl ester. Specimens were prepared using either open or closed moulds, and were thermally cured under either air or nitrogen atmosphere. It was found that the flexural moduli of nitrogen-cured and closed-mould specimens were 3 % and 9 % higher than for air-cured specimens, respectively. Moreover, the mean flexural strength for open-mould air-cured specimens (with their sides exposed to air loaded in tension) was 65% lower than the mean flexural strengths of open-mould nitrogen-cured or closed-mould specimens. The authors attributed the reduction in flexural properties to incomplete vinyl ester curing due to the exposure of the curing polymer to ambient oxygen. Oxygen diffuses into the free surface region of the open-mould, air-cured specimens creating gradients in the local stiffness and strength in the near-surface region, due to lower cross-link density. It can thus be understood that this effect may be particularly important for thinner specimens.

2.2.3. Concluding Remarks

In conclusion, vinyl ester resins have been previously identified as diphasic structures, which consist of highly cross-linked methacrylate epoxy compounds surrounded by a lightly cross-linked, styrene-rich region. Curing in vinyl ester resin is achieved through free radical polymerisation and has been associated with the formation of microgel structures. These are a

product of the resin heterogeneity, i.e. the difference in vinyl ester and styrene monomer reaction rates. Thus, the cure kinetics and conversion of vinyl ester resins are highly dependent on the individual thermal behaviour and conversion of the styrene and vinyl ester monomers. It has been found that even though the reaction rate of the vinyl ester monomer is higher than that of styrene at the early stages of the polymerisation process, styrene conversion becomes increasingly higher. Moreover, styrene has the ability to keep reacting once the conversion of the vinyl ester monomer has been terminated [17,23–27].

Vinyl ester properties are highly dependent on parameters involved in the polymer preparation process, such as solvent, conversion, styrene content, cure environment and temperature employed as well as the initiator used [28,29]. It can be concluded that the thermal behaviour of vinyl ester (cross-link density, Tg, conversion) is primarily related to the cure and post-cure temperature [17,20,25,32]. Particular attention during polymer preparation must be given to the exclusion of oxygen from the polymerisation medium since oxygen is known as a free radical polymerisation retarder [24,28]. Resin formulation can also influence the cure kinetics of the material. A high styrene content vinyl ester resin can have higher maximum conversion due to the ability of styrene to keep reacting once the polymerisation is complete. A low styrene content can contribute to higher cross-linking and an insignificant Tg increase short-term [24,27,34]. An increased initiator concentration has been found to increase the reaction rates of vinyl ester resins but has no effect on polymer conversion [24]. Furthermore, inhibitors, which are used to increase the shelf life of the resin can also affect polymerisation [17].

DSC analysis of vinyl ester curing has been associated with the feature of a shoulder present prior to the main exotherm curve. This initial maximum has been attributed to several manufacturing parameters discussed above, such as oxygen introduction and inhibitor evaporation during cure. Induction time has been found to decrease for an increased initiator concentration [20,26].

Most to-date studies are focused on measuring fractional conversion for vinyl ester resin, in its liquid state, which is cured in the DSC furnace. However, FTIR can also be used for the assessment of the cure kinetics of vinyl ester over the entire conversion and despite the thermoset undergoing different state transitions during polymerisation. Thus, FTIR can potentially be utilised for the evaluation of the fractional conversion of a cured vinyl ester matrix as a function of scale. Limited information is currently available on the thermal behaviour of vinyl ester on the microscale [36], as opposed to other thermoset matrices, such as epoxies [49].

2.3. MECHANICAL AND MICRO-MECHANICAL TESTING OF FIBRE REINFORCED POLYMERS

2.3.1. Introduction to Micro-mechanical Testing

Interfacial properties can be determined through various testing methods, either directly or indirectly. Indirect methods include macro-mechanical testing, i.e. a series of non-destructive or destructive techniques which involve the study and testing of bulk laminates, such as the 3-point bending and short-beam shear tests, which provide information on the flexural properties and Interlaminar Shear Strength (ILSS) of the material.

Although bulk composite testing can provide useful information on the macroscopic properties of the material, the need to understand in more depth the role of the fibre/matrix interface has led to the development of micro-mechanical testing techniques. These are particularly sensitive to interfacial changes and can provide a direct characterisation of the stress transfer capability at the interface. The stress transfer capability at the interface can be assessed as a measure of interfacial shear strength (IFSS), which nonetheless cannot be determined directly through bulk composite testing methods. Direct characterisation of the composite interface can be a fast and efficient way to evaluate the performance of an FRP. Some commonly used micro-mechanical testing techniques are the microbond test, the fragmentation test, the single fibre pull-out test and the fibre indentation test [2,15,50,51].

Even though the scalability of the properties of the fibre/matrix interface to the bulk laminate performance is complex, it has been established that a strong interface can potentially contribute to an FRP with high mechanical and chemical resistance, and an interfacial failure is likely to compromise the performance of the bulk material and even lead to its failure. Studies have also shown that whenever there was any improvement in the micro-mechanical properties of a composite, there was a corresponding improvement in its macroscopic properties too [1,2,4].

Single Fibre Pull-out test

The single fibre pull-out test is one of the longest established micro-mechanical testing methods, introduced in the mid-1960s by Kelly and Tyson [52]. This method involves the placement of a fibre perpendicularly in a large volume of resin prior to cure, and is essentially operated by the pulling of a fibre out of the matrix. The matrix is usually present in the form of a disc or a rod [53,54]. A schematic presentation is shown in *Figure 2-7*. The test complies with the assumption that the measured debond force is equal to the pulling, shearing force

applied to the entire interface and is uniformly distributed [55]. The main limitation of the pull-out test is its incapability to support fine fibres, such as carbon, glass and Kevlar fibres. This is due to fibre breakages initiated by high pulling forces. For fibres ranging in diameter from 5 to 50 μm, the maximum embedded length that can be used is in the range of 50 ± 1000 μm. It is particularly challenging to keep the embedded length to such small geometries and to handle such test specimens [53]. However, despite the limitations of the testing method, Piggott and Xiong [56] observed that when carried out under appropriate conditions, results can be obtained for interface yielding stress and interface work of fracture without the values having to be corrected for friction.

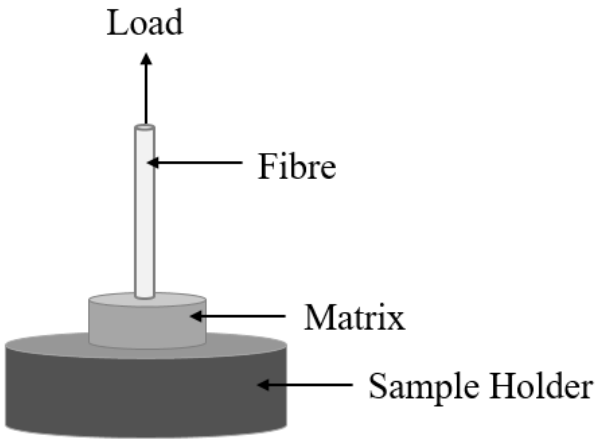

Figure 2-7: *Schematic presentation of the single-fibre pull-out test.*

Single-fibre Fragmentation Test

The fragmentation test involves tensile loading of single fibre specimens encapsulated in a cured dogbone-shaped matrix. When external tensile stress is applied to the dogbone sample, the stress is transferred by shear stress across the interface. The external tensile load is increased inducing fibre fracture. As the tensile load increases, the tensile strain in the fibre will eventually exceed the ultimate tensile strain of the fibre, and fibre fracture will occur. As loading takes place, further fractures occur resulting in shorter length fragments. The test is complete when the fragment length becomes too short for the available interface to transfer sufficient stress onto the fibre to break it. The shortest fragment length that can be broken upon stress application is referred to as “critical length” and can be used with the tensile strength of the fibre for the evaluation of IFSS. A schematic presentation is shown in *Figure 2-8.* The use of a polarised light microscope is employed for transparent matrices so that the fragmentation

process can be observed in situ. This is one of the main benefits of fragmentation test over other micro-mechanical testing techniques [57,58]. The fragmentation test can be carried out on both thermosets and thermoplastics. In the case of thermoset matrices, specimens are typically cast in open silicone moulds, whereas in the case of thermoplastics compression moulding is employed [58–63]. The main limitation of the fragmentation technique is the fact that the fibre failure strain must be approximately three times lesser than the matrix failure strain for the production of accurate and reliable data [14,64]. Additionally, Weibull analysis must be used to extrapolate a value for the fibre strength at the critical length, which can often be misleading [65]. Nairn et al [66] reported that since real composite laminates are not fragmented into short critical lengths, the use of a critical length measurement to predict bulk composite behaviour may be inaccurate. Lastly, over-predictions of the output IFSS may be made due to the presence of higher transfer normal stresses induced by Poisson's effect, while interfacial voids, such as cracks may further confuse the calculation [55].

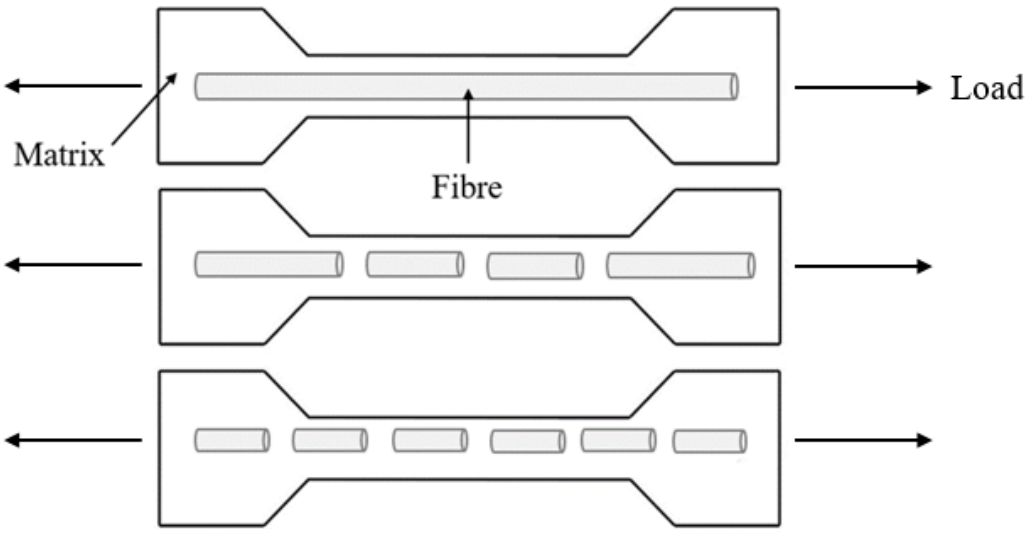

Figure 2-8: *Schematic presentation of the single-fibre fragmentation test.*

Microbond Test

The microbond test technique was developed in the late 1980s by Miller et al [67] and is to this day one of the most widely used micro-mechanical testing methods. In the microbond test sample preparation is easier when compared to the pull-out test, which involves the use of large matrix blocks. Microbond samples are fabricated by applying several matrix micro-

droplets on a single fibre. The droplets are formed concentrically around the fibre and are of an ellipsoidal shape. The test involves the clamping of the test specimen between a pair of shearing blades/thin plates so that the fibre can move freely, while the resin droplet remains restrained. In such a manner, the fibre is pulled out of the droplet by the application of a tensile force to the free end of the fibre. The resulting effect can be referred to as a "debond". The force resulting from the matrix debond is recorded and the average shear stress is calculated by dividing this force by the embedded fibre area. A schematic presentation is shown in *Figure 2-9*. As of yet, there is not any standardisation regarding sample preparation or testing apparatus. Therefore, laboratories tend to develop their own testing setup, as observed in the literature [4,67–71].

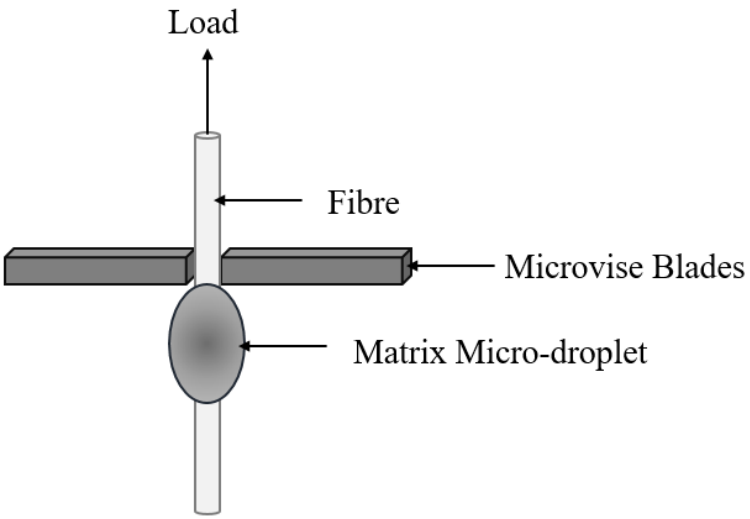

Figure 2-9: *Schematic presentation of the microbond test.*

The microbond test is sensitive to matrix and fibre properties, such as cure schedule, cross-link density, chemical modifications and, diameter, surface treatment, sizing, respectively. It can be hence used in the screening and characterisation of different micro-composite combinations employing a wide range of materials, such as thermosets, elastomers, amorphous, semi-crystalline, thermoplastics, liquid crystalline polymers as well as a broad range of reinforcing fibres, such as glass, carbon and polymeric fibres [53]. The method is associated with a great deal of scatter in the results, which can nonetheless be minimised by maintaining a constant test configuration, such as equipment setup and consistency in specimen dimensions and geometry [53,70].

The scatter in data has been attributed to several testing parameters, such as:

- Droplet gripping [72,73].
- The effect of the microvise blade gap width, which as reported, when altered can potentially cause dramatic changes in the magnitude and location of shear stress [74]. Such claims have been disputed by several thorough investigations and attributed the scatter to another of the testing parameters on this list (see non-uniformity of fibre surfaces).
- Non-uniformity of fibre surfaces. This is due to the microbond test being conducted only on one moment of the fibre, which can vary from the rest of the material [75,76]. Moreover, fibre surface variation was observed due to the use of different fibre filaments. Such issues may be countered by increasing the test specimen range [77].
- Meniscus formation on the fibre, which can influence embedded length measurements. Changes in measured embedded length can have an impact on measured IFSS and have also been associated with premature micro-droplet failures [70,74].
- The "hand" of the operator [78,79]. Such claims have been countered by Wagner et al [80] who highlighted that this is not an issue provided the operators are well trained. Laurikainen et al [77] and Järvelä al [81] conducted microbond testing using several operators with no notable changes in the output data.

Single-fibre Indentation Test

The indentation or micro-indentation test involves the determination of interfacial properties through the use of a "real", bulk composite. The test is operated by the application of compressive load on a fibre or region of fibres on a polished specimen surface to produce debonding. It is conducted by the insertion of a sharp indenter in a polished laminate area. An individual fibre aligned normal to the polished surface is then located and a compressive load is applied, producing a debond [82,83]. A schematic presentation is shown in *Figure 2-10*. The primary benefit of indentation testing is the fact that it uses bulk composite samples which allow a more realistic simulation of thermal stresses, polymer morphology and the influence of neighbouring fibres [84]. The main limitation of this testing technique is that it requires the cutting and polishing of a sample area, which may possibly result in a change in the residual stress state and interfacial damage. Moreover, complications may be introduced regarding result interpretation; the presence of neighbouring fibres requires accounting for the onset of frictional stresses and can lead to an over-estimation of IFSS values. This can become an issue when selecting the appropriate failure criterion and can often lead to errors when used in

industry for the calculation of safety factors. Moreover, the extrapolation of interfacial to bulk properties may be exaggerated [14,74,84].

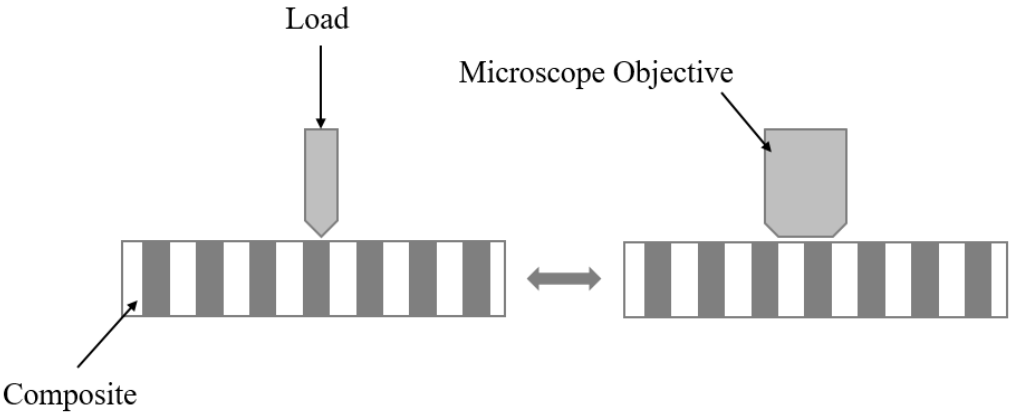

Figure 2-10: *Schematic presentation of the indentation test.*

Single-fibre Micro-indentation Push-out Test

The push-out test is a slight deviation from the indentation test. Its main difference is that the test is carried out on a thin material polished surface allowing fracture of the whole interface and, that the fibre is entirely removed from the matrix when pulled [85–87]. The IFSS is calculated by dividing the maximum applied load required to push out a single fibre by the polished area the test is conducted on [86]. The main advantage of the technique is that it enables a thorough understanding of interfacial mechanics, including response to fracture and interfacial failure modes, such as fatigue and environmental conditioning, as well as monitoring the "health" of in-service parts [87,88].

In the same fashion as in the indentation test, the effect of neighbouring fibres can affect the evaluation of IFSS. Successful conduction of the test is also challenging and rigorous sample preparation is required. Interfacial damage may also be induced when polishing the thin sample area [14,74,84,89].

Benefits and Limitations of Micro-mechanical Testing

The main advantage of micro-mechanical testing is its capability to provide direct data about the stress transfer capability at the interface. Moreover, the material consumption, testing time and operation costs involved in micro-mechanical testing are minimal compared to indirect,

macro-mechanical or meso-mechanical testing methods. This allows an economical and time-efficient characterisation and screening of composite interfacial adhesion as a function of various treatments. For instance, the effect of different fibre sizings on the fibre/matrix interface can be assessed, as well as interfacial durability in various environmental ageing conditions, which otherwise is a lengthy and costly procedure involving continuous monitoring of potentially large components or structures [3,90,91].

Nonetheless, micro-mechanical testing possesses various challenges and limitations, which if not adequately considered, may lead to misleading and inaccurate conclusions. The primary challenge of micro-mechanical testing is the accurate interpretation of material property transferability from a micro-composite scale to a bulk laminate scale [49,91,92]. This is due to potential variations of the cure kinetics, chemical, mechanical and physical adhesion of a bulk composite interface when compared to its micro-composite counterpart. The small scale often involved in sample preparation of micro-composites makes the sample sensitive to a series of parameters. For instance, temperature variation in the test environment of thermoplastics can influence their adhesion [93–95]. Additionally, a small error in thermoset mixing ratios can alter the stoichiometry of the final material [96,97]. Diffusion and evaporation effects may become more prominent (e.g. styrene or curing agent evaporation, adsorption of curing agent to fibre surface) changing the cure kinetics of the system [68,92,98–101]. Surface oxidation may also appear [92,93], while the use of additional cure or post-cure steps may be required to achieve optimum conversion [92,98]. All challenges involved in the use of the microbond test, which has been employed in the characterisation of the glass fibre vinyl ester interface throughout this study, as well as the potential of the method to obtain useful information for a bulk composite, are discussed in detail below. One needs to be fully aware of the issues mentioned above for an accurate and realistic determination or understanding of bulk composite interfacial properties, although a qualitative assessment may not be achieved.

A common indicator of the thermal performance of micro-composites is Tg, which is usually compared to the Tg of their counterpart in the bulk scale. However, the small size of micro-composites is restrictive for an accurate Tg evaluation via the established thermal analysis techniques, such as DSC and DMA. Several methods have been suggested in the literature with the most prominent being the use of thin film models, which exhibit the embedded length of matrix micro-droplets. Other methods include the stacking of micro-droplets in a DSC pan or the TMA-Tg method [49,92]. The latter uses single fibre micro-composites exhibiting a cluster of micro-droplets [49].

Several authors have reported the detection of a notably lower Tg in microscopic matrices than in their bulk composite counterparts. Rao et al [49] found that epoxy micro-droplets possessed a Tg of 60 °C, less than that of the bulk composite, due to curing agent evaporation. Artefacts were also observed in smaller droplets, induced by IFSS measurements through the microbond test, due to curing agent evaporation. Zinck and Gérard [102] found that the Tg of polyepoxide thin films used as micro-droplet models was 50 °C less than that of the bulk matrix, due to differences in the stoichiometric ratio. A similar observation was made by Zinck et al [92], who highlighted that due to evaporation effects, cure schedule employed, surface oxidation and probable hydrolysis of the curing agent at the first step of cure, epoxy micro-droplets showed a significantly lower Tg (-20 to -50 °C) than the bulk matrix. This resulted in changes in the interfacial stress distribution and in turn reduced adhesion in the micro-composites. Moreover, IR analysis of amine cured films used as micro-droplet models, featured two additional spectral bands at 1661 cm^{-1} (C=N imine) and 1723 cm^{-1} (C=O carbonyl), which were not apparent in bulk epoxy samples. The Tg reduction was attributed to the formation of imine groups and their reaction with oxirane groups. The authors thus concluded that the curing of amine-based micro-droplets should be carried out in an inert atmosphere and/or at temperature below 120 °C.

Haaksma and Cehelnik [103] reported on incompletely cured epoxy micro-droplets used in the microbond test. Regardless of the fibre used, the authors failed to record IFSS due to curing issues of the droplets. The degree of cure was assessed by FTIR microscopy, which showed complete unreacted species in the matrix and curing agent loss upon curing at elevated temperature. The degree of cure was also influenced by the dimensions of micro-droplets; samples with diameters lower than 1 mm appeared to be particularly tacky, which is an indication of low Tg and thus incomplete cure. Curing agent loss was attributed to evaporation effects. Liao and Tung [101] reported the incomplete cure of epoxy micro-droplets on carbon fibre due to the adsorption of m-Phenylenediamine (m-PDA) curing agent onto the fibre surface. The issue was counteracted by increasing the curing agent concentration of the matrix. Such limitations were not faced when a methylene dianiline (MDA) curing agent was used.

Ash et al [104] observed varying degrees of stiffness and IFSS in polyester micro-droplets. It was observed that when micro-composites were tested in DMA, as sample stiffness decreased, there was a subsequent decrease in IFSS. This was not the case during fibre testing, which translates into varying degrees of stiffness of the matrix, solely. The authors attributed the stiffness scatter to styrene loss. FTIR of polyester micro-droplets showed that 50 – 60 % of their initial styrene content was evaporated. A correlation between IFSS and stiffness was also

proposed by Yang and Thomason [105] for glass fibre/polypropylene samples, due to changes in residual interfacial stresses. There were generated due to changes in the polypropylene matrix, such as oxidation and temperature degradation.

Dirand et al [106] reported styrene loss in vinyl ester micro-droplets on glass fibre, which resulted in poor interfacial adhesion. According to the authors, styrene loss was facilitated by the particularly high surface-to-volume ratio of micro-droplets and the absence of a mould, which would prevent evaporation effects. However, in this case, the effect of styrene evaporation is solely an assumption and no actual experimental evidence was provided by the authors. Laurikainen [68] observed that for a glass fibre/vinyl ester system, attempts to cure vinyl ester micro-droplets were unsuccessful, regardless of post-cure temperature. Incomplete curing was attributed to styrene loss, as per the conclusion of Dirand et al [106], mentioned above. Laurikainen [68] suggested that the effect of styrene evaporation could be countered by curing specimens in a styrene-rich atmosphere.

Bénéthuilière et al [45] conducted a comparison between the interfacial adhesion of a conventional styrenated and a more environmentally friendly, styrene-free vinyl ester resin, 1,4-butanediol dimethacrylate-based (BDDMA), reinforced with glass fibre. The comparative studies include an IFSS assessment through the microbond test, a wettability evaluation of fibre bundles by uncured vinyl ester and a bulk scale mechanical characterisation (ILSS) of moulded unidirectional (UD) composites using the short-beam shear test (SBS). Comparative wettability studies on the two resins in their wet state on sized glass fibre filaments showed that styrene-based vinyl ester exhibited a lower contact angle and better work of adhesion. In addition, sizing solubility was also found to be lower in the styrene-free resin. In agreement with wettability observations, the SBS results showed a lower ILSS for the styrene-free specimens. However, microbond test results suggested that the styrene-free resin possessed slightly higher IFSS than the conventional vinyl ester resin in contrast to the wettability and SBS observations. The fracture mode in both systems was similar. The former observation clashes with the observations of Laurikainen [68] and Dirand [106], who suggested that styrene evaporation resulted in incomplete curing which translated into reduced interfacial adhesion. Bénéthuilière et al [45] proposed that styrene evaporation was more intense at the microscale due to the high surface-to-volume ratio of microdroplets, leading to an under-estimation of IFSS for the styrene-based micro-composites. Thermal analysis studies entailed in section *2.2.1. The Chemistry of Vinyl Ester* showed that in bulk vinyl ester a reduction in styrene had a minor influence on the Tg of the resin. In fact, the degree of cure of vinyl ester resin was found to be complex and a function of more than one parameter. Such parameters

are initiator concentration, styrene volatility and the influence of oxygen and cure schedule [20,24–28]. One can hence conclude that the curing kinetics of microscopic vinyl ester specimens (high surface-to-volume ratio), and in turn interfacial adhesion, still remain unresolved topics and the margin of understanding vinyl ester curing on the microscale is still high.

Several authors have reported the use of different cure conditions, to produce a testable micro-droplet which can reflect the polymer properties on the macroscale. Bryce et al [98] highlighted the influence of evaporation effects on epoxy micro-droplets, which can notably affect the IFSS of the system and even lead to "soft", tacky droplets. The introduction of a pre-cure standing time step was proven to contribute to better curing in epoxy-based micro-droplets and prevent curing agent vaporisation [49,98,99]. Bénéthuilière et al [45] employed a gradual temperature elevation involving isothermal steps to prevent loss of reactive diluents, such as styrene.

Mak et al [107] were unable to achieve the same degree of cure in thermoplastic reinforced epoxy micro-composites as that achieved on a bulk scale when using bulk scale cure conditions. Monitoring of micro-droplet cure showed that when a lower cure temperature was employed, the microstructure of the bulk composite could be achieved. Contrarily, Charlier et al [108] observed that a higher temperature schedule was used to achieve optimum cure in epoxy and acrylic micro-droplets. The authors also suggested that in micro-droplets, whereby only a minute volume of pre-polymer mix is used, autoacceleration effects were not present, as opposed to bulk scale, and thus the reaction extent was lower. Paraffin wax also added to acrylic micro-droplets to prevent vaporisation of acrylic monomers.

Rao et al [49] managed to compensate successfully for epoxy curing agent evaporation by curing epoxy samples in an amine-rich environment but no improvement was shown when double the amount of curing agent was used. On the contrary, the attempt of Biro et al [109] to cure epoxy micro-droplets in an amine-rich environment did not improve the curing process. Zinck et al [92] suggested an inert nitrogen cure environment for epoxy systems and a temperature level lower than 120 °C to prevent imine formation and a subsequent Tg loss. Nonetheless, Biro et al [109] observed no improvement in epoxy curing under inert nitrogen conditions.

Comparison of Micro-mechanical Test Methods

In 1991, Galiotis highlighted the lack of standardised experimental methods, either in isolation or in a "real" composite scale, to assess interfacial performance. The issue remains dominant

in the present times with no established method standardisation [110]. Piggot [111] carried out a comparison between the pull-out, fragmentation and microbond methods. They noted that although comparative results can be considered, great care must be taken in results interpretation, due to the limitations and different levels of complexity involved in each method. Discrepancies were attributed to force imbalance between friction and debonding stresses.

Mandell et al [88] studied three different micro-composite systems through the fragmentation and push-out tests enabling a method comparison. IFSS values obtained by the fragmentation test were notably higher than those obtained by the push-out test. Namely, for the graphite/epoxy, glass fibre/epoxy and glass fibre/polyester systems, IFSS values measured by the fragmentation test were nearly 35 %, 30 % and 20 % higher, respectively.

Similar observations were made by Galiotis [110], who reported notably lower IFSS values resulting from fragmentation tests, when compared with results obtained by the pull-out test, for a Kevlar 49/epoxy system. In fact, fragmentation tests resulted in an under-estimation of IFSS, due to debonding occurring at particularly low strains making the assessment of critical length more challenging. When a different epoxy matrix was used, IFSS values produced by the microbond and pull-out tests were in close proximity. Pull-out tests were prone to the output of lower IFSS values when considering that the test complies with the assumption that the applied force is equal to the uniformly distributed shearing force along the interface. The microbond test showed that the average IFSS was lowered with an increase in embedded length, attributed to the non-uniform distribution of the force applied to the micro-droplet. Nonetheless, microbond results obtained for an embedded length of 50 – 100 μm were in line with data obtained through Raman spectroscopy.

Favre and Jacques [64] produced comparative results between the fragmentation and pull-out tests. They found that IFSS values generated by the fragmentation test were two times lower than the ones obtained by the pull-out test when a bare carbon fibre/epoxy system was used. Large discrepancies in values were also noted when a thinner diameter fibre was used. The replacement of epoxy with a tougher tetraglycidyldiaminodiphenyl methane (TGDDM) resulted in particularly high IFSS measured by the pull-out test, while on the other hand, the fragmentation test was deemed incapable of yielding results for such a tough matrix.

Herrera Franco and Drzal [74] attempted to create a comparison between results obtained by micro-mechanical testing methods, such as the fragmentation, microbond and indentation tests and, bulk composite mechanical tests, such as tensile, Iosipescu, and short beam shear, using a carbon fibre/epoxy system. The authors noted significant discrepancies between micro-

mechanical testing techniques. In particular, IFSS results produced by the microbond test were lower than fragmentation values. The effect was attributed to the high surface-to-volume ratio of epoxy micro-droplets, facilitating the vaporisation of the curing agent. On the other hand, the fragmentation test involves the use of a bulk matrix encapsulating the single fibre and in turn such effects are minimised. Although indentation tests resulted in the highest IFSS values, the authors proposed refinement of the method, due to apparent limiting factors, such as debonding criteria, free surface, residual stresses, effects of neighbouring fibres, and surface damage induced by specimen polishing. Upon the application of fibre sizing, IFSS values measured by the indentation tests only showed a small improvement, whereas fragmentation and microbond values were significantly amplified. It was hence suggested that micro-mechanical testing techniques were sensitive to interfacial conditions. Correlation was shown between fragmentation and short-beam shear tests since they involve the measurement of the same shear stress component. Greater agreement was shown between fragmentation and 45° off-axis tensile tests. The authors concluded that despite these correlations, reliance on micro-mechanical tests should be avoided until further research on the transferability of composite properties is conducted.

Wagner et al [80] enabled a comparison between the fragmentation and microbond test methods using a Kevlar/epoxy system. The fragmentation test was found to measure a higher IFSS value than the microbond test by 50 %. This was in contradiction to the observations by Herrera Franco and Drzal [74], who attributed the effect to curing agent vaporisation in microbond droplets. The authors supported that an over-estimation of IFSS was shown by fragmentation tests, due to fragmentation occurring only when minimum interfacial bond strength is reached. Moreover, they suggested that an underestimation of IFSS was obtained by the microbond test, due to the method being restrictive in measuring droplets of a large embedded length and in turn higher IFSS. The conclusion of this work was that true IFSS values fall somewhere between the two.

A joint, round-robin study between different laboratories was conducted in order to allow a thorough evaluation of the compatibility of different micro-mechanical test methods, such as the single fibre pull-out, microbond, fragmentation, and indentation methods [112]. Pull-out tests showed that although different values were obtained between different laboratories, there was agreement that fibre sizing enhanced interfacial adhesion. The measured IFSS increase varied by between 7.3 and 38.7 MPa between different laboratories. Microbond tests showed a similar trend with IFSS values falling between 31.6 MPa and 63.2 MPa for bare carbon fibre. An increase by a factor of 1.2 to 2 was observed upon the addition of fibre sizing. A smaller

IFSS increase upon sizing application by a factor of 1.1 resulted from the indentation test, although high data scatter was recorded. Fragmentation values were lower than the ones observed in other methods in accordance with Favre and Jacques [64], and in argument with Herrera-Franco and Drzal [74]. Although some laboratories suggested that IFSS dependent on embedded length, others reported that for treated fibres, IFSS was independent of embedded length. However, confidence in data was established, despite the scatter. Lastly, the authors highlighted the potential of establishing method standardisation to reduce scatter in data. One can conclude that micro-mechanical testing results are based on comparison and even though discrepancies in data might be present, accurate material screening may be enabled.

2.3.2. Macro-mechanical and Meso-mechanical Testing

Macro-mechanical (or meso-mechanical) tests involve the application of transverse loading on a 3-point bending configuration that initiates a mode II or in-plane shear fracture from which ILSS values can be obtained. Such tests are considered indirect since failure fractures are interlaminar in nature. Furthermore, more macro-mechanical tests have been developed to measure the in-plane shear strength, moduli, and failure strains of bulk composite laminates. Even though macro-mechanical and meso-mechanical testing techniques do not allow measurements of properties exclusive to the interface and cannot provide qualitative interfacial data directly, they can be useful for comparative evaluation of bulk composites. This is simply due to macroscopic tests involving the failure of composites not necessarily induced by an interfacial failure. However, macro-mechanical tests designed for the measurement of interface-dominated properties, such as parallel shear and transverse tension can provide valuable qualitative information on changes related to interfacial strength. Furthermore, such properties have been found to reflect the presence and evolution of cracks during loading [2,83].

The short-beam shear (SBS) test can only be used for ILSS calculation. SBS testing can also be employed for comparative testing of composites, given that failures occur consistently in the same mode. The basis of the SBS test is derived from the elementary beam theory and is conducted through the use of a 3-point bending configuration with a span-to-width ratio selected to initiate interlaminar failure. The shear distribution along the thickness of the specimen is expressed as a parabolic function, symmetrical about the neutral axis. Thereby, ILSS reaches a maximum value and, a zero value is attained at both ends of the specimen. However, a number of researchers have reported inaccuracies in the classical beam theory when applied to composite laminates. In reality, normal stress distribution varies non-linearly throughout the specimen thickness. Parabolic distribution can occur on planes midway

between the loading nose and support points and stress distribution may appear to be unbalanced away from these points. Subsequently, peak stresses may occur in the region near the loading noses and supports. Failure can often occur in the region of the loading due to the combined action of shear stresses and, transverse and in-plane compressive stresses. For ductile matrices, this may not necessarily be the case since other failure modes are known to take place, such as bottom surface fibre tensile fracture. Hence, care must be taken in the interpretation of non-homogeneous materials such as composites, and simply assuming mid-plane interlaminar failure will not necessarily provide an accurate shear strength value [74,113–115]. Horizontal shear load diagrams for a curved beam and a flat laminate are shown in *Figure 2-11* [113].

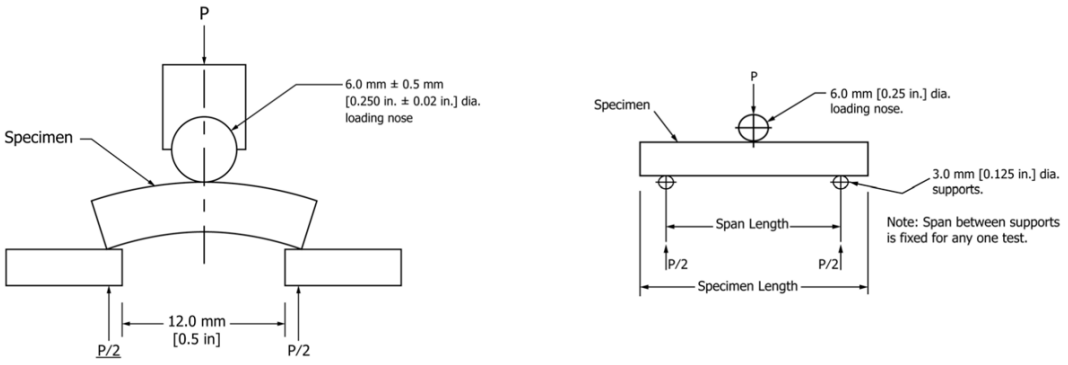

Figure 2-11: *LHS horizontal shear load diagram (curved beam), RHS horizontal shear load diagram (flat laminate)* [113].

Flexural testing, such as 3-point or 4-point bending tests can be used for the evaluation of composite strength, stiffness, and load/deflection behaviour. Both tests are conducted on a rectangular bar supported as a beam. In 3-point bending mode, the bar is placed on two supports and is loaded by means of a loading noise in the midpoint between the supports. In the 4-point bending configuration, the bar is placed on two supports and, is loaded by means of two loading noses at two fixed points. These are set at an equal distance from the adjacent support point. The distance between the loading noses is one-half of the support span. The tests are operated by the application of loading; resulting deflection at the centre of the span is monitored until failure takes place on either one of the outer surfaces, or deformation reaches a pre-determined value. The 3-point and 4-point bending configurations are shown in *Figure 2-12* [116].

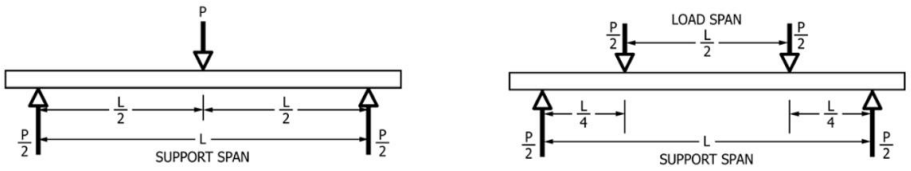

Figure 2-12: *LHS 3-point bending configuration, RHS 4-point bending configuration* [116].

2.3.3. Concluding Remarks

Micro-mechanical composite testing is widely used for the evaluation of IFSS, as a measure of the stress transfer capability at the interface. The major testing techniques with their benefits and limitations have been discussed. Although IFSS is the main output property, methods vary on sample geometry and the manner data is interpreted. The assumptions made for the assessment of interfacial adhesion and the use of different materials have been found to generate disparity and often disagreement occurs between output values obtained from different laboratories. Nonetheless, the round robin study of Pitkethly et al [112] showed that the data scatter for results obtained within the same laboratory was limited. Stress-transfer conditions are critical for the function of the interface/interphase region and in turn the performance of the bulk composite. However, stress-transfer conditions cannot solely be expressed in terms of adhesion. The role of the fibre within the composite interface, interfacial toughness, and stress-redistribution are also important for the optimum function of the interface/interphase region [55].

Although micro-mechanical testing allows the screening of different treatments, such as environmental ageing and fibre sizing, the extrapolation of quantitative data to a bulk composite scale remains in question [49,85,91,92]. In most studied cases, a clear correlation between macromechanical and micromechanical properties could not be established. This was mainly due to the volatility of thermoset micro-droplets (evaporation of curing agent in epoxies and styrene in vinyl esters) owing to their high surface-to-volume ratio [68,92,98–101], or thermal instability of thermoplastic micro-droplets [93–95]. Other impeding effects included surface oxidation [92,93], high possibility of human error in thermoset stoichiometry ratios due to small sample volumes involved in sample preparation [96,97] and adsorption of curing agent to the fibre surface [101]. Such effects may change the chemistry of the matrix and can often lead to incomplete curing and reduced apparent adhesion, which nevertheless

may not be evidenced in a "real" composite scale. A series of reports were presented suggesting that vaporisation effects were counteracted by adding extra cure steps or controlling the curing atmosphere (i.e. curing vinyl ester in a styrene-rich environment to account for styrene evaporation) [49,98,99]. Even though the latter measure has been reported to contribute to more sufficient curing in vinyl esters [68,106], Bénéthuilière et al [45] reported that a styrene-free resin produced slightly higher IFSS values than a conventional styrene-based vinyl ester resin. In addition, several reports have stated that a potential styrene loss in vinyl ester has only a minor influence on the Tg of the resin [24,34]. However, given that the latter observation was made for bulk scale specimens and that the styrene-free samples employed by Bénéthuilière et al [45] did include an alternative reactive diluent (BDDMA), this leaves a "blurred" image on the topic allowing further investigation.

2.4. MOISTURE DIFFUSION KINETICS

Diffusion is a process by which penetrant matter is transported from one part of a system to another through the motion of random molecular segments [117]. The diffusion of aqueous solutions in polymer composites is a complex phenomenon. The diffusion kinetics are directly dependent on the variation of the effects of hydrothermal ageing on the performance or chemistry of the exposed material. The diffusivity of a polymeric composite has been found to be a function of specimen geometry, moisture concentration, temperature and time, and is often modelled using Fick's law [68,118]. According to Thomason [1,9], abnormalities in the structure of polymer composites, such as voids can significantly affect moisture diffusion. Neat resin specimens usually follow a diffusion pattern that resembles Fick's laws of diffusion, although a clear Fickian diffusion is rarely achieved [68].

Moisture uptake of polymeric materials occurs through two different phenomena; "absorption" and "adsorption". "Absorption" is characterised by the capillary transfer of moisture through the existing pores of a material, such as voids, micro-cracks and interfacial gaps. "Absorption" results in the occupation of free space within the material and is not associated with the plasticisation of the matrix and does not generate much heat or swelling. On the other hand, "adsorption" is a process by which a solution is formed. It is associated with the generation of heat and swelling of the polymeric materials when they are exposed to organic solutions. In the case of void-containing polymers and polymeric composites, both processes may take place. Thus, the terms "sorption" or "water/moisture uptake" are used, representing both "absorption" and "adsorption" [6,36].

The mass/moisture gain (%) for an aged specimen can be obtained by *Equation 2-4* [119].

$$M,\% = \frac{M_i - M_o}{M_o} * 100$$

2-4

where: $M,\%$ is the mass gain (%), M_i is the aged specimen mass and, M_o is the oven-dry specimen mass (pre-ageing) [119].

An example of the moisture absorption of a carbon fibre/epoxy (0,45,–45,0)s eight-ply laminates at 49 °C is shown in *Figure 2-13* [119].

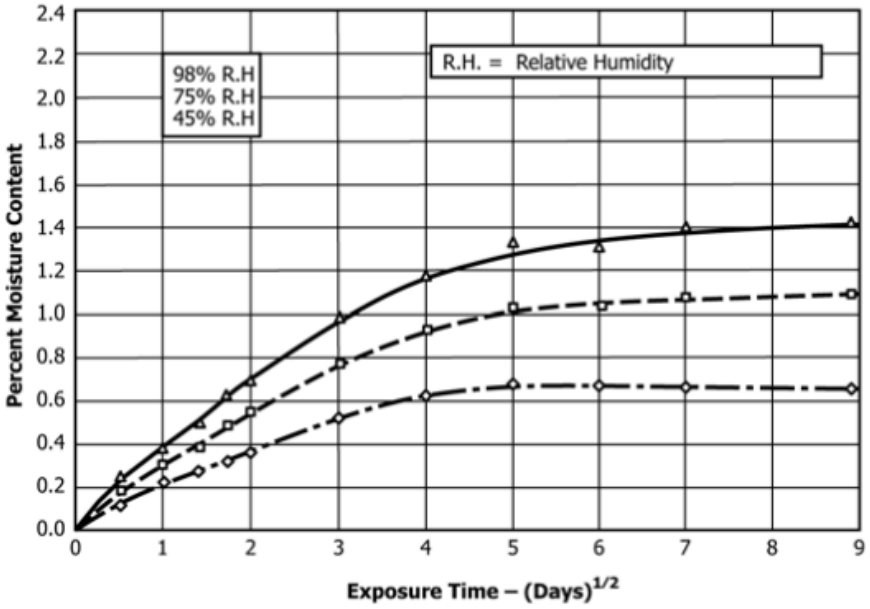

Figure 2-13: *Example of the moisture absorption of carbon fibre/epoxy (0,45,–45,0)s eight-ply laminates at 49 °C* [119].

The classical diffusion approach can be described by Fickian diffusion. In Fickian diffusion, the rate of diffusion of the penetrant is much less than that of polymer segment mobility. Assuming a 1-D form, Fickian diffusion is described by Fick's 2nd Law of diffusion – *Equation 2-5* [36].

$$\frac{dC}{dt} = -D\frac{d^2C}{dx^2}$$

2-5

where: $\frac{dC}{dt}$ represents the change in moisture concentration as a function of time t and D is the diffusion coefficient or diffusivity across any X plane [36]. The relationship of the diffusion coefficient and temperature can be shown by the Arrhenius equation – *Equation 2-6* [2].

$$D = D_0 e^{-E_D/kT}$$

2-6

where D_0 is the pre-exponential factor, E_D is the activation energy for the reaction, k is the Boltzmann constant and T is the absolute temperature [2].

The moisture equilibrium level (M_∞) for a material undergoing Fickian diffusion is illustrated in *Figure 2-14* [2].

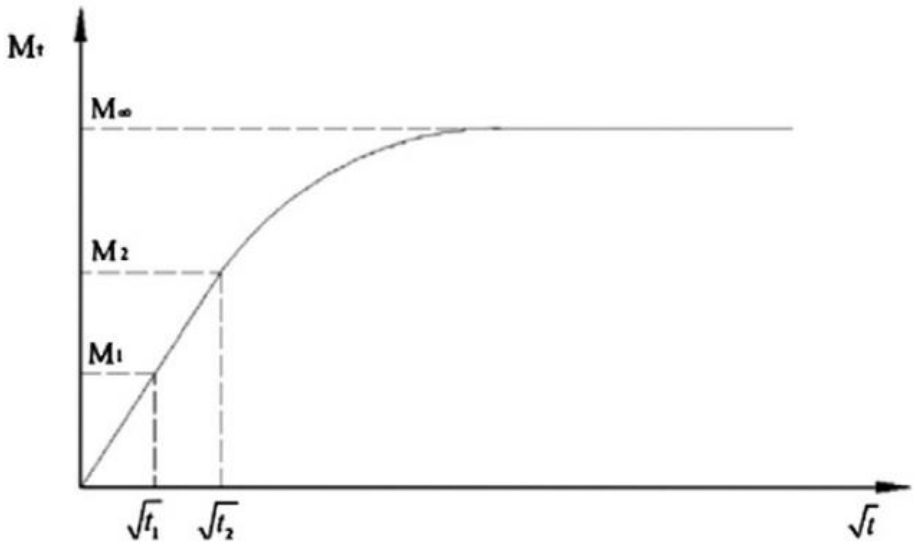

Figure 2-14: *Fickian diffusion plot, mass vs ageing time* [2].

The diffusion coefficient, D can be determined from the initial slope of the linear region of the moisture gain (%) vs ageing time curve as follows – *Equation 2-7* [119].

$$D = \pi \left(\frac{h}{4M_m}\right)^2 \left(\frac{M_2 - M_1}{\sqrt{t_2} - \sqrt{t_1}}\right)^2$$

2-7

where: h is the average specimen thickness, M_m is effective moisture equilibrium content, %, $M_2 - M_1$ is equal to the slope of moisture absorption plot in the initial, and $\sqrt{t_2} - \sqrt{t_1}$ to the linear portion of the curve, $\sqrt{seconds^{-1}}$ [119].

By obtaining the diffusion coefficient of the neat resin, D_m, the diffusion coefficient of the composite laminate, D_c of the same matrix in the direction normal to the surface can be estimated through the following equation – *Equation 2-8* [120]:

$$D_c = D_m[(1 - v_f)\cos^2\varphi + \left(1 - 2\sqrt{\frac{v_f}{\pi}}\right)\sin^2\varphi]$$

2-8

where: v_f is the volume fraction of the laminate and φ is the angle of the fibre orientation relative to the surface [120]. In the current investigation, the thickness was significantly less than the other two dimensions for specimens used for moisture uptake studies, and because the reinforcement laid within the plane of the panel (i.e. φ = 90°), edge effects were assumed to be negligible, leading to the following approximation – *Equation 2-9* [120]:

$$D_C = \left(1 - 2 * \sqrt{\frac{v_f}{\pi}}\right) * D_m$$

2-9

The time required for the composite laminate to attain 99.9% of its maximum possible moisture content is given by *Equation 2-10* [119]:

$$t_m = 0.93 * \frac{h^2}{D_c}$$

2-10

where: h is the thickness of the laminate [119].

Even though moisture concentration may reach a certain plateau as shown in *Figure 2-14*, plasticisation may keep increasing over time. For inhomogeneous materials, diffusion within the polymer can vary, leading to non-uniform moisture concentrations along the structure of the specimen. This type of diffusion can be referred to as non-Fickian [118]. For such cases, models that employ concentration-dependent coefficients $D = D\ (m)$ can be used. However, the functions $D = D_{(m)}$ are mainly of a phenomenological nature and their physical significance is yet unclear [117,121]. The potentially different moisture concentrations within the different regions of polymeric materials (non-Fickian) can result in localised stresses, as

well as matrix cracking. In that case, moisture ingress can be characterised by a combination of diffusion and stress or strain or a combination of diffusion and damage [117,118]. The diffusion process coupled with strain is a time-dependent process, whereas the diffusion coupled with stress is a time-independent process and may also result in creep. In the case of damage, such as cracks or voids the diffusion process can be accelerated significantly [1,117].

The chemistry and molecular structure of the exposure medium have a significant effect on the sorption process. It has been observed that saturation levels of polymers are subjected to change when they are exposed to chemically aggressive environments, such as acidic fluids and methylene chloride (CH_2Cl_2) and n-hepatine solutions. Moreover, the diffusion of high molecular weight solutions in polymeric materials has been found to be rather slow [117].

A widely observed diffusion type in polymers and their composites is "two-stage diffusion". "Two-stage diffusion" is characterised by a weight gain that initially reaches an equilibrium after a short exposure period and then continues to increase until it reaches another equilibrium level, which represents the final equilibrium that can be attained. This phenomenon is attributed to the coupling of diffusion with a viscoelastic response. More specifically, the combined effect of coupling between diffusion and polymeric relaxation is governed by two distinct yet interrelated phenomena: diffusion across the thickness of an area of a polymeric material and time-dependent relaxation of the polymeric chains. For instance, moisture diffusion until saturation in a film will occur rapidly, due to its reduced thickness. Therefore, the establishment of a uniform distribution across the film thickness will take place before the relaxation process starts taking place. In this case, moisture ingress is governed by the diffusivity of an unrelaxed polymer. On the other hand, moisture diffusion in a thick slab of a polymer will occur slower than relaxation and therefore the diffusion will be governed by the diffusivity of fully relaxed polymeric chains. However, for intermediate slabs, the phenomena of diffusion and relaxation will occur in combination [117]. The weight gain against $\sqrt{time}$ plot for a carbon fibre/epoxy exposed to an aqueous environment illustrating a typical two-stage diffusion weight gain pattern is shown in *Figure 2-15* [122].

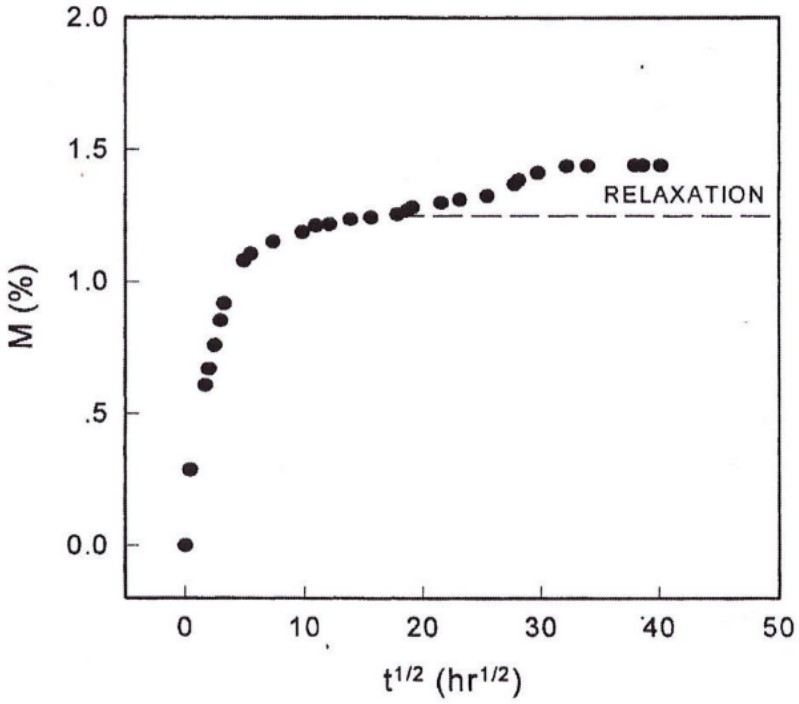

Figure 2-15: *Additional water uptake of unidirectional laminate measured at 70°C exhibiting two equilibrium stages seemingly due to polymer swelling and physical relaxation* [122].

Moisture can enter the structure of polymeric materials by capillary action through areas of air entrapments, such as voids and micro-cracks [2]. FRPs, when exposed to hydrothermal environments or mechanical loading are particularly vulnerable to the formation of micro-cracks located parallel to the direction of the fibres [117]. Additionally, moisture can permeate the structure of polymeric composites through their interface by wicking effects. Moisture concentration at the interface can modify the level of adhesion and thus the performance of the composite [2,117].

Weitsman divided the weight gain behaviour vs $\sqrt{t^*}$ of polymeric materials in six different categories, which are referred to with an abbreviation.

LF: Linear Fickian behaviour

A: Weight gain never attains equilibrium, such as for two-phase diffusion

B: Two-stage diffusion

C: Rapid increase in fluid content-damage growth and material breakdown

D: chemical/physical breakdown of the material; separation between fibre and matrix, leaching along the interface, hydrolysis, chain scission

S: moving diffusion front [117].

Cases *A* and *B* are mostly observed in both polymers and polymer composites exposed to benign fluids causing reversible degradation. *C* and *D* are mostly attained by polymer composites and are associated with irreversible changes, such as loss of material integrity and potential failure. The weight gain pattern against ageing time, $\sqrt{t^*}$ for all six cases is illustrated in *Figure 2-16* [117].

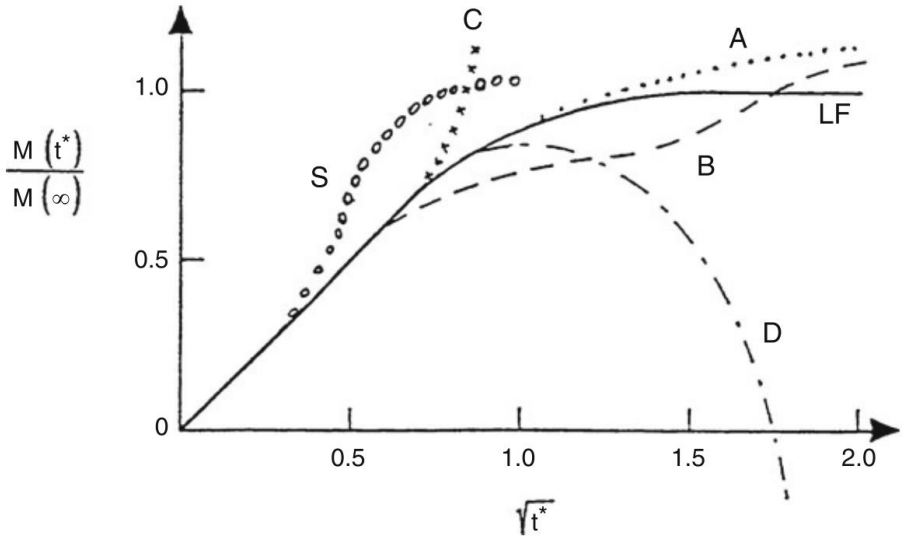

Figure 2-16: *Various weight gain vs ageing time, $\sqrt{t^*}$ patterns/behaviours for polymers and polymer composites exposed to hygrothermal ageing conducted by Weitsman* [117].

2.5. MOISTURE AGEING OF FIBRE REINFORCED POLYMER COMPOSITES

2.5.1. Introduction to Ageing

Physical and Chemical Ageing

The growing demand for lightweight materials with favourable mechanical properties for industrial use has broadened the variety of applications for which composites materials are being considered. However, despite the industrial demand, uptake of polymer composites in industrial applications, which involve any kind of long-term environmental exposure has been rather slow, since their environmental durability may be questionable in some environments.

Such applications include aerospace and marine structures, transport vehicles, wind turbines and civil infrastructure, with the latter two being the primary focus of this study.

The process of change in properties of a material or structure as a function of time is loosely referred to as "ageing". Depending on the type of degradation mechanisms acting, ageing can be classified into two main categories: "physical" and "chemical". The rate and degree of degradation throughout ageing are uniquely defined by material type, environmental and mechanical loading, and its duration relative to the expected durability limit [118]. "Physical" ageing is referred to the exposure of materials or components to environmental agents which do not result in chemical changes in their structure and have reversible effects. It is associated with the free volume evolution and the change of properties relative to an equilibrium state. For instance, a common physical ageing agent in thermosetting resins is moisture-induced plasticisation caused by moisture diffusion into the polymer network. Moisture-induced plasticisation is known to cause measurable changes in the mechanical properties, as well as Tg reduction of polymeric materials, which nonetheless can be reversed [4,68,118].

The difference between "chemical" and "physical" ageing is primarily defined by the reversibility of the effect, i.e. the ability of an FRP to regain its properties after it has been exposed to a humid environment. Three of the most important chemical ageing mechanisms are thermo-oxidation, thermal and moisture-induced, and hydrolytic degradation. The latter two effects have been studied in more detail since hydrothermal ageing was a primary focus of this study. "Chemical", moisture-induced ageing is associated with irreversible degradation and changes in the polymer chain/network, mainly occurring through the mechanisms of hydrolysis, chain scission, or even cross-linking for incompletely cured polymeric materials [22,34].

Chemical ageing is more probable when degradation mechanisms, such as moisture and heat or moisture and mechanical loads act simultaneously. For instance, for a thermoset FRP exposed to a humid environment, a temperature increase will accelerate degradation and may cause chemical irreversible changes to the material. Similarly, the presence of mechanical loads and residual stresses in a polymeric material may increase the probability of bond rupture (molecule dissociation) and promote chain scission. Chemical ageing can change the properties of polymeric materials and therefore change their diffusion kinetics [3,118].

Accelerated Ageing

The performance and integrity of in-service materials or structures undergoing natural ageing – exposed to real-life ageing conditions – can be assessed by condition monitoring through

non-destructive testing (NDT) or by the physical examination of material components taken out of service. However, in-service monitoring can only provide information on the current state of components and not on the serviceable lifespan of the material or component. Therefore, a validation of the future performance and durability of the components or materials under study may be provided by the implementation of accelerated ageing and potentially accurate modelling [3,118].

The basic concept of accelerated ageing is to increase the degradation conditions, such as temperature or humidity, to a higher level than that experienced in real-life operating environments, accelerating the testing procedure and minimising testing times. The material that is subjected to accelerated ageing should therefore reach the same end-state, as that in the real-life operating environment in less time. Another common way to accelerate ageing is to reduce the thickness or size of the exposed specimen [3,118].

Accelerated ageing is often employed to assess the life expectancy of new materials used in long-term or critical applications, where the knowledge of their potential failure mechanisms still remains limited. The major limitation concerning accelerated ageing is that the increased degradation rates may alter the effect of the degradation agents, when compared to real-life operating conditions and weaken the validity of the prediction. Therefore, accelerated ageing results should be coupled with analytical methods to accurately predict future performance and durability. For instance, multiphysics approaches are usually employed to correlate physical ageing with the diffusion of moisture through polymeric materials and its effect on their mechanical performance [3,118]. Additionally, spectroscopic methods, such as FTIR are often employed for the coupling of gravimetric measurements, quantifying the moisture gain of polymer composites [13].

In general, material testing is associated with high costs, involving many material-related disciplines and a variety of laboratory equipment. It is apparent that although long-term, real-life testing can fully assess the durability and life expectancy of materials, accelerated laboratory-scale ageing can significantly lessen the time and costs required. The latter can be achieved by narrowing or screening the field of acceptable candidate materials that would go into long-term qualification tests and thus provide information on the remaining service life of existing structures. Furthermore, improved standards for product and material development are established by defining the performance and behaviour of materials under environmental degradation [118].

Ageing Degradation Mechanisms

The degradations mechanisms acting during environmental ageing mainly take place on the polymeric matrix of composites and the fibre-matrix interface (provided the fibre constituent is adequately tailored) [13,118]. Even though the polymer matrix offers many advantages to the FRP, such as easy processing, low cost and corrosion resistance, it can be a major cause of its failure [118]. The main degradation agents acting during environmental ageing include:

- Thermal-high/low temperatures and thermal cycling.
- Moisture-hydrothermal environments, high humidity, water immersion, moisture cycling (transition from wet to dry and inversely).
- Weathering-UV light exposure combined with rain and/or sand erosion.
- Chemicals-acidic and alkaline environments, solvents and oxygen.
- Irradiation-UV or high-energy radiation.
- Biological-micro-organisms.
- Mechanical degradation (cracking, delamination, voids, fibre fracture).
- Static fatigue/creep rupture [3].

These mechanisms can act either alone or in combination. Combined action can have severe effects on the performance of polymeric materials and may result in complex reactions and, irreversible degradation [3]. For instance, it was found that for a glass fibre polyester composite system, moisture-induced plasticisation and subsequent Tg depression were reversible phenomena only if the system was not exposed to thermal degradation and mechanical loads [61].

Background of Moisture and Hydrothermal Ageing

This literature study is focused on the effect of moisture – humidity and water – ageing in thermoset matrices and their composites. Thermosets and thermoset FRPs exposed to humid environments will generally experience weight gain over time as a result of moisture sorption. Moisture-induced degradation is a common cause of failure for most polymeric materials and can be present from the manufacturing stage of the material to its end of life. As previously discussed, moisture sorption can result in both reversible and irreversible changes in the properties and performance of polymers and FRPs [2]. The severity of the effect depends on the amount of moisture absorbed by the material, but even small amounts can have a negative effect on its performance [3]. It has been established that moisture uptake is often accelerated by combined degradation agents acting on the polymer or FRP, such as thermal degradation and external loading, which may lead to irreversible changes in the material structure and

performance [61]. Moisture penetrates the structure of polymeric materials following a diffusion-controlled process. In the case of FRPs, moisture uptake by capillary action is also common, particularly in regions of air entrapment such as voids, cracks and delaminated regions. Moreover, small amounts of moisture may be located in the fibre/matrix interface. In GFRPs/CFRPs the majority of moisture is usually attracted by the matrix constituent, with the fibres being the most hydrophobic constituent of the composite, provided they are tailored adequately. This imbalance in moisture sorption can lead to induced localised stress and strain fields in FRPs [1,2,13,18,118,123].

Moisture sorption takes place until equilibrium is reached. When Fickian diffusion is dominant, the moisture uptake rate and equilibrium level are directly proportional to relative humidity, whereas the time to equilibrium is a function of temperature. The term equilibrium can be explained as the maximum amount of moisture that a material can absorb, and when it is reached, the aged material can be considered saturated. Equilibrium can be either absolute or effective. Absolute equilibrium is achieved when the moisture content of a material has reached its maximum capacity and remains constant. On the other hand, effective equilibrium is reached when the material has reached its maximum, average moisture content, which is characterised by small changes over a specified period of time [119]. The moisture uptake period until equilibrium may be several weeks, months or even years [3]. However, significant quantities of moisture can be absorbed within shorter periods of time and still affect the properties of the material. The moisture content of a polymeric material is strongly dependent on the inherent properties of the material, the environment of exposure (i.e. relative humidity, water immersion, temperature) and the geometry of the specimen [124]. It is evident that thinner specimens of the same material tend to reach equilibrium in significantly shorter periods of time [3,118]. It can be concluded that moisture uptake rate is dependent on several factors, such as:

- Material type and geometry/polymer chemistry.
- Length of the ageing period.
- Temperature.
- Environmental and mechanical load [2,3,118].

Ageing Failure Modes in Thermoset Matrices and FRPs

One of the most common moisture-induced degradation forms in polymers and FRPs is plasticisation. Plasticisation is most often a reversible form of degradation. It is associated with an increase in the movement of polymer chains and may lead to softening and swelling of the

matrix, reductions in stiffness and $T_{g,}$ and decreased stress transferability between the fibre and the matrix [2–4,11,68,125]. Plasticisation and swelling are also known to increase the capillarity of moisture in FRPs [16]. The main degradation effects induced by swelling are the reduction of mechanical and tensile strength of the matrix, the generation of localised stress, cracking and crazing, as well as increased capillarity [18,68,117,126].

Moisture ingress in FRPs can also induce the effect of hydrolysis. Hydrolysis is a chemical decomposition process which mainly occurs at elevated temperatures. During hydrolysis, a water molecule ruptures one or more chemical bonds. Consequently, both the molecule and the bond(s) compound are separated and, a hydrogen and hydroxyl group are formed. As opposed to plasticisation, hydrolysis may cause permanent degradation, since it affects the bonds in the polymer matrix and the fibre/matrix interface [2–4,11,68,118]. In fact, hydrolysis can result in reduced stress transfer in the composite interface and affect all matrix dominated properties. These include T_g, off-axis tensile strength, compressive strength, and ILSS [4,127].

Hydrolysis is primarily associated with matrix decomposition – leaching [29,128]. Leaching involves the irreversible extraction of low molecular, organic additives of the matrix, such as fillers, catalysts, hardeners and pigments, to the ageing medium. The thermal decomposition of the matrix can be followed by its stiffening as well as reduced adhesion and (or) failure of the fibre/matrix interface [5,16,129]. Incompletely polymerised or void-containing and cracked matrices have been found to be particularly sensitive to leaching effects. Thus, it can be summarised that leaching through hydrolysis can lead to cyclic and long-term, irreversible degradation [2,3,6,22,128–130]. The rate of hydrolytic degradation and hence leaching are primarily governed by the temperature of the ageing environment (i.e. aqueous solution, humid environment, temperature), as well as the thermal properties of the polymer. Elevated temperature has been described as an accelerator of moisture-induced degradation. When the temperature of the exposure medium (i.e. water) is higher than the T_g of the material and hence the material is in the rubbery state, molecular mobility is increased enabling an easier passage of moisture through the polymer. On the other hand, when the temperature of the exposure medium is lower than the T_g of the material and the material is in the glassy state, molecules "freeze" and thus the diffusion rate is lower [3,16,118].

Generally, matrix degradation and interface debonding may result in an anomalous moisture uptake rate and an unclear equilibrium level, and in turn change the diffusion kinetics of the material. The rate of water absorption is likely to increase once polymer properties have been compromised and degradation has started to take place [18,36,118,131].

It has been observed that exposure to aqueous environments with a higher salinity content results in reduced absorption due to the ability of salt crystals to inhibit moisture diffusion [129]. However, high salinity aqueous mediums can still induce hydrolytic degradation and impair the properties of thermoset matrices, as well as fibre/matrix adhesion [129,132,133].

As previously discussed, thermosets are often unable to polymerise fully even at high cure temperatures. Elevated post-cure temperatures are employed to increase chain mobility and reactivity within the matrix. However, unreacted polymer sites and curing agent molecules may still be present in post-cured polymer matrices. These are called volatiles and are known as matrix plasticisers. Volatiles exhibit a hydrophilic profile and can be leached out during hydrothermal ageing [68]. Reactions between volatiles and permeated water create stresses both in the matrix and in the interface of FRPs. These stresses along with the chemical hydrolytic attack may generate swelling, osmotic effects and therefore cracking, crazing and blistering [18,68,117,126]. Hydrolytic and leaching effects on partly polymerised polymeric materials have been associated with secondary cross-linking. Secondary cross-linking can be classified as chemical ageing since it induces irreversible changes in the matrix network [33] [34]. Secondary cross-linking through ageing can be induced for polymeric materials that still possess unreacted polymer molecules. Physical and chemical ageing can act simultaneously. Moreover, synergistic chemical ageing effects of cross-linking and leaching have been previously observed by several workers. Leaching followed by matrix embrittlement and a subsequent Tg increase can be referred to as “anti-plasticisation”. These effects can significantly affect the final properties of the polymer [22,33,34].

According to Han and Drzal [134], two types of bound water have been identified in epoxy polymers. Type I was found to be responsible for an increase in polymer weight and a decrease in polymer Tg induced by plasticisation. Type II was associated with changes in mechanical properties. The authors attempted to carry out a thermomechanical assessment of glucose maleic acid ester vinyl resin (GMAEV) and epoxy resins cured at both low and high temperatures, by DMA and Thermogravimetric analysis (TGA). From comparisons of the bound water effects on the polymer cured under different conditions, it was concluded that the bound water in the polymer contributes to the changes of the thermomechanical properties differently depending on the cross-link structure. Polymers cured at low temperature exhibited higher evaporation of water content in the temperature regime of 100 - 200 °C. This indicated the existence of hydroxyl groups on the surface of the matrix, which were easily removed after heating the polymer above 100 °C. On the other hand, the matrix cured at the higher temperature contains higher concentrations of bound water that evaporates at temperatures

over 200 °C. This is an indication that water exists in the tight cross-links of the polymer network, which may result in micro-cracks and mechanical changes.

A similar observation was presented by Zhou and Lucas [135], who also identified two types of absorbed water. Type I possesses a lower activation energy than type II, forms a single hydrogen bond with the polymer and acts as a plasticiser. Type I water can be desorbed more easily than type II. Type II water forms multiple hydrogen bonds with the matrix network. As opposed to type I, type II does not act as a plasticiser, but it forms bridges within structural networks of the resin, forming secondary cross-linking. The amount of type II water taken up by the polymer is dependent on the hydrothermal conditions and exposure duration.

According to Zhou and Lucas [136], the Tg of a hydrothermally aged epoxy system can be re-gained, even when residual water remains in the polymer network upon drying. Additionally, it was observed that the greatest Tg depression was apparent when the polymer first reached saturation. A greater depression in Tg was associated with type I water than with type II. This is due to secondary cross-linking in the polymer induced by type II water. It was observed that the Tg of epoxies was not dependent solely on the water content, but it was also influenced by the hydrothermal history of the polymer. Moreover, for a given epoxy system, a longer exposure time and higher exposure temperature may result in higher Tg values. The effect of type I and type II water on the Tg of epoxy varies; Type I acts as a plasticiser and causes Tg reduction. On the other hand, type II lessens this Tg reduction by causing secondary cross-linking. Tg values obtained experimentally are a result of the combined action of both type I and type II water.

According to Zafar et al [137], re-drying an epoxy polymer at 190 °C helped to re-gain its properties. Furthermore, the same TGA onset (temperature of decomposition) was observed at around 320 °C for samples immersed in DI and seawater for a different duration, which indicates heat stability and therefore reversibility. Zafar et al also observed that water acts as a plasticiser and when trapped within the polymer network can induce chemical changes (chain scission). However, a competing mechanism of post-curing happened during the heating cycle for re-drying the sample, which recovered the properties of the conditioned material.

Freeze and Freeze-thaw & Moisture Ageing

The response of FRPs conditioned under the synergistic action of moisture and freeze-thaw temperatures remains under investigation and the research around the matter is yet limited. However, there is a clear understanding of the effect of low-temperature thermal cycling. At low temperatures, the matrix undergoes shrinkage and thermal contraction is present at the

fibre/matrix interface causing an increase in residual stresses. These tend to increase further as the temperature decreases. Residual stresses may subsequently result in micro-crack formation and debonding of the fibre/matrix interface. The resulting effects are reflected on the macroscopic performance of the laminate in the form of reductions in stiffness, strength, dimensional stability and fatigue resistance. At low temperatures, the moisture that may have been absorbed by the laminate through capillary effects and subsequently stored in areas of air entrapment or voids might start turning into ice. Generally, as opposed to room or elevated temperature hydrothermal ageing in FRPs, which promote matrix swelling and compromised mechanical properties, freeze-thaw cycles are associated with the formation of ice particles, which can result in augmented localised stresses and can lead to matrix embrittlement, cracking and even fracture [3].

Karbhari et al [23] studied the response of ambient cure E-glass/vinyl ester composites after short-term exposure to freeze (-10 °C) and freeze-thaw (-10 to 22.5 °C) conditions, both with and without immersion in water. At low temperatures, the authors observed matrix stiffening followed by a minor increase in tensile strength and stiffness of the composite. Nevertheless, freeze-thaw ageing compromised the overall performance of the composite. The introduction of water as an ageing agent to the freeze-thaw environment resulted in pronounced degradation of the composite in the forms of matrix hydrolysis and fibre/matrix debonding.

2.5.2. Ageing of Vinyl Ester Matrices and Vinyl Ester-based Composites

During their service-life vinyl ester composites are exposed to a variety of hydrothermal conditions and therefore it is essential to have a strong understanding of their response in such environments. However, the number of studies on the environmental exposure of vinyl esters and VE-based composites is limited and thus the knowledge about their durability and life expectancy is deficient [6,22,23]. A thorough review of the literature follows in chronological order of publication. Diffusivity coefficients for vinyl ester matrix immersed in water at different temperatures that were available in this literature study are presented in *Table 2-2* below.

Water Immersion Temperature (°C)	Diffusivity x 10^{-6} (mm^2/s)	Reference
RT	0.69*	[36]
RT	0.78	[138]
RT	0.625	[22]
40 °C	2.19	[39]
40 °C	2.84	[138]
40 °C	1	[22]
60 °C	0.85	[34]
60 °C	0.19*	[36]
60 °C	0.97	[32]
60 °C	8.7	[138]
60 °C	1.5	[22]
80 °C	15.6	[39]
80 °C	2.4	[22]

*thickness = 0.23 – 0.26 mm

Table 2-2: *Vinyl ester diffusivities at different immersion temperatures*.

Ghorbel and Valentin [34] reported on the hydrothermal effects on the physicochemical properties of neat vinyl ester and polyester matrices, as well as vinyl ester-based and polyester-based FRPs. Both neat matrices followed Fickian diffusion after ageing in water at 60 °C, while the diffusion of both FRPs can be described by the Langmuir model. In disagreement with previously recorded literature results, the vinyl ester and VE-based FRP had higher moisture gains than the polyester and polyester-based FRP. This was attributed to incomplete curing of the vinyl ester, as opposed to polyester, validated by studying the DSC exothermic reaction. Plasticisation effects were present, which induced secondary cross-linking for the neat vinyl ester matrix manifested by the decrease of the exothermic reaction in DSC, without, however, Tg being affected. The polyester-based FRP experienced a Tg reduction during ageing, attributed to synergistic hydrolysis and plasticisation. Degradation was also apparent for the vinyl ester-based FRP in the forms of leaching, cracking and debonding at the interface. Secondary cross-linking was observed for the VE-based FRP upon long-term ageing, marked by a Tg increase, and after the Tg was initially reduced. The effect was attributed to

plasticisation, hydrolysis and post-curing acting in combination, confirmed by DMA results. Moisture-induced degradation in the FRPs resulted in higher sorption than in neat matrices.

Karbhari et al [139] investigated the flexural and impact properties of E-glass fibre/vinyl ester in cold regions. The authors highlighted the suitability of vinyl ester matrices for use in marine and cold-region applications due to their exceptional chemical properties, resistance to osmotic blistering and high impact resistance. It was observed that the substitution of the reinforcement from continuous strand mat to woven layer could potentially increase the damage resistance of the composite. However, this was only the case when the woven surface was placed on top and towards the impact point. Water-induced plasticisation was reported through the formation of hydrogen bonds. These generated bridging within the preform architecture damaged by impact resulting in increased strength in certain occasions. It was actually found that under certain conditions VE-based RTM composites improve in impact strength and flexural strength at temperatures of -18 °C more than those at room temperature. Frozen water followed by freezing resulted in the highest moisture absorption, three times higher than room temperature water absorption. Freezing water and room temperature water immersion resulted in cracking which facilitated further moisture absorption.

Buck et al [140] investigated the durability of E-glass/vinyl ester composites subjected to environmental conditioning and sustained loading. Durability was assessed by means of Ultimate Tensile Strength (UTS). Water immersion was conducted between room temperature and 66 °C. Sustained loading during ageing gave rise to degradation, resulting in lower UTS and strain-to-failure values. Synergistic ageing and loading effects notably decreased UTS, even upon short-term exposure. Degradation effects were amplified at higher temperatures. More specifically, in the temperature range of 38 – 49 °C, the UTS of conditioned samples decreased abruptly. At 66°C, degradation was amplified regardless of loading. Moreover, morphology changes became evident during ageing. Namely, water ageing resulted in the removal of the vacuum side resin layer and left fibres exposed to the ageing medium. Samples aged at room temperature had a similar appearance independent of loading, while greater morphology changes were induced with an increase in temperature and ageing time. Creep effects and sample elongation were observed, which increased with loading and exposure temperature. Matrix cracking and fibre pitting effects were identified which resulted in debonding at the interface and delaminations.

Chin et al [36] conducted a characterisation of the sorption and transport of distilled water, salt solution, and a simulated concrete pore solution (23 °C and 60 °C) in free films of vinyl ester, isophthalic polyester (isopolyester) and epoxy resins. It was observed that all matrices

followed Fickian diffusion at all ageing conditions. Uptake was found to be rapid in the first 10 h of ageing but decayed between 10 h and 100 h, after which equilibrium was attained. Epoxy proved to be the most hydrophilic matrix of the three. The authors attributed this to the high polarity of epoxies as opposed to vinyl esters and isopolyesters. As expected, the increase in temperature resulted in higher moisture uptake levels and moisture uptake rates. Equilibrium levels did not show correlation with the polymer polarity measured by contact angle measurements. This was attributed to the fact that the obtained polarity values were related to the surface and near-surface of the films, and not the bulk polymer. Moreover, the authors noted that microstructures and cross-link density may have influenced uptake kinetics. Surprisingly, isopolyester films aged in salt and pore solution exhibited lower uptake levels at elevated temperatures and weight loss through leaching upon equilibrium. It is noteworthy that there was no indication of hydrolytic behaviour in vinyl ester matrices, even at elevated temperature ageing.

Boinard et al [18] reported on the influence of resin chemistry on water uptake and environmental ageing effects on GFRP polyester and vinyl ester laminates. A DMA characterisation including re-scanning runs of the polyester and vinyl ester laminates revealed incomplete curing. Anomalies in the moisture sorption were observed for both laminates and neither of them followed Fickian behaviour. For the polyester laminate, an increase in the temperature of the water medium resulted in amplified degradation. Higher degradation rates were also apparent for water ageing followed by ageing in air. Leaching in water was observed, subsequently followed by anti-plasticisation and stiffening of the material. DMA revealed weakening of the interface, either due to debonding or fibre sizing loss. For vinyl ester laminates, unreacted monomer sites plasticised the polymer, through anti-plasticisation effects revealed by DMA. Unreacted monomer was leached out during water ageing creating gaps within the FRP network, which allowed excess moisture ingress. However, the ageing effect was found to be reversible, as validated after drying the samples. It can be concluded that the vinyl ester laminate exhibited a less hydrophilic nature and was more resilient to moisture-induced degradation that the polyester laminate.

McBagonluri [141] carried out a characterisation of fatigue and combined ageing environments on the durability of glass/vinyl ester composites. Cyclic and non-cyclic ageing environments of fresh-water and saltwater from room temperature to 65 °C were employed. Regarding quasi-static laminate performance following moisture ageing and cycling, no major differences between water and salt water were seen. Namely, in saltwater, reductions of 11 % and 32 % and an increase of 6 % were evident for the quasi-static modulus, UTS and Poisson's

ratio, respectively. Similar values were obtained for fresh-water ageing, except for the Poisson's ratio, which remained unchanged from that of the dry specimen. Cyclic moisture results showed that although quasi-static material properties were notably reduced after the first cycle, no further reductions were observed from the additional cycles. However, the addition of ageing cycles introduced irreversible ageing affecting the matrix and the interface. A partial recovery in strength values was only apparent upon re-drying specimens after the first cycle and complete irreversibility was introduced upon the addition of extra cycles. SEM indicated that fresh-water ageing promoted cracking around the interface. Fatigue tests indicated that failure occurred due to degradation of the load-bearing fibres and was independent of the ageing environment, test parameters (i.e. frequency) and, the matrix and interface nature, in the short term. However, long-term ageing induced matrix toughening and plasticisation, which affected the fatigue performance of the material.

Karbhari and Zhang [6] reported on the behaviour of E-glass/vinyl ester composites in various lay-up designations, in aqueous environments. Specimens were aged by full immersion in deionized water at 23 °C and 60 °C. As expected, the increase in temperature increased the water uptake rate and the equilibrium level. Moisture-induced degradation was evident in the forms of micro-cracking, discolouration and visual changes, volume micro-cracking and transverse crack formation generated by micro-crack coalescence, interfacial debonding and morphology changes. All aforementioned effects increased the rate of uptake further. Absorption was highest for the triaxially reinforced specimens and lowest for uniaxial specimens. Nonetheless, all lay-up orientations exhibited a two-stage diffusion. This was attributed either to changes in the viscoelastic response marked by a change in boundary conditions or the following combined effects; relaxation of elastic forces induced by the cross-linked network after the initial weight-gain plateau and, degradation at the interface and (or) fibres, enabling wicking, resulting in further moisture gain. At 60 °C, tensile strength and ILSS decreased notably with ageing time. Fibre pitting through fibre decomposition (loss of K_2O and Na_2O) was noted. This was detected through optical microscopy through the composite structure and was validated by FTIR on leached components. Fibre degradation was attributed to interfacial debonding and cracking. At 23 °C, secondary cross-linking in the matrix was observed after long-term immersion and although tensile strength was initially reduced, it then followed a notable increase reaching higher values than those of the un-aged composites. Variations in tensile strength values were apparent after ageing at all conditions. Finally, a Tg increase was observed upon short-term ageing but reductions were observed after the full ageing period of 52 weeks.

Fraga et al [39] studied the effects of water absorption on unsaturated isophthalic polyester and vinyl ester matrices and their composites reinforced with glass fibres. The viscoelastic response of the materials was assessed by DMA after re-drying the specimens. Interfacial adhesion was studied by SBS tests and SEM. DMA results of the dry vinyl ester matrix and composite showed a double peak in the tan δ, which was attributed to thermal instability by the authors. However, as discussed in section *2.2.2.* this may be an indication of the diphasic nature of the resin.

At 40 °C, Fickian behaviour was displayed by the vinyl ester matrix, with most water being absorbed during the first 140 h of immersion. No equilibrium was reached for the polyester samples, which showed a continuously increasing weight gain pattern and a significantly higher moisture gain. The effect was attributed to their high void content and the high polar-hydrogen donors in the hydrogen bonding-carboxylic chain of polyester samples making them more hydrophilic. The void content of both matrices increased with ageing, although polyester was more susceptible to the effect. Moreover, the polyester matrix exhibited a notably lower Tg (78 °C) than vinyl ester (110 °C) contributing further to the hydrophilicity of the former. The weight gain of the polyester matrix was also higher than the vinyl ester at 80 °C ; nonetheless, after a maximum weight gain had been reached for the former matrix, an abrupt decrease to negative values followed. The effect was attributed to leaching of unreacted monomers or oligomers – no extraction of actual reacted polymer occurred. When a higher styrene content was introduced to the polyester matrix, its hydrophobicity increased. The lesser the styrene concentration was in the resin, the easier the extraction of residual unreacted components was [39].

The composites treated at 40 °C featured similar weight change trends to the neat matrices; nevertheless, both composites attained similar saturation levels to each other. The water uptake of the polyester composite was higher than expected, due to interfacial degradation and cracking of the matrix. At 80 °C, a weight gain maximum was attained by both composites, which was then followed by abrupt weight decreases, eventually dropping to negative values. This effect was greater for the vinyl ester composite. The authors attributed the effect to a combination of hydrolytic degradation of the matrix and the silane-coupling agent on the fibre. The latter is known to be activated upon immersion in water between 50 °C and 100 °C. Poor interfacial adhesion was identified by SEM even in un-aged specimens, attributed to the non-compatibility of sizing. At 40 °C, the matrix of the polyester composites exhibited a brittle nature, whereas swelling was induced at 80 °C resulting in a primarily ductile matrix. The matrix of the vinyl ester composites was found to be brittle at both ageing temperatures.

Although ILSS values were found to be higher for the vinyl ester composite, the fractional strength retention upon ageing was similar for both composites [39].

Secondary-cross-linking through anti-plasticisation was observed for both matrices, manifested by increases in Tg and cross-link density (decrease in tan δ). Similar behaviour was exhibited by the composites. Although, not a clear Tg increase is shown for the vinyl ester laminate the two tan δ peaks shown for the dry specimen were integrated into one main peak upon ageing, indicative of anti-plasticisation [39].

Hammami and Al-Ghuilani [44] examined the durability of glass fibre/vinyl ester composites in seawater and corrosive fluids in, hot, humid or dry conditions for 3 and 6 months. A high fibre content resulted in poor wetting and therefore reduced interface adhesion, while it also promoted micro-crack formation and layer delamination. Such failure mechanisms can accelerate water diffusion through the composite structure and thus degradation. For seawater ageing, a decrease in flexural modulus of 18.5 % was recorded between 3 and 6 months of ageing. An initial linear water uptake trend of 1 – 1.5 % gain was observed between 25 and 100 days, respectively, followed by a secondary plateau of approximately 2.5 % gain after approximately 185 days. Matrix leaching was reported, which resulted in reduced interface adhesion leaving fibres without protection. Moreover, water ingress resulted in volumetric expansion and in turn in the formation of micro-cracks. Similar observations but with increased degradation effects were recorded in hot (exceeding 50 °C) and humid environments. A hot and dry climate up to 60 °C and after 6 months of exposure resulted in secondary cross-linking and an increase in flexural modulus. An increase in corrosive fluid concentration and (or) ageing time resulted in increased degradation for the FRP. Degradation was observed in the form of corrosive behaviour, including hydrolytic and oxidative corrosion as well as pit formation and blistering. Decreased ILSS values, attributed to the presence of micro-cracks, were found for laminates exposed to both humid and acid-rich environments. On the other hand, an increase in ILSS values was observed for hot and dry environments.

Karbhari and Wang [33] conducted a multi-frequency dynamic mechanical thermal analysis of moisture uptake in E-glass/vinyl ester composites laminates. Residual cure of the laminates was accelerated by the presence of moisture. More specifically, ambient exposure of FRPs led to notable a Tg increase after 6 months. During that period, a Tg increase was observed for ageing in DI water and pH 4 buffer solutions. On the contrary, Tg decreased for pH 7 buffer and 24 h ‘wet–dry’ cycling conditions, while fluctuations in Tg were seen for pH 10 buffer solution immersion. When trying to understand all aforementioned Tg changes, the competing effects of secondary cross-linking and environmental attack were considered. Water-induced

degradation was present in the forms of leaching and anti-plasticisation. Moreover, the authors reported that DMA testing of the FRP in the longitudinal direction produced higher Tg values than testing in the transverse direction. Lastly, an increase in the DMA test frequency resulted in an increase in the output Tg value without influencing the format of the thermal curve.

Chu and Karbhari [22] studied the effect of water sorption on the performance of pultruded E-glass fibre/vinyl ester composites. Composites were aged by full immersion in DI water at 23, 40, 60, and 80 °C. Aged specimens followed Fickian behaviour at all conditions and, the uptake rate and weight gain increased with temperature. At high-temperature ageing, wicking along the interface and micro-cracks of the composites, and thus moisture storage were observed, increasing the total gain to values higher than the theoretical values. This was due to the activation of damage at the interface and bulk resin level. A change in the colour of specimens was also featured, indicative of hydrolysis. Short-term ageing of 5 weeks led to a small, initial decrease in Tg. Upon this initial decrease and after 10 – 15 weeks a Tg increase was noted along with a decrease in storage modulus. The storage modulus decrease was attributed to hydrolysis, which was confirmed by a preliminary FTIR analysis. Higher ageing temperatures resulted in an overall lower decline in glass transition temperatures. This was attributed to leaching effects which led to matrix embrittlement, followed by chain scission. Nevertheless, the effect was not apparent upon low-temperature ageing. At 80 °C, fibre pitting, cracking and weakening of the interface were confirmed. In the first 5 – 10 weeks of ageing, most of the loss of tensile strength was recovered upon re-drying the laminate. The reduction was attributed to plasticisation effects, which as previously discussed, are mostly reversible. At 23 °C exposure, ILSS loss was found to be linear with ageing time. At 40 °C, a stepped reduction was observed – mostly irreversible damage - attributed to failure at the interface in the forms of debonding and osmotic cracking. At higher temperatures, leaching, debonding, micro-crack coalescence to form transverse cracks, and therefore higher moisture uptake and increased degradation were observed. The levels of ILSS and tensile strength retention decreased with ageing time and conditioning temperature.

Yu et al [142] reported on the hydrothermal ageing of pultruded carbon fibre/vinyl ester resin composites. Specimens were exposed to distilled water and brine (3% NaCl) at a temperature range of 65 – 95 °C. Fickian diffusion plateaus were observed at all conditions with increased uptake rates observed as a function of temperature. Although the interface was more resilient during absorption due to the hydrophobicity of the reinforcement, water-induced plasticisation of the matrix after long-term ageing was reported resulting in two distinctive Tgs. The authors reported that long-term moisture ageing induced secondary cross-linking and a subsequent rise

in Tg. However, the effects of dual Tg appearance and cross-linking were reversible upon re-drying of the specimens. SEM imaging showed debonding at the interface after long-term exposure which in turn contributed to reduced flexural strength and ILSS. Lastly, no major difference was observed between the distilled and salt solutions.

Sobrinho et al [29] reported on the effects of water absorption on a neat epoxy-based vinyl ester. Fickian-like behaviour was observed in the first stages of sorption followed by small but abrupt weight increases. Thereafter, a subsequent weight drop was reported, whereby leaching dominated sorption. After 16 days of ageing in water at 60 °C, discolouration and voids were identified in the samples, which were amplified with ageing time. Mechanical testing and thermal analysis showed matrix embrittlement through secondary cross-linking of the matrix in the hydrothermal medium. Long-term ageing resulted in decreased Tg and Young's modulus and an increase in strain and fracture toughness, after the latter two properties had undergone an initial decrease upon short-term ageing. It is noteworthy that samples used for this ageing study were only cured at room temperature but were compared to un-aged samples post-cured at 120 °C. As previously discussed, the post-cure step is highly important for the performance of vinyl esters, while incompletely cured vinyl esters are more susceptible to hydrolytic degradation [25,44].

Narasimha Murthy et al [123] investigated the seawater durability of glass fibre/epoxy, glass fibre/vinyl ester, carbon fibre/epoxy and carbon fibre/vinyl ester composites. All aged composites exhibited a Fickian-like weight gain pattern. Seawater resulted in expansion and shrinkage and in turn fibre/matrix debonding, cracking and voids, which functioned as water storage regions and increased total moisture gain. Overall, VE-based composites were found to be less hydrophilic than epoxy-based composites, achieving lower weight gains. As a result, VE-based composites featured greater flexural strength, ILSS, and tensile strength retention than epoxy-based specimens. All aforementioned mechanical properties underwent notable degradation during water uptake prior to equilibrium. The lowest maximum was observed upon moisture equilibrium, while stability was reported beyond that point.

Visco et al [32] presented a comparative study on the effects of hydrothermal seawater ageing at 60 °C on an isopolyester and a vinyl ester matrix. Vinyl ester was found to be more hydrophobic and less susceptible to seawater degradation than the isopolyester. Thus, the vinyl ester matrix retained better mechanical and physical behaviour than the isopolyester. Fickian trends were observed for both matrices. A change of specimen colour was detected upon long-term ageing indicative of hydrolysis, along with secondary cross-linking which is in line with the observations of Chu and Karbhari [22]. Progression of ageing-induced void formation and

thus further degradation of the isopolyester was reported. In vinyl ester, degradation was primarily present on the outer surface of the resin; detached surface layers by hydrolytic attack were apparent. This observation was in accordance with the findings of Buck et al [140], who detected the removal of the outer resin layer of vinyl ester-based GFRPs upon hydrothermal ageing. Visco et al highlighted that the structural features of the matrix need to be considered for its potential use as a laminate constituent. These can dictate the stability of polyester and vinyl laminates in seawater, especially when taking into account the different chemical reactivity of the ester groups of the two resins. In line with the observations of Ghorbel and Valentin [34], it was found that the moisture uptake kinetics of the matrices were strongly dependent on their degree of cure. The authors identified the margin for improvement in the field for the establishment of a clearer relationship between the moisture uptake and degree of cure of matrix polymers and in turn their composites.

Eslami et al [133] reported on the effects of moisture absorption on the degradation of E-glass fibre/vinyl ester composite pipes and modelling of transient moisture diffusion using finite element analysis (FEA). Fickian behaviour was attained by all aged specimens at all conditions. Composites aged in seawater reached equilibrium faster but exhibited lower diffusivity and moisture gain levels than composites aged in water. In buckling tests conducted, the failure force and displacement were reduced with an increase in temperature of water and when the exposure medium changed from seawater to water. Moreover, SEM confirmed weakening at the interface with an increase in ageing temperature. Finally, the authors reported that Abaqus could successfully predict moisture diffusion rates and equilibrium values for the aged specimens.

Fragassa [143] found a diffusion coefficient of 6.25×10^{-8} mm^2/s for a neat vinyl ester matrix aged in seawater at 15 °C. Even though the moisture uptake plateau was not distinctly Fickian and the saturation level was unclear, Fickian behaviour was assumed and an equilibrium level was approximated.

Sarlin et al [126] conducted an ageing comparison of glass fibre/vinyl ester laminates made of bisphenol-A-based and novolac-based vinyl ester matrices. The final composite was in the form of a pipe. Water immersion was found to induce higher levels of degradation, in the forms of leaching and weakening of the interface, than those promoted by the corrosive solution. Novolac-based laminates noted a higher weight gain, which nonetheless was unexpected since novolac-based vinyl esters are known to be more hydrophobic than bisphenol-A-based vinyl esters. Water immersion resulted in the greatest weight gain of all ageing mediums. The second largest weight gain was obtained in a 5 % H_2SO_4 medium, while

the lowest weight gain was noted in the environmental chamber (70 °C, 95 % RH). Subsequently, the greatest tensile strength reduction of up to 65 % was observed in the water medium and the lowest tensile strength reduction of 10 – 25 % after 12 months was shown in the environmental chamber. Although one of the novolac-based FRPs noted the highest weight gain in all ageing mediums, this was not correlated with the tensile strength loss of the laminate, which achieved the highest tensile strength retention, long-term. The highest tensile strength reduction was featured by one of the bisphenol-A-based FRPs. Moreover, the authors confirmed that a reduction in tensile strength is not necessarily translated into changes in FRP stiffness; for instance, one of the bisphenol-A-based FRPs underwent the highest tensile strength reduction, but its stiffness remained unaffected. The highest resistance to plastic deformation was achieved by one of the novolac-based FRPs, which possessed the most brittle base resin.

Yin et al [138] reported on the uptake, hydrothermal expansion, and thermomechanical properties of a vinyl ester matrix intended for FRP applications when immersed in water or an alkaline solution. As expected, in water immersion, the total moisture gain was increased with an increase in the temperature of the ageing medium. However, the inverse effect was observed in the alkaline solution but the decrease was considered minor. According to the authors, weight change levels were affected by water-induced relaxation and leaching. For water immersion, matrix relaxation was the dominant effect over leaching resulting in an increase in weight gain. In both ageing mediums, diffusivity values increased with an increase in ageing temperature. The alkaline medium induced higher hydrolytic rates than water, resulting in higher mass loss, due to catalysing effect of the solution. Tg reductions were observed in both ageing mediums. These were attributed to plasticisation effects reflected in the tan δ curves, which appeared to become broader upon ageing. The effect was therefore primarily reversible and leaching was considered to occur only on the specimen surface. Lastly, an increase in tensile strength and elongation at break was observed after 6 months of ageing.

2.5.3. Ageing of Glass Fibres

The glass fibre surface yields a change in the structure of the polymer when used as a reinforcement, when compared to an un-reinforced polymer. The addition of glass fibres to a polymer can produce a fibre/matrix interface of a high cross-link density and as a result yield less free volume to be occupied by water molecules during sorption [144]. As previously discussed, fluid presence in FRP structures may promote residual stresses, which in turn can affect mechanical fields by enhancing the creep and relaxation processes. Besides, probable hydrolysis of the interface can introduce osmotic pressure and weakening of the fibre/matrix

bonding, and subsequent degradation of glass fibres. Degradation in glass fibres can be in the form of chemical decomposition and corrosion-induced defects [117,145]. Although, the majority of fluid attack is concentrated on the matrix constituent and the fibre/matrix interface affecting shear-driven properties, degradation of glass fibres is associated with reductions in FRP tensile resistance. The compromise of tensile properties may be completely or partially irreversible. In the case of FRPs, observations suggest the development of regularly spaced ring-shaped cracks encircling the glass fibre, upon water exposure. The formation of such cracks has been attributed to the swelling of the matrix and the swelling of reactive components [117].

Glass fibres exhibit a hydrophilic nature and can corrode and degrade significantly when exposed to humid conditions. Once glass fibres have been exposed to moisture, hydrolysis begins to take place and ions are removed from the surface into the exposure medium, resulting in deterioration of the fibre surface. Hydrolysis reduces the mechanical strength of the fibre, with the effect being amplified to the bulk FRPs performance [12]. Exposure to humid air can weaken the load-bearing capacity of the fibres and consequently increase the strength variability across the fibres, and reduce their strength. For instance, the tensile strength of freshly drawn glass fibres is typically 2.5 GPa. Exposure to atmospheric moisture can result in a reduction in tensile strength of up to 40 % [3]. The reduction level in tensile strength and generally the severity of the effect of moist environments on glass fibres depends on conditioning times, temperature and humidity content [3,146]. The degradation of the glass fibres in moist environments is almost immediate after exposure, even in a standard laboratory environment. More specifically, the tensile strength of the fibres is reduced by around 15 % after a 3-week exposure in a standard laboratory environment and 20 % in water at room temperature for the same period. If the fibre is not handled carefully when it is initially drawn, then its properties may be significantly compromised [3,146].

Although only a few studies have been conducted on the diffusion kinetics of water on glass fibre, information has been recorded on the dissolutive behaviour of E-glass fibre under water. The dissolution of E-Glass fibres in water is mainly attributed to the leaching of alkali oxides, such as sodium and potassium oxide from the surface of the fibre. Once leaching starts taking place, the water becomes an alkali solution which further promotes the dissolution of the fibres. As a result, permanent strength loss of the fibres can take place [3].

The hydrothermal resistance of glass fibre is of utmost importance for the overall performance of the composite. Hydrothermal protection, fibre strength and the need for a high stress transfer capability across the fibre-matrix interface are the primary reasons that have led glass fibres

manufacturers in the development of fibre sizings. Fibre sizings can be referred to as protective surface coatings used in glass fibre manufacturing. Reports suggest that un-sized fibres tend to lose their strength rapidly when conditioned in hydrothermal environments. Thomason [12] suggested that silane sizings can increase the hydrophobicity of glass fibres. Maxwell and Broughton [3] have reported that the aqueous resistance of glass fibres can be enhanced by increasing their alkaline content.

2.5.4. Micro-mechanical Characterisation of the Interface of Hydrothermally Aged Micro-composites

Zinck and Gérard [102] attempted to assess the thermo-hydrolytic resistance of glass fibre/polyepoxide interfaces through the microbond test. Neat matrix thin film models were used for the estimation and evaluation of the moisture uptake gain and behaviour of microbond droplets, respectively. It was observed that differences in the stoichiometric ratio of the bulk and thin film matrix resulted in different moisture uptake behaviour and the form of moisture-induced degradation that took place. Therefore, the microbond test approach was deemed insufficient to provide information on the composite interface region at a macroscopic level. Moreover, the Tg of films was found to be around 50 °C less than that of the bulk matrix. Hence, one can understand the reason behind the severity of the ageing effect on the microscale. The performance of the polymer is strongly dependent on the difference between the temperature of the ageing medium and the Tg, with the effect being more drastic on microscopic specimens. Accordingly, Tg reduction in microscopic specimens can have a more severe impact than in bulk specimens. In this case, the ageing of thin films for 24 h at 60 °C and 98 % RH was followed by a Tg decrease to a level below the ageing temperature, resulting in the film specimens to be in their rubbery state. Nonetheless, this was not the case for bulk specimens, which remained in their glassy state.

Pandey et al [4] reported on the ageing effect on micro-mechanical properties of fluorinated and non-fluorinated epoxy-based single fibre micro-composites through the microbond test, before and after boiling water degradation. A notable number of experiments were reported in unwanted failure modes, such as tensile failure, cohesive failure of microbond droplets, or handling failures. The IFSS of fluorinated micro-composites was found to be higher than that of the non-fluorinated counterpart. However, the non-fluorinated micro-composites were found to be more resilient to boiling water degradation, measured after the ageing period of 48 h. Namely, the IFSS of fluorinated micro-composites was reduced by 43 %, whereas the IFSS of the non-fluorinated counterpart experienced an IFSS loss of 9 %. By carrying out a

post debonding friction analysis, the authors observed an increase in IFSS with a reduction in the embedded length of micro-composites.

Biro et al [109] studied the hydrothermal effect on the micro-mechanical properties of unsized carbon fibre/epoxy micro-composites, assessed by the microbond test. After DI water ageing, micro-composite samples were re-dried under vacuum prior to testing. IFSS reductions up to 19 % and 41 % were observed after 2 and 6 h of ageing, respectively. Decreases in IFSS were not solely attributed to the surface chemistry of the interface; friction-related mechanical interactions, stress-induced relaxation effects, moisture storage between interfacial bonds, initiating degradation and resulting plasticisation effects were considered too.

Bian et al [61] investigated the effect of water uptake on the micro-mechanical performance of an E-glass fibre/nylon system, and in particular the role of glass fibre sizing in the protection of the micro-composite from aqueous attack, assessed by the fragmentation test. Ageing took place by immersion in room temperature water. Glass fibre sizing was indeed proven to be crucial for the IFSS retention of the system upon ageing. In fact, no IFSS loss was noted when a sized carbon fibre was used, whereas ageing of the system using bare E-glass fibre resulted in a 25 % IFSS reduction. IFSS values were recorded upon re-drying the test samples.

Schultheisz et al [59] investigated the effect of moisture on the interfacial properties of an E-glass fibre/epoxy system by the use of the fragmentation test. Samples were conditioned at 25 °C and 75 °C by full immersion. One of the main objectives of the study was to provide information on the durability of the fibre and interface constituents of the bulk composite by obtaining direct micro-mechanical information through the fragmentation test. Simple mathematical models were used, such as the Weibull criterion. Obtained results were encouraging in acquiring qualitatively data in fibre strength for the prediction of fibre-dominated failures. In addition, accurate trends were generated, regarding quantitative prediction of strength. However, the models used for the prediction of composite strength over-predicted fibre degradation; glass fibres in single fibre fragmentation tests were affected by stress corrosion induced by matrix swelling. Regarding transferability of interfacial properties between the microscale and macroscale, fragmentation tests provided a clearer image, which was however somewhat obfuscated by fibre bridging in the bulk composite testing hindering a direct measurement of interfacial properties. More complex mathematical models could be used to provide a more accurate image of property transferability between testing in the two scales. As previously discussed, the fragmentation test features several significant drawbacks including data discrepancies upon the use of the Weibull criterion, and

the assumption made in obtaining IFSS through critical fibre length measurements [57,65,66,139].

Gautier et al [147] conducted an interface damage study of hydrothermally aged glass-fibre-reinforced polyester composites. Although the largest volume of experiments was carried out on bulk composites, the microbond test was used to provide direct information on interfacial adhesion upon ageing in water at 30 °C. The IFSS was reduced to an extent of 50 %. Re-gaining of IFSS was observed upon re-drying the specimens after 1 h of ageing, attributed to plasticisation effects, whereas irreversible degradation was recorded after 4 h of immersion. The same result was documented after depositing a water droplet on top of the resin droplet under test, in its dry state. Although micro-mechanical testing was a local approach and was incapable of providing direct information on the bulk composite interface, it was useful to monitor interfacial damage evolution and provided the knowledge that moisture-induced interfacial damage can be both reversible and irreversible and must therefore be taken into consideration.

Yu et al [148] found that for carbon fibre/epoxy assessed by the microbond test, the use of sizing increased IFSS retention in freshwater and marine environments notably. Laurikainen [68] highlighted that single fibre micro-composite ageing in water can compromise fibre sizing properties and therefore alter the interface. The use of accurate sizing can increase adhesion retention in hydrothermal environments, although matrix incompatible sizing can still provide relatively high IFSS but can undergo significant adhesion loss upon ageing [59,68] Furthermore, it has been observed that the application of a resin particle coating on carbon fibre can increase adhesion and resilience to moisture. The latter result was produced for a maleic anhydride grafted polypropylene (MAPP) system on carbon fibre assessed by the microbond test. However, the resin used for fibre coating was not specified [149].

Bénéthuilière et al [45] conducted an ageing study (95 % RH & 70 ˚C) of a conventional styrene-based and a styrene-free vinyl ester resin, assessed by the microbond test. The IFSS of the dry styrene-based vinyl ester was approximately 40 MPa. An IFSS loss of 22 % was present for the styrene-based matrix, while no IFSS loss was apparent for the styrene-free matrix. The authors attributed the effect to hydrolysis through bond rupture of polyester pre-polymer found in the styrene-based matrix. These results were in disagreement with ageing results obtained on bulk-scale UD laminates. Cracks and porosities induced by ageing were featured in styrene-poor composites in the bulk scale, attributed to the hydrolysis of the 1,4-butanediol dimethacrylate (BDDMA) reactive solvent. Nonetheless, no hydrolytic effects were observed for the styrene-based composites.

2.5.5. FTIR & Vinyl Ester Ageing

FTIR offers the capability of providing an accurate evaluation not only of moisture concentration within aged polymers, but also information on their structure and chemistry, which can be altered by interaction with moisture. It is vital to understand whether any measured polymer weight loss is due to polymer degradation or to the extraction of monomers and (or) oligomers [39]. All to date studies regarding moisture ageing of vinyl esters have been focused on the study of hydrolytic effects rather than the quantification of absorbed moisture. Therefore, FTIR studies of aged epoxy resins were also investigated to provide insight into moisture content quantification. Although this literature review is focused on the FTIR analysis of actual polymeric specimens, the possibility of hydrolysis can also be determined by scanning the ageing medium for extracted polymer molecules [36,150,151].

Most literature reports involve the use of the ATR-FTIR interface, which is one of the most effective and versatile FTIR interfaces. A great benefit of using this interface is that ATR-FTIR-specific spectral libraries are widely available [152,153]. ATR-FTIR is operated by probing the surface area of the sample in contact with a suitable optical element by an evanescent wave. The penetration depth of the interface can vary from 0.5 to 5 μm. It can be therefore understood that this interface can only provide information on a polymer surface level rather than the inner polymer network. Furthermore, the accuracy of a quantitative analysis, such as ageing, is strongly dependent on the contact between the sample and the crystal. Thus, the geometry of the specimens should facilitate this contact. Pressurizing gas can be used but this may alter the diffusion kinetics, in the case of aged polymers [152]. Clamping using a standard force can be used but this may be damaging to the thin and brittle polymer films which are used in this study [154]. It has been reported that in the case of thin polymer films, which often feature a heterogeneous morphology through their thickness (multiple layers, surface effects), data interpretation can be complex [152].

Transmission is the first FTIR method developed and despite its wide use it has a significant drawback when used for (thin) brittle polymer samples; it can be a destructive FTIR method. Transmission FTIR requires infrared light to be completely transmitted through the specimen. Several techniques can be employed, such as powdering or pressing the sample in the form of an optical window allowing penetration of the light beam. However, this implies geometrical restrictions for the test sample and in turn restricts the use of the interface [153].

A non-destructive, contact-free interface with a high penetration depth is specular reflectance. Specular reflectance allows the sampling of non-infrared transparent specimens and is

operated by illuminating the sample with broadband infrared light and then collecting its reflection. The main limitation of specular reflectance is that despite its versatility, there is a lack of available data and spectral libraries in literature. This is due to specular reflectance data appearing to be less distinct than that generated by the previously mentioned methods, discouraging potential users. Therefore, data interpretation and in particular a qualitative analysis can be challenging. An example of spectral comparison obtained through the ATR and specular reflection interfaces, for a gum Arabic coating on a modern salt print was presented by McClelland et al [153], as shown in *Figure 2-17*.

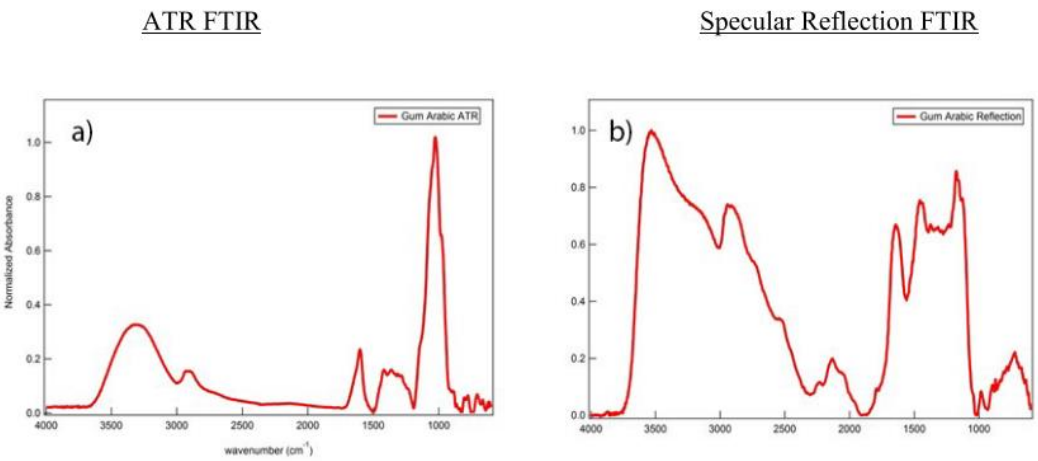

Figure 2-17: *Comparison of ATR and specular reflection/reflectance spectra of gum Arabic coating on a modern salt print, as presented by McClelland et al* [153].

FTIR has been extensively used for the evaluation of hydrothermal ageing effects on polymers. Visco et al [32] proposed the use of hydrolysis indices (HI) for the quantification of hydrolytic changes in hydrothermally aged vinyl ester polymers assessed by ATR-FTIR. The ageing conditions involved exposure to seawater at 60 °C, followed by re-drying at 50 °C for 24, prior to being measured. The following equations were used – *Equations 2-11, 2-12, 2-13*.

$$HI_{C-Oester} = \frac{A_{C-Oester}}{A_{ref}}$$

2-11

$$HI_{C=Oester} = \frac{A_{C=Oester}}{A_{ref}}$$

2-12

$$HI_{C-Oalchohol} = \frac{A_{C-Oalchohol}}{A_{ref}}$$

2-13

where: HI refers to hydrolysis index, A_{ref} is the peak area -CH_3, -CH_2 and -CH stretching, within the 3130 – 2750 cm^{-1} range, used as reference. $A_{C-Oester}$ is the C-O stretching signal of ester group peak area, within the 1190 – 1340 cm^{-1}, $A_{C=Oester}$ is the C=O stretching signal of ester peak area, within 1650 – 1790 cm^{-1}, and $A_{C-Oalchohol}$ is the C-O stretching signal of the alcohol group peak at 1040 cm^{-1}. The first two indices are indicative of ester group concentration [32,34]. A potential depletion of these can be indicative of bond rupture. Modifications in the last index are indicative of secondary alcohol bonding, and hydrolytic degradation in vinyl esters. Namely, upon ageing, the C-O ester stretching vibration at 1230 cm^{-1} and 1280 cm^{-1} was reduced by 25 % and, the ester carbonyl C=O at 1725 cm^{-1} was reduced by 38 %. An increase in the C-O stretching signal of the alcohol group of 38 % was observed, due to hydroxyl stretching of alcohol groups. The authors highlighted that the FTIR was only capable of providing information on the outside layer of the resin and thus coupling with experimental data obtained from other techniques, such as gravimetric analysis, thermal analysis and microscopy may be required to fully understand the hydrolytic reaction [32].

Ghorbel and Valentin [34] attempted to conduct a qualitative FTIR analysis of neat and reinforced bisphenol-A vinyl ester in their dry state and after 4000 h exposure to water at 60 °C. The analysis was used to study the potential of hydrolysis of a vinyl ester matrix and the secondary cross-linking of a vinyl ester-based FRP. Peaks investigated were those subjected to changes during ageing. The Beer-Lambert law was employed for the calculation. The band used for reference was the one at 1510 cm^{-1}, representing the vibration of aromatic compounds C=C. For the neat matrix, network changes induced by hydrolysis and post-curing were observed but quantification was challenging. Decreases in the alkene and styrene bands were identified for the vinyl ester-based FRP, indicative of secondary cross-linking. Observed changes below an ageing period of 3000 h included a change in the form of the peak at 1045 cm^{-1}, due to the stretching vibration of an aliphatic acid, indicative of hydrolysis. Spectral

changes evident after the ageing period of 3000 h included an increase in intensities of epoxy group bands at 1250 cm^{-1} and 950 cm^{-1}, attributed to the dehydration reaction following hydrolysis.

Chin et al [151] conducted a transmission FTIR analysis on vinyl ester aged in water at room temperature, 60 °C and 90 °C. The authors provided quantitative data on hydrolytic changes of vinyl ester induced by water. The quantification was carried out by evaluating certain fractions, of which the denominator was the aromatic C-H stretch peak at 3027 cm^{-1} used as internal standard, and the numerator included the areas of spectral regions that changed with ageing. These were the C-O stretching peak at 1182 cm^{-1}, the C-O stretching peak at 1245 cm^{-1} and the O-H stretching peak at 3473 cm^{-1}. All specimens, except for those aged at 90 °C showed an increase at 3473 cm^{-1} and decreases at 1182 cm^{-1} and 1245 cm^{-1}. Minor changes were also featured in the C=O peak at 1727 cm^{-1}. Such changes were attributed to ester hydrolysis, in which ester functional groups are converted to hydroxyl and carboxylic acid by-products. In addition, according to the authors, an increase in the concentration of hydroxyl and carboxylic acid groups would also contribute to the increase in the intensity of the O-H stretching peak. However, such changes were considered minor indicative that no major hydrolytic changes took place. More pronounced changes were recorded at 90 °C and after 10 weeks of ageing; the O-H stretching peak at 3473 cm^{-1}, C-H bending peak at 1509 cm^{-1} and the C-O stretching peak at 1182 cm^{-1} were depleted significantly. Moreover, there was a significant increase in the intensity of the carbonyl stretching peak at 1727 cm^{-1} and a shift in the position of C-O stretching peaks from 1182 cm^{-1} and 1108 cm^{-1} to lower wavelengths. Nonetheless, an explanation for these spectral changes has not been provided.

Chu and Karbhari [22] reported on moisture-induced hydrolysis of E-Glass/vinyl ester composites assessed by FTIR. Hydrolysis was confirmed by monitoring the decrease of the vinyl ester band at 1452 cm^{-1} (combination of C-O stretch and O-H). A gradual depletion of the C-O stretching peak 1182 cm^{-1} was also reported. The depletion increased further with an increase in the ageing temperature and ageing period. FTIR band assignments for the vinyl ester matrix are shown in *Table 2-3*.

≈ Band (cm^{-1})	Assignment	Reference
3600–3100	O-H of hydroxyl	[55]
1715	carbonyl group C=O group of vinyl ester	[40]
1641	double C=C bond of vinyl ester	[40]
1612	double C=C bond of styrene	[40]
1510	vibration of aromatic compounds C=C – benzene ring	[40]
1295	O-H of alcohol	[34]
1230	C-O stretching signal of ester group peak	[32]
1170	C-O-C stretching of VE	[40]
1109	O-H of alcohol	[34]
1040	C-O stretching vibration of an aliphatic acid	[32]
946	act of plane bending C-H of vinyl ester	[40]
910	wagging CH_2 in the vinyl group of styrene	[27,34]
830	bending of aromatic C-H in vinyl ester	[34,40]
695	bending of aromatic C-H in styrene	[34,40]

Table 2-3: *FTIR band assignments for the vinyl ester matrix.*

Gonzalez et al [155] summarised all vibration modes used for the quantification of moisture concentration in epoxy resins. Water in its liquid state can be detected by monitoring the increase of the O-H bond (≈ 3800 - 3600 cm^{-1}) and O-H bending (≈ 1650-1590 cm^{-1}). Hydrogen bonded water bonded can be detected in wavenumbers lower than 3600 cm^{-1}. The authors have used the band at 5215 cm^{-1} for the quantification of water, when normalised for sample thickness with respect to a spectral band that does not change with ageing. The 5215 cm^{-1} band resulted from the combination of asymmetric stretching and bending of O-H. Using Fick's law principles, the quantification of moisture can be carried out, as follows – *Equation 2-14*.

$$\frac{\Delta w_t}{W_0} = \frac{\frac{A_{t,5215}}{A_{t,ref}} - \frac{A_{0,5215}}{A_{0,ref}}}{\frac{A_{0,5215}}{A_{0,4623}}}$$

2-14

Equation 2-15, which obeys the Beer-Lambert law, can be used to account for volume changes (swelling) induced by moisture, using a reference band [155].

$$\frac{\Delta V(t)}{V_0} = \left(\frac{A_0}{A_{ref}}\right)^{3/2} - 1$$

2-15

Wu and Siesler [156] studied the water sorption of epoxies by monitoring the change of the O-H stretching bands at 3900 – 2800 cm^{-1}. They identified the main intensity increase to be at around 3450 cm^{-1}, due to the presence of water. The band became progressively broader as a function of ageing. The 3900 – 2800 cm^{-1} band was divided into three components:

1. 3610 cm^{-1} water hydrogen bonded with epoxy resin.
2. 3450 cm^{-1} weak hydrogen bonded with epoxy resin and partially dissolved.
3. 3240 cm^{-1} strong water – water hydrogen bonded or cluster of water.

Antoon et al [157] studied the water uptake of an epoxy system by monitoring the intensities at the peak of 1650 cm^{-1} and the spectral region at around 3500 cm^{-1}, observing an intensity increase, and broadening along with an intensity increase, respectively, as ageing progressed. However, no quantitative data was produced regarding moisture gain levels in the polymer.

Jana and Zhong [158] conducted an FTIR analysis of a hydrothermally aged epoxy network. They found that although the intensities of the hydroxyl O-H stretching at 3440 cm^{-1} and the O-H bending vibration at 1650 cm^{-1} can increase with water uptake, the production of hydroxyl units during epoxy curing can complicate the accurate interpretation of results. The O-H stretching vibrational bands can be affected by intramolecular and intermolecular hydrogen bonding, while hydroxyl formation at around 3400 cm^{-1} can broaden the O-H band. Increases in O-H stretching 3900–2800 cm^{-1} concentration as a function of epoxy curing were also identified by Sharma et al [159] and Gonzalez-Benito [160].

2.5.6. Influence of Voids in the Ageing Behaviour of FRPs

It is commonly accepted that it is difficult to manufacture entirely void/defect-free composite materials. Manufacturing defects are one of the factors that can compromise the mechanical performance of composites [1,161]. As previously mentioned, moisture is particularly attracted to areas of air entrapment in FRPs, such as voids, cracks and delaminated regions. These can be catastrophic for polymeric composites exposed to humid environments since they function as moisture passages into the structure of the material through capillary action and diffusion. Regardless of the application, once cracks have formed within polymeric materials, their structure is significantly compromised [2].

Voids can appear in many sizes and shapes in FRPs. The two main causes for void formation are air entrapment and vaporisation of volatile components or contaminants during curing. Air entrapment usually appears in the initial manufacturing stage of polymeric composites either due to air bubbles being trapped in viscous resin formulations during their preparation or due to incomplete wetting of the filaments or fibre bundles. Poor wetting can be attributed to the high viscosity of resins, which hinders the penetration of the latter into the fibre bundles creating air gaps. The second reason for void formation is particularly related to high-temperature curing resins, such as epoxies. During high-temperature cure, voids may be formed by the vaporisation of volatile components or contaminants, such as curing agents. It has been observed that such voids can significantly weaken the mechanical properties of composites [1]. Another common cause for the appearance of voids, cracks and interface failures in FRPs is the differential coefficient of thermal expansion between the fibre and the matrix, especially when accompanied by large temperature fluctuations. This mismatch can result in the generation of residual stresses and in turn activate failure mechanisms [2,16]. Fibre fracture, delamination and cracks can be classified as the most common failure mechanisms of FRPs [2].

Crack growth and propagation are known to accelerate hydrothermal action but are also dependent on the performance of the interface [2,117]. A strong interface creates an FRP with high strength and stiffness. However, this in turn can lead to composite being brittle in nature, thus enabling easy crack propagation through the matrix and fibre. On the other hand, a weaker interface can result in reduced applied stress transfer to the load-bearing fibres resulting in lower strength and stiffness. In a weak interface, a crack that is propagating transversely through an FRP is more likely to deviate from its path and propagate along the interface, resulting in interfacial debonding and (or) fibre pull-out [1,2]. A precise manner for the tailoring of the composite interface to ensure optimum laminate performance and prevent

failure modes is yet to be established. Besides, it is yet unclear whether high levels of interfacial adhesion are essential for the best balance of mechanical properties to be achieved [1].

Resins which are cured at elevated temperatures, such as epoxies can be adversely affected by cracks. Although such densely cross-linked structures possess exceptional mechanical properties, such as high modulus, high fracture strength and solvent resistance, they are susceptible to damage induced by high stresses, since they result in the formation and propagation of cracks. Strain fields located around cracks and voids control the properties of thermosets such as fatigue and fracture strength. Micro-cracking induced by hydrothermal exposure is a severe issue for the durability of polymeric composites. As previously mentioned once cracks have appeared in an FRP, its structure is significantly compromised [2,16]. Therefore, the durability of an FRP is strongly dependent on the ability of the matrix to resist cracking during service [147].

As soon as an FRP has been exposed to a humid environment, moisture concentration starts increasing on the outer surface of the material. It then continues to penetrate the FRP structure over time, while cracks tend to grow parallel to the free surface. This damage is often localised, resulting in a small number of large cracks (crack coalescence). Crack growth is strongly dependent on the different degrees of loading applied to the material. At low magnitudes of loading, crack growth is primarily governed by chemical reactions. At moderate loading magnitudes, crack growth is mainly controlled by the diffusion process, while at higher levels of loading, cracking is affected by stress-assisted corrosion [2,117]. According to Gagani and Echtermeyer [162], cracks located at the external layers of FRPs, which are in direct contact with the ageing fluid can accelerate diffusion significantly. On the contrary, cracks located within the internal layers of the materials had no significant impact on the diffusion kinetics.

The exposure of FRPs in aqueous environments has been associated with the activation of osmotic effects. These are initiated immediately after the exposure of the material to water. Once the water has started entering the structure of the material, reactions with its hydrolysable components will start occurring resulting in the formation of micro-cavities. These moisture-containing micro-cavities lead to crack propagation and delamination initiation enabling further moisture diffusion through the material. This effect is commonly known as “osmotic cracking” and is one of the most common failure modes of composites exposed to aqueous environments [3,130].

Delamination is a critical damage mode of thermoset composites, which is often induced by the presence of moisture at the interface of the two adjacent fibre plies. Delaminations develop

due to excessive out-of-plane or interlaminar stresses produced at the interfaces between adjacent fibre plies [163]. It takes place when the resultant transverse shear force exceeds a threshold value. Similar to cracking, delamination allows the storage of moisture within the laminate and accelerates diffusion [2]. According to Gagani and Echtermeyer [162], fluid diffusion in multi-directional laminates was increased by five times by the presence of delaminations. The causes of delamination in a hydrothermally exposed FRP are usually the same as the ones of cracking, such as hydrolysis and volumetric expansion, osmosis and blistering, residual stresses, thermal fatigue and interfacial failures [2,3]. Even though delamination can compromise the life of a laminate through premature buckling, stiffness degradation and moisture permeation, in certain cases it may improve stress relief and enhance its properties [2]. More specifically, in short-term moisture ageing, delamination may result in damage growth and premature failure. On the contrary, in long-term ageing, delaminated areas can function as load-bearing layers in a laminate [2].

To the author's best knowledge, the data on the effect of manufacturing voids on the water absorption of polymeric composites are limited. This is probably due to the difficulty of manufacturing composite samples with a controlled void content [164]. To-date reports suggest a rather abstract manner of manufacturing voids and, their control and quantification remain challenging. Mehdikhani et al [161] have summarised some primary techniques of artificial void manufacturing, as follows:

1. Employment of inappropriate cure pressure, vacuum or temperature conditions.
2. Introduction of moisture or foaming agents between laminate plies during manufacturing.
3. Introduction of void-initiating additives, such as polytetrafluoroethylene (PTFE) filament during manufacturing.
4. Selection of inappropriate liquid composite moulding input parameters.
5. Inadequate degassing prior to infusion.
6. Air injection before consolidation.

However, according to the few data that have been recorded, the effect of voids on the water uptake kinetics of polymeric materials and their performance after water exposure is crucial and should not be neglected [1,165]. According to Thomason [1,9], voids act as stress concentrators in FRPs and tend to weaken their performance. They also reduce interfacial strength due to lack of bonding at these points. Thomason found that the magnitude of the ILSS of a UD epoxy GFRP is strongly dependent on its void content. The author measured a reduction of 2-10 MPa in ILSS for every 1 %, by volume of voids. According to Harper et al

[164], the moisture equilibrium level and the uptake rate are dependent on the void content of the FRP. The authors reported on the water absorption of epoxy/graphite composites with a 1-6 % void content by volume. They observed a notable change in the diffusion kinetics of the composites, marked by an increase in moisture gain and high variation in the level of equilibrium when compared to "void-free" composites. Diffusion anomalies were also reported by Choi et al [166], who noted that diffusion coefficients reached a minimum value at 2 – 3 % void content, by volume. Thomason [1,9] reported that the initial absorption rate and the final moisture equilibrium level of different epoxy-based FRPs increased significantly with increased void content. Thomason also observed that only composites with a void content of less than 1 % exhibited an absorption behaviour similar to the one of the unreinforced matrix. Moreover, he concluded that voids form paths within the composite structure, which enable accelerated water ingress since the surface area exposed to moisture is increased. The author attributed the increased moisture gain of void-containing composites to the fact that voids provide sites for moisture storage at much higher concentrations than in the matrix. This is also suggested by Woo and Piggott [167], who carried out a theoretical analysis of the diffusivity of composites and showed that void-containing composites have a diffusivity fifteen times greater than that of the neat epoxy.

Youssef et al [168] attempted to predict the hydrothermal response of porous composites by creating a model whereby the fibres, matrix and voids were featured as three distinct phases. They reported on the strong relationship between voids and moisture kinetics and suggested that an increased void content may alter the form of homogenised compressive stress to tensile stress. Costa et al [169] suggested that voids and hydrothermal ageing can have a similar influence on the mechanical properties of FRPs, such as ILSS and, compressive and flexural strengths. Moreover, the authors highlighted the effect of hydrothermal forces on magnifying further the effect of voids in the mechanical properties of FRPs. By comparing woven-fabric epoxy and bismaleimide-based FRPs, they found that the hydrothermal effects on the fracture parameters of the composites were strongly dependent on their constituents, as well as the type of loading. More specifically, the ageing effect on ILSS, and for void-containing composites, was more significant for carbon/epoxy FRPs than for carbon/bismaleimide and UD carbon/epoxy FRPs. The authors also reported an increase of 45 % in the toughness of carbon/bismaleimide FRPs. According to compression test results, the latter void-containing FRPs were the most susceptible to ageing, while the other two FRPs were barely affected.

Allred [170] studied the effect of temperature and moisture on the flexural response of Kevlar/epoxy void-containing FRPs. Voids reduced the flexural strength of the laminate with

a void content of 2 – 4 % at 120 °C by 20 % but had a minor effect at room temperature. The author attributed the latter effect to the toughness of the Kevlar filaments or to the distinctive failure modes which they exhibit. Additionally, Allred reported a flexural strength reduction for moisture-containing composites with a high void content exposed to freeze-thaw cycling. The effect was attributed to crack initiation at voids during the freezing phase.

Zhang et al [171] investigated the effect of hydrothermal environments on void-containing, woven and epoxy-based CFRPs. Their findings confirmed that voids amplify moisture-induced degradation in FRPs and can further increase void growth. For aged, unaged and re-dried composites, the mechanical properties including ILSS, compressive and bending strength were impaired with an increase in void content and (or) ageing time. The most pronounced strength reductions were observed for the matrix and interface-dominated properties, such as ILSS and compressive strength. The latter mechanical properties were partly regained upon re-drying the specimens. However, the bending strength of the re-dried specimens was found to be higher than that of the un-aged specimen. The authors attributed this effect to the process of re-drying the specimen at 70 °C, which they believed resulted in further cross-linking while eliminating residual stresses and improving adhesion at the interface.

Almeida and Santacreu [172] studied the hydrothermal response of carbon fibre/epoxy composites with a high void content. The authors highlighted that evaluating the impact of hydrothermal ageing on the mechanical properties of void-containing FRPs is a complex matter involving a large number of variables. The ageing conditions employed were dry and wet environments in the temperature range of 54 - 65 °C, followed by a small number of thermal shock cycles. Mechanical properties, evaluated as a measure of ILSS were found to be independent of void content and ageing environment, for low and medium void content laminates. On the other hand, reduced ILSS was found for high void content at all ageing conditions. Samples that were exposed to moisture but not thermal shock noted an increase in ILSS. On the contrary, for the same laminates in wet environments, ILSS decreased with an increase in temperature and independently of void content. Additionally, results conflicting with the aforementioned literature were reported by the authors. Namely, a 30 % ILSS decrease was reported for all void content and ageing conditions after thermal shock except for dry, elevated temperature environments which showed the least ILSS decrease of 20 %. Moreover, high-void-content composites were found to be insensitive to environmental ageing. For laminates not submitted to thermal shock, humidity increased laminate toughness

and reduced void content. The inverse effect was reported for increased temperature environments.

2.5.7. Concluding Remarks

The environmental ageing of polymeric materials and in particular vinyl ester matrices and their composites has been thoroughly analysed. The term “ageing” is referred to the process of change in properties of a material or structure as a function of time. The growing demand for composite materials in infrastructure applications, where exposure to environmental conditions is inevitable, makes durability studies a necessity. However, the in-service examination of large composite structures can be a time-consuming process involving large costs. Therefore, in laboratory-based composite research “accelerated ageing” conditions are widely employed. The basic concept of “accelerated ageing” is the increase of degradation conditions, such as temperature or humidity to a higher level than that achieved in real-life operating environments. Ageing can be reversible (physical ageing) and (or) irreversible (chemical ageing). Chemical ageing primarily involves the combined action of degradation agents, such as moisture and temperature, known as hydrothermal ageing. Thus, one can conclude that particular attention should be devoted when accelerated ageing is applied on a composite research base since the increase of degradation effects can induce irreversible damage modes in the material, which would not be apparent in a “real life” ageing environment [3,22,34,68,118]. The most common moisture-induced degradation modes in thermosets and their FRPs can be summarised as follows:

- Weight gain [3,124].
- Plasticisation and dimensional changes (swelling and shrinkage of the material) [2–4,11,68,125].
- Surface degradation and damage (colour, gloss, crazing, blistering, etc) [3,18,32,68,117,126].
- Reduction in the glass transition temperature (T_g) [3,33].
- Hydrolysis and leaching [29,128].
- Reduction in mechanical and physical properties (i.e. stiffness, strength, localised strain, hardness, creep initiation) [3,140].
- Cracking (micro-cracking, osmotic cracking) and void formation [3,39,118].
- Changes in cross-link density and anti-plasticisation [22,34].
- Reduced fibre/matrix adhesion and debonding [3,22].

Although moisture-induced degradation primarily affects the matrix and interface of FRPs, the role of the reinforcing fibres is critical. In fact, the degradation of the fibre can result in the degradation of the composite interface and subsequently the overall composite performance may be compromised. Protective layers, known as “sizings”, are therefore coated on fibre surfaces to increase interfacial adhesion and ensure higher resilience to ageing-induced degradation [3,13,118].

The study of the literature regarding moisture ageing of vinyl ester and its composites showed that vinyl esters are fairly hydrophobic matrices. This justifies their use in industrial applications, where contact with moisture is allowed. In fact, comparative studies showed that vinyl ester matrices can be less susceptible to moisture attack than polyesters, isopolyesters and epoxies, provided they are sufficiently cured. When sufficiently cured, diffusion in vinyl esters was primarily marked by Fickian trends. However, for incompletely cured or void-containing matrices, and (or) when high-temperature ageing is deployed, diffusion kinetics can vary. Water uptake in vinyl esters and their composites induced two main degradation effects: plasticisation after short-term ageing, and hydrolysis after long-term ageing.

It can be summarised that degradation effects induced by plasticisation are primarily reversible or partly reversible and can affect the mechanical properties, moisture levels and Tg of vinyl ester and VE-based composites. On the other hand, hydrolysis is associated with irreversible degradation and chemical changes in the polymeric material. Hydrolysis is governed by leaching which can in turn result in fibre/matrix weakening and debonding, mechanical property and Tg depression, cracking and micro-cracking, delaminations, increased levels of moisture and, secondary cross-linking through anti-plasticisation effects. Vinyl ester matrices, and in turn their composites, may be particularly sensitive to secondary cross-linking and anti-plasticisation since they often exhibit incomplete curing due to their high degree of heterogeneity and microgel formation during curing.

The number of studies using micro-mechanical testing methods for the direct evaluation of the durability of the composite interface is limited, especially regarding the use of a vinyl ester matrix. Since, as previously discussed, the interface of single fibre micro-composites is different from that of bulk composites one can understand that direct property transferability between the two scales upon ageing can be ambiguous. However, encouraging indications have been recorded regarding the understanding of damage modes and evolution, as well as strength retention trends at the interface. Taking into account the benefits and capabilities of micro-mechanical testing discussed in former sections it can be concluded that if micro-

mechanical testing methods are used with caution, they can provide fundamental information for the bulk composite material, as a function of environmental history.

FTIR can be a useful tool for the assessment of vinyl ester integrity upon hydrothermal ageing. Although no quantitative data is currently available regarding moisture sorption levels in vinyl esters, hydrolytic effects have been evaluated accurately. Attempts to evaluate moisture gain using FTIR have been conducted on epoxy resins. Nonetheless, such an assessment is challenging due to moisture-induced changes in the thermoset structure which may lead to misleading conclusions.

Last but not least, a thorough literature search on the effect of voids on the ageing behaviour of FRPs was conducted. One can conclude that the manufacturing of controlled void specimens remains a challenging task and therefore information around the particular effects of voids in synergy with hydrothermal ageing is still limited. Voids have been found to have similar effects to hydrothermal ageing in FRPs. Therefore, the degradation rate is amplified for void-containing FRPs exposed to hydrothermal environments. The diffusion kinetics of the composite may be altered, including changes in moisture uptake behaviour and equilibrium level. Voids, cracks and delaminations are known to accommodate moisture within polymer networks and thus further increase moisture-induced degradation and crack/void growth and propagation rates. The resulting effects on the mechanical properties of FRPs, mainly the ones governed by the matrix and interface, have been reported to be critical. In fact, the selection and nature of the FRP constituents were found to be of utmost importance in the influence of voids and ageing in the material. Nonetheless, conflicting results have been reported by Almeida and Santacreu [172]. Finally, reports suggest that FRP delamination in combination with short-term ageing can result in premature failure, while, on the other hand, delamination in long-term ageing may actually be beneficial for the laminate.

CHAPTER 3: INVESTIGATION OF THE EFFECTS OF SCALE AND CURE ENVIRONMENT ON PHYSICAL AND CHEMICAL PROPERTIES OF THE VINYL ESTER RESIN

During the literature study, three fundamental conclusions were reached regarding the cure kinetics of vinyl esters:

- A styrene reduction in bulk scale specimens does not affect the Tg of vinyl ester polymers, provided they are adequately cured.
- Oxygen introduction during polymerisation can complicate and retard the reaction.
- Incomplete curing and (or) reduction of micro-mechanical properties were observed for single fibre VE-based micro-composites, without strong supporting evidence, nevertheless.

These points must be well understood for a more comprehensive understanding of this study. This study is an attempt to produce a link between these points and shed light on the "blur" around the cure kinetics of vinyl ester and matrix property transferability from a bulk scale to a microscale. Thermal analysis techniques, such as Differential Scanning Calorimetry (DSC) and Dynamic Mechanical Analysis (DMA), as well as Fourier-transform Infrared Spectroscopy (FTIR), have been utilised.

3.1. EXPERIMENTAL

3.1.1. Materials

Two different matrices were used throughout this study; one commercial vinyl ester resin and one experimental vinyl ester resin. Both matrices were made available by Polynt, as part of the DACOMAT project.

The commercial vinyl ester resin used was the Polynt DION 1260 bisphenol-epoxy vinyl ester with a styrene content of 48 – 52 % by weight. The resin is designed for vacuum infusion; it has low viscosity and therefore improved wetting, exceptional mechanical properties, high toughness and good crack resistance, as well as improved high-temperature stability.

The experimental resin used was the Polynt DION 1273, a matrix consisting of a complex polymer network comprised of different monomers. DION 1273 is a pre-accelerated, modified vinyl ester resin, primarily based on methyl methacrylate-based (MMA) and styrene (< 20 % by weight). This resin was also designed for vacuum infusion; it is a low viscosity resin with very high fracture toughness and exceptional adhesion.

Both resins were cured using a PBC-21 UN 3103 Organic peroxide type C initiator from United Initiators GmbH. The initiator was added to the resin at a ratio of 97.5 : 2.5 by weight prior to use.

3.1.2. Specimens Used and Cure Conditions

All specimens used in this chapter are entailed in *Table 3-1* for the DION 1260 resin and in *Table 3-2* for the DION 1273 resin. A more detailed analysis was carried out on the DION 1260, since it was considered the "baseline" resin for the DACOMAT project. The cure conditions and specimen geometry employed were selected to examine the following parameters, which have been found to affect the cure kinetics and thermal behaviour of vinyl esters:

- scale/varying thickness
- styrene content
- oxygen intrusion during polymerisation
- post-cure temperature.

Specimen	Cure 24 h at RT	Post-cure (P-C)	Max. P-C Temperature (°C)	Scale
Polynt Standard*	Sealed Mould		60	Macroscale - Bulk
Polynt FC*	Sealed Mould		100	
UoS Op. Mould 60 °C	Open Mould/Ambient		60	
Full Atm.	Ambient	Ambient	100	Microscale - Film
Standard	N_2	Ambient	100	
Standard + 150 °C Air P-C	N_2	Ambient	150	
Full N_2 100 °C	N_2	N_2	100	
Full N_2 150 °C	N_2	N_2	150	

*Resin casting supplied by Polynt.

Table 3-1: *DION 1260 specimens used*

Specimen	Cure 24 h at RT	P-C	Max. P-C Temperature (°C)	Scale
Polynt Standard*	Sealed Mould		60	Macroscale - Bulk
Polynt Standard	N_2	Ambient	100	Microscale - Film
Full N_2 150 °C	N_2	N_2	150	

*Resin casting supplied by Polynt.

Table 3-2: *DION 1273 specimens used.*

The effect of scale on the cure kinetics of the specimens was examined using three different thickness ranges:

- $3.9 \leq t \leq 4.5$ mm *(macroscale – bulk).*
- $0.1 \leq t \leq 0.2$ mm *(microscale – thin film).*
- $t < 0.1$ mm *(microscale – thin film).*

The suggestion of the manufacturer regarding cure and post-cure (P-C) cycles were:

- Macroscale – bulk:
    - Cure: 24 h in a closed mould at (room temperature) RT at 60 °C.
    - P-C: 24 h at 60 °C.
- Microscale – films:
    - Cure: 24 h under N_2 at RT at 60 °C.
    - P-C: 24 h at 60 °C, 3 h at 80 °C, 1 h at 100 °C.

The above cure cycles have been identified as "standard" cure cycles, as shown in *Table 3-1* and *Table 3-2*. The N_2 environment used in the initial cure phase of thin films was recommended by the resin manufacturer to prevent probable oxygen interaction and volatile component vaporisation from the high-surface-to-volume ratio curing polymer. Moreover, the additional elevated temperature post-cure phase of 100 °C was used for thin films to ensure optimum conversion, as also recommended by the resin manufacturer. Although as per the manufacturer macroscale specimens were to be post-cured at 60 °C, further post-cure at 100 °C was applied to some samples to allow comparison with the "standard" cured thin films.

The assessment of ambient oxygen during the manufacturing of vinyl ester specimens was carried out at both scales:

- Bulk neat resin samples fabricated both in a sealed mould (hindering oxygen introduction) and an open mould (allowing interaction with ambient oxygen). The sealed mould samples “Polynt Standard - 60 °C” and “Polynt FC - 100 °C” were supplied by Polynt.
- Thin films were cured both in an inert nitrogen environment, as recommended, and in an ambient atmosphere, for the first part of the cure. Inert nitrogen and ambient environment were also employed in both phases of the cure to allow comparison. The effect of elevated post-cure temperature was also examined.

The effect of styrene content on the microscale was studied by reducing the styrene content of a “standard” cure film within the thickness range of $0.1 < t < 0.2$ mm. The resin styrene content was reduced by approximately 67 % by applying vacuum evaporation to unreacted resin. A styrene-rich environment was also used to reduce potential styrene loss and allow comparison between varying styrene content.

Bulk open mould specimens were manufactured in a silicone rubber mould fabricated in-house. The manufacturing of thin film specimens was found to be a challenging task. The low viscosity and high adhesion of the resins made it difficult to obtain a uniform thickness and to remove the final specimen of the substrate, respectively. Several substrates and manufacturing techniques were attempted, such as spin coating on glass slides, spreading resin on a silicone mould, using a seam roller and manufacturing between metal plates. Nonetheless, not all aforementioned techniques resulted in an adequate finish. The most effective manufacturing method was found to be the use of a metallic drawdown bar for the application of the film on a nylon substrate, adhered onto a steel plate. The latter technique produced films of the most uniform thickness finish. Thickness was measured by the use of a digital micrometer. The use of drawdown bars of different thicknesses allowed the manufacturing of films of varying thicknesses.

3.1.3. Differential Scanning Calorimetry (DSC)

DSC analysis was carried out to provide insight into the Tg of the matrix manufactured with different thicknesses. A Q20 differential scanning calorimeter (TA Instruments) with a cooling unit was used for all tests. The following heating programme was used for each specimen: equilibrate at -10 °C and hold isothermally for 10 min (cycle 1), temperature ramp at 10 °C /min up to 180 °C and hold isothermally for 10 min (cycle 1), temperature ramp at 10 °C /min

to -10 °C and hold isothermally for 10 min (cycle 2) and finally temperature ramp at 10 °C /min up to 180 °C (cycle 2). Nitrogen was used as purge gas at 50 ml/min for all tests. The glass transition temperature could then be assigned from a clear step change visible on the resultant thermal curve of heat flow plotted against temperature.

All specimens were accommodated in an standard aluminium pan sealed with a lid. Regarding bulk specimens, a small piece of material was cut from the specimen and was placed in the pan. Therefore the actual thickness of the tested specimen was lower than the one exhibited by the bulk specimen. Regarding film specimens, one film layer was used. Even though these possessed a slightly lower mass than bulk specimens (films ≈ 2-3 mg, bulk ≈ 20 mg), the stacking of multiple layers was avoided to prevent uneven heat transfer between the different layers

A fractional conversion calculation was also carried out for varying sample thicknesses. The fractional conversion of monomer to polymer for each system was evaluated by using *Equation 3-1*.

$$a = (1 - \frac{H}{H_t})$$

3-1

where a is the degree of cure, H is the heat of the reaction of the specimen and H_t is the total heat of reaction measured from an unreacted sample.

The unreacted resin baseline specimen was subjected to vacuum for approximately 10 minutes while in the DSC pan for removal of oxygen prior to testing. Universal Analysis software was used for data analysis.

3.1.4. Dynamic Mechanical Analysis (DMA)

DMA was conducted to provide information on the Tg and thermal behaviour of the matrix manufactured at different thicknesses and under different cure conditions. DMA analysis was carried out using a Q800 Dynamic Mechanical Analyser (TA Instruments). Measurements were performed on thick specimens in 3-point bending mode in accordance with ASTM D5023-15 [173]. The specimen dimensions used were 64 x 13 mm with a thickness of $3.9 \leq t \leq 4.5$ mm; the span length during testing was 50 mm. All microscale thin film specimens were

tested in tension mode according to ASTM D5026-15 [174]. The test parameters for the thin film specimens tested in tension were kept as close as possible to the macroscale, rectangular bars to allow a comparison between the two scales. However, a significant reduction in amplitude was required as a function of scale. Specimen details are presented in *Table 3-3*. All specimens were equilibrated at 25 °C for 5 minutes, then ramped at 2 °C/min up to 150 °C . The Tg assignment was conducted in agreement with ASTM D7028 − 07 [175], by taking an onset of the storage modulus curve presented on a logarithmic scale.

Thickness Range, t (mm)	Amplitude (µm)	Preload Force (N)	Frequency (Hz)	Force Track (%)	Test Mode
$0.1 < t \leq 0.2$	10	N/A	1	105	Film Tension
$t \approx 3.9$	50	0.1	1	120	3-Point Bending

Table 3-3: *DMA test parameters.*

3.1.5. Fourier-transform Infrared Spectroscopy (FTIR)

Fourier-transform infrared spectroscopy (FTIR) was used to assess the degree of cure of vinyl ester as a function of scale, cure environment and (or) temperature. Spectra collection was carried out on a 4100 ExoScan FTIR using a spherical diamond attenuated total reflectance (ATR) interface. Analysis was performed in the 650 cm^{-1} to 4000 cm^{-1} range with a spectral resolution of 8 cm^{-1} and 64 scans per sample. Background scans were taken every ten minutes and the crystal was cleaned with acetone between measurements. Data processing and normalisation were conducted through the OriginPro software. A quantitative analysis was performed through the use of SpectraGryph software using the “integration with baseline” tool.

For both matrix systems, the degree of cure was monitored by the depletion of the C=C at 946 cm^{-1} and 910 cm^{-1} for the vinyl ester and styrene monomers, respectively. The C-H of styrene and vinyl ester at 695 cm^{-1} and 830 cm^{-1} were used as internal reference. Lastly, the large variation in styrene content of different specimens and the lack of information regarding the molar ratio of the two resins were restrictive parameters for the calculation of the total polymer fractional conversion. The individual styrene and vinyl ester monomer conversions were

calculated using the following equations derived from the Beer-Lambert law – *Equations 3-2* and *3-3*.

$$\alpha_{VE}(t) = 1 - \left(\frac{ABS\ (t)945\ cm^{-1}}{ABS\ (t=0)945\ cm^{-1}}\right) * \left(\frac{ABS\ (t=0)830\ cm^{-1}}{ABS\ (t)830\ cm^{-1}}\right)$$

3-2

$$\alpha_{ST}(t) = 1 - \left(\frac{ABS\ (t)910\ cm^{-1}}{ABS\ (t=0)910\ cm^{-1}}\right) * \left(\frac{ABS\ (t=0)700\ cm^{-1}}{ABS\ (t)700\ cm^{-1}}\right)$$

3-3

3.2. RESULTS AND DISCUSSION

3.2.1. The Chemistry and Thermal Properties of DION 1260

Thermal Analysis – Effect of Scale

A more detailed analysis was conducted for the DION 1260 resin since it was considered the "baseline" resin for this project. First and foremost, it was essential to identify the variation (if any) between the thermal behaviour of bulk scale and microscale vinyl ester. A DSC study of cured vinyl ester as a function of material thickness was established. Results are shown in *Figure 3-1*. All Tg values as a function of specimen thickness from the first and second heating cycles are included in *Table 3-4.* It was clearly observed that film specimens, representative of the microscale, featured a broad, lower-temperature transition than the bulk specimens, which was in fact reduced when the material thickness was lower. This transition was featured at 55 °C and 65 °C for the films of a thickness of 0.03 mm and 0.15 mm, respectively. Although the transition of the 0.15 mm film was rather broad, it was still apparent and detectable by the analysis software. For both film specimens, this initial transition was followed by a hint of a secondary transition, which was nonetheless "masked" by the presence of the exothermic peak. It was found that when these specimens were re-heated (2nd DSC cycle), the Tg observed was closer in range for all specimens with the exception of the t = 0.03 mm film, which only reached a Tg (2) of 81 °C. The Tg (2) increase was an indication of initial incomplete curing of the specimens and post-curing effects induced by the introduction of a higher temperature

in the DSC furnace. Nonetheless, for the thinnest specimen of t = 0.03 mm, it was shown that the potential for achievement of "bulk scale" cure was clearly unfeasible, at least when "standard" cure conditions were employed. This was a strong indication that the chemistry of the thinner films varied notably from that of "bulk scale" specimens.

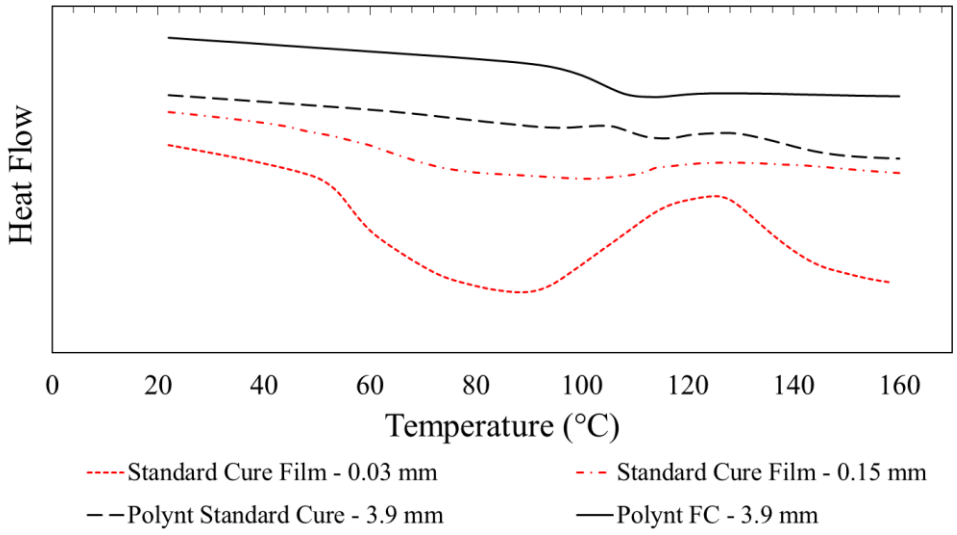

Figure 3-1: *Comparison of DSC thermograms – 1st heating cycle – as a function of "standard" cured DION 1260 thickness. Curves were stacked by using an offset in the Y axis and therefore Y axis values are arbitrary.*

Thickness (mm)	Tg_1 (1) (°C)	Tg_2 (1) (°C)	Tg (2) (°C)	Exothermic Reaction Energy (1) (J/g)
3.9 ± 0.2*	N/A	105	108	1
3.9 ± 0.2 **	N/A	109	110	1.5
0.15 ± 0.02	65	101	110	7
0.03 ± 0.02	55	81	90	17

* Polynt FC, **Polynt Standard

Table 3-4: *Tg change vs thickness of DION 1260. Tg_1 (1) and Tg_2 (1) represent the step changes in Heat Flow in cycle 1, and Tg (2) in cycle 2. Exothermic Reaction Energy (1) was calculated by integration with linear baseline in cycle 1.*

No major variation was detected between the Tg values and exothermic reaction energies of the bulk specimens. The effect of post-curing at a higher temperature was thus found to be insubstantial and that a cure temperature of 60 °C was adequate for the specimen to react "fully". Regarding film specimens, the increase in exothermic reaction energy for decreasing material thickness was another clear indication of reduced cure. Based on that observation, a monomer conversion calculation was conducted using *Equation 3-1*. A resulting bar graph is presented in *Figure 3-2*. The potential of an over-prediction of the degree of conversion was considered. This was due to the curing reaction in the DSC furnace occurring notably faster than the cure of test specimens. Please note that sufficient cure of test specimens involves a two-part cure procedure, involving an initial cure phase for 24 h, prior to post-curing. As a result, the exothermic reaction energy of unreacted vinyl ester obtained by rapid heating in DSC, which was used for the calculation may be exaggerated, resulting in higher conversion for the test specimens. Nevertheless, even though the quantification may be inaccurate, on a qualitative basis, it can be accepted that the degree of conversion is lowered when material thickness is reduced.

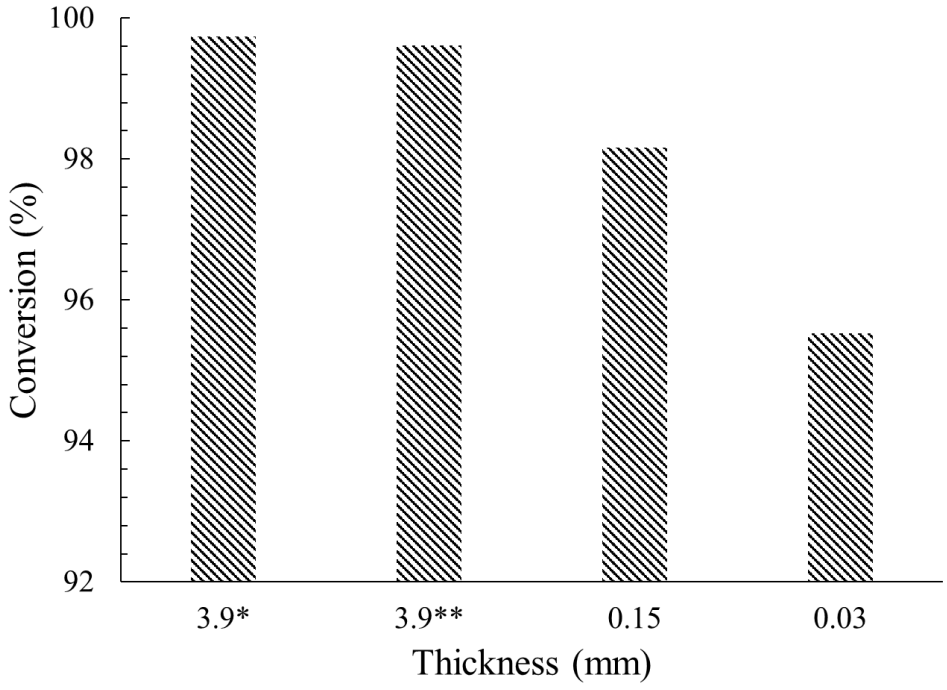

Figure 3-2: *DSC conversion calculation as a function of DION 1260 thickness.*

A DMA was conducted for the study of the thermal behaviour of film specimens, as a complement to DSC results. Storage and loss modulus curves for a "standard" cure film of a thickness of 0.13 mm and a "Standard Polynt" plate of a thickness of 3.9 mm are presented in *Figure 3-3(a)* and *Figure 3-3(b)*, respectively. The resulting Tg values from storage modulus, loss modulus and tan δ obtained by DMA are contained in *Table 3-5*.

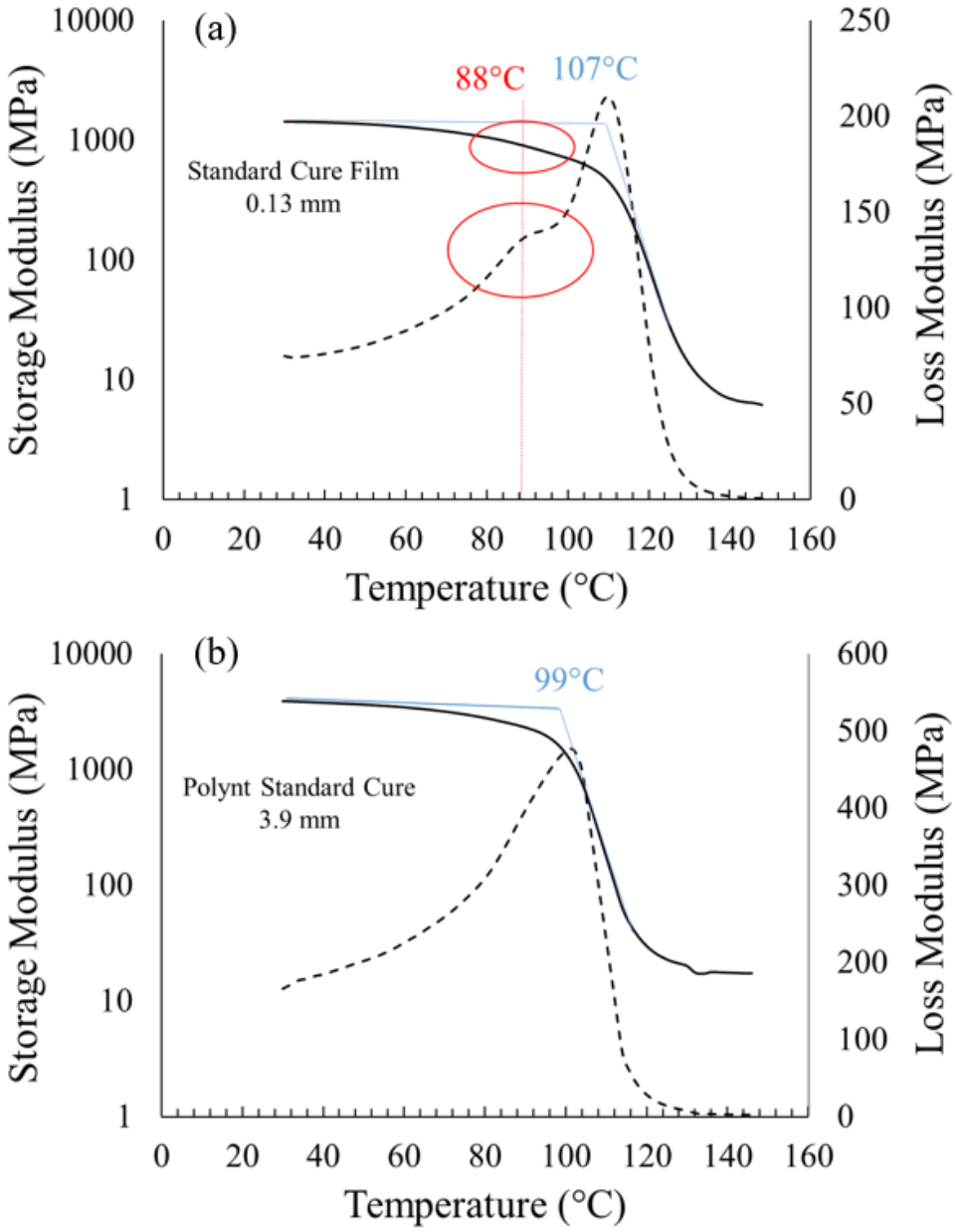

Figure 3-3: *(a) DMA thermal curve of a DION 1260 "standard" cure film of a thickness of 0.13 mm, (b) DMA thermal curve of a DION 1260 "Polynt Standard" plate of a thickness of 3.9 mm.*

It was found that a broad shoulder stretching between 70 °C and 90 °C was apparent in the film loss modulus curve prior to the main peak. Moreover, a slight downward change in the slope of the storage modulus curve can be observed in the same range. This result was found to be in agreement with the first DSC transition of a film in the same thickness range (0.15 mm), which as described previously was at 65 °C. As shown in *Table 3-5*, the Tg range indicated by DMA was around 88 °C to 122 °C, bounded between the first onset of the log of the storage modulus and the maximum value obtained from the tan δ peaks. The Tg of the macroscale plate was found to be between 99 °C and 115 °C. In this case, the transitions shown in the thermal curves were clear and the shoulder apparent in the loss modulus of the film was not present. Moreover, the storage modulus values of the bulk specimen at the viscoelastic range were found to be significantly higher than those of the film (≈ 1000 MPa for film and ≈ 3950 MPa for plate at room temperature). This was indicative of notably higher stiffness for the bulk specimens and was a validation of the effect of scale on vinyl ester properties. As described in the experimental section, different test setups were used for the film and plate specimens and hence deviation was expected between Tg values in the different scales. In theory, so long as the applied strain lies within the linear viscoelastic region for the material at the same frequency, the Tg position should not change. In our case, the strain level chosen for bulk polymer plates (amplitude of 50 um) was appreciably higher than the one employed in thin film testing (amplitude of 10 um). Such a change likely affects the sensitivity to detect the early stages of the transition – higher strain levels may detect the Tg onset earlier, lower levels later into the transition once softening is more significant. DSC is generally more effective in detecting Tg as a function of thickness, due to the smaller specimen mass employed (low thermal lag) and the fact that the specimen is sitting on top of the thermocouple. On the other hand, with DMA, specimen mass is more significant, the thermocouple is positioned a few mm from the specimen and the furnace is heating radiantly, and not via conduction, as is the case with DSC. Thus, DMA is less efficient when it comes to temperature uniformity, which is why lower heating rates are usually employed when compared to DSC. A slight deviation between DMA and DSC results is also common due to the different sensitivity of the two thermal analysis techniques. Varying Tgs as obtained by DMA and DSC for the same matrix were presented in *Table 2-1*.

Specimen Type	Storage Modulus - Onset (°C)	Loss Modulus - Shoulder (°C)	Loss Modulus - Peak (°C)	Tan δ - Peak (°C)
"Standard" Cure Film	107	88	110	122
"Polynt Standard"	99	N/A	99	115

Table 3-5: *Tg values obtained by DMA thermal curves for a DION 1260 "Standard" cure film of a thickness of 0.13 mm, and a "Polynt Standard" plate of a thickness of 3.9 mm.*

The appearance of a low-temperature transition in microscale vinyl ester specimens may be indicative of the diphasic nature of the resin. Although this effect was not apparent on bulk scale specimens, literature results suggest that a diphasic nature may still be present but cannot be deconvoluted by thermal analysis software [21]. This is due to the two transitions existing within the same temperature region. In this case, it can be assumed that the low-temperature Tg is exhibited by the styrene-rich region of the resin, considering the volatility of the styrene monomer and the fact that the styrene-rich region is known to have a lower cross-link density than the vinyl ester region. However, this assumption required further evidence, which was attempted to be provided in the following sections of this thesis.

Effect of Reduced Styrene – A Microscale Study

Although it has been established that a reduction in the styrene content of bulk vinyl ester specimens has a minor effect on their Tg [24,34], to this author's best knowledge the transferability of the effect to the microscale, which involves the handling of small matrix volumes is yet to be examined. The potential of styrene loss during manufacturing and curing of film specimens was considered, due to the volatility of the styrene monomer as opposed to the stable chemistry of the vinyl ester monomer. Nonetheless, it should be taken into account that reducing the amount of styrene of the pre-polymer mix used for films to 67 % of "standard" would simply reduce styrene content further, if styrene was already evaporated during the manufacturing of "standard" cure specimens. Considering literature mentions regarding incomplete polymerisation of vinyl ester and polyester micro-droplets due to styrene vaporisation, it was essential to determine whether the lower temperature Tg of vinyl ester

films was caused by such an effect. Laurikainen [68] stated that vinyl ester micro-droplet curing could only be achieved under a styrene environment (in air). On that basis, the effect of a styrene-rich environment on the thermal behaviour of film specimens was explored. Storage and loss modulus curves for a "standard" cure film of a thickness of 0.13 mm, a "standard" cure film cured under a styrene environment of a thickness of 0.15 mm and a reduced "standard" cure film of reduced styrene of a thickness of 0.16 mm are shown in *Figure 3-4*.

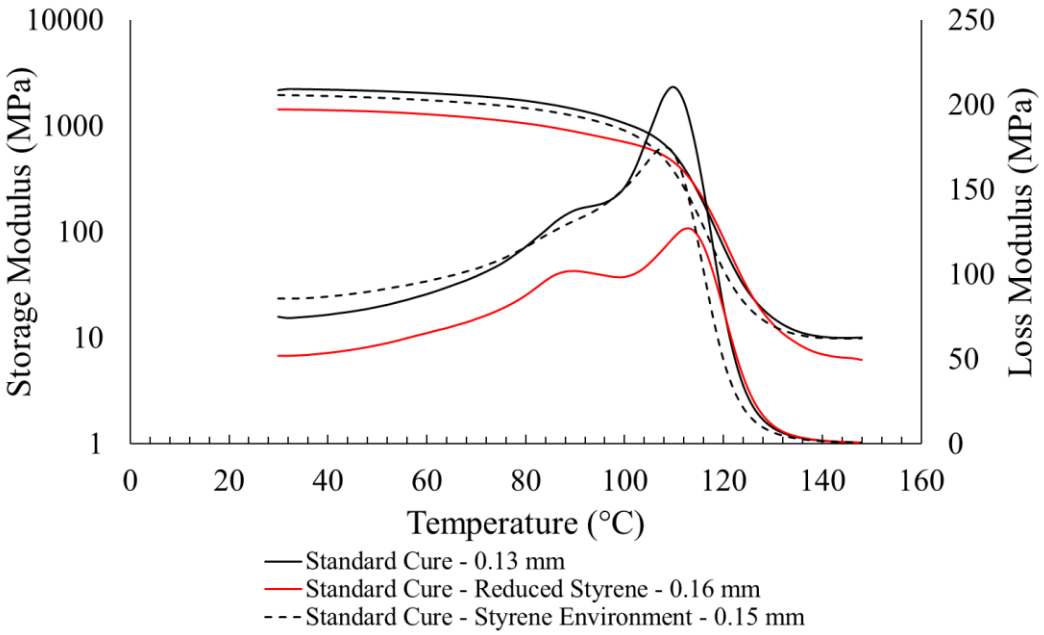

Figure 3-4: *DMA thermal curve comparison of DION 1260 "standard" cure films of varying styrene content in the thickness range of 0.1 < t ≤ 0.2 mm.*

All Tg values were found to be within the same temperature range. Nevertheless, as clearly featured in the storage modulus curve, the Tg of the film cured under a styrene-rich environment exhibited a slightly lower Tg, while the styrene-poor specimen showed a slightly higher Tg. This was in line with bulk vinyl ester results as a function of varying styrene content reported by Scott et al [24]. However, in this case, a discernible pattern in the format of the low-temperature transition of the loss modulus was featured, as a function of styrene content. The breadth of the shoulder was increased with increasing styrene content, while a more pronounced shoulder was seen in the case of the reduced styrene film. Moreover, by studying the storage and loss modulus curves of films of varying styrene content, it can be seen that the reduced styrene film exhibited a slightly lower storage modulus magnitude below Tg and in the rubbery region, as well as a lower loss modulus magnitude, when compared to other two films. Typically, the above observations, along with the small Tg increase of the reduced

styrene film are indications of a higher cross-link density. This was in line with the observations by Scott et al [24], who found a reduction in crosslink density with increased styrene content. Nevertheless, generally, small variations in storage and loss modulus magnitudes are to be expected, even when testing the same material due to experimental error, which is more likely when testing such thin specimens. Such errors may arise from non-uniformity of test specimens and inaccurate specimen dimension measurements, as well as specimen alignment and clamping in DMA.

In agreement with DMA results, comparative DSC results between "standard" cure and reduced styrene "standard" cure films of different thickness ranges confirmed the presence of a low-temperature transition. DSC thermograms are shown in *Figure 3-5*. All Tg values obtained by the styrene content study are contained in *Table 3-6*. This transition was within the same temperature range for "standard" cure and "standard" cure, reduced styrene specimens of a similar thickness. For $t < 0.1$ mm, both standard" cure and reduced styrene, "standard" cure films exhibited similar lower temperature Tgs of 55 °C and 54 °C, respectively. A similar effect was observed for films of $0.1 \leq t \leq 0.2$ mm, whereby an initial Tg between 65 °C and 70 °C was featured by both film specimens. The exothermic reaction energies obtained through DSC were slightly higher for the "standard" cure films containing the original styrene content, as opposed to the ones of a reduced styrene content. These were measured by the integration tool in the Universal Analysis software. Nevertheless, the variation was considered minor and most likely unrelated to the change in styrene content after studying the results of a wide range of specimens.

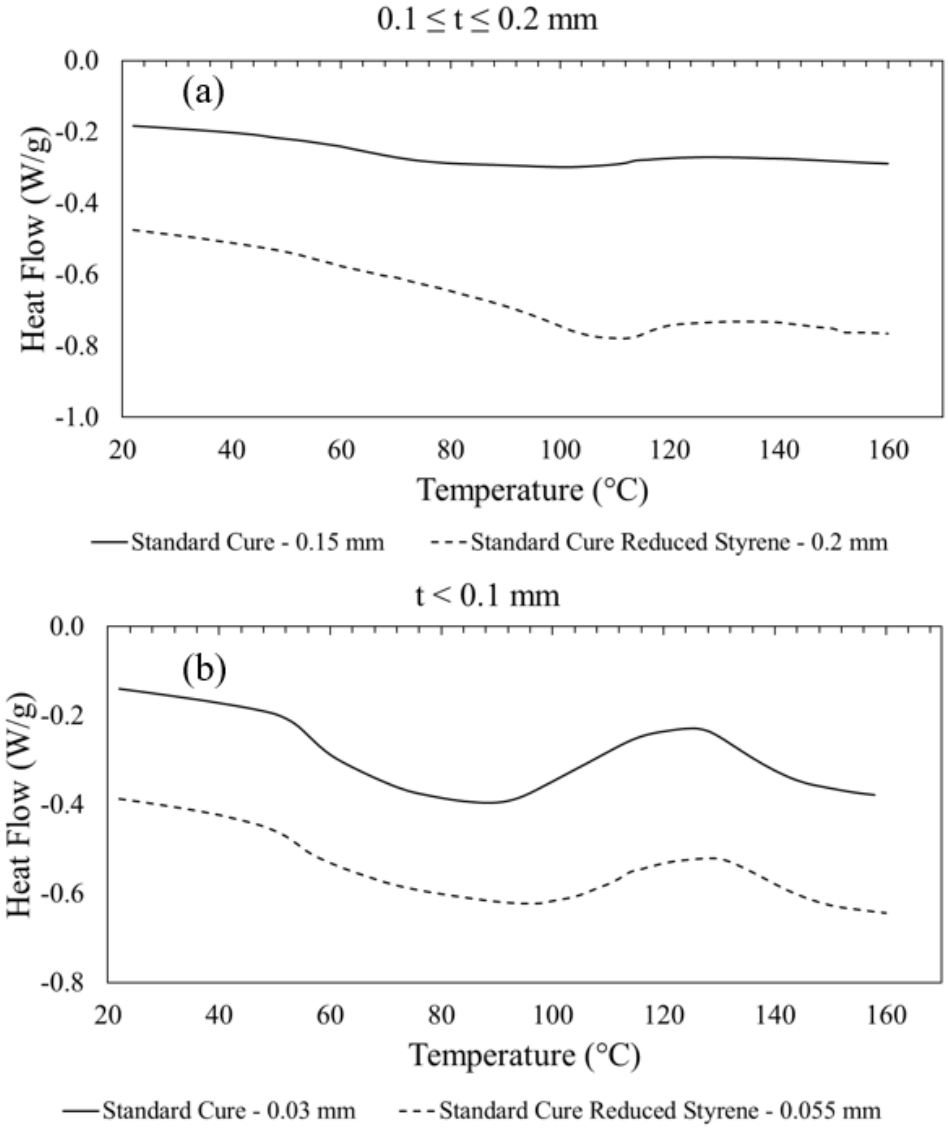

Figure 3-5: *(a) DSC thermograms of DION 1260 "standard" cure films with original and reduced styrene content of a thickness of $0.1 < t \leq 0.2$ mm, (b) DSC thermograms of DION 1260 "standard" cure films with standard and reduced styrene content of a thickness of $t \leq 0.1$ mm.*

Thickness, t (mm)	Designation	Tg_1 (°C)	Tg_2 (°C)	Exothermic Reaction Energy (J/g)
$t \leq 0.1$	Standard	55	81	17
	Reduced Styrene	54	83	11
$0.1 < t \leq 0.2$	Standard	65	101	7
	Reduced Styrene	70	101	6

Table 3-6: *Tg change for DION 1260 "standard" cure of original and reduced styrene content for different thickness ranges. Tg_1 and Tg_2 were obtained by the step change in temperature DSC thermogram during the first heating cycle. Exothermic Reaction energy was calculated by integration with a linear baseline.*

It can be concluded that the Tg and cross-linking of styrene-poor films were found to be slightly higher than those of "standard" cure and films cured under a styrene environment. However, the shoulder in the loss modulus DMA curve was found to be more pronounced for reduced styrene films and was depleted as a function of increasing styrene. Nonetheless, this shoulder was apparent in all tested films, regardless of the styrene content. Thus, the reason behind the presence of the shoulder, indicating a Tg reduction of one of vinyl ester phases (presumably that of the styrene-rich phase) was still to be explored further.

Effect of Oxygen in Vinyl Ester Polymerisation

The presence of oxygen in the polymerisation of vinyl ester has been classified as a "scavenger" [28]. Reports suggested that the effect can compromise the performance of bulk vinyl ester specimens and is likely to be catastrophic when vinyl ester specimens of a high surface-to-volume are employed [48,176]. To this author's best knowledge the latter case still remains unexplored. In this work, the effect of the interaction of vinyl ester with the ambient environment – specifically oxygen in the atmosphere – during cure has been studied thoroughly using DMA. Several DMA thermal curves for vinyl ester specimens on the microscale and macroscale cured under different cure environments and temperature regimes are presented in *Figure 3-6*.

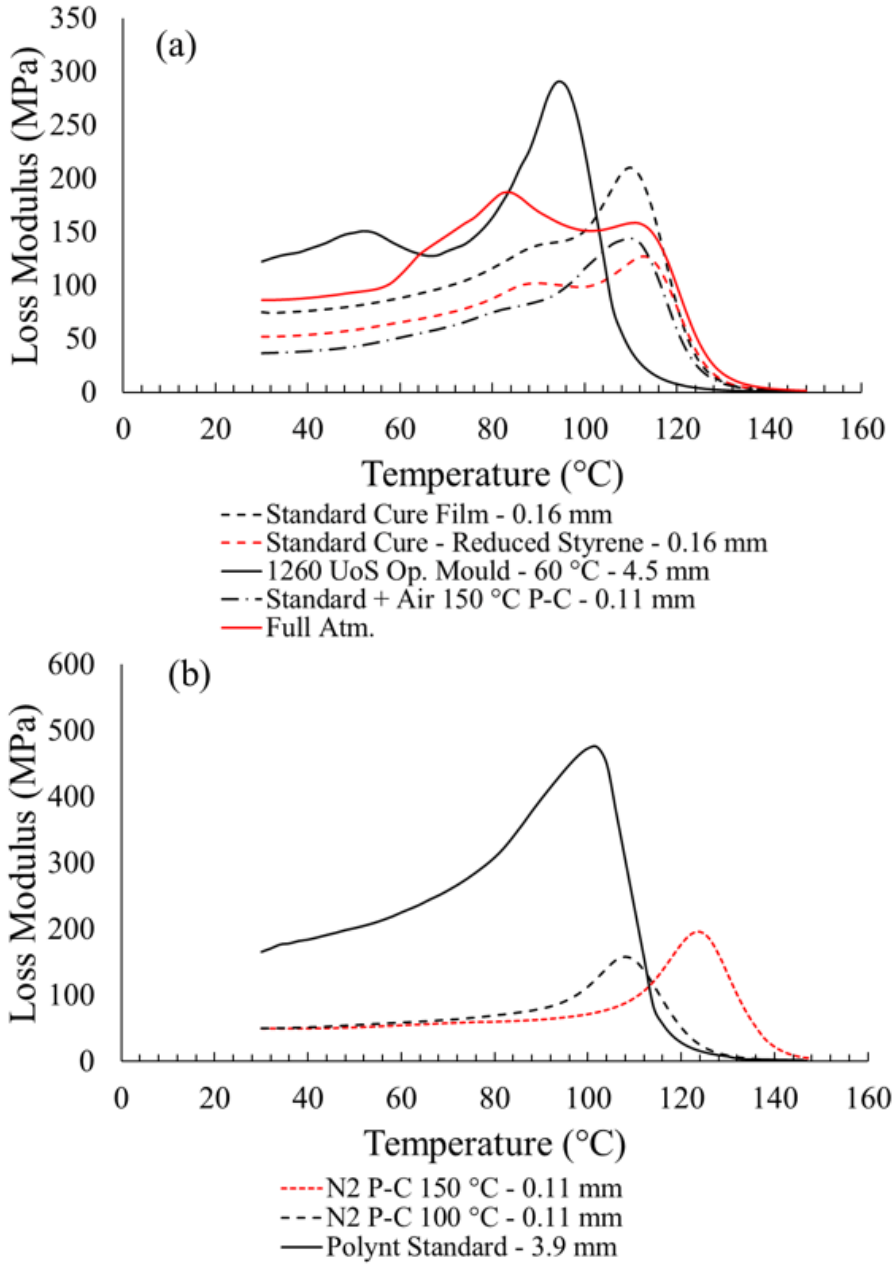

Figure 3-6: *(a) DMA thermal curves of DION 1260 specimens cured allowing interaction with oxygen during the cure and (or) post-cure phases, (b) DMA thermal curves of DION 1260 specimens cured allowing no interaction with oxygen during the cure and P-C steps.*

A low-temperature shoulder was present in the loss modulus curve of cured vinyl ester specimens regardless of the scale when, during the specimen preparation, there was exposure to ambient atmosphere at some point in the curing process. Although film specimens were cured under a nitrogen environment for the first part of the cure cycle, their particularly high surface-to-volume ratio makes them more susceptible to oxygen introduction during the

second stage of the cure in a convection oven under an air atmosphere. On the other hand, when an inert nitrogen atmosphere was used for the initial room temperature cure and elevated temperature post-cure, the shoulder in the loss modulus was no longer apparent. The effect of cure temperature was also found to be clear in the case of thin films; post-cure in an inert nitrogen atmosphere and a higher temperature of 150 °C resulted in a significantly higher Tg of 124 °C, while inert post-cure at 100 °C resulted in a Tg of 106 °C. If the post-cure temperature was set at 150 °C but no inert nitrogen atmosphere was used, the shoulder in the loss modulus was still apparent. This was another validation that the only case where the shoulder was present was when the vinyl ester resin had an interaction with oxygen, either in the initial or post-cure stages of the matrix.

In the previous section, it was observed that a styrene-rich environment resulted in a less pronounced shoulder in the loss modulus curve. It is also possible that a nitrogen environment may prevent potential retardation of styrene upon interaction with oxygen [47]. The fact that it is not solely styrene evaporation that causes the decrease in the Tg of one of the vinyl ester phases, presumably the styrene-rich phase, was that the loss modulus shoulder remained apparent regardless of the styrene content. Moreover, styrene loss is facilitated prior to solidification of the resin, whereas in this case interaction of the polymer with oxygen, even during the post-cure phase, was enough to result in the appearance of a lower temperature Tg. It is noteworthy that the "Full Atm" film, which was cured under the influence of oxygen at both cure phases featured two clear peaks in the loss modulus curve (*Figure 3-6a)*. The first peak was highly pronounced and broad, while the second peak, presumably indicative of the Tg of the vinyl ester phase remained at the same temperature level. This is expected since vinyl ester monomer conversion is completed before that of styrene [24], and the vinyl ester monomer is not a volatile component, as is styrene. It is thus likely that when styrene loss and oxygen inhibition act in combination, this results in reduced copolymerisation between styrene and vinyl ester, and in turn phase deconvolution, reflected in a double loss modulus transition.

Although research around oxygen inhibition of vinyl ester polymerisation remains limited, the following information was obtained by studying the literature. Oxygen has been associated with the formation of an inhibited layer on the surface of the free radically polymerised resins in contact with ambient air. The thickness of this layer has been found to be related to monomer composition and activating systems. Materials which possess lower viscosities have been found to have a greater thickness of un-polymerised resin, and lower exothermic heat releases during cure. This observation is in correlation with the DSC conversion results – *Figure 3-1* and *Figure 3-2*, which showed that as vinyl ester thickness was reduced, the exothermic

reaction peak of the cured material was increased. This inhibited layer has been reported to still possess the capacity of being polymerised further. This was in fact shown in the Tg (2) values presented in *Table 3-4*; when vinyl ester films were heated with a second heating cycle, the Tg obtained from the second heating ramp was increased [177]. According to Nouranian et al [48], the diffusion of oxygen into the free surface region of air-cured vinyl ester specimens can result in gradients in the inhibited layer, due to its lower cross-link density. As aforementioned, such effects may be amplified when sample thickness is significantly reduced [48,176]. Moreover, oxygen presence within polymer links has been associated with thermal instability [28]. The latter observation was evidently featured in the presented DMA results.

Fourier-transform Infrared Spectroscopy (FTIR)

The role of FTIR as a complement to thermal analysis results was crucial for a more thorough understanding of the cure kinetics of vinyl ester as a function of scale. Although a quantitative assessment of the degree of conversion was not possible for all specimens, qualitative indicators were sufficient to provide a clear image regarding the evolution of cure as a function of scale. Spectral comparisons between unreacted resin - film specimens and unreacted resin – bulk specimens cured under different conditions are featured in *Figure 3-7(a)* and *Figure 3-7(b)*, respectively. Individual styrene and vinyl ester monomer conversions for the "Polynt Standard" (thickness, t = 3.9 mm) resin casting and the "Full N_2 150 °C" (thickness, t = 0.11 mm) thin film are presented in *Table 3-7*. A quantitative conversion calculation could not be achieved for film and bulk specimens, which were cured allowing air interaction for either phase of the cure (initial cure, P-C). This was attributed to two primary reasons. One of them was excess styrene evaporation confusing the calculation and resulting in inaccuracies. The reduction in the styrene content of the resin was identified by studying the C-H backbone of styrene at 695 cm^{-1}. It is clear that the decrease in styrene was least for the "Polynt Standard" and the "Full N_2 – 150 °C" film. On the other hand, styrene evaporation reached a maximum for the "UoS Op. Mould" and the "Full Atm." film, for which interaction with the ambient atmosphere was allowed in both phases of the cure. Styrene evaporation was also evident in the "standard" cure film specimen with the spectral area at 695 cm^{-1} being found in-between the specimens cured for both phases under an ambient and an inert N_2 environment. Thus, a pattern of increasing retained styrene was featured, as interaction with oxygen was minimised. The depletion in the C=C of styrene at 910 cm^{-1}, indicative of styrene monomer reaction, increased as the cure became more rigorous, as shown in *Figure 3-7*. Notable depletion of the latter spectral band was featured by the specimens in which the largest styrene evaporation occurred ("UoS Op. Mould", "Full Atm."). Nonetheless, it should be taken into account that

there was only a very small portion of styrene left to react and thus an over-prediction of the cure degree of the specimen could be made. A similar observation was made by Scott et al [178], who stated that "*at low styrene levels, the copolymerisation does not need to proceed very far before most of the styrene is consumed, and so high styrene conversions are observed*".

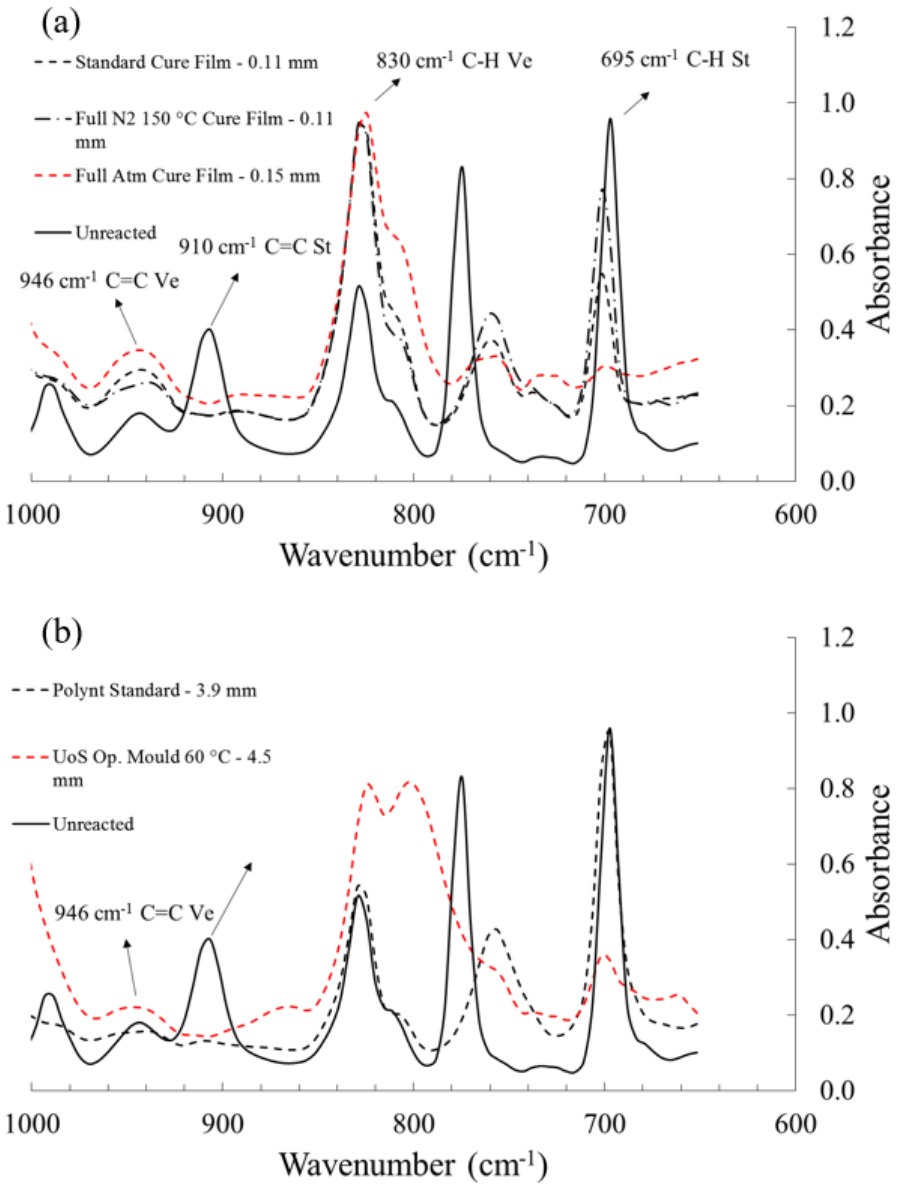

Figure 3-7: *(a) FTIR spectra of unreacted DION 1260 and film specimens cured under different conditions, (b) FTIR spectra of unreacted DION 1260 and bulk specimens cured under different conditions.*

DION 1260 Specimen	Thickness (mm)	VE Conversion (α_{VE})	St. Conversion (α_{St})
Polynt Standard	3.99	0.38	0.94
Full N_2 150 °C	0.11	0.17	0.91

Table 3-7: *DION 1260 vinyl ester (VE) and styrene (St) monomer conversions obtained through FTIR.*

The second reason why a quantitative analysis was infeasible was that a different chemistry could be identified for the specimens affected by the presence of oxygen when compared to specimens cured by minimising oxygen interaction in both cure phases. More specifically, an unexpected increase in the C=C of vinyl ester at 946 cm^{-1} was of particular interest. In fact, the measured spectral area featured by oxidised specimens was higher than the spectral area of the unreacted resin, instead of the spectral band being depleted with cure. It is yet uncertain whether this increase also took place for "Full N_2 150 °C", but was less amplified. Generally, the effect was more discernible on film specimens, which exhibited a higher surface-to-volume ratio. Similar results have been reported by Arrieta et al [179], who presented an increase in the spectral area of C=C for vinyl ester films oxidised at different temperatures. A shoulder was also present between around 1730 cm^{-1} and 1775 cm^{-1} for specimens affected by oxidation, as shown in *Figure 3-8*. This shoulder is indicative of the build-up of carbonyl products and in particular the conversion of an ester into an anhydride [179]. The shoulder was found to be more significant for specimens cured under air for both phases of the cure, such as the "UoS Op. Mould" and the "Full Atm", whereas it was least apparent for the bulk "Polynt standard" and the "Full N_2 150 °C". Although the shoulder appeared to be smaller for the "standard" cure film, the spectral band is rather broad indicating that the specimen may still be affected by oxygen.

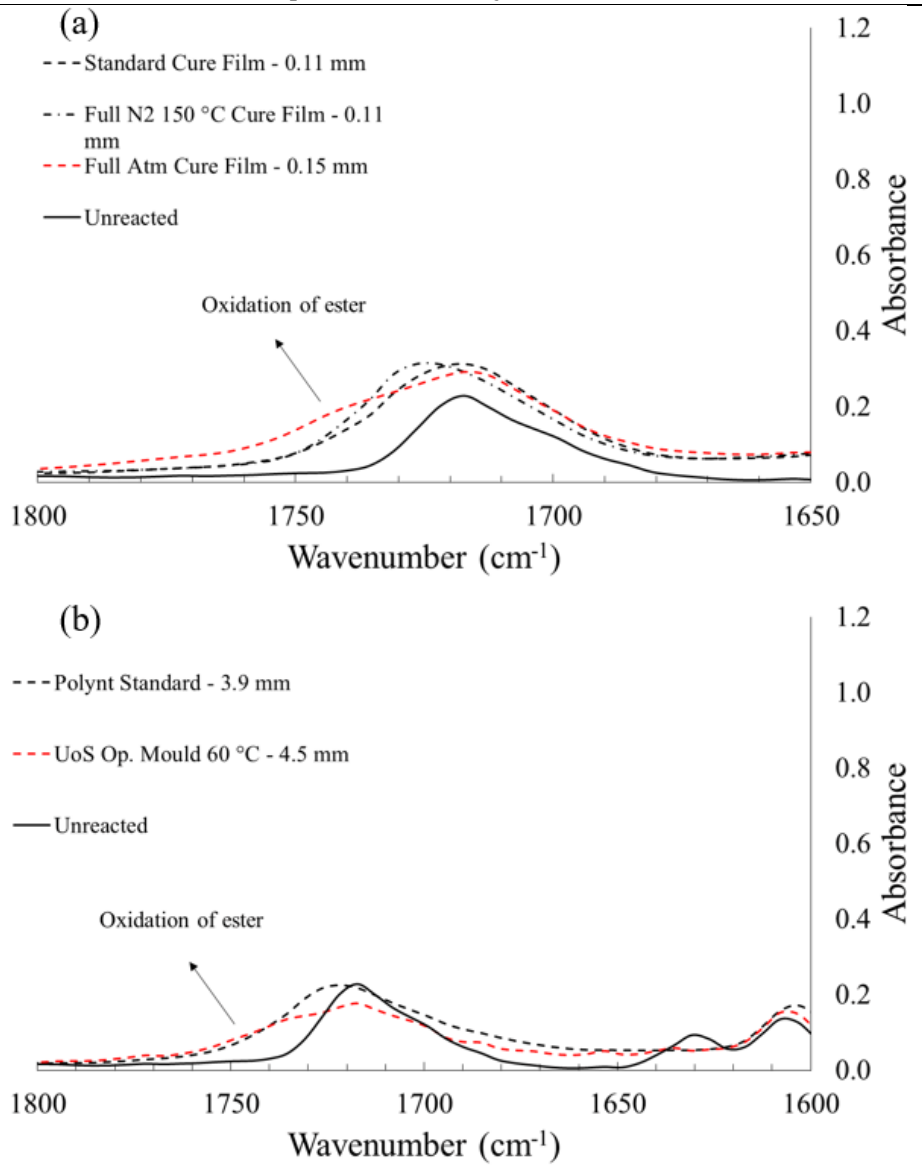

Figure 3-8: *(a) FTIR spectra of unreacted DION 1260 and film specimens cured under different conditions revealing oxidation of ester group, (b) FTIR spectra of unreacted DION 1260 and bulk specimens cured under different conditions revealing oxidation of the ester group.*

A notable increase of the C-H backbone of vinyl ester at 830 cm^{-1} was also observed for all specimens, except for the bulk "Polynt Standard". Thus, it should be noted that since the peak was used as internal reference for the conversion calculation of the vinyl ester monomer, it is likely that there was an under-prediction in the vinyl ester conversion of the "Full N_2 150 °C" film. The increase was maximum for the bulk "UoS Op. Mould" specimen, while the formation of two clear peaks was also observed. The reason for the latter, as well as the increase in the spectral area, was believed to be either interaction with oxygen or styrene

evaporation. However, such an effect could not be identified in the studied literature. The increase in 830 cm^{-1} was found to begin to take place from the manufacturing stage but was exaggerated in the presence of oxygen during curing. On that basis, the following experiment was conducted; unreacted resin spectra were compared with spectra of unreacted resin, which was spread on a substrate in the format of a thin film and degassed for 10 minutes to resemble the procedure carried out in film manufacturing. A spectral comparison between unreacted and degassed resin is shown in *Figure 3-9*. It can be seen that the increase in C=C took place upon the processing of the unreacted resin, while the C-H of styrene at 695 cm^{-1} remained the same (no significant styrene evaporation). Although it is still uncertain of what can cause such a change in chemistry, the effect of oxygen is suggested, since it is the only variable parameter in the experiment, upon the spectral indication that the styrene content remained at a similar level after the degassing of the resin. It is likely that an oxygen-inhibited layer discussed in the previous section started to develop when the resin was spread onto the substrate and subsequently degassed, as the surface-to-volume ratio of the resin layer increased.

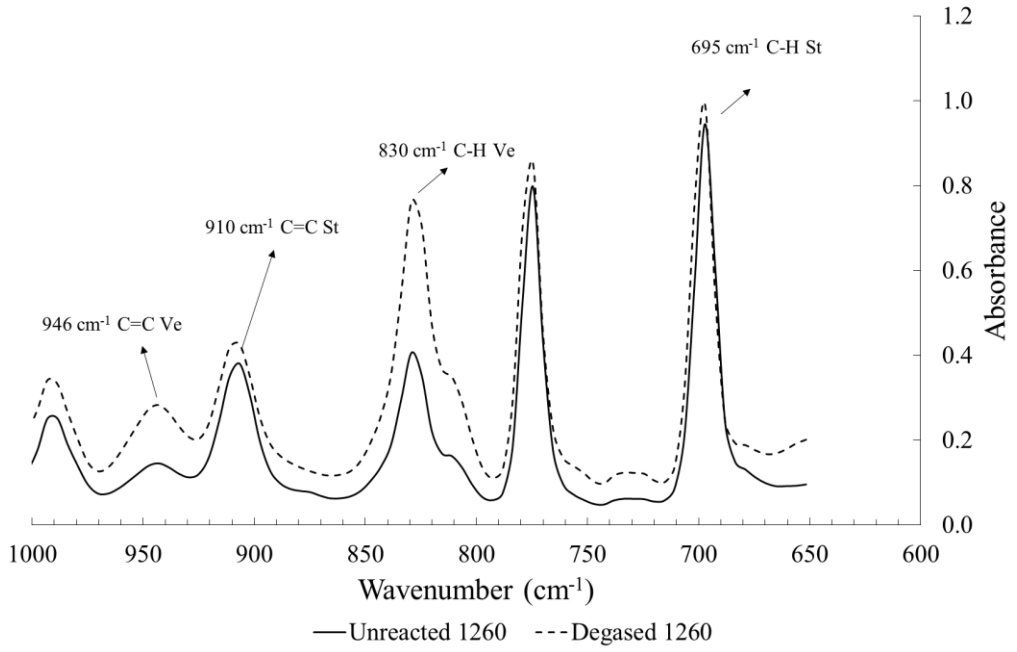

Figure 3-9: *FTIR spectra of unreacted vs degassed DION 1260.*

3.2.2. The Chemistry and Thermal Properties of DION 1273

Thermal Analysis – Effect of Scale and Effect of Oxygen on Polymerisation

A more preliminary study was conducted for DION 1273 when compared to DION 1260. The purpose of this analysis was to provide a better understanding of the behaviour of the resin used as a composite/micro-composite matrix in the following chapters, and to allow basic comparison between the two resin systems. DSC thermograms of DION 1273 as a function of specimen thickness are shown in *Figure 3-10*. Tg values from both heating cycles are tabulated in *Table 3-8*. A clear Tg reduction was featured between the bulk scale "Polynt Standard" resin casting and the "standard" cure films, in a similar fashion to the DION 1260. However, despite a notable Tg variation between the microscale and macroscale, both film specimens exhibiting different thickness ranges, $0.1 < t < 0.2$ mm and $t \leq 0.1$ mm, featured the same Tg of 68 °C and a single transition. The Tg of thin films revealed by DSC was similar to that of DION 1260 in the thickness range $0.1 < t < 0.2$ mm. However, the transitions featured in *Figure 3-10* appear to be rather broad and complementary DMA results were produced.

A DMA thermal curve comparison of DION 1273 films post-cured at different conditions, and a "Polynt Standard" 3.9 mm plate are presented in *Figure 3-11*. A Tg study as a function of material thickness was not allowed by DMA, due to the use of different strains and test methods (film tension vs 3-point bending). However, *Figure 3-11* allowed a comparison of the thermal behaviour between thin film and bulk plate specimens, as well as the effect of the cure environment on Tg between films of a similar thickness.

First of all, the Tg of a 0.14 mm thick DION 1273 film was found to be 87 °C. This was notably lower than the high-temperature Tg obtained for DION 1260 of a similar thickness (107 °C) but similar to the low-temperature Tg indicated by the DION 1260 loss modulus shoulder (88 °C). Please note that this result was obtained using DION 1260 and DION 1273 films of a similar thickness as well as the same DMA input parameters, thus a direct comparison was allowed. Post-curing DION 1273 under N_2 and a higher temperature resulted in a Tg of 98 °C, which was considered a significant improvement. This was nonetheless notably lower than the Tg obtained by DMA (using the same test parameters) for its DION 1260 counterpart – 124 °C. It can be deduced that DION 1273 possesses a lower Tg than DION 1260 on the microscale, but such a statement is not definitive given the low-temperature transition for DION 1260.

In *Figure 3-11*, it can be seen that particularly in the glass region, the loss modulus curve of the "standard" cure film is broader than that of the "Full N_2 150 °C" film and that of the bulk "Polynt Standard". The broadening of the loss modulus curve in the glassy state of the "standard" cure film may be a hint of a secondary transition starting to appear. In addition, for films within the same thickness range, there was a clear increase in the storage modulus magnitude for the "Full N_2 150 °C" film in the rubbery region, when compared to that of a "standard" cure film. This may be an indication of higher cross-linking for the film specimen post-cured under nitrogen at a higher temperature when compared to the "standard" cured film. That was despite a potential higher styrene loss for the latter which is known to increase cross-link density. In particular, styrene loss was found experimentally for DION 1260 to result in a cross-link density increase, while similar results have also been previously reported in the literature [45]. Besides, the cross-link density increase for "Full N_2 150 °C" was accompanied by a Tg increase, as discussed. All the above observations lead to the conclusion that in a similar fashion to DION 1260 there is a change in the material properties of DION 1273 when its surface-to-volume ratio is increased, which may be compensated only when rigorous cure and post-cure conditions are employed.

Overall, DION 1273 showed a lower Tg than DION 1260 on the macroscale. This is probably true on the microscale too, if one compares the Tg of DION 1273 to the high-temperature Tg of DION 1260, as indicated by DMA. Nonetheless, DION 1273 exhibited a more stable thermal behaviour on the microscale than DION 1260. The latter statement refers to the attainment of a similar Tg between thicker films (0.13 mm thick) and thinner films (0.03 mm thick), which was not the case in DION 1260. Moreover, although there was broadening of the loss modulus curve of "standard" cure films, a pronounced shoulder was not apparent, as was the case in DION 1260. Oxygen inhibition during DION 1273 polymerisation was considered when the surface-to-volume ratio of the material was increased, and despite the employment of an initial N_2 cure step. Although probable oxygen inhibition did not result in a profound Tg deconvolution between the styrene and the vinyl ester phases of the polymer, as in DION 1260, based on DSC results they led to Tg depression. Thermal analysis results on DION 1273 were deemed preliminary and future work on the topic may be desirable.

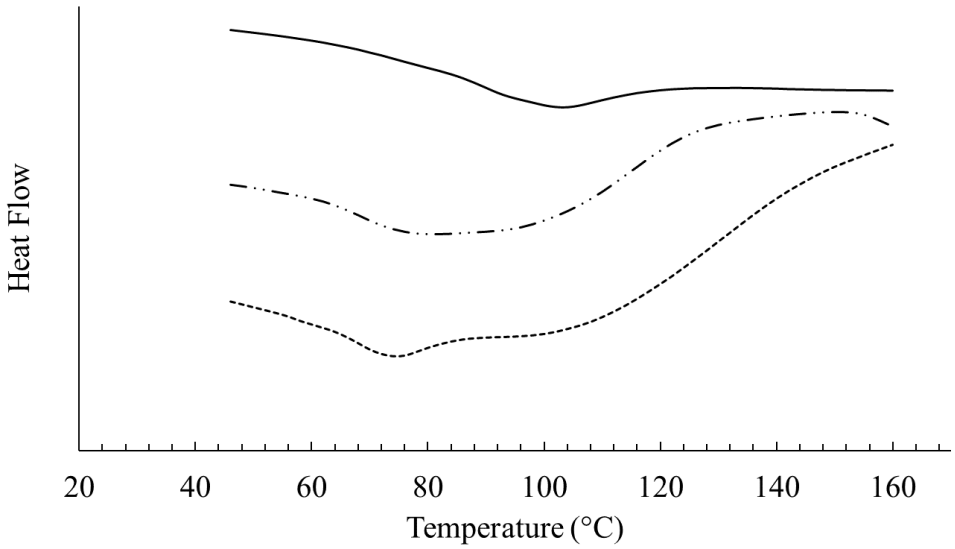

Figure 3-10: *Comparison of DSC thermograms – 1st heating cycle – as a function of "standard" cured DION 1260 thickness. Curves were stacked by using an offset in the Y axis and therefore Y axis values are arbitrary.*

Thickness (mm)	Tg (1) (°C)	Tg (2) (°C)
3.9 ± 0.2*	90	96
0.13 ± 0.02	68	94
0.03 ± 0.02	68	92

Table 3-8: *Tg change vs thickness of DION 1273. Tg (1) represents the step change in temperature in cycle 1 and Tg (2) in cycle 2.*

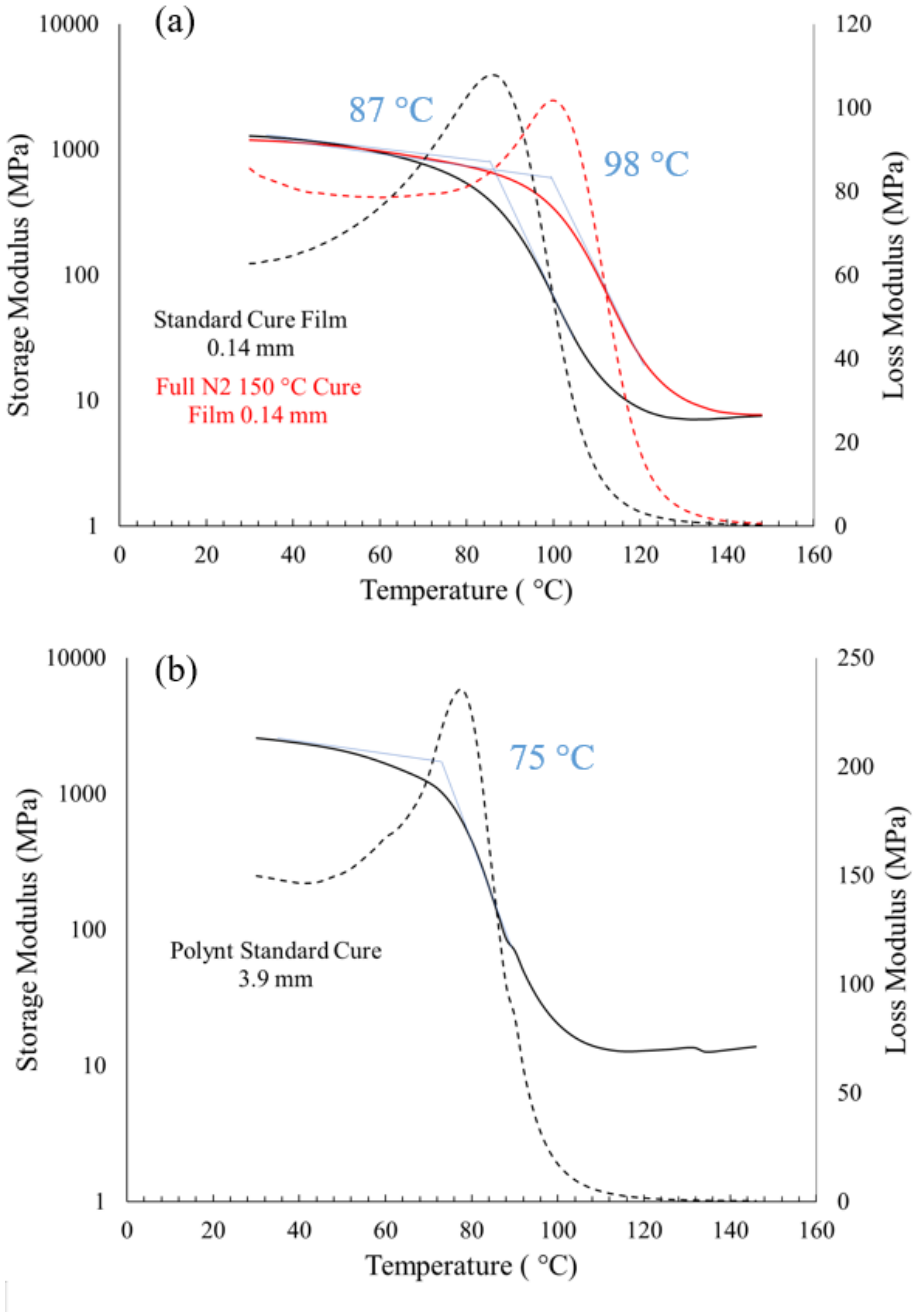

Figure 3-11: *(a) DMA thermal curve of DION 1273 films cured under different conditions, (b) DMA thermal curve of a DION 1273 Polynt "standard" cure plate.*

Fourier-transform Infrared Spectroscopy (FTIR)

Due to the complex and confidential network of DION 1273, a preliminary ATR-FTIR study was conducted as a complement to thermal analysis results. A spectral comparison between unreacted matrix and polymers cured under different conditions is presented in *Figure 3-12*. Despite the complexity of DION 1273, some general conclusions can be drawn. First and

foremost, the spectra confirm the variation in the degree of cure between "standard" cure bulk and thin film specimens. Substantial styrene evaporation was confirmed for the "standard" cure film by monitoring the C-H of styrene at 695 cm^{-1}. The use of N_2 reduced styrene evaporation and enhanced the overall degree of cure. This was confirmed by monitoring the C=C of styrene and vinyl ester at 910 cm^{-1} and 940 cm^{-1}, respectively. In a similar fashion to FTIR results on DION 1260, a shoulder appeared around 1730 cm^{-1} and 1775 cm^{-1} for thin film specimens, as shown in *Figure 3-12*. The appearance of this shoulder has been previously associated with the formation of carbonyl products and in particular the conversion of an ester into an anhydride in vinyl esters [179]. Furthermore, an increase in several band intensities was observed for both "standard" and "Full N_2 – 150 °C" cure film specimens, which was believed to be due to oxidation effects. In particular, a notable increase in the C-O stretch of ester groups between 1040 cm^{-1} and 1115 cm^{-1} was observed. Similar results have been reported by Namouchi et al [180] for oxidised polymethyl methacrylate (PMMA) specimens. The intensity increase was in fact found to be greater for the "standard" cure film, which was post-cured in air. Besides, there is clear variation in the shape of the peaks for the "standard" cure film, but the reason for this change remains unknown. Other significant band intensities between "Polynt Standard" and the film specimens were seen at the spectral regions between 1184 cm^{-1} and 1220 cm^{-1}, and 1465 cm^{-1} and 1565 cm^{-1}. Even though a band assignment for these was challenging due to the confidential polymer network of DION 1273, oxygen inhibition was considered, as per the observations of Namouchi et al for an intensity increase in all IR bands for oxidised PMMA. On a qualitative basis such pronounced changes between film specimens and the bulk "Polynt Standard" confirm variation in the chemistry between microscopic and macroscale specimens.

A conversion calculation was conducted for the styrene and vinyl ester monomers for all specimens and the results are shown in *Table 3-9*. As opposed to the DION 1260, the calculation could be achieved even for the "standard" cure film, which underwent styrene evposation. It should be noted that the DION 1273 formulation already contained an appreciably lower styrene content than the DION 1260 and so potential styrene loss may have a smaller impact on the cross-linking of the final polymer. The conversion calculation showed a rather low styrene conversion for the "standard" cure film, which nonetheless reached a level close to the bulk polymer when N_2 cure was employed. The vinyl ester monomer conversion remained at a relatively high level for the latter specimen and was fully reacted when an N_2 environment was used in the post-cure phase. Nonetheless, it is noteworthy that significant changes were observed at the C-H vinyl ester backbone at 830 cm^{-1}, used as internal reference and therefore some deviation from the reported values may be possible.

In conclusion, despite the complex network of DION 1273, the conducted FTIR analysis was useful in confirming variations in chemistry between a fully cured bulk specimen, a "standard" cure film and a post-cured in N_2 at a higher temperature. Effects of oxygen inhibition of the curing polymer and excess styrene evaporation were detected by FTIR in DION 1273 films. In a similar fashion to DION 1260, such effects were promoted by the particularly high surface-to-volume ratio of the films. A conversion calculation was achieved for DION 1273, showing rather poor curing for "standard" cure films and improved curing when matrix films were post-cured in N_2 at a higher temperature. However, the analysis may be deemed preliminary due to the large shift in the C-H vinyl ester backbone at 830 cm^{-1}, used as internal reference.

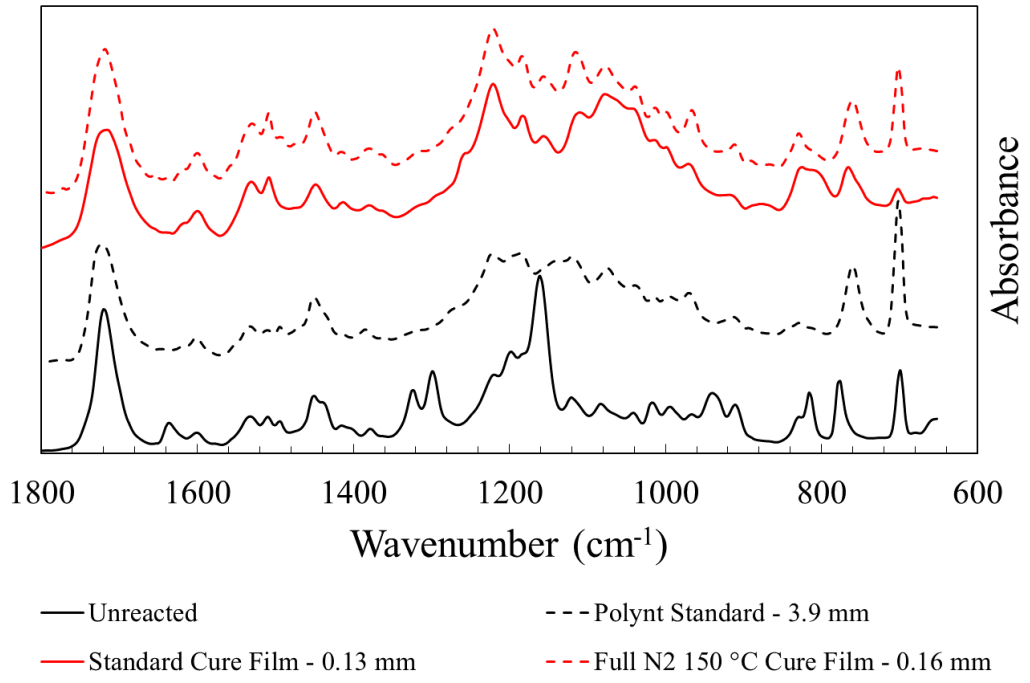

Figure 3-12: *FTIR spectra of unreacted DION 1273, bulk and film specimens cured under different conditions.*

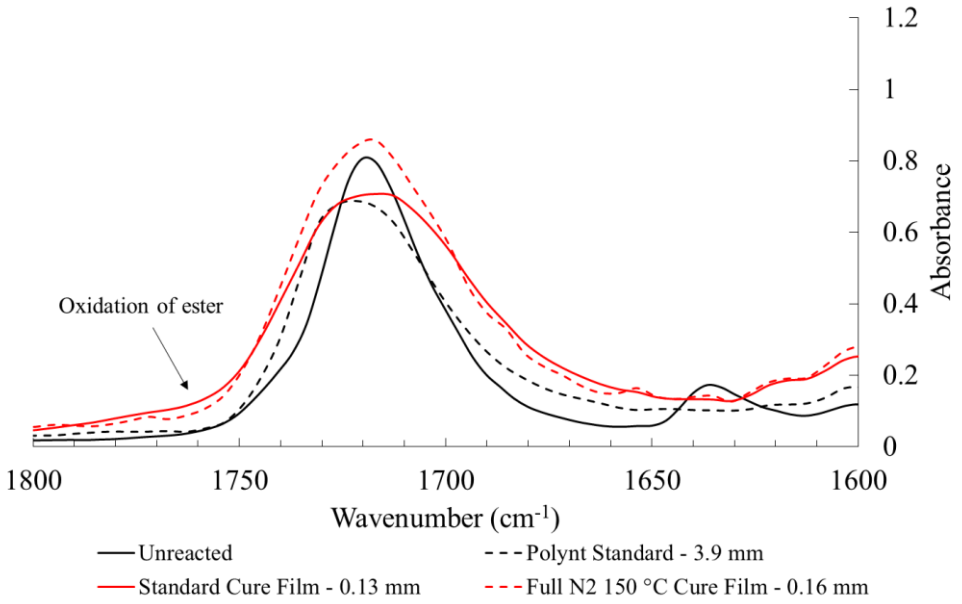

Figure 3-13: *FTIR spectra of unreacted DION 1273 film specimens cured under different conditions, and bulk DION 1273 "Polynt Standard" revealing oxidation of ester group.*

DION 1273 Specimen	Thickness (mm)	VE Conversion (αVE)	St. Conversion (αSt.)
Standard	0.13	0.8	0.03
Full N_2 150 °C	0.16	1	0.57
Polynt Standard	3.9	1	0.64

Table 3-9: DION 1273 vinyl ester (VE) and styrene (St) monomer conversions obtained through FTIR.

3.3. CONCLUDING REMARKS

This study aimed to provide a better understanding of the cure kinetics and thermal behaviour of vinyl ester as a function of scale. DSC provided an indication of a dual Tg in DION 1260 thin film specimens, consisting of a low-temperature transition between 55 °C and 65 °C, and a higher temperature transition between 81 °C and 101 °C. Re-heating the specimens in DSC resulted in a single, higher-temperature transition, indicative of incomplete cure in the original specimens. The lower-temperature transition of thin films was also revealed by the appearance of a shoulder in the DMA loss modulus curve. A study of varying styrene content in DION 1260 films showed that the loss modulus shoulder was more pronounced for styrene-poor films

and less apparent when a styrene-rich environment was used. The Tg of films was found to be loosely dependent on styrene; nonetheless, a minor Tg increase, as well as an indication of increased cross-link density, were obtained for styrene-poor films. The loss modulus shoulder was found to disappear fully when a full N_2 environment was employed during curing, while the Tg of DION 1260 films was increased further when a higher P-C temperature of 150 °C was used. Thus, data clearly suggested that the exposure of high surface-to-volume ratio specimens to atmospheric conditions, even during the post-cure phase, accompanied by styrene loss, reduced copolymerisation of styrene and vinyl ester monomers, and was the driver of the lower temperature transition that can be found in thermal analysis data. Regarding the deconvolution of the diphasic vinyl ester network in DION 1260 thin films, the lower temperature Tg was attributed to the styrene-rich phase of the matrix, given the excess monomer evaporation and knowing that the cross-link density of the styrene-rich phase is lower than that of the vinyl ester phase.

Regarding the thermal behaviour of DION 1273, the matrix showed a lower Tg than the DION 1260 on the macroscale, and possibly on the microscale if one compares that to the high-temperature Tg obtained by DION 1260. Nevertheless, DION 1273 showed a more stable thermal behaviour than DION 1260 on the microscale; the Tg of DION 1273 films was found to be the same regardless of film thickness, while only a single transition was featured. Oxygen inhibition during DION 1273 thin film polymerisation was considered responsible for the Tg reduction in films. A hint of a secondary transition was also detected for "standard" cure DION 1273, which was depleted when an N_2 environment was employed at both cure phases.

FTIR results confirmed excess styrene loss from DION 1260 films during curing and suggested that oxidation effects start to take place at the manufacturing stage. Nevertheless, the use of an N_2 environment throughout the full cure of DION 1260 films showed higher conversion, closer to that of the bulk specimens. Similar effects were found to take place on the DION 1273, even though the analysis remained at a preliminary level as a predecessor to the following chapters where the resin is used as a composite constituent.

The obtained results confirm that one must be very wary when making the extrapolation from a macroscale to a microscale regarding vinyl ester curing and material property transferability. However, despite the complicated change in the vinyl ester network between the two scales, an encouraging indication was shown regarding the "design" of a cure environment, which will prevent degradation effects during curing of specimens with a high surface-to-volume ratio. In particular, oxidation and styrene loss effects were significantly reduced by the use of more rigorous cure conditions.

CHAPTER 4: THE INTERFACE OF GLASS FIBRE/VINYL ESTER AND THE INFLUENCE OF THE FIBRE FIXING ADHESIVE ON SINGLE FIBRE MICROBOND SPECIMENS

This chapter is aimed at providing insight into the micro-mechanical performance of glass fibre/vinyl ester micro-composite systems, assessed by means of the microbond test. The transferability of cure kinetics of films presented in *Chapter 3* to vinyl ester microbond droplets is discussed. A novel observation regarding the interaction of glass fibre sizing with the cyanoacrylate glue (CA) adhesive widely used to adhere the fibre onto the substrate accommodating single fibre specimens is presented. Lastly, a comparison between the DION 1260 and DION 1273 matrices on vinyl ester-compatible glass fibres made of a different glass formulation, but of the same sizing is enabled – SE 3030 (Advantex), W 3030 (HiPertex). Scanning Electron Microscopy (SEM) was also employed to observe possible differences in the morphology and structure of the micro-composites, as a complement to micro-mechanical testing.

4.1. EXPERIMENTAL

4.1.1. Materials

Matrix

The DION 1260 vinyl ester resin was used and was considered the "baseline" matrix in this and the DACOMAT study, and the majority of experiments involved its use. This is a bisphenol epoxy-based vinyl ester resin with 48 – 52 % styrene, supplied by Polynt. The resin was mixed with a BC-21 UN 3103 Organic peroxide type C initiator supplied by United Initiators GmbH at a ratio resin-to-styrene of 97.5 to 2.5 by weight. The cure schedule was 24 h at RT under an inert N_2 environment and post-cured at 24 h at 60 °C, 3 h at 80 °C, and 1 h at 100 °C in an air circulating oven ("standard" cure). DER 332 bisphenol-A diglycidyl ether (DGEBA) epoxy-based matrix was used for comparative purposes. The resin was mixed with a triethylenetetramine (TETA) tetrafunctional amine curing agent at a stoichiometric ratio of 14.3 phr. The cure schedule of the epoxy resin was 2 h at 60 °C, followed by 1 h at 120 °C, at a heating rate of 2 °C/min, in an air circulating oven.

Fibres

Fibre details of all glass fibres used in this study are contained in *Table 4-1*. All experiments were carried out with boron-free E-glass fibre. All fibres came in the form of large rovings.

SE 3030 and W 3030 are commercial glass fibres, fully sized and multi-compatible, provided by 3B. The SE 3030 fibre with DION 1260 resin was the "baseline" composite/micro-composite combination used throughout this project, according to the material combination selection for DACOMAT laminates. SE 3030 and W 3030 were tested in all combinations with the DACOMAT vinyl ester resins DION 1260 and DION 1273 to allow comparison between the same sizing on different fibre substrates. The 2002 and 2026 fibres were supplied in the latter stages of the project were used for comparative purposes. These also exhibited a multi-compatible sizing and were supplied by Nippon Electric Glass. The SE 2020 fibre is a commercial epoxy-compatible fully sized fibre and was also supplied by 3B fibreglass.

Designation	Sizing Compatibility	Avg. Measured Fibre Diameter (µm)	Nominal Tex (gr/km)	Supplier
SE 3030	Vinyl ester, polyester, epoxy	19	1200	3B
W 3030	Vinyl ester, polyester, epoxy	19	1200	3B
2002	Vinyl ester, polyester, phenolic, epoxy	18.8	2400	NEG
2026	Vinyl ester, polyester, epoxy	17.6	2400	NEG
SE 2020	Epoxy	19.4	1200	3B

Table 4-1: *Glass fibre details.*

4.1.2. Microbond Test

Microbond Rig and Sample Preparation

In this study, microbond testing was conducted using both card frames as well as a stainless steel rig fabricated in-house. Card frames are commonly employed in single fibre microbond testing and are used as a default setup by the Advanced Composites Group (ACG) [90,181,182]. The purpose of a stainless steel rig was to allow the conditioning of single fibre micro-composites in hydrothermal environments. Single fibre micro-composites were adhered onto stainless steel washers. A high-grade stainless steel material was selected for the manufacturing of the rig to prevent moisture-induced rusting. Although ageing results are not included in this chapter, the majority of microbond testing was conducted using stainless steel rigs and washers to allow comparison between un-aged and aged specimens. The rig was

designed using Solidworks 2018 and was manufactured at the University of Strathclyde MAE workshop by water jet cutting. A 2-D CAD drawing with dimensions and a picture of the rig are featured in *Figure 4-1 (a)* and *Figure 4-1 (b)*, respectively. Each microbond rig exhibited a length of 130 mm, a width of 70 mm, and a thickness of 2.5 mm. It contained ten circular incisions – five on each side opposing each other and divided by a window. The width of the window was 20 mm. The role of the incisions was to enable the position of the washers, which accommodated the single fibre micro-composites. Each pair of washers opposing each other produced two microbond specimens, as fibres were positioned along the length of the inner window, aligned along the vertical axis.

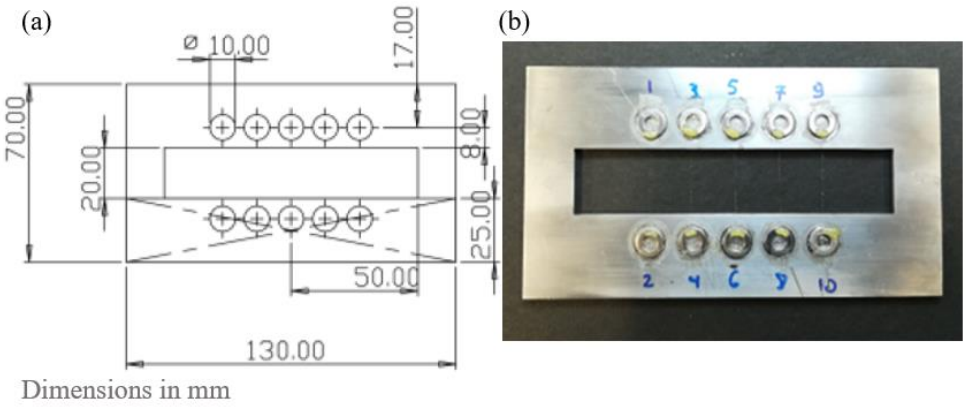

Figure 4-1*: (a) CAD drawing of microbond rig with dimensions, (b) microbond rig containing single fibre, microbond specimens.*

The washers exhibited an outside diameter of 9 mm and were adhered onto the circular incisions of the rig by double-sided tape. Double-sided tape was also introduced on the top end of each for the mounting of fibres. The fibres were then secured onto the washers with Araldite epoxy. The latter was placed on the inner end of the washer, closer to the gap of the rig, and was left to cure for a minimum of 2 hours prior to micro-droplet application. Extensive care was taken in the application of Araldite epoxy to the inner end of the fibre to prevent spreading on the fibre and thus avoid discrepancies in the gauge length value. Each fibre was selected from a fibre bundle, approximately 20 cm long. Each fibre bundle was removed from the inside of a larger fibre roving in order to reduce to ensure the integrity of the fibre and avoid the probability of failure during transport.

The effect of the fibre-fixing adhesive on the IFSS of vinyl ester was also investigated. Although Araldite epoxy (EP) was used to fix fibres on stainless washers to allow ageing in

water, cyanoacrylate glue (CA) – commonly known as "superglue" – has been the default adhesive for fixing fibres on card windows by the ACG [90,181,182]. Upon application on the fibres (at the edge of the card), CA was left to react fully for 24 h, prior to microbond droplet application.

Vinyl ester resin was maintained in a fridge at a temperature of 8 °C. It was removed from the resin container by the use of a pipette, was transferred into small capsule-like, air-tight containers preventing styrene vaporisation, and was left to reach room temperature 24 h before use. Prior to use, liquid resin was placed into a small plastic container by the use of a pipette and curing agent was gradually introduced to the pre-polymer mix by the means of a syringe with a fine needle point to ensure precision in the stoichiometric ratio. Approximately 2 g of resin were used per application. The mixture was weighed using a microbalance and was stirred thoroughly for at least 30 seconds. Vinyl ester preparation was carried out under a fume cupboard to avoid human exposure to styrene. Epoxy was degassed under vacuum for 10 min to remove entrapped air from the mixture and enhance mixture homogeneity, prior to application. Several micro-droplets were applied onto each fibre by the means of a short steel wire of 0.125 mm in diameter. The resin application involved the "tapping" of the end of the wire, including a minute volume of resin onto each fibre, forming a micro-droplet. Several droplets were applied on each fibre and a dry area was left in the mid-section to define each pair of specimens. The micro-droplet application was followed by the curing of the specimens, and post-curing, wherever applicable. A schematic illustration of the sample preparation procedure is presented in *Figure 4-2.*

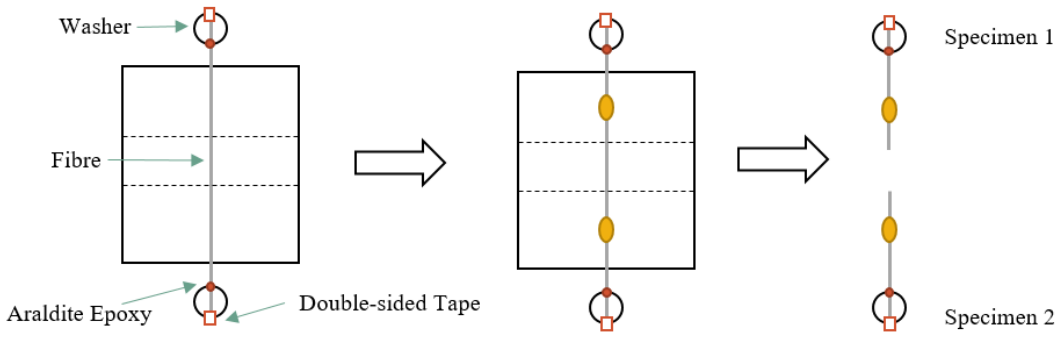

Figure 4-2: *Schematic illustration of the microbond test sample preparation.*

Upon post-cure, micrographs of microbond droplets were captured by the means of a Leitz Ergolux optical microscopy, at 200x magnification. The most suitable, axisymmetric droplets

were identified for each specimen. Droplets that were too large, small or non-axisymmetric were not tested due to concerns regarding fibre fracture, slippage between shearing blades, and uneven load distribution, respectively. The dimensions of each specimen, such as fibre diameter, droplet embedded length and droplet diameter were measured using the image processing software ImageJ, and were used as an input for the operation of the test. Acceptable droplet dimensions were approximately within the range of 100 - 180 μm in embedded length, and 65 - 105 μm in diameter. The micrograph of a typical microbond specimen is presented in *Figure 4-3*. Prior to testing, fibres were cut across the horizontal axis and in the mid-point of the extending fibre, producing two specimens. Each specimen was removed from the rig by carefully disjoining the washer from the circular incision to hang from the load cell hook and enable the testing procedure. The sample preparation method remained consistent throughout the project and each batch consisted of a minimum of 15 specimens (maximum of 30 specimens). Confidence limits of 95 % were used allowing for sufficient data for a valid statistical analysis.

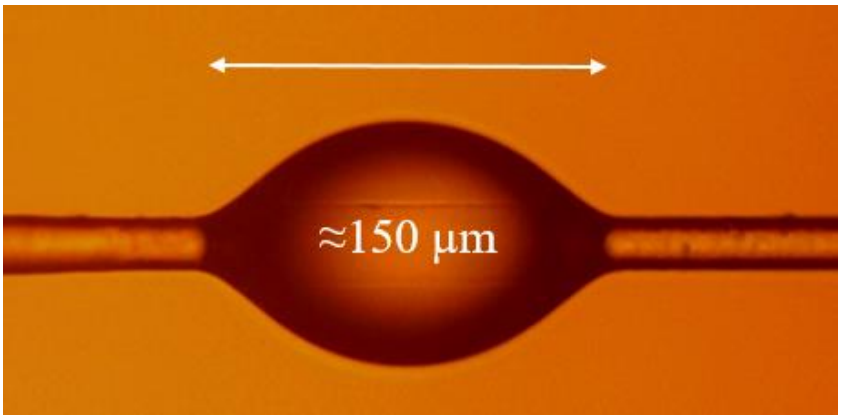

Figure 4-3*: Micrograph of a typical microbond droplet captured at 200x magnification.*

Microbond Testing Procedure

The microbond test is operated by adjusting the shearing blades to the diameter of a fibre filament restraining its movement, followed by the application of a load and while the test droplet is restrained. The test is ended upon the debonding (loss of adhesion) of the micro-droplet and the IFSS required to result in the debond is then recorded. The test apparatus featured a linked network of a tensile testing machine (Instron 3342), a stereo microscope (max magnification: 45x) and a DCM130 camera with output on a computer screen. The experimental rig was operated through a computer by using the Bluehill 2 software. The movement of the searing blades was controlled at a resolution of 1 μm by two micrometres

adjusted on each side of the microvice. The development of the testing ring was conducted by Yang and Thomason [69].

The specimen was positioned on the rig by hanging the washer from the load cell hook. It was then moved vertically using a fast crosshead velocity until the droplet to be tested was identified. The crosshead velocity was then reduced and the LHS blade was brought close to the fibre, creating contact. It was then moved slightly backwards to prevent excess "dipping" and the RHS blade was then brought close to the fibre carefully until a slight bend of the fibre was achieved. Subsequently, the RHS blade was also drawn slightly to set the gap width, enabling the free vertical movement of the fibre, and while the droplet remained constrained. During the test, the fibre was pulled upwards by a shearing force at a rate of 0.1 mm/min using a 10 N load cell. Loss of adhesion occurred when the shearing force surpassed the IFSS. Whenever the shearing force was higher than the ultimate fibre tensile strength, fibre fracture was apparent. Moreover, due to the difficulty of aligning the washer and in turn the fibre in a precise vertical position, fibre twisting was frequently observed, resulting in lower IFSS values. When the latter two cases were evident, generated results were excluded from the analysis. The apparatus setup used for the microbond test is presented in *Figure 4-4*.

Figure 4-4: *Microbond test rig setup.*

The calculation of IFSS was carried out through the use of the following equation – *Equation 4-1*.

$$IFSS = \frac{F_{max}}{A_e} = \frac{F_{max}}{\pi * L_e * D_f}$$

4-1

where: $IFSS$ is the interfacial shear strength, F_{max} is the maximum applied load, A_e is the embedded area of the micro-droplet, L_e is the embedded length of the micro-droplet (including the meniscus) and D_f is the fibre diameter.

The test output was in the form of an applied force vs crosshead displacement plot. Depending on the type of debond produced, three typical plot trends were identified, as follows:

1. Successful debond; slight curve at the region of the maximum load. The appearance of a frictional component, due to the debonded micro-droplet being dragged downwards along the surface of the fibre, as the fibre is pulled upwards – *Figure 4-5 (a)*.
2. Successful debond; slight curve at the region of the maximum load. Significant deformation and removal of the droplet from the fibre surface, and thus no presence of a frictional component - *Figure 4-5 (b)*.
3. Premature fibre fracture. In this case, the load usually follows an abrupt drop after it has reached its maximum magnitude - *Figure 4-5* (c).

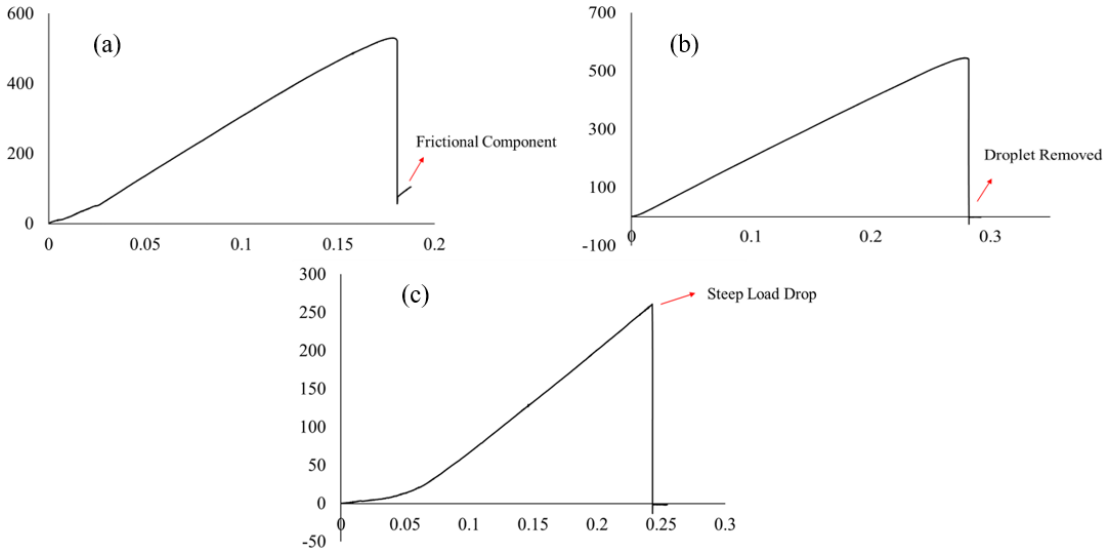

Figure 4-5: *Load vs Displacement plots; (a) a typical example of a successful microbond test (b) a typical example of a successful microbond test without a frictional region. (c) a typical example of a microbond test of premature failure dictated by a steep load drop.*

4.1.3. Scanning Electron Microscopy (SEM)

Scanning Electron Microscopy (SEM) was used to examine the morphology and structure of DION 1260 and DION 1273 microbond droplets bonded on SE 3030 and W 3030 glass fibres, respectively. Micro-composite specimens were prepared on steel washers accommodated on

the stainless steel plate presented in the previous section. Once post-cured, these were transferred on specimen stubs used for SEM. Double-sided carbon tape was used on the stub surface for the adherence of the micro-composite specimens. Twelve single fibre specimens containing several micro-droplets were used on each stub. These were then gold coated using an Agar sputter coater. Sputter coating was performed under an argon atmosphere with an operating pressure of 0.08 mbar, 30 mA current, and a 40 s coating time. Analysis was performed using a Hitachi SU 6600 scanning electron microscope with an accelerating voltage of 15.0 kV and a 10 mm working distance.

4.1.4. Fourier-transform Infrared Spectroscopy (FTIR)

An ATR-FTIR study was conducted to establish the variation in the cure kinetics between thin film specimens and microbond droplets. FTIR data on thin film specimens has been previously presented and discussed in *Chapter 3*. Spectra collection was carried out on a 4100 ExoScan FTIR using a spherical diamond attenuated total reflectance (ATR) interface. Analysis was performed in the 600 cm^{-1} to 4000 cm^{-1} range with a spectral resolution of 8 cm^{-1} and 64 scans per sample. Background scans were taken before every scan and the crystal was cleaned with acetone between measurements. Data processing and normalisation were conducted through the OriginPro software. The FTIR analysis was conducted on large microbond droplets manufactured on steel wire. The steel wire was wiped with acetone before use to prevent potential contaminations. The average embedded length of the droplets was approximately 0.4 mm and the diameter of the steel wire was 0.05 mm.

4.2. RESULTS AND DISCUSSION

4.2.1. Effect of Curing Conditions on Vinyl Ester Micro-droplets

In *Chapter 3*, the effect of curing conditions on vinyl ester thin films was investigated. It was found that the curing environment can have a huge influence on the cure kinetics of DION 1260. As per the resin manufacturer, high surface-to-volume specimens, such as thin films, may not be sufficiently cured when the cure conditions of bulk specimens are used, and the employment of an N_2 environment was recommended (for the first 24 h of the cure schedule). Initially, thin films were manufactured as models of microbond droplets, since they exhibited a similar surface-to-volume ratio; the thickness of thin films in the range of $0.1 < t \leq 0.2$ mm used in this study is in fact similar to the embedded length of a microbond droplet of, L_e = 100 - 180 μm, as shown in *Figure 4-6*. The plot was obtained by an estimation of the surface-to-volume ratio for cured DION 1260 microbond droplets and thin films. The volume and surface

area of microbond droplets was estimated by using the droplet length and diameter dimensions in accordance with the hypothesis that their shape is close to that of an ellipsoid. The contribution of the glass fibre embedded in the microbond droplet was subtracted from the calculation. The surface area and volume of films were determined by using a length and width of 280 mm and 10 mm, respectively, which are the approximate dimensions of the film slab manufactured by means of a drawdown bar. A range of thicknesses between 0.01 mm and 0.2 mm was explored.

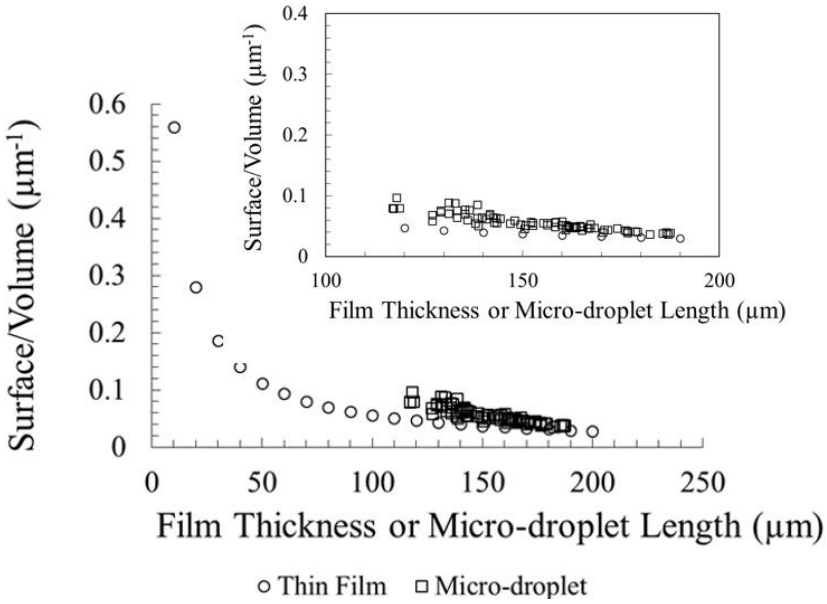

Figure 4-6: *Surface-to-volume ratio of thin films and micro-droplets vs film thickness or micro-droplet length.*

Results presented on the curing of DION 1260 films are in correlation with the findings of Thomason et al [182] regarding the micro-mechanical properties of the SE 3030/1260 system, assessed by the microbond test. Reported results were obtained on micro-composites on card frames, where fibres were fixed with CA glue. The authors found that when microbond droplets were initially cured under air, instead of inert N_2, incomplete curing was evident, with the average IFSS being below 5 MPa. Similar results were observed when a styrene environment was employed in the initial curing which resulted in the IFSS being slightly higher, but still below 5 MPa. When initial cure was carried out under an N_2 environment, which is the cure condition employed throughout the current study, the output IFSS was around 14 MPa. Lastly, when droplets were cured under N_2 for both cure phases, a higher IFSS close to 20 MPa was obtained. For films of a thickness of $0.1 < t \leq 0.2$ mm, DMA measurements presented in section *3.2.1*. showed an initial loss modulus peak/shoulder. As presented in *Chapter 3*, a clear loss modulus peak was featured for films cured fully under air

at 83 °C. A loss modulus shoulder at 90 °C was seen for "standard" cure films. These were followed by a secondary transition – loss modulus peak – at around 110 °C, while a single transition was identified also at 110 °C when both cure and post-cure were conducted under N_2. It can be deduced that curing films fully under air, either for the first or both stages of the cure, resulted in incomplete polymerisation and Tg deconvolution between the two phases of the resin (VE and styrene). Thus, both results presented by Thomason and those presented in section *3.2.1.* of this thesis show that DION 1260 properties are impaired (oxygen inhibition and styrene evaporation) when manufactured specimens are in the form of micro-droplets or films, i.e. possessing a high surface-to-volume ratio.

Scalability effects on the degree of cure between a film and microbond droplet were further examined by FTIR on a qualitative basis. A plotted comparison of thin film spectra for a 0.15 mm thick film and microbond droplets manufactured on steel wire is shown in *Figure 4-7*. It can be observed that no significant variation is shown between the spectra obtained by the two between 600 cm^{-1} and 1000 cm^{-1}. As previously discussed, this is the most important spectral region for the monitoring of cure kinetics in vinyl esters. However, an intensity increase was featured in the 695 cm^{-1} C-H of styrene for the thin film, which can be an indication of increased styrene concentration in the film specimens, when compared that of of the droplets. This was despite films displaying a higher surface-to-volume ratio than the large microbond droplets. Even though this may be an indication of styrene loss, intensity changes can take place when the geometry of the specimen is altered. Thus this result requires further validation.

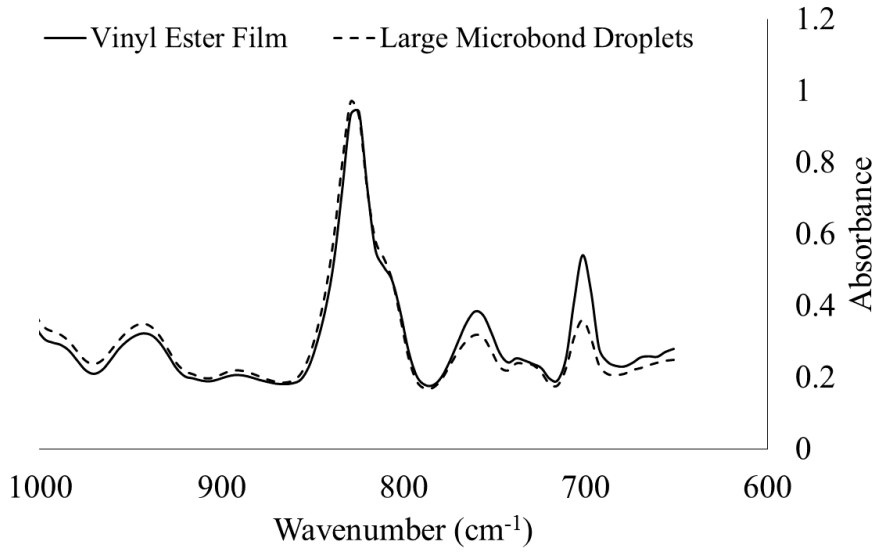

Figure 4-7: *Spectral comparison between a large microbond droplet and a thin film with an average thickness of 0.15 mm.*

4.2.2. Effect of Glass Fibre Sizing and Mounting Adhesive on IFSS Results

The use of Araldite EP as a fibre fixing adhesive was introduced, when stainless steel washers took the place of the mounting card to allow ageing of microbond specimens in water. When CA glue was used on stainless steel washers, the adhesion (between the fibre and the washer) was not enough to keep the fibre intact and as a result, the fibre was removed from the minute volume of CA glue during testing. The replacement of CA and card with Araldite EP and washers surprisingly resulted in an almost doubling of the IFSS of the SE 3030/1260 system. Thomason et al [182] reported an average IFSS of 12 – 14 MPa for SE 3030/1260 on card with CA glue. However, conducting the experiment on washers with EP as the mounting adhesive resulted in IFSS with an average value of 36.9 MPa. A debond force vs embedded length plot for the SE 3030/1260 adhered with CA on card vs EP on washer is shown in *Figure 4-8.* Results using CA on card were obtained by the ACG and were reported by Thomason et al [182], whereas results on EP on washer were obtained experimentally in this work. The plot reveals the variation in performance between specimens mounted with CA and EP. To this author's best knowledge, such discrepancies in IFSS due to the mounting adhesive have never been reported in the literature. It is noteworthy that upon the use of EP on card, it was concluded that the rise in IFSS was not related to the change of substrate from card to stainless steel, but to the substitution of CA with EP.

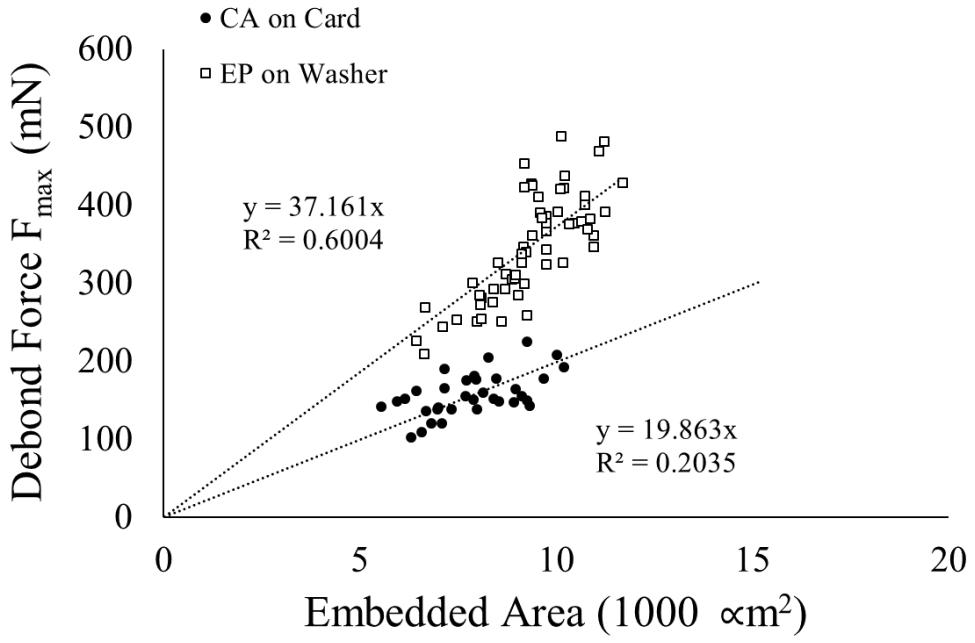

Figure 4-8: Comparison of debond force vs embedded are for the SE 3030/1260 mounted with CA on card vs EP on washer.

At this stage, it was of utmost importance to establish whether the compromise in micro-mechanical performance was owed to an interaction between CA and glass fibre sizing, or CA and the matrix. Thomason et al [182] reported that when a bare (un-sized) fibre was used with the DION 1260, the effect of the mounting adhesive was not apparent and similar IFSS values were obtained when either of the two adhesives was used. Similar results were shown on MoPTMS silane sized glass fibres, a component known to exist in vinyl ester-compatible sizings [12,182]. This led to the conclusion that the effect was owed to the interaction of CA with the film former or other non-silane sizing components [182].

The investigation was extended to a series of vinyl ester-compatible fibres and a commercial epoxy-compatible fibre. The main reason behind that was to find out whether the effect under study was solely related to the SE 3030/1260 system and (or) its constituents. Output IFSS values of various glass fibres with DION 1260 are featured in *Figure 4-9*. It can be clearly observed that when the vinyl ester-compatible sized fibre was tested with DER 332 epoxy droplets, the mounting adhesive effect was also apparent. This showed that the IFSS reduction was not related to the resin formulation, provided a glass fibre with a vinyl ester-compatible sizing was in contact with CA glue. Moreover, the following observation by Thomason et al [182] was critical; no IFSS variation was obtained when the mounting adhesive was altered in a SE 2020/DER 332 full epoxy system. However, when the SE 2020 epoxy-compatible fibre was used on the DION 1260 vinyl ester, the effect of mounting adhesive was observable. Reduction in IFSS was also evident when the DION 1260 vinyl ester was used on the 2002 and 2026 glass fibres with a vinyl ester-compatible sizing. The latter observation confirmed that the effect was evident in various vinyl ester systems. This was further validated by Thomason et al [182], who reported that the mounting adhesive effect was apparent when various vinyl ester resin formulations were used with a series of vinyl ester-compatible fibres. A simple matrix containing all examined glass fibre/matrix combinations is presented in *Table 4-2* to provide more clarity on the systems affected by the mounting adhesive effect. It can be concluded that the negative effect on IFSS with the use of CA adhesive does not occur upon interaction with epoxy matrix or epoxy-compatible sizing components, but only with some component of the VE-compatible sizing and (or) possibly vinyl ester resins. Furthermore, results showed reduced IFSS of vinyl ester on epoxy-compatible sizing under the presence of CA, but in the meantime, no effect was shown when vinyl ester was used on bare fibre. It can hence be suggested that there is a potential simultaneous interaction between a sizing component, vinyl ester and CA.

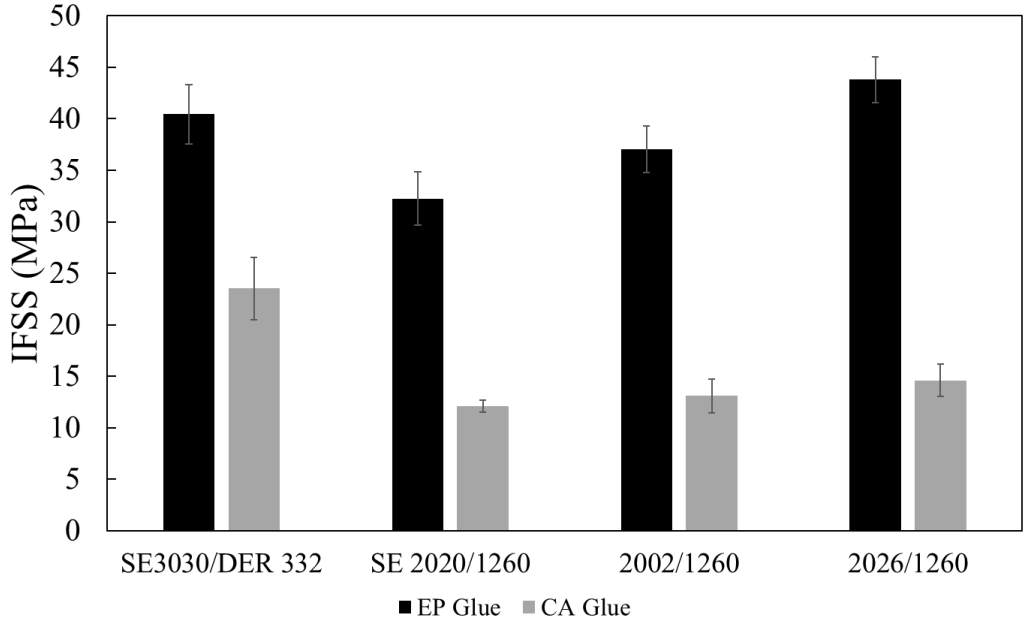

Figure 4-9: *Effect of mounting adhesive on various glass fibre/matrix formulations.*

Glass Fibre/Matrix	Effect of Mounting Adhesive
VE/VE	YES
VE/EP	YES
EP/VE	YES
EP/EP	NO [182]

Table 4-2: *Effect of mounting adhesive on various glass fibre/matrices.*

4.2.3. Possible Interactions of Fibre/Matrix and CA Adhesive

Despite the lack of knowledge on commercial glass fibre sizing components, it was important to gain more precise information on the form of reaction between vinyl ester and (or) vinyl ester-compatible sizing with CA. On that basis, the two following hypotheses were made: either wicking of CA occurs along the glass fibre affecting adhesion, or there is an interaction between CA glue vapour and the glass fibre/vinyl ester system. The following experiments were carried out to test these hypotheses; SE 3030/1260 microbond specimens were manufactured on card and a large EP glue droplet was used for the mounting of the fibres. CA glue was placed above the EP droplet, and after the latter was fully cured. In this case, potential wicking/capillary of the CA onto the fibre would be prevented by the bulky EP droplet. A schematic representation of the arrangement is shown in *Figure 4-10*.

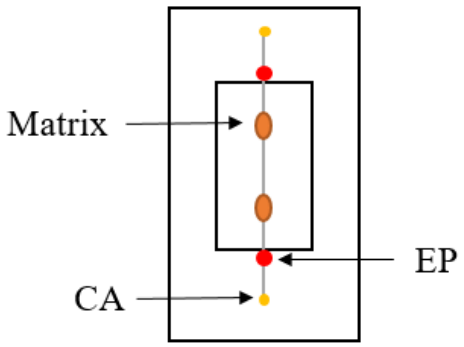

Figure 4-10: *Schematic representation of EP and CA on SE 3030/1260 for the study of CA wicking.*

The second experiment was conducted on stainless steel washers on the stainless steel frame, using the same micro-composite system. The experiment involved the mounting of fibres using EP, but CA droplets were placed across the thickness of the stainless steel frame, in very close proximity but not in contact with the glass fibres. A capture of the arrangement is featured in *Figure 4-11*. The resulting IFSS from the two experiments is shown in *Figure 4-12*.

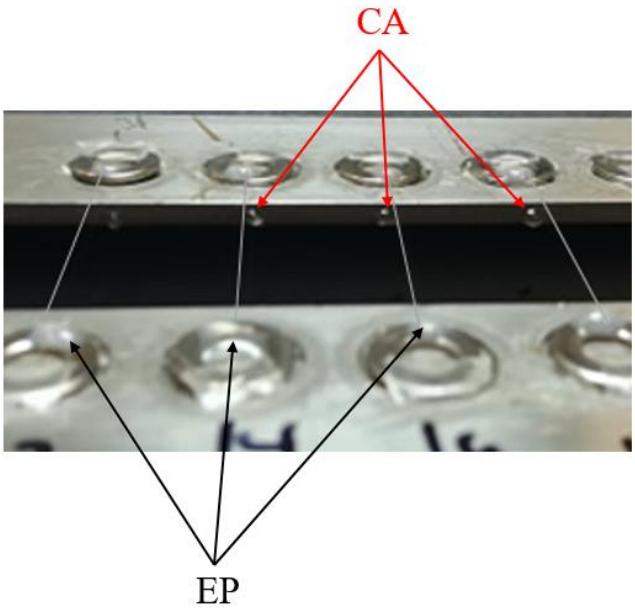

Figure 4-11: *Capture of CA on steel for SE 3030/1260 and EP-mounted fibres*.

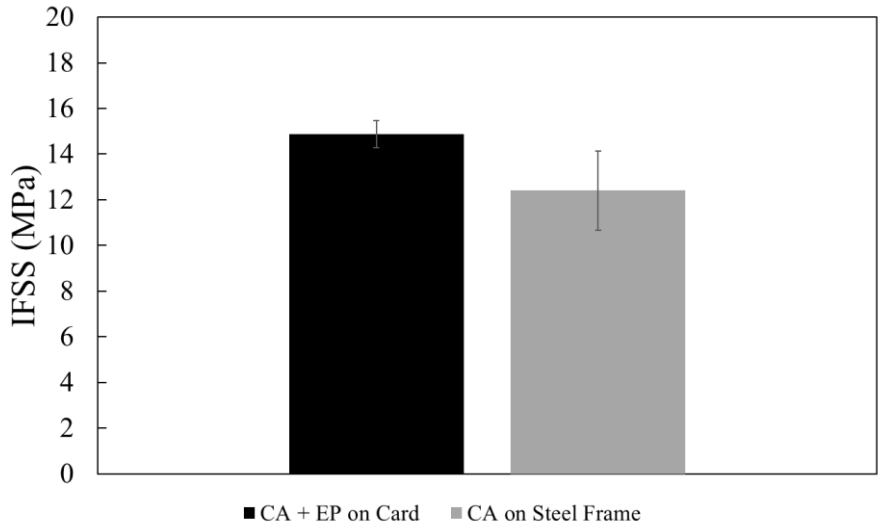

Figure 4-12: *Resulting IFSS for CA and EP on card vs CA on steel frame for SE 3030/1260.*

Both experiments resulted in an approximate 50 % IFSS reduction. Results also indicated that there was no wicking effect between the CA adhesive and the micro-composite since there was no direct contact between the two in either of the cases. In fact, the resulting average IFSS for the CA + EP on card, and the CA on steel frame were 14.9 MPa and 12.4 MPa, respectively. The former value is closer to the higher values, whereas the latter value is closer to the lower values obtained within the ACG for the SE 3030/1260 on card and with CA [182]. It is possible that this small IFSS variation was due to the distance of CA from the fibre, and that the placement of CA droplets in particularly close proximity to the fibre further reduced adhesion. However, further validation would be desirable.

It has been well-established that CA-based adhesives generate vapour that is capable of initiating reaction with chemical compounds or any nearby surface. This ability of CA adhesives is known to be utilised by criminal investigators for the development of latent fingerprints [183]. Preliminary tests showed that CA vapours interact with the fibre surface prior to droplet application. It was concluded that CA fumes induce an interaction with certain component(s) found in vinyl ester-compatible glass fibre sizing or may possibly locally influence the curing reaction of applied vinyl ester droplets. Although glass fibre sizing formulations are confidential and the exact reaction components could not be found, it can be suggested that one needs to be wary when using CA glue as a mounting adhesive for microbond specimens, especially when vinyl ester is present in the system.

4.2.4. Characterisation of DACOMAT Fibres and Resins

Microbond Test

The microbond test was used for the interfacial characterisation of the SE 3030 (Advantex) and W 3030 (HiPertex) glass fibres with DION 1260 and DION 1273. All tests were conducted using washers and EP as the fibre fixing adhesive. The resulting apparent IFSS for all fibre and matrix combinations is shown in *Figure 4-13*. It can be observed that W 3030/1273 provided the highest IFSS of around 43.5 MPa. All other IFSS values were found to be within the same range between 35 MPa and 37 MPa. No significant variation in IFSS was found when DION 1260 was used on different glass fibre substrates of the same sizing. Nonetheless, it can be seen that although all IFSS values were close in magnitude, DION 1273 provided slightly higher adhesion than DION 1260 when used on either of the two fibres. Bryce [55] has conducted a thorough study involving the interfacial assessment of a wide range of epoxy-compatible sizings with epoxy resins via the microbond test. The author found that interfacial adhesion was entirely independent of the glass fibre formulation upon testing SE 2020 (Advantex) and W 2020 (HiPertex) with the same epoxy matrix. However, when changing from an EP matrix and EP-compatible fibre to a VE matrix and a VE-compatible fibre, respectively, one should consider that the chemistry of the interface may be altered. This refers primarily to the individual reactions of the silane and coupling agent with the glass formulation and in turn with the matrix. It is yet unclear whether the glass formulation and in particular the superior properties of HiPertex to Advantex [184] contribute to an increase in IFSS in DION 1273. Nevertheless, given the tendency of DION 1273 to provide higher IFSS values than DION 1260 when tested in either of the two fibres, it can be concluded that DION 1273 has been tailored to offer strong interfacial adhesion. This is validated by Polynt, who have clearly stated in the DION 1273 datasheet that the resin has been particularly designed to offer exceptional adhesion.

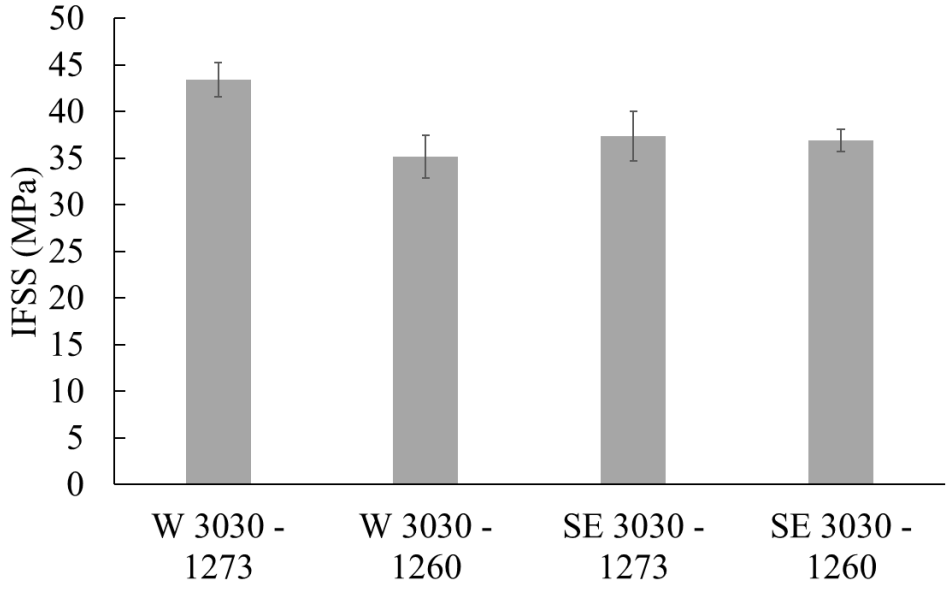

Figure 4-13: *Resulting IFSS for all fibre/matrix combinations using DION 1260 and DION 1273 resins, and SE 3030 and W 3030 fibres.*

Scanning Electron Microscopy (SEM)

SEM images of DION 1260 and DION 1273 microbond droplets mounted on SE 3030 and W 3030 fibres, respectively, are featured in *Figure 4-14*. DION 1260 micro-droplets were found to possess a featureless surface. However, cracking around the droplet meniscus was evident in certain droplets, as shown, while the resin layers around the meniscus appeared to be thin. Upon investigating a wide range of specimens, the cracking appeared to be on a surface level but still remained an indication of a weak interfacial bond between the fibre and the matrix. It can be suggested that such cracks may act as promoters of the debonding process during the microbond test, and may consequently reduce the required debonding force and hence IFSS.

This was not the case for W 3030 and DION 1273, which showed good bonding featuring a solid resin layer around the droplet meniscus and no cracking. However, some of the droplets featured small micro-cavities, which nonetheless also appeared to be on a surface level after examining a wide specimen range. Considering the results recorded through the microbond test, it is likely that the cracking between the fibre and the matrix is what results in a lower IFSS for the SE 3030/1260 system. On the other hand, the interfacial bond for W 3030/1273 appears to be strong in SEM images, which justifies the higher IFSS for that system. It would certainly be useful to obtain SEM images on all SE 3030 and W 3030 with DION 1260 and DION 1273 configurations to understand in more depth the differences in interfacial adhesion between the two fibre and resin systems.

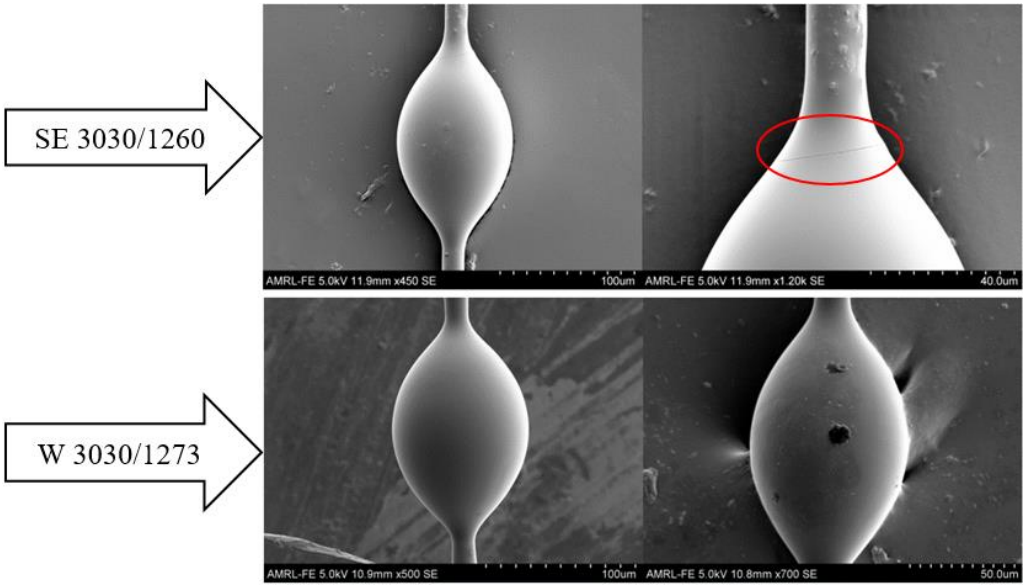

Figure 4-14: *SEM images of DION 1260 and DION 1273 microbond droplets mounted on SE 3030 and W 3030 fibres, respectively.*

4.3. CONCLUDING REMARKS

In conclusion, a surface-to-volume ratio estimation for thin films and microbond droplets showed that the thickness of the thin films investigated in this study was more or less equivalent to the embedded length of a microbond droplet. Close correlation between the curing of microbond droplets and thin film vinyl ester specimens of DION 1260 was confirmed through FTIR. This in turn allowed a better understanding of the cure kinetics of vinyl ester microbond droplets. More specifically, microbond droplets exhibit masses in the nanoscale range and they are particularly challenging to handle and study, whereas as thin films can be more easily studied by thermal analysis (TA) and FTIR. It was further confirmed that the use of more rigorous cure schedules should be employed to achieve bulk scale cure in vinyl ester microbond droplets. FTIR showed that vaporisation may be greater in droplets than in films of a similar surface-to-volume ratio, even though this required further validation. Furthermore, according to ACG findings reported by Thomason et al [182], adequate micro-droplet curing could not be achieved in a styrene environment as previously suggested by Laurikainen [68]. However, enhanced interfacial adhesion can be achieved by preventing oxygen interaction with the pre-polymer mix.

In addition, it was unexpectedly discovered that the type of adhesive used for the mounting of different glass fibre vinyl ester microbond specimens can have a huge influence on the IFSS

results obtained. A series of experiments were conducted suggesting that there are probable reactions of CA vapour with glass fibres coated with vinyl ester-compatible sizings or when vinyl ester matrix is used on other sized fibres. The interaction was found to occur upon the adherence of CA glue to the fibre ends prior to the deposition of the matrix on the fibre. The resulting effect was a probable contamination of the glass fibre surface with CA glue vapour, which reacted with certain sizing components and (or) affected the cure kinetics of matrix droplets. However, when the CA adhesive was substituted with an EP adhesive, the IFSS of glass fibre vinyl ester was approximately doubled.

Last but not least, an interfacial comparison between DACOMAT fibres of the same sizing but of a different glass substrate – SE 3030 and W 3030, with DACOMAT vinyl ester resins DION 1260 and DION 1273 was enabled via the microbond test. No significant variation was found between the IFSS of DION 1260 on either glass fibre substrates. Nevertheless, the highest IFSS was attained by the W 3030/1273 system. SEM images on SE 3030/1260 and W 3030/1273 revealed cracking in the meniscus of the former, whereas a stronger interfacial bond was evident for the latter. The effect of glass formulation on output IFSS remained unclear. It was nonetheless concluded that DION 1273 has been tailored by the resin manufacturer to offer higher adhesion than a commercial vinyl ester, such as DION 1260, despite possessing inferior properties in its neat form on a macroscale.

CHAPTER 5: THE INFLUENCE OF MOISTURE AGEING ON GLASS/FIBRE VINYL ESTER LAMINATES

The primary objective of this chapter is to evaluate the durability of glass fibre/vinyl ester laminates in wet environments. The moisture uptake kinetics of the neat matrix, cured at different conditions, and the composite laminate are studied. A DMA characterisation of both the aged matrix and the composite is presented. Last but not least, the monitoring of the mechanical properties of the composite as a function of ageing is performed.

5.1. EXPERIMENTAL

5.1.1. Materials

Two DACOMAT unidirectional (UD) composite laminates were used to investigate the effects of hydrothermal ageing on glass fibre/vinyl ester systems. Material specifications are included in *Table 5-1*. The SE 3030/1260 laminate was considered a "baseline" material both for this project and DACOMAT, since it consisted of a commercially available matrix and reinforcement, the DION 1260 resin and SE 3030 fibres, respectively. On the other hand, the W 3030/1273 laminate was a newly developed composite consisting of the DION 1273 experimental matrix and the W 3030 fibre. Composite laminates were supplied by Polynt in 80 x 80 cm panels. The thickness of the laminates was 3.9 mm. According to the manufacturer, both laminates were produced by a symmetric stacking that is mirrored at the mid-plane, as shown in *Figure 5-1*. These were cut to appropriate specimen sizes by water-jet cutting at the University of Strathclyde, Mechanical & Aerospace Engineering workshop. Prior to ageing, specimen edges were sealed by using an Araldite Epoxy, which is marketed as a 2-part, high viscosity, hydrophobic adhesive. Two thin coating layers of coating were applied in succession to ensure thorough sealing.

Designation	Glass Fibre Sizing	Glass Fibre Type	Matrix	Avg. Measured Fibre Weight Fraction, W_f
SE 3030/1260	SE 3030	3B Advantex 17μm 1200 tex fibre	DION 1260	71.54
W 3030/1273	W 3030	3B HiPer-tex 17μm 2400 tex fibre	DION 1273	71.13

Table 5-1: *Laminate details.*

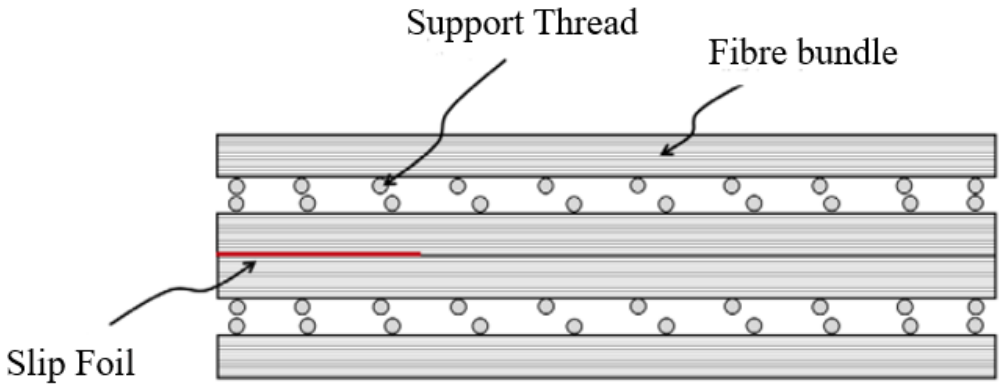

Figure 5-1: *Composite laminate structure.*

Neat resin specimens were also employed for a better understanding of the hydrothermal response of the matrix material on a bulk scale. The specimens used were the:

- DION 1260 and DION 1273 Polynt Standard; post-cured at 60 °C, defined in *Chapter 3*. All DION 1273 specimens used were cured at "standard" conditions, while deviations from the "standard" schedule were attempted for DION 1260 for comparative purposes. These specimens were supplied by Polynt.
- DION 1260 P-C 100 °C. Same as above but post-cured at 100 °C. This is the post-cure temperature employed for microscale specimens. It was only used for preliminary results in DION 1260 macroscale plates to examine whether a higher post-cure temperature can contribute to the hydrophobicity of the matrix.

- DION 1260 UoS Op. Mould - 100 °C, post-cured at 100 °C, as also defined in *Chapter 3*. The use of a higher post-cure temperature was chosen to ensure greater thermal properties and higher conversion. These specimens were manufactured in-house in open silicone rubber moulds.

5.1.2. Diffusivity Calculations

The weight gain of the matrix and composite laminates was calculated using *Equation 2-4* presented in the literature section. The apparent diffusivities of the matrix and composites were calculated using *Equation 2-7*. *Equation 2-9* was used for the prediction of composite laminate diffusivities for the SE 3030/1260 and W 3030/1273 systems, using the apparent diffusivity value obtained for the matrix. Fibre volume fractions of 51.95 % and 51.4 % were obtained for SE 3030/1260 and W 3030/1273, respectively. The volume fraction calculation was carried out using the rule of mixtures for composite laminates shown below – *Equation 5-1* [185]:

$$w_f = \frac{\rho_f v_f}{\rho_f - \rho_m * (1 - v_f)}$$

5-1

where w_f is the fibre weight fraction, %, – measured values shown in *Table 5-1*, ρ_f and ρ_m are the densities of the fibre and matrix, provided by 3B and Polynt, respectively, and v_f is the fibre volume fraction. An estimation of the moisture gain of the composite laminates was conducted by using the weight fraction of the matrix multiplied by the moisture gain of the neat matrix at equilibrium.

5.1.3. Mechanical Testing of Composites

Short-beam Shear (SBS)

All short-beam shear (SBS) tests were performed in the Advanced Materials Research Laboratory (AMRL). The largest volume of the tests was conducted by James Gillespie and without the presence of the author due to covid-19 safety regulations. However, adequate training was offered to the author, when covid-19 restrictions were lifted. The main objective of SBS tests was to monitor the change of Interlaminar Shear Strength (ILSS) as a function of environmental ageing. Therefore, both dry and aged specimens were tested in SBS. Aged specimens were measured for their weight change the day before the tests and were then kept in a desiccator of 100 % RH overnight, to ensure they were kept wet during the test. Each

specimen was removed from the desiccator only prior to testing. A total of 6 specimens were tested per batch, as per ASTM D2344/D2344M – 16 to ensure an adequate statistical basis [113]. The span length used was 16 mm and specimen dimensions were 24 x 8 mm, and approximately 3.9 mm in thickness. Upon the completion of the tests, all specimens were kept so that they could undergo ignition loss tests and be examined for their void content. The test apparatus used was the 50 kN Instron Electromechanical 5969 Tester, with a short-beam shear configuration. A diagram of the test setup with dimensions is shown in *Figure 5-2*. The experimental rig was operated through a computer by using the Bluehill 2 software.

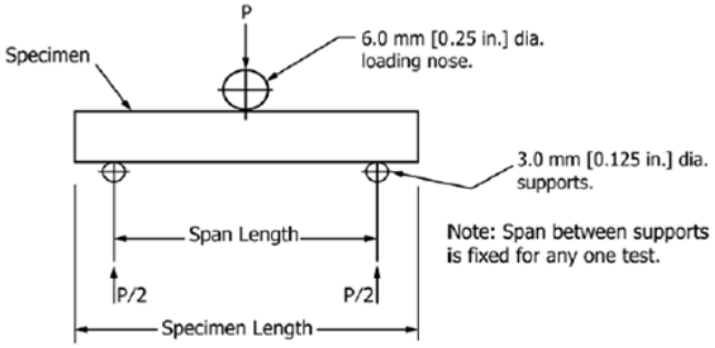

Figure 5-2: *Test setup for short-beam shear mechanical testing.*

The ILSS calculation was carried out according to *Equation 5-2* and ASTM D2344/D2344M – 16 [113].

$$F_{SBS} = 0.75 * \frac{P_m}{b * h}$$

5-2

Where F_{SBS} is the short-beam strength, or apparent interlaminar shear stress, P_m is the maximum load observed during the test, b is the measured specimen width and h is the measured specimen thickness**.**

3-Point Bending

All 3-point bending tests were performed in the AMRL. Similar to the SBS tests, the largest volume of the tests was conducted by James Gillespie. The main objective of 3-point bending tests was to monitor the change of flexural strength and Young's modulus (in the fibre direction) as a function of environmental ageing, and thus both dry and aged specimens were

tested. Aged specimens were measured for their weight change the day before the tests and were then kept in a desiccator of 100 % RH overnight to ensure they were kept wet during the test. Each specimen was removed from the desiccator only prior to testing. A total of 5 specimens were tested per batch, as per ASTM D7264 to ensure an adequate statistical basis [116]. The span length used was 122 mm and specimen dimensions were 146 x 13 mm, and approximately 3.9 mm in thickness. The test apparatus used was the 50 kN Intron Electromechanical 5969 Tester, with a 3-point bending configuration. The test setup is shown in *Figure 5-3*. The experimental rig was operated through a computer by using the Bluehill 2 software.

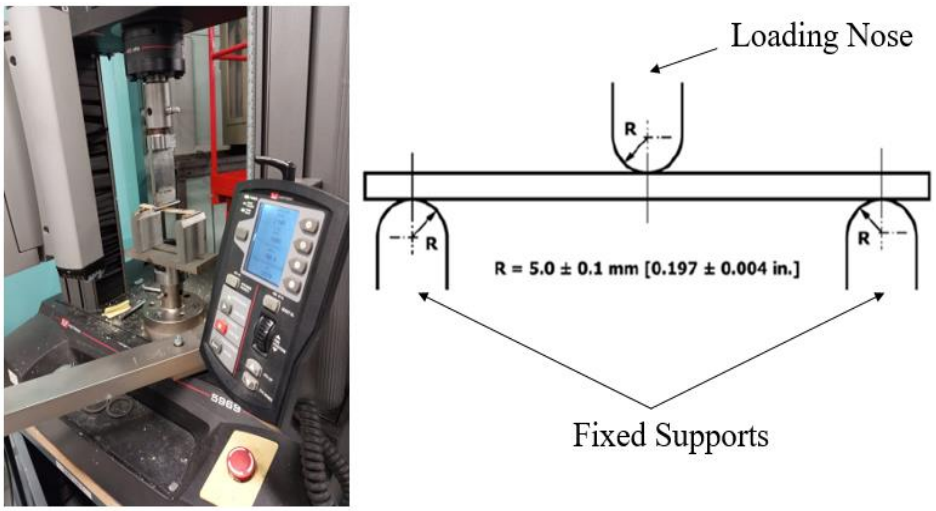

Figure 5-3: *Test setup for 3-point bending mechanical testing.*

The flexural strength calculation was carried out according to the equation below and ASTM D7264 – *Equation 5-3* [116].

$$\sigma_f = \frac{3}{2}\frac{P_{max} * L}{b * d^2}$$

5-3

Where σ_f is the flexural strength, P_{max} is the load at the highest point on the load-deflection curve, L is the support span, b is the width of the beam and d is the depth of the beam. In this

case, the calculation was performed by the Bluehill 2 software used for the analysis and the output flexural strength value was provided.

5.1.4. Dynamic Mechanical Analysis

Dry and aged DACOMAT composite laminate and neat resin specimens were tested by DMA in a 3-point bending configuration to provide insight into the effect of ageing on the thermal behaviour of the system. The analysis was performed using a Q800 Dynamic Mechanical Analyser (TA Instruments) and according to ASTM D5023-15 [173]. The input test parameters were: frequency of 1 Hz, amplitude of 50 μm, pre-load force of 0.1 N and a force track of 120 %. The specimen dimensions were 64 x 13 x 3.9 mm. All specimens were equilibrated at 25 °C for 5 minutes, then ramped at 2 °C/min up to 150 °C. The Tg assignment was conducted in agreement with ASTM D7028 − 07 [175]. Tested specimens were the DION 1260 and DION 1273 – "Polynt Standard", DION 1260 "UoS Op. Mould - 100 °C", as well as the SE 3030/1260 and W 3030/1273 laminates.

5.1.5. Void Content Calculation

The purpose of the void content calculation was to examine the relationship between the void content of glass fibre/vinyl ester laminates and the ageing environment they were conditioned in. Void content measurements were conducted on SE 3030/1260 SBS specimens upon ageing and mechanical testing. The void content measurement procedure involved the ignition loss of the composites to obtain the fibre weight content. This was conducted in ceramic crucibles according to ASTM D2734 – 94 [165]. The heating schedule used was 45 minutes at 600 °C. Upon the completion of the heating cycles, specimens remained in the furnace until cool, prior to being weighed.

The calculation involved the calculation of the percentage difference between the theoretical composite density and the measured composite density. The theoretical density was calculated by *Equation 5-4*, as follows;

$$\rho_{theoretical} = 100/(\frac{w_m}{\rho_m} + \frac{w_f}{\rho_f})$$

5-4

where: $\rho_{theoretical}$ is the theoretical density of the composite, W_m is the matrix weight fraction of the composite, w%, ρ_m is the density of the matrix, w_f is the weight fraction reinforcement of the composite and ρ_f is the density of the reinforcement.

The void content for each composite specimen can be then determined by *Equation 5-5* as follows:

$$Void = 100(\rho_{theoretical} - \rho_c)/\rho_{theoretical}$$

5-5

where: $Void$ is the void content of composite, volume v%, $\rho_{theoretical}$ is the theoretical composite density and ρ_c is the measured composite density.

The matrix density of 1.127 g/cm^{3}was provided by Polynt. The density of Araldite epoxy - 1.165 g/cm^3 used as a sealant was also accounted for. A density value of 2.62 g/cm^3 for bare SE 3030 was provided by 3B. Since the ignition loss of the composites was conducted at 600 °C, at which SE 3030 undergoes annealing, a density increase of 0.02 g/cm^3 was used.

Laminate Density Calculation

Composite density was measured by recording the weight of each specimen in air and in deionized water. All measurements were conducted using a Metler Toledo density kit, which was mounted on a Metler Toledo analytical balance. Factors influencing the accuracy of the measurement, such as air bubbles were considered and limited as thoroughly as possible. Moreover, the immersion depth of the basket in the DI water was kept constant at every test. The following equation – *Equation 5-6* – was used for the calculation;

$$\rho = \frac{M_A}{M_A - M_L}(\rho_0 - \rho_L) + \rho_L$$

5-6

where: ρ is the density of the specimen, M_A is the mass of the specimen in the air, M_L is the mass of the specimen in the auxiliary liquid, ρ_0 is the density of the auxiliary liquid, and ρ_L is the density of the air.

In addition, the volume of the specimen was determined by *Equation 5-7* as follows:

$$V = c\frac{P_A - P_L}{\rho_0 - \rho_L}$$

5-7

where: V is the volume of the specimen, and c is a weight correction factor (0.99985) accounting for the atmospheric buoyancy of the adjustment weight into account. The temperature of the water remained constant throughout the measurement (20 °C) resulting in a density of 0.998203 g/cm^3 [186].

5.1.6. Ageing Conditions

All laminates and "standard" cured matrix specimens were aged by full immersion in DI water at 23 °C and 50 °C and in a humid environment of 100 % RH at RT. These are referred to as "23 °C", "50 °C" and "100 % RH" throughout this manuscript. The selection of immersion in water was used to simulate accelerated degradation mechanisms which may be acting through rainwater in large infrastructure applications. However, since the chemistry of rainwater is variable, DI water was selected in order to simplify the nature of the degradation reactions. The temperature of 50 °C was used as a means of ageing acceleration and to create an ageing environment, similar to ones present in hot and wet climates. The increased humidity environment was chosen to replicate degradation conditions acting in highly humid climates, such as in Northern European countries. Four water baths were employed for the DI water ageing, while sealed desiccators were used for the controlled humidity conditions. The 100 % RH humidity level was achieved by placing DI water at the bottom of a desiccator and was checked by a digital hygrometer. The ageing conditions remained consistent throughout this study and were applied both in bulk specimens, results of which are presented in this chapter, and microscale specimens, results of which are entailed in the following chapter. "DION 1260 UoS Op. Mould - 100 °C" specimens were only aged at 23 °C and 50 °C. Specimens of 80 x 80 x 3.9 mm of both composites and neat matrix were used to monitor moisture uptake at all conditions and allow comparison. All specimens were dried for at least 24 h under vacuum prior to ageing for removal of probable ambient moisture.

5.2. RESULTS AND DISCUSSION

5.2.1. Neat Resin: Moisture Uptake

Moisture Uptake Kinetics of DION 1260 Vinyl Ester

A weight gain vs ageing time plot of the DION 1260 "Polynt Standard" at different ageing conditions is shown in *Figure 5-4*. DION 1260 diffusivity and moisture gain values are shown in *Table 5-2*. Diffusivity values were calculated assuming 1-D Fickian diffusion for all specimens. In certain cases, equilibrium was unclear and was approximated. The "standard" cure samples – "Polynt Standard" exhibited a similar water uptake behaviour when immersed at 23 °C in DI water and when conditioned in a 100 % RH desiccator at room temperature. In both cases, an initial Fickian-like weight gain was observed until around 50 days (≈ 2000 √s). The weight gain began to stabilise but followed a slow and gradual increase for the remaining ageing period, indicative of matrix relaxation. Matrix relaxation is essentially the moisture-induced plasticisation of the matrix and can be marked by a Tg decrease as a function of moisture content [166]. At equilibrium and as presented in *Table 5-2*, the weight gain in both conditions was found to be similar. The time to equilibrium was between 85 (≈ 2700 √s) and 110 days (≈ 3000 √s) at both conditions. Diffusivity values at all ageing conditions were close to ones reported in the literature [22]. Generally, the comparison of the two ageing conditions provides evidence that exposure to a highly moist environment, and direct immersion in an aqueous medium, have a similar effect on vinyl ester. However, as expected, the moisture gain at 100 % RH was slightly lower than the ones obtained in water at 23 °C, while similar diffusivities were obtained.

At 50 °C, Fickian-like behaviour was featured with a higher weight gain, nonetheless, as expected, due to elevated temperature ageing. On that basis, attaining equilibrium was accelerated, when compared to 23 °C and 100 % RH and took place within 35 days (≈ 1700 √s). The weight gain recommended by the resin manufacturer was 0.65 %. A lower equilibrium level was obtained at 23 °C and 100 % RH (0.58 % and 0.53 %, respectively), whereas a higher level was obtained upon equilibrium at 50 °C (0.77 %). Although matrix relaxation was apparent at RT ageing and is nevertheless more likely to take place in higher temperatures [138], this was not the case when DION 1260 "Polynt Standard" was aged at 50 °C. A possible explanation for this is that ageing at elevated temperatures induced anti-plasticisation effects, i.e. a combination of leaching and secondary cross-linking, instead of plasticisation. As discussed in the literature review section, Han and Drzal [134] have proposed the presence of two types of bound water in thermoset networks; type I, which is associated with a reduction

in Tg and plasticisation (relaxation) and Type II bound water is responsible for secondary cross-linking and increased Tg. Further claims made by Apicella et al [128] suggest that hydrothermal environments of a high temperature are associated with Tg increases in thermosets through post-curing, often accompanied by leaching. In addition, the authors have stated that such effects can reduce the degree of plasticisation of the matrix (anti-plasticisation). Leaching and secondary cross-linking effects have been previously observed by Visco et al [187] for a vinyl ester matrix aged at 60 °C in water. Similar effects have also been observed by Apicella et al [128] for incompletely polymerised styrene-containing unsaturated polyester.

Despite the observation of Fickian-like plots, irreversible weight loss was confirmed for all specimens. All specimens were re-dried upon the completion of ageing after 530 days (≈ 7240 √s). Re-drying was conducted at 45 °C for 72 h, following storage in a dry desiccator of 10 % RH at RT for a minimum of 24 h. A re-drying temperature notably lower than the Tg of the materials was selected to avoid weight loss during the re-drying cycle. Namely, 0.24 %, 0.27 % and 0.23% weight losses were observed for the conditions of 23 °C, 50 °C and 100 % RH, respectively. As presented in the literature review, matrix ageing has been associated both with matrix leaching (matrix decomposition) – hydrolysis, and (or) leaching polymer unreacted oligomers – not an indication of hydrolysis. A common indicator for hydrolysis is the change of matrix colour after ageing. In this case, a mild change of colour in the matrix was observed at 23 °C and 100 % RH whereas a more profound discolouration was featured at 50 °C – *Figure 5-5*. The latter observation confirms matrix hydrolysis at 50 °C, while the former is an indication that hydrolytic effects had only started to take place at RT ageing. DMA measurements were required to further elucidate the ageing effects on the matrix.

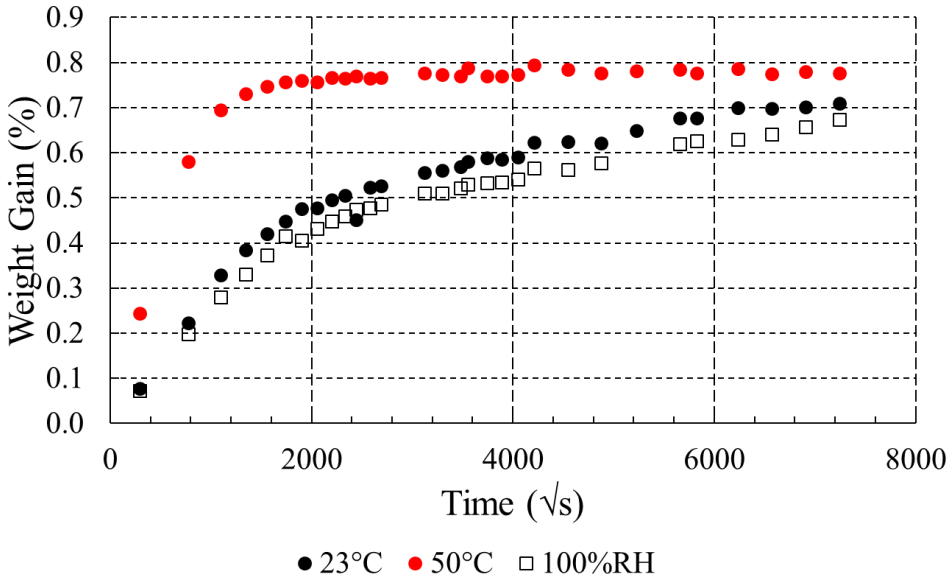

Figure 5-4: *Weight gain vs ageing time plot for neat DION 1260 "Polynt Standard" matrix at different ageing conditions.*

DION 1260	Condition	Equilibrium (%)	Diffusivity x 10^{-6} (mm^2/s)	Max. Ageing Period (Days)	Max. Weight Gain (%)
Polynt Standard	23 °C DI	0.58	0.36	530	0.7
	50 °C DI	0.77	1.8	530	0.78
	100 % RH	0.53	0.43	530	0.67
Polynt - P-C 100 °C	23 °C DI	0.61	0.73	175	0.6
	50 °C DI	0.74	1.96	175	0.74
	100 % RH	0.6	0.33	175	0.6
UoS Op. Mould – 100 °C	23 °C DI	0.90	0.5	658	1.37
	50 °C DI	1.41	1.3	389	2.6

Table 5-2: *Weight gain and diffusivity of DION 1260 at different ageing conditions.*

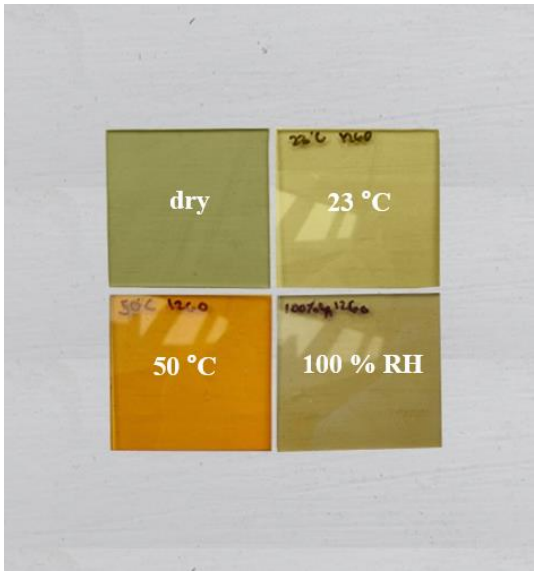

Figure 5-5: *Neat DION 1260 colour retention at different ageing conditions.*

Post-curing the DION 1260 matrix at a higher temperature of 100 °C, as in microscale/microbond specimens did not have a great effect on moisture uptake kinetics, as shown in *Figure 5-6*. Despite the ageing period of the DION 1260 P-C 100 °C specimens being shorter than the "Polynt Standard", similar water uptake plateaus are shown, while the moisture gain values and diffusivities were also found to be within the same range, as shown in *Table 5-2*.

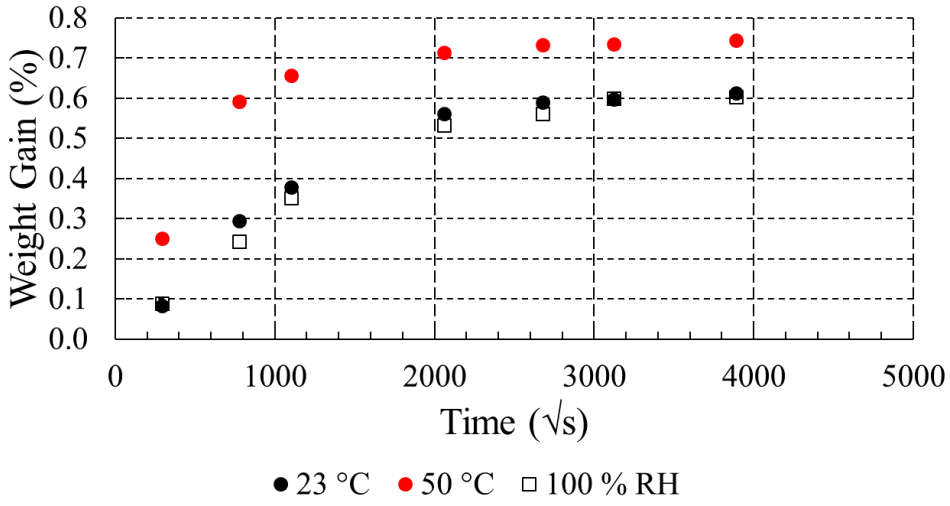

Figure 5-6: *Weight gain vs ageing time plot for neat DION 1260 matrix post-cured at 100 °C, at different ageing conditions.*

A notably different ageing behaviour was observed for the specimens cured in an open mould for the first part of the cure, allowing oxygen interaction with the curing specimen. In fact, two

different water uptake trends were seen for the three specimens aged at 23 °C, as shown in *Figure 5-7*. Specimen 1 followed a Fickian-like behaviour and reached equilibrium after approximately 2 months (≈ 2300 √s) absorbing approximately 0.87 % of water. However, specimens 2 and 3 noted a gradually increasing weight gain plateau, despite forming a Fickian-like curve for the first part of conditioning. These reached a temporary equilibrium of 0.85 % (specimen 2) and 1 % (specimen 3) at approximately 85 days (≈ 2700 √s). Diffusivity was calculated using the curve of Specimen 3, assuming Fickian diffusion, while the moisture gain values presented in *Table 5-2* were averaged. The notable increase in weight gain when compared to "standard" cure, as well as the variation in weight gain and weight gain behaviour between the three open mould specimens could be attributed to varying void content (i.e. air gaps), and the fact that the interaction of oxygen with the curing polymer, as well as styrene evaporation during cure, may be happening in an uncontrolled manner. It is noteworthy that pronounced styrene evaporation, which was apparent in this case, as presented in *Chapter 3*, can significantly decrease the hydrophobicity of the matrix. Moreover, the thickness uniformity across all specimens was slightly variant, since they were cured in an open mould without being compressed in shape. The increasing weight gain was indicative of matrix relaxation and volumetric expansion – swelling. Despite the moisture gain of all three specimens being higher than that of "Polynt Standard", diffusivity values and equilibrium times were found to be relatively close in magnitude.

A different response to hydrothermal ageing was exhibited by the specimens exposed at 50 °C. The curve featured in *Figure 5-7* is an average of three specimens, which noted a similar behaviour with each other with slightly varying moisture gain, reflected in the 95 % error bars shown. Even though a stabilisation in the moisture gain of the matrix was observed after 30 days (≈ 1600 √s) of exposure at around 1.41 % gain indicating equilibrium, an unexpected, abrupt increase in weight was observed after around 3.3 months (≈ 3000 √s) – two-stage diffusion. This increase can be attributed to probable plasticisation and matrix relaxation. Nonetheless, leaching was apparent and dominated sorption after an average, maximum weight gain of 2.6 % was obtained, resulting in a pronounced weight loss.

Similar to 23 °C, the obtained diffusion coefficient, as well as the time to equilibrium for the open mould specimens at 50 °C were found to be particularly close in magnitude to the ones of "Polynt Standard". It should be noted that in the case of the former only the "Fickian" part of the curve was considered for the diffusivity calculation, and the secondary weight increase was not accounted for.

Re-drying of the aged specimens took place in order to examine probable leaching effects. At 23 °C, leaching was confirmed upon re-drying all three specimens. Specimens 1 and 2 were found to have lost approximately 0.18 % after 658 days of ageing (≈7540 √s), whereas specimen 3 returned to its original weight upon being re-dried after 360 days of ageing (≈5580 √s). At 50 °C, only one of the aged specimens was re-dried, after 322 days (5275 √s) of exposure, measuring a notable weight loss of 0.6 %. Unfortunately, the other two specimens remained in the water bath during the first Covid-19 lockdown, which had been fully drained upon the author's return to the laboratory. Nevertheless, these noted a weight loss of 1 %, further confirming irreversible degradation.

Difficulty in extracting absorbed moisture was present in both "Polynt Standard" and open mould specimens. Re-drying open mould specimens was particularly challenging, and rigorous drying schedules were employed for most specimens. A decaying weight loss was recorded for all specimens, upon heating in an air circulation oven (at 45 °C – below the Tg of the materials) and their placement in a dry desiccator. The difficulty of re-drying the matrix was an indication of water molecules trapped within micro-cavities and capillaries, found in the polymer network of the thermoset making it susceptible to hydrolysis. This effect has been previously studied by Han and Drzal [134] and is an indication of chemical ageing. Thus, it was challenging to provide definitive answers on weight loss, especially when some of the specimens were eventually used for thermal analysis purposes. On that basis, although it was observable that open mould specimens underwent a smaller weight loss than the "Polynt Standard", one should consider the possibility of residual entrapped moisture in the former, which may lead to erroneous interpretations.

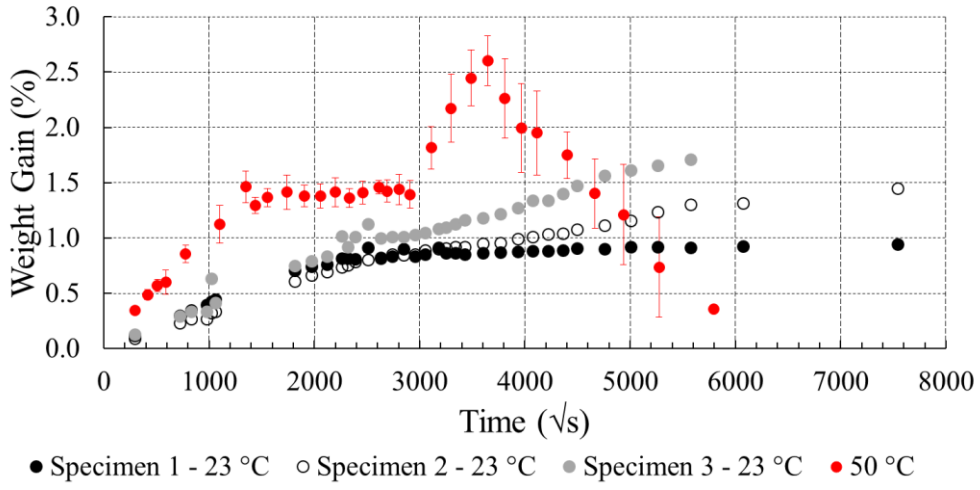

Figure 5-7: *Weight gain vs ageing time plot for neat DION 1260 "UoS Op. Mould - 100 °C" matrix at different ageing conditions.*

Moisture Uptake Kinetics of DION 1273 Vinyl Ester

The weight gain behaviour and diffusivity values of DION 1273 "Polynt Standard" were found to be relatively close to the ones of DION 1260, although the former absorbed more moisture at equilibrium. Due to an increasing weight gain in all cases, equilibrium was assumed when the weight gain reached a temporary plateau – at the "flattest" point of the curve. Weight gain vs time plots for DION 1273 are presented in *Figure 5-8*, while diffusivity and moisture gain values are contained in *Table 5-3*. The weight gain behaviour and diffusivity values recorded for DION 1273 at 23 °C and 100 % RH were similar to each other, confirming the likeness of the two conditions. The format of the curves shown in *Figure 5-8* appears to resemble Fickian diffusion in the linear part, followed by a continuous weight gain increase. The flattest point of the curve was attained between 63 (≈ 2300 √s) and 69 days (≈ 2440 √s), significantly faster than in DION 1260, which reached equilibrium between 85 (≈ 2700 √s) and 110 days (≈ 3000 √s). The moisture gain at this point was notably higher than the one of DION 1260 at both conditions. Namely, 0.75 % was recorded at 23 °C, as opposed to 0.58 % found for DION 1260, and 0.68 % for 100 % RH, compared to 0.53 % noted for DION 1260. The continuous weight gain increase is indicative of matrix relaxation, which means that the matrix undergoes plasticisation (swelling) as a function of water absorption. This became more pronounced as a function of ageing, and upon the assumed "equilibrium" between 63 and 69 days.

DION 1273 attained a similar weight gain pattern at 50 °C to 23 °C and 100 % RH but absorbed more moisture. A short-term equilibrium was assumed at around 42 days (≈ 1904 √s), approximately at a similar ageing period as DION 1260, which equilibrated at approximately 35 days (≈ 1700 √s). Nonetheless, the moisture gain at the assumed "equilibrium" of 1.17 % for DION 1273 was much higher than that of DION 1260, which attained approximately 0.77 %. In addition, for an ageing period of 530 days, the maximum moisture gain obtained by DION 1273 at 50 °C was 1.4 %, whereas a significantly lower maximum moisture gain of 0.77 % was attained by DION 1260 (*Table 5-2* and *Table 5-3*). A possible reason for this is that DION 1260 possess a notably higher styrene content than DION 1273, which is known to increase the hydrophobicity of the matrix [44]. Moreover, the two resins consist of two different primary monomers, methyl-methacrylate (MMA) – DION 1273, and bisphenol-epoxy – (DION 1260), which in turn produce a matrix with entirely different polymer networks from each other. N'Diaye et al [188] have reported that although methyl-methacrylate polymers (PMMA) are hydrophobic, they have been found to absorb up to 2 % of water and can undergo swelling and plasticisation, as did DION 1273 at all ageing

conditions. Although DION 1273 is not a thermoplastic, as is PMMA, a significant portion of the resin consists of an MMA monomer, similarly to PMMA.

All "Polynt Standard" cure DION 1260 and DION 1273 specimens were re-dried under the same drying schedule to allow direct comparison. Re-drying was conducted at 45 °C for 72 h, following storage in a dry desiccator of 10 % RH (produced be means of silica gel) at RT for a minimum of 24 h. A re-drying temperature notably lower than the Tg of the materials was selected to avoid weight loss during the re-drying cycle. All weight loss values after re-drying are contained in *Table 5-4*. At 23 °C and 100 % RH, the weight loss of DION 1273 was slightly less than DION 1260, despite the former absorbing more moisture. However, at 50 °C, DION 1273 noted a significantly higher weight loss than DION 1260, indicative of the susceptibility of the matrix to hydrothermal attack at elevated temperatures. Pronounced discolouration was also observed for all DION 1273 at all ageing conditions, indicative of chemical ageing, as shown in *Figure 5-9*.

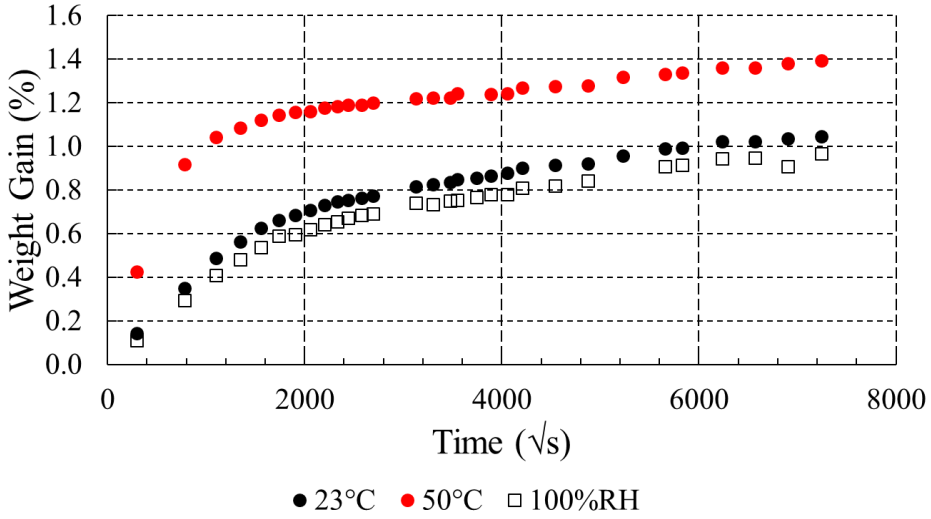

Figure 5-8: *Weight gain vs ageing time plot for neat DION 1273 matrix at different ageing conditions.*

DION 1273	Condition	Equilibrium (%)	Diffusivity x 10^{-6} (mm^2/s)	Max. Ageing Period (Days)	Max Weight Gain (%)
Polynt Standard	23°C	0.75	0.84	530	1.05
	50°C	1.17	2.18	530	1.4
	100 % RH	0.68	0.59	530	0.97

Table 5-3: *Weight Gain and diffusivity of DION 1273 at different ageing conditions.*

	Weight Loss (%)		
	23 °C DI	**50 °C DI**	**100 % RH**
DION 1260	0.24	0.27	0.23
DION 1273	0.18	0.42	0.19

Table 5-4: *Weight loss (%) of neat DION 1260 and DION 1273 ("Polynt Standard") upon ageing and re-drying.*

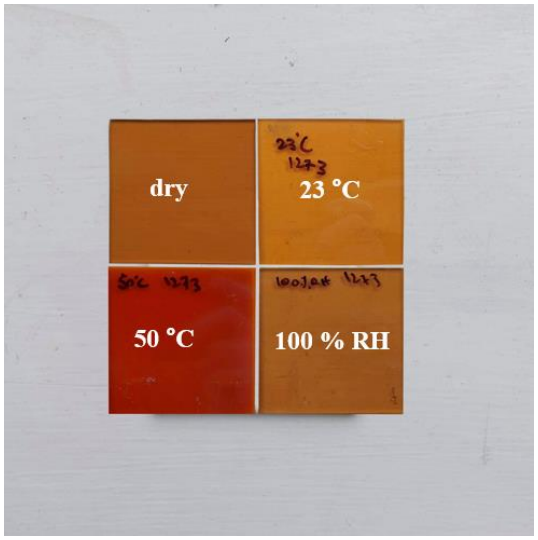

Figure 5-9: *Neat DION 1273 colour retention at different ageing conditions.*

5.2.2. Neat Resin: Dynamic Mechanical Analysis (DMA)

DMA Characterisation of Moisture-aged DION 1260 Vinyl Ester

The Tg of DION 1260 "Polynt Standard" in its un-aged state was measured by DMA to be 99 °C. Tg retention and weight gain vs ageing time plots are featured in *Figure 5-10*. The weight gain was measured for the rectangular bar specimens employed in the DMA measurements. Moisture values recorded for these were similar to the ones of 80 x 80 mm specimens, discussed in the previous section *5.2.1*. Tg depression was greater as the exposure conditions became more amplified. At 50 °C, all measurements were conducted beyond equilibrium. A Tg depression of approximately 10 % was noted after 1 month of ageing. Tg was further depressed after 3.5 months of ageing and was then stabilised for a total ageing period of 6

months. At 23 °C and 100 % RH, Tg depression increased as a function of weight gain. Both moisture gain and Tg depression at these conditions were on a similar level, but slightly lower for specimens aged at 100 % RH. Measurements at 100 % RH were only taken after 1 month and 6 months, and no measurement was taken at 3.5 months. This was due to the lack of available matrix material and upon observing that the gravimetric trends at 23 °C and 100 % RH were similar. Tg depression has been previously associated with plasticisation [3,134,166]. Hydrolytic degradation was also probable, as indicated by the results of the gravimetric analysis conducted in matrix plates. Please note that in this case DMA was conducted on wet specimens and at different ageing periods. A scouting experiment showed similar values for the same system post-cured at 100 °C.

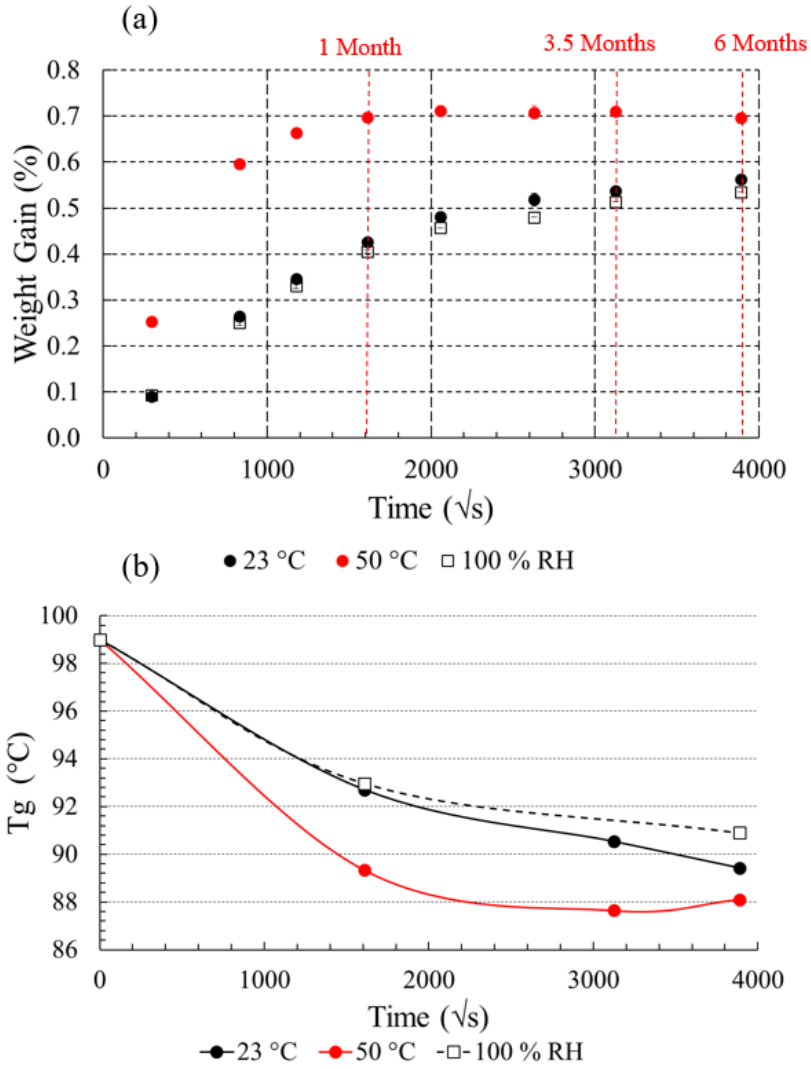

Figure 5-10: *Tg depression and weight gain vs ageing time of neat DION 1260 ("Polynt Standard") in "wet" state at different ageing conditions. The red gridlines in plot "a" indicate the ageing period in "months".*

A complement to this analysis were the Tg measurements, conducted by DMA, on rectangular specimens extrapolated from the aged and re-dried 80 x 80 mm specimens at all three ageing conditions. The Tg of un-aged "Polynt Standard" was 99 °C. The Tg values for the aged and re-dried specimens were 101 °C, 102 °C and 101 °C at 23 °C DI, 50 °C DI and 100 % RH, respectively, as shown in *Table 5-5*. These are notably higher than the ones measured during the ageing period of the specimens (*Figure 5-10*) but only slightly higher than the Tg value of the dry DION 1260 specimen. This implies that the majority of degradation can be attributed to plasticisation – reversible degradation, especially for specimens aged at 23 °C and 100 % RH. This is in correlation with the moisture sorption behaviour of the specimens, which exhibited a continuously increasing weight pattern, indicative of matrix relaxation through plasticisation. However, narrowing of the loss modulus peak upon ageing at either of the three ageing conditions may be a hint of secondary cross-linking. In particular, as shown in *Figure 5-11*, the narrowing of the loss modulus peak followed the intensity of the ageing conditions. It was the broadest at 100 % RH and the narrowest at 50 °C. Such changes may be indicative of anti-plasticisation effects starting to take place after room temperature ageing, and being more apparent at a higher temperature. Besides, these were denoted by the weight loss of the samples upon ageing and their discolouration. Please note that discolouration was mildest at 23 °C and 100 % RH and more amplified at 50 °C, which is in line with the observation regarding anti-plasticisation effects. Increased cross-linking did not result in a huge Tg increase, but anti-plasticisation effects may be nonetheless counteracted by subsequent moisture-induced degradation. It is possible that further ageing would have resulted in amplified anti-plasticisation effects and a higher Tg.

Gravimetric and DMA results on "Polynt Standard" plates can be summarised as follows. For specimens aged at 23 °C and 100 % RH, plasticisation/relaxation was the dominating moisture-induced degradation effect. This was manifested by the continuous weight increase of the specimens and was confirmed by a Tg decrease as a function of ageing. The majority of degradation was indeed physical and was confirmed upon re-drying the specimens and measuring their Tg, which remained close to the Tg of the un-aged specimens. However, chemical ageing did take place in the form of leaching. Leaching effects were apparent indicated by the discolouration and weight loss of the aged specimens. Leaching seemed to have introduced secondary cross-linking, indicated by the narrowing of the loss modulus curve. The latter effect, along with discolouration was more pronounced for the specimen aged at 50 °C. The weight uptake vs ageing behaviour of the plate aged at 50 °C resembled Fickian diffusion, and relaxation effects were not apparent. Despite the attainment of a Fickian curve, DMA results during ageing showed a notable Tg decrease – plasticisation, whereas DMA

results after ageing and re-drying indicated a small Tg increase and narrowing of the loss modulus curve which may imply cross-linking. It can thus be concluded that competing ageing effects took place at 50 °C. Similar degradation did indeed take place at all ageing conditions, but evidently at a slower rate, which is expected considering that 50 °C is an accelerated ageing environment.

"Polynt Standard"	Max. Ageing Period (Days)	Tg (°C)
Dry	N/A	99
23 °C	530	101
50 °C	530	102
100 % RH	530	101

Table 5-5: *Tg of aged and re-dried DION 1260 "Polynt Standard" 80 x 80 x 3.9 mm plates, obtained by the onset of the storage modulus curves presented on a logarithmic scale, and produced by DMA.*

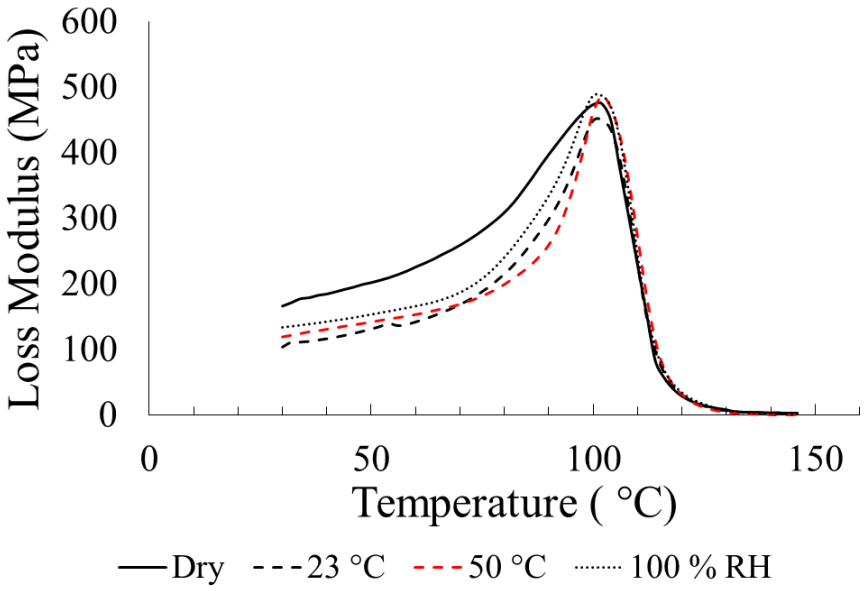

Figure 5-11: *DMA loss modulus thermal curve for aged and re-dried neat DION 1260 ("Polynt Standard") specimens.*

DMA thermal curves obtained on DION 1260 "UoS Op. Mould – 100 °C" specimens extrapolated by the 80 x 80 mm plates used for ageing are illustrated in *Figure 5-12*. Tg values

obtained both by the onset of the storage modulus and the two loss modulus peaks upon the completion of ageing and re-drying of open mould DION 1260 specimens are contained in *Table 5-6*. A shoulder was present in all loss modulus curves of open mould specimens. As discussed in *Chapter 3*, the presence of a loss modulus shoulder may be an indication of poor cross-linking in vinyl esters, resulting in phase separation, whereby its phase has its own distinct Tg. Tgs obtained by the onset of the storage modulus were similar, but slightly higher, for the aged specimens, compared to those of the dry matrix. After ageing at 23 °C, the shoulder evident prior to the main loss modulus peak was broadened and shifted to a lower temperature, indicating plasticisation. On the other hand, the loss modulus shoulder had almost disappeared after ageing at a higher temperature of 50 °C and within a shorter timescale. This was an indication of further reaction of the lower Tg phase of the vinyl ester matrix. Similar observations have been made by Fraga et al [39], who found that two tan δ peaks apparent in the thermal curve of dry VE specimens were integrated into one upon ageing. In all cases, environmental attack may be acting in combination with secondary cross-linking, "balancing out" the Tg values to a level closer that of the dry matrix. Such observations have been made by a series of researchers [18,33,34].

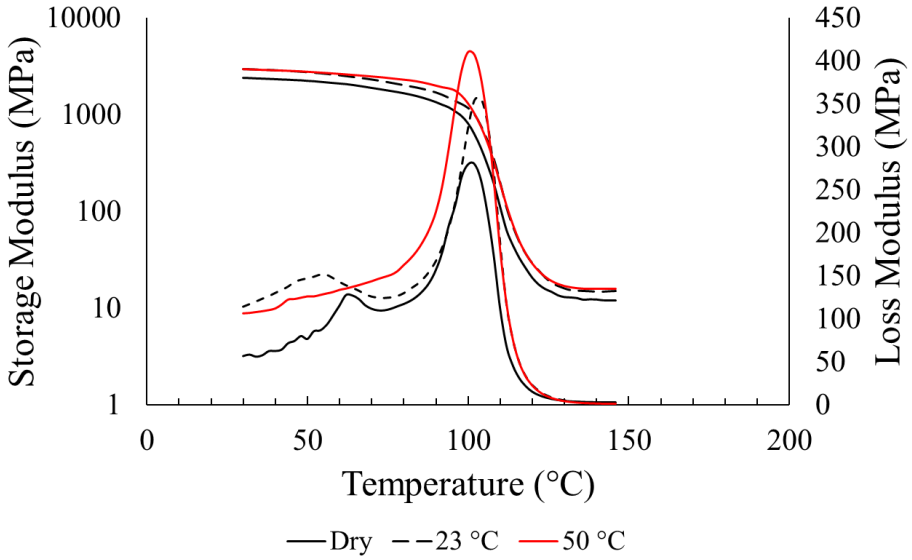

Figure 5-12: *DMA thermal curves for DION 1260 "UoS Op. Mould – 100 °C" specimens; un-aged and aged (re-dried) specimens at 23 °C and 50 °C for 21 and 10.5 months, respectively.*

" UoS Op. Mould – 100 °C	Ageing Time (Months)	Loss Modulus - 1st Peak	Loss Modulus - 2nd Peak	Storage Modulus - Onset
Dry	N/A	62	101	100
23 °C DI	21	55	103	102
50 °C DI	10.5	N/A	101	101

Table 5-6: *Tg of aged and re-dried DION 1260 "Op. Mould" obtained by the storage (log. scale) and loss modulus curves produced by DMA.*

DMA Characterisation of Moisture-aged DION 1273 Vinyl Ester

The Tg of the un-aged DION 1273 "Polynt Standard" was measured by DMA to be 77 °C. This was notably lower than that of DION 1260 (99 °C). DMA-suitable "Polynt Standard" DION 1273 specimens were extracted from the 80 x 80 mm plates upon the completion of ageing (530 days) and re-drying. A clear Tg increase was shown at all conditions, which was amplified upon elevated temperature ageing. More specifically, Tg values of 80 °C were found after ageing at 23 °C and 100 % RH, and 86 °C after ageing at 50 °C. The Tg increase upon ageing was a clear indication of moisture-induced cross-linking. Secondary cross-linking has been previously associated with anti-plasticisation effects [22,33,34]. In this case, these were probable, indicated by the pronounced discolouration of the specimens and their weight loss through leaching. Nevertheless, DION 1273 plates underwent a continuous weight increase during ageing, indicative of relaxation through plasticisation which is a form of physical ageing. It is thus likely that competing relaxation and secondary cross-linking effects were apparent, whereby relaxation dominated but was reversed upon re-drying the specimens.

5.2.3. Composite: Mechanical Testing

Mechanical Property Assessment of Moisture-aged SE 3030/1260 Composite Laminate

During this study, specimens of different geometries were aged, since they were employed for different purposes, such as mechanical testing and thermal analysis. Firstly, a weight gain vs time plot is shown in *Figure 5-13* for 80 x 80 x 3.9 mm SE 3030/1260 laminates at different ageing conditions. The specimen geometry was selected to allow direct comparison with the neat resin plates, presented in the previous section. Laminate edges were sealed so that diffusion coefficients can be obtained from a simplified 1-D analysis ignoring edge effects. Composite diffusivity and weight gain values obtained experimentally vs diffusivity and

weight gain values predicted by neat matrix ageing are compared in *Table 5-7*. An average SE 3030/1260 weight fraction of 0.29 % was considered for the evaluation of the predicted moisture gain. In all cases, obtained diffusivity and weight gain values were higher than the ones predicted. This was attributed to three main reasons taking into account the observations of Karbhari and Zhang [6]; relaxation of elastic forces induced by the cross-linked network after the initial weight-gain plateau, and (or) wicking at the interface, and (or) the presence of manufacturing voids and the likelihood of them being increased by ageing.

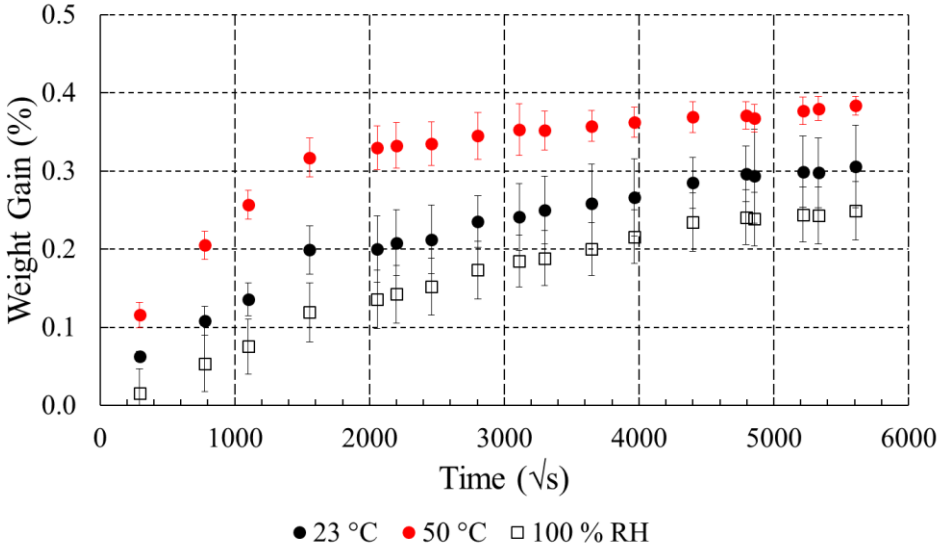

Figure 5-13: *Weight gain vs ageing time plot for 80 x 80 x 3.9 mm, SE 3030/1260 composite specimens at different ageing conditions.*

	Condition	Equilibrium Prediction (%)	Obtained Equilibrium (%)	Diffusivity Prediction x 10^{-6} (mm^2/s)	Obtained Diffusivity x 10^{-6} (mm^2/s)
SE 3030/1260	23 °C DI	0.17	0.24	0.067	0.5
	50 °C DI	0.22	0.33	0.34	1.1
	100 % RH	0.15	0.19	0.08	0.55

Table 5-7: *Experimental vs predicted SE 3030/1260 composite diffusivity and weight gain values.*

Despite the thickness of all different specimens employed in this study being the same, varying absorption curves and moisture gain levels were attained by specimens of different geometries. A comparison of the weight gain vs ageing time of SE 3030/1260 specimens of different geometries is shown in *Figure 5-14*, aged by full immersion at 50 °C. Generally, it was found that smaller specimens absorbed more moisture. This could be attributed to several reasons,

such as increased void content, wicking along the interface, variation in volume fraction, and weak seal around laminate edges and corners. In particular, the edge sealant was proven to be particularly hydrophilic, even at room temperature and after short-term ageing. The removal of the seal during ageing is a common issue in the ageing of composites. According to the literature, simplistic 1-D diffusion models can lead to erroneous results, especially when removal of the sealant occurs. More complex diffusion models may thus be employed to understand the full effect of ageing when changing specimen geometry [189].

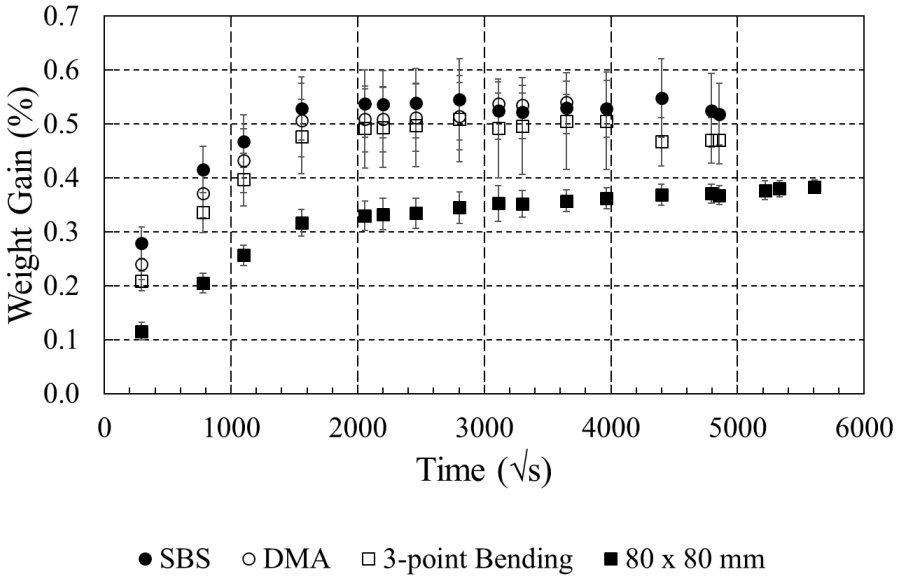

Figure 5-14: *Weight gain vs ageing time comparison for SE 3030/1260 specimens of different geometry aged 50 °C by immersion in DI water.*

A void content study was carried out on aged and tested SBS specimens, and the results of it are shown in *Figure 5-15*. Certain specimens were impaired upon mechanical testing resulting in an extremely high void content. These refer primarily to the first two tested batches, such as the "dry" specimens and some of the specimens aged at 23 °C, which were not accounted for. Hence, the void content of a similar laminate in its dry state was measured for reference. This comprised of the same matrix – DION 1260 and reinforced with the same fibre, but with a different vinyl ester-compatible sizing, namely S 001. The void content of S 001/1260 was measured to be 0.78 %, by volume. Assuming a similar void content for the SE 3030/1260 laminate, it can be accepted that void content was increased upon ageing. The increase was observed after 3 months of ageing, followed by a plateau for the remaining ageing period. The void content of aged specimens was found between 1.65 % and 2.46 %, by volume.

The highest void content increase was observed after ageing at 50 °C. However, at most conditions and time intervals, void content error bars were found to overlap each other. The lowest void content increase was attained at the "mildest" condition of 100 % RH. At 23 °C, the greatest void content fluctuations as a function of ageing were seen. In particular, at 3 months the void content measured at 23 °C was the greatest of all conditions, and the lowest of all conditions and close to the value was obtained at 100 % RH at 6 months. It was then followed by a subsequent increase of approximately 20 % after 9 months of ageing.

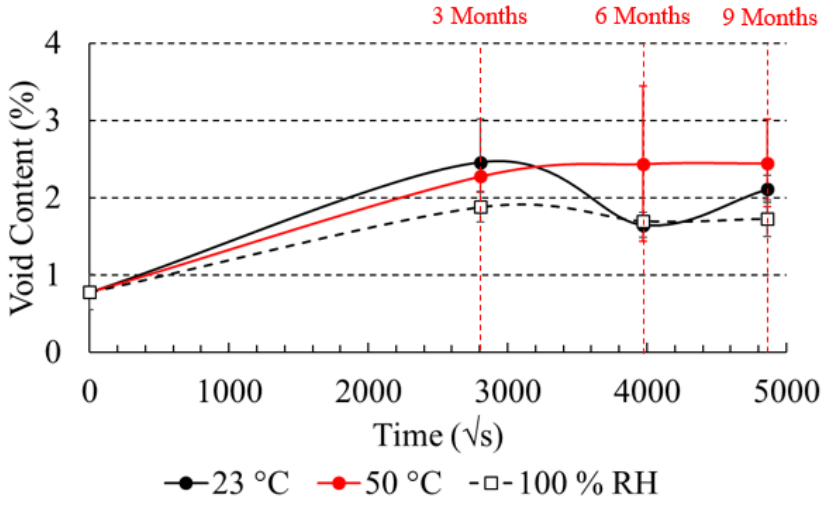

Figure 5-15: *Measured void content (%) vs ageing time for SBS, SE 3030/1260 composite specimens at different ageing conditions.*

The average sealant used for the SBS specimens was the highest of all other specimens used – approximately 3.5 % in average. Weight gain for SBS specimens and ILSS retention vs ageing time plots are presented in *Figure 5-16*. Fickian-like curves were recorded at all ageing conditions followed by some weight fluctuations in certain cases. The highest weight gain for the greatest part of the ageing period was featured at 50 °C. However, large and overlapping error bars were featured in all cases. The variation in weight gain was attributed to the weakening of the sealant. This was more pronounced at the ageing conditions of 23 °C and 100 % RH, resulting in a shift of the weight gain values close to those obtained at 50 °C. Large weight fluctuations were seen beyond an ageing period of 6 months for the conditions 23 °C and 100 % RH when the number of the immersed specimens was reduced (specimens were used for mechanical testing). In the literature review, it was established that if moisture is allowed to enter the FRP structure it can be stored within voids, and in turn gradually increase degradation and moisture gain. Such an effect, along with leaching of the sealant, potential leaching of the matrix constituent, and probable leaching along the interface can act in combination and result in anomalous sorption.

The ILSS of dry SE 3030/1260 was found to be 59.5 MPa. Generally, the varying void content did not seem to have a discernible effect on the ILSS of the composite. It may indeed have affected the resulting ILSS, but the extent of the effect remains unclear since similar void content was exhibited by SBS specimens at all ageing conditions. In fact, it was observed that ILSS was greatly dependent on the severity of the ageing conditions. One main ILSS retention trend was identified. ILSS depression was greatest at 50 °C and also noted the highest decline as a function of ageing. ILSS retention was similar for both 23 °C and 100 % RH and recorded retention, % values were found to overlap. At 50 °C, the ILSS retention of the laminate was reduced to just over 60 % after 3 months of ageing, remained at a similar but slightly lower level after 6 months and dropped gradually to 50 % after 9 months. ILSS at 23 °C and 100 % RH was retained between 83 % and 90 % after 3 months of ageing, it was then increased to a level between 90 % and 95 % after 6 months, and was subsequently reduced to approximately 80 % after 9 months. Trends similar to the latter, whereby strength is increased upon short-term ageing and subsequently decreased upon long-term ageing have been previously identified in the literature [6]. The short-term strength increase may be an indication of secondary cross-linking of the matrix upon ageing. However, such changes were small and mostly contained within the error bars featured, thus the latter statement is not definitive. ILSS has been identified as a property which is highly dependent on the integrity of both the matrix and the fibre/matrix interface [74]. Thus, moisture wicking along the interface was considered to be one of the acting degradation mechanisms on the composites, which can weaken interfacial bonds and result in a reduction in mechanical properties. Such degradation may be more amplified at elevated temperatures due to leaching and subsequent void and (or) cracking formation, as well as fibre pitting [6,22]. The provision of a more definite answer on whether degradation of the fibre, matrix constituents or their interface (or a combination) may be causing the reduction in mechanical properties would benefit from an assessment of the mechanical properties of the matrix itself as a function of ageing. Nonetheless, DMA results presented in the previous section showed that the Tg of the matrix was not majorly affected by ageing and was regained upon re-drying the specimens. Based on these observations, it can be deduced that weakening on the interface may be playing a significant role in ILSS reduction, although further experimentation would be desirable. Interfacial testing presented in *Chapter 6* may also be useful to provide insight into the integrity of the interface as a function of ageing.

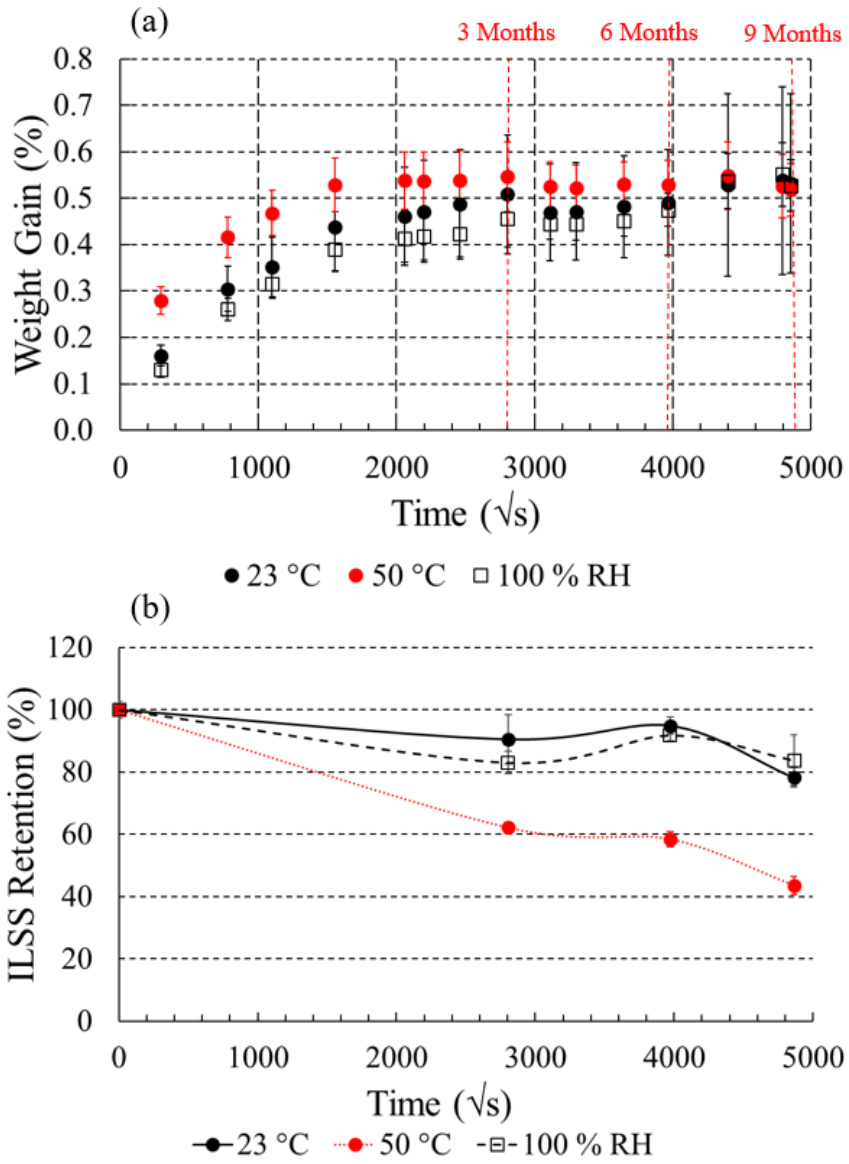

Figure 5-16: *(a) Weight gain vs ageing time plot for SBS, SE 3030/1260 composite specimens at different ageing conditions. The red gridlines indicate the ageing period in "months". (b) ILSS retention vs ageing time plot for SBS, SE 3030/1260 composite specimens at different ageing conditions.*

The weight gain of 3-point bending bar specimens and flexural strength retention vs ageing time are presented in *Figure 5-17*. Fickian-like behaviour was observed in all cases, but the weight gain remained at relatively lower levels than in SBS specimens. When direct exposure to water by immersion (23 °C DI and 50 °C DI) was allowed, the total weight gain was higher than that attained by 80 x 80 mm specimens. Additionally, the error bars were quite high in both cases. On the other hand, at 100 % RH slightly lower weight gain was attained than that of 80 x 80 mm specimens, along with lower error bars. As previously discussed, such changes

in the weight gain behaviour can be attributed to numerous reasons. In this case, sealant removal in some of the specimens was the most apparent reason when direct exposure to water was enabled, resulting in varying moisture content and higher error bars. Additionally, removal of sealant may have allowed an easier pathway through the composite enabling wicking and may have in turn enabled deterioration of the fibre/matrix interface.

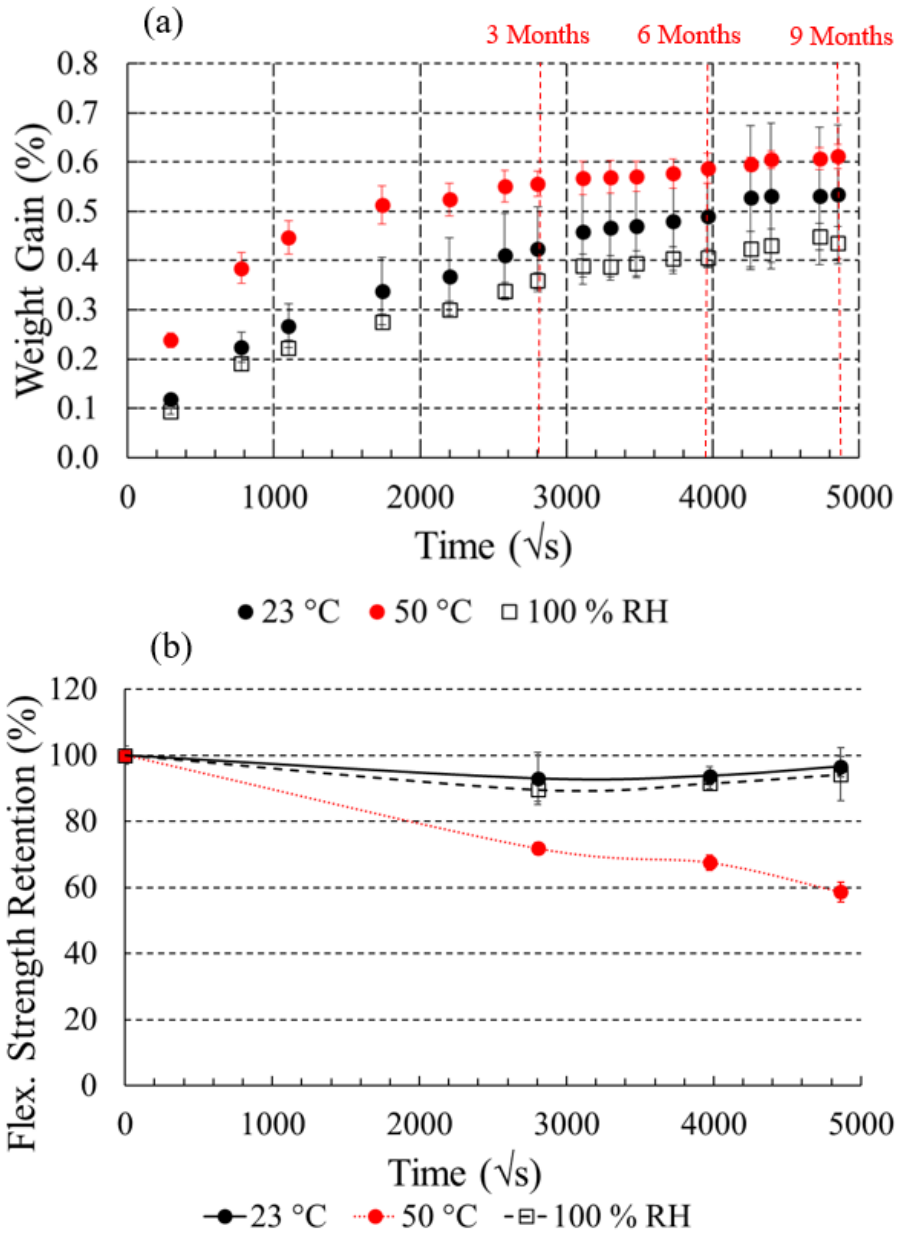

Figure 5-17: *(a) Weight gain vs ageing time plot for 3-point bending, SE 3030/1260 composite specimens at different ageing conditions. The red gridlines indicate the ageing period in "months". (b)Flexural strength retention vs ageing time plot for 3-point bending, SE 3030/1260 composite specimens at different ageing conditions.*

According to Bowles and Frimpong [190], a linear relationship between flexural strength and short-beam shear measurements can be established. This was also more or less applied in this case, as shown in *Figure 5-18*, which features a comparison of the average flexural strength values plotted against the average ILSS values. Thus similar degradation mechanisms may have been promoted by ageing in both SBS and flexural strength specimens. In a similar fashion to SBS, one main trend was featured regarding flexural strength retention; the highest flexural strength loss was noted at 50 °C, notably higher than the one seen at 23 °C and 100 % RH. At 50 °C, the main flexural strength loss took place after 3 months of ageing, close to 30 %. It was then followed by smaller reductions of around 32.5 % and 41 % after 6 and 9 months, respectively. Similar trends were obtained at the conditions of 23 °C and 100 % RH. After an initial drop of 7 %, the flexural strength remained relatively constant throughout the ageing period. It was then followed by a gradual increase as conditioning continued. The greater depression at 50 °C may be attributed to matrix plasticisation and hydrolytic effects, commonly apparent in VE-based FRPs and amplified at elevated temperatures. Glass fibre degradation, such as sizing loss, and moisture penetration along the interface, thus interfacial weakening were also considered [6,22]. At room temperature exposure, even though a relatively small initial depression was seen, part of the strength was regained as a function of ageing. The latter wass an indication of ageing-induced secondary cross-linking, even though recorded data points are contained within the same featured 95 % error bars, and such a statement is not definitive.

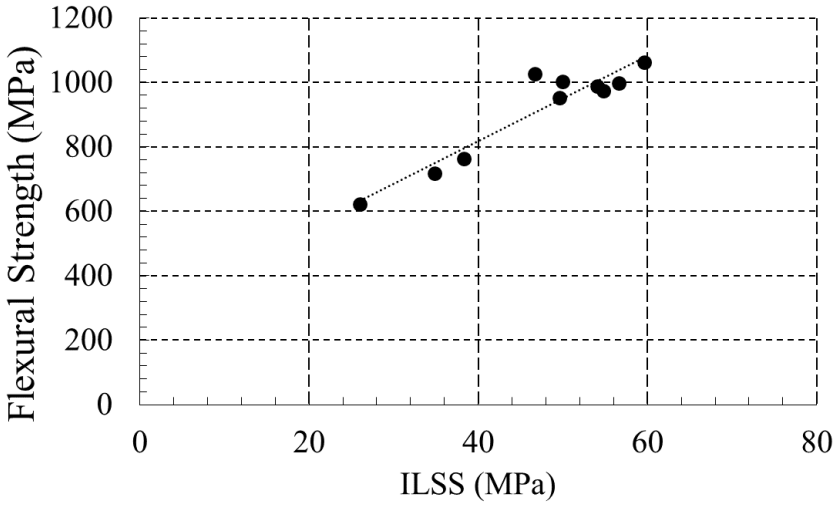

Figure 5-18: *Plotted comparison of the average measured flexural strength vs ILSS values for SE 3030/1260.*

A Young's modulus retention vs ageing time plot is shown in *Figure 5-19*. The average Young's modulus of the SE 3030/1260 composite in its un-aged form was determined experimentally to be 40.8 GPa. It can be observed that Young's modulus does not change appreciably as a function of ageing time. There are some small fluctuations in the property but contained within 95 % error bars featured. Flexural testing was measured in a 3-point bending configuration in the fibre direction, and output Young's modulus was thus heavily influenced by the reinforcement. The Young's modulus retention trend was in contrast with the trend featured in flexural strength and ILSS retention. The latter were indeed severely affected by ageing, attributed primarily to the weakening of the interface and the matrix. It can be deduced that Young's modulus results were an indication that the stiffness of the composite, which is heavily influenced by the stiffness of the fibre, was not largely affected by ageing.

.

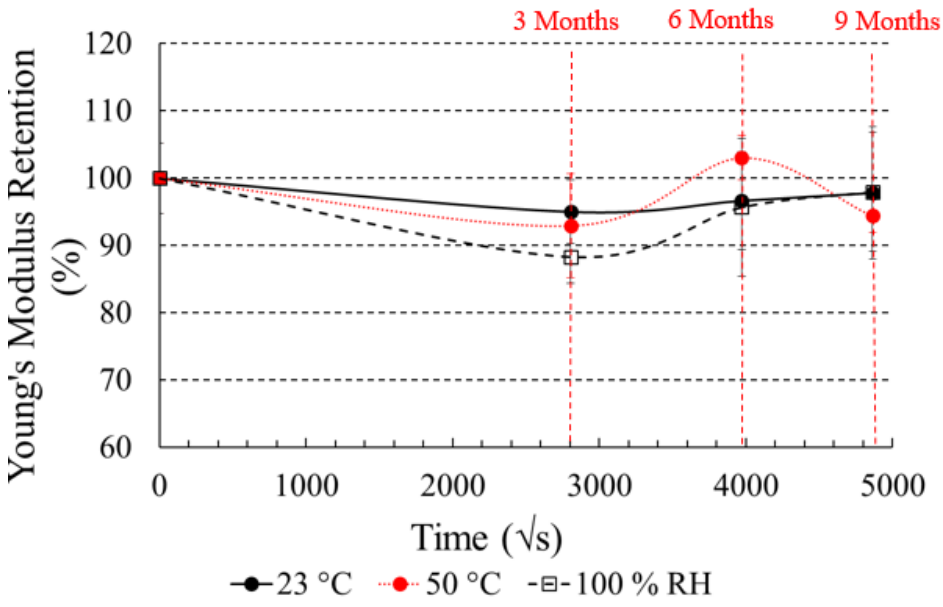

Figure 5-19: *Young's modulus retention vs ageing time plot for 3-point bending, SE 3030/1260 composite specimens at different ageing conditions.*

Further investigation could be carried out by SEM to study in more depth the manner the laminates are affected by ageing, the impact of the variation between water immersion and humidity exposure, as well as the effect of the increase of the ageing temperature on the structure and morphology of the FRPs. However, given that SBS measurements can be sensitive to both interfacial changes and the integrity of the matrix, and that the latter was relatively resilient to hydrothermal degradation when adequately cured, mechanical property depression may be attributed to the weakening of the fibre matrix interface and (or) weakening

of the fibre [6,22]. Weakening of the glass fibre refers to sizing hydrolysis when exposed to moisture and heat, and (or) ageing-induced reduction of sizing reactivity with matrix [191]. Nonetheless, Young's modulus vs ageing measurements showed exceptional stiffness retention, towards which the contribution of the fibre clearly contributed. A potential sizing loss may still be apparent in affecting the interface, but such changes may not be apparent in the stiffness values of the composite. Reduced interfacial performance may have been facilitated by the removal of the sealant, which can in-turn enable the wicking of moisture along the fibre/matrix interface. Furthermore, according to Hammami and Al-Ghuilani [44] composites with a high fibre content (≈ 75 %), as is the case with the FRPs employed in this study, tend to exhibit poor wetting and thus reduced interfacial adhesion. Such composites are also known to be more susceptible to delamination and micro-crack formation, which can accelerate water diffusion through the composite structure and thus degradation. As presented in *Chapter 4* the presence of micro-cracks was commonly observed in the meniscus of SE 3030/1260, which was a sign of reduced adhesion between the fibre and the matrix. Although in reality the interface of an FRP varies from that of a micro-composite, the presence of cracks in the SE 3030/1260 FRP interface was considered. These can potentially be amplified during ageing producing micro-cracking coalescence, and in turn result in an increased moisture uptake and degradation at the interface [22]. Lastly, since SBS measurements can be sensitive to interfacial changes, as per the observations of Herrera-Franco and Drzal [74], a direct characterisation of the SE 3030/1260 interface (by the microbond test) as a function of ageing is presented in the following chapter.

Mechanical Property Assessment of Moisture-aged W 3030/1273 Composite Laminate

In a similar fashion to the SE 3030/1260, W 3030/1273 specimens of a smaller overall size showed a different total moisture gain and slightly different behaviour in certain cases. However, the moisture uptake of specimens of a smaller geometry was not as exaggerated as in the SE 3030/1260. This was primarily due to a more effective sealant application, and possibly a lower void content. Each Araldite epoxy mixture produced was used for the sealant of 2 specimens at a time, instead of 3 – 4 specimens used for the SE 3030/1260. Although the sealant application was more successful, sealant loss during ageing was still apparent.

A weight gain vs ageing time plot recorded for 80 x 80 x 3.9 mm W 3030/1273 specimens at diffeferent ageing conditions is demonstrated in *Figure 5-20*. A continuously increasing weight gain as a function of ageing was evident at all conditions. This may be indicative of matrix relaxation, wicking at the interface, or storage of moisture in air gaps, such as delaminations and interfacial micro-cracks [6,22,44]. Such a weight gain behaviour was in

close correlation to the weight gain pattern exhibited by the neat matrix. The highest sorption was attained at 50 °C. The composites aged at 23 °C and 100 % RH exhibited similar sorption levels, although slightly higher sorption was attained with full immersion (23 °C DI). Composite diffusivity and weight gain values obtained from this data and weight gain values predicted by using *Equation 2-9*, neat matrix ageing are compared in *Table 5-8*. Considering an average matrix weight fraction of 29 %, predicted weight gain (at equilibrium) values were lower than those obtained experimentally. Firstly, there was no actual equilibrium obtained by the laminates, but equilibrium was assumed at the stage when water uptake was slower to facilitate the calculation. Similarly to SE 3030/1260 the increased weight gain and continuously increasing weight gain pattern may be attributed either to matrix relaxation, and (or) to wicking at the interface. However, experimentally obtained diffusivity values assuming 1-D Fickian diffusion were close to those expected. These were determined using *Equation 2-8*, taking into account the fibre volume fraction of the composite. Again, in this case, due to no equilibrium, obtained diffusivity values are an approximation and do not fully represent the water uptake behaviour of the composite. Overall, the moisture gain of W 3030/1273 was found to be higher than that of the SE 3030/1260, in line with the observations made for the DION 1273 and DION 1260 matrices, respectively.

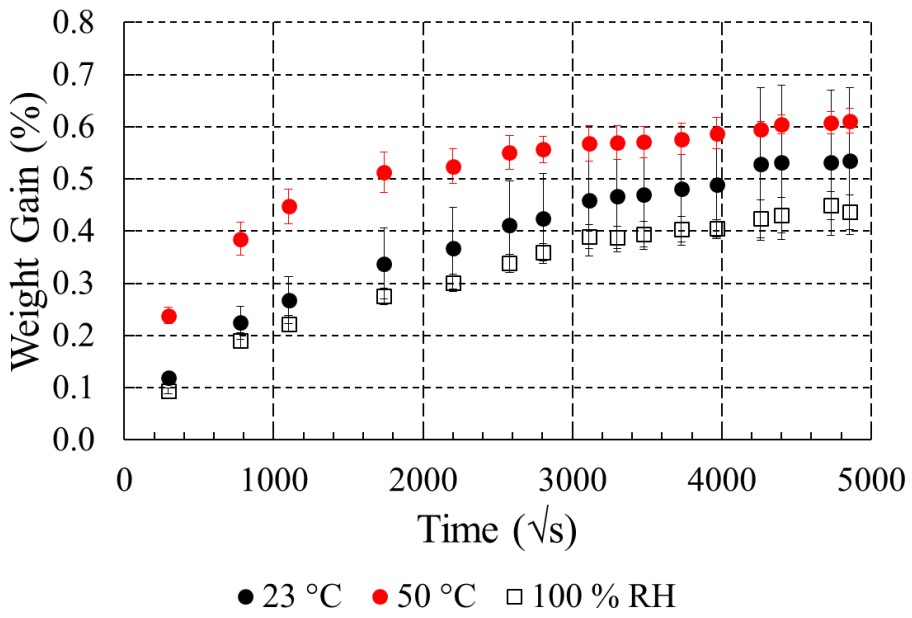

Figure 5-20: *Weight gain vs ageing time plot for 80 x 80 x 3.9 mm, W 3030/1273 composite specimens at different ageing conditions.*

	Condition	Equilibrium Prediction (%)	Obtained Equilibrium (%)	Diffusivity Prediction x 10^{-6} (mm^2/s)	Obtained Diffusivity x 10^{-6} (mm^2/s)
W 3030/1273	23 °C DI	0.22	0.33	0.16	0.17
	50 °C DI	0.34	0.41	0.42	1.6
	100 % RH	0.2	0.29	0.11	0.17

Table 5-8: *Experimental vs predicted W 3030/1273 composite diffusivity and weight gain values.*

Weight gain of SBS specimens and ILSS retention vs ageing time plots are shown in *Figure 5-21*. The water uptake behaviour of SBS specimens was similar to the one recorded for the 80 x 80 mm plates, noting nevertheless a higher moisture gain. An average ILSS of 45.3 MPa was obtained for dry W 3030/1273, close to 25 % less than that of SE 3030/1260. Despite SE 3030/1260 having a higher ILSS in its dry state, it was overall proven to be more susceptible to ageing-induced mechanical degradation regarding ILSS retention, especially at elevated temperature, upon long-term ageing and when direct immersion in the ageing medium was enabled. Generally, the level of ILSS reduction for W 3030/1273 was similar at all ageing conditions.

In fact, upon short-term ageing at 50 °C, a reduction of approximately 14 % was measured for the W 3030/1273, as opposed to a loss of almost 40 % obtained for SE 3030/1260. Moreover, upon 9 months of ageing at 50 °C, the ILSS reduction for W 3030/1273 was close to that obtained by SE 3030/1260 at the milder ageing conditions of 23 °C and 100 % RH. Upon short-term ageing at 23 °C, W 3030/1273 underwent a slightly higher ILSS loss than SE 3030/1260. However, after 9 months of ageing and after following small fluctuations, ILSS returned to a similar level to that lost short-term. At 100 % RH and after ageing for 9 months, similar values were recorded for both laminates.

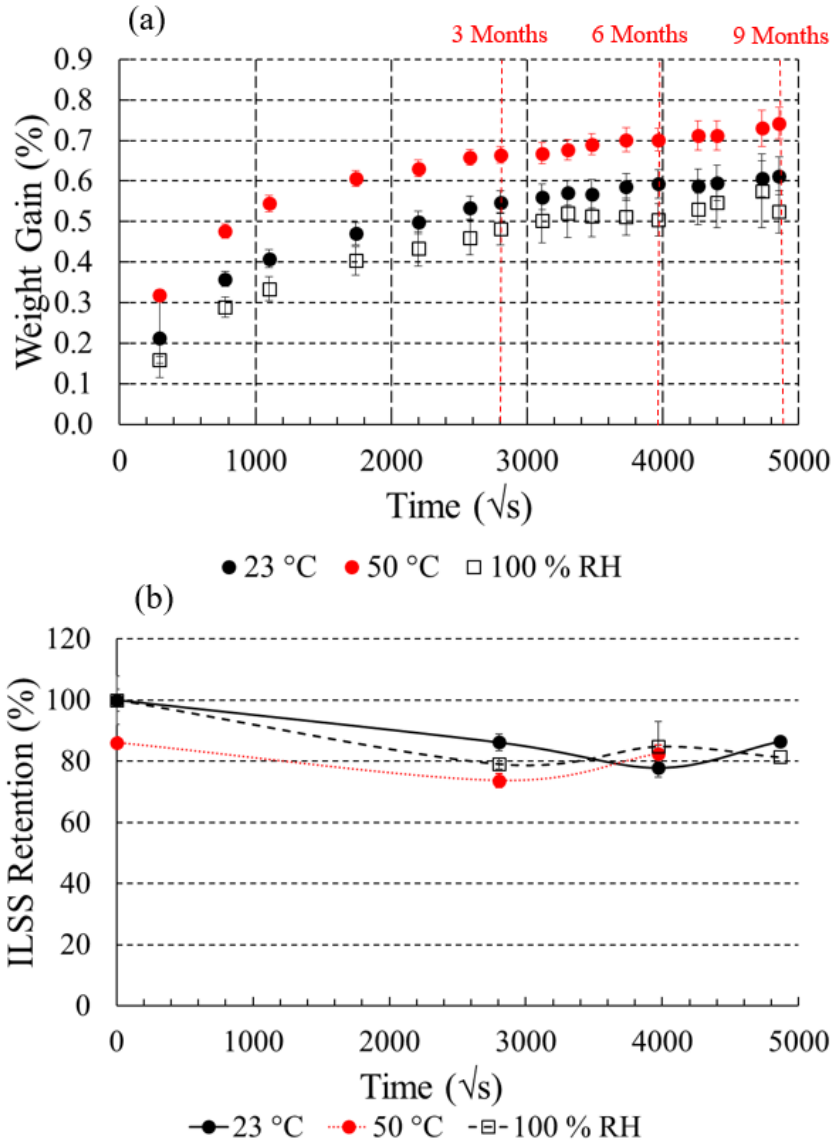

Figure 5-21: *(a) Weight gain vs ageing time plot for SBS, W 3030/1273 composite specimens at different ageing conditions. The red gridlines indicate the ageing period in "months", (b) ILSS retention vs ageing time plot for SBS, W 3030/1273 composite specimens at different ageing conditions.*

Weight gain of 3-point bending specimens and flexural strength retention vs ageing time plots are shown in *Figure 5-22*. The resilience of W 3030/1273 to elevated temperature conditioning shown in the ILSS results was also evident in the results obtained in flexural tests. In a similar fashion to SBS tests, results remain relatively close at all conditions, whereas one main trend was identified in SE 3030/1260 specimens – increased mechanical degradation at 50 °C, lower level of degradation at 23 °C and 100 % RH.

At 100% RH, a 7 % flexural strength increase was noted after 3 months of ageing. Even though the increase was considered minor, it was consistent for all tested specimens (small error bar).

Thus this may be an indication of moisture-induced secondary cross-linking. A small decrease of around 8 % from the values recorded for the un-aged specimen was then measured after 6 months of ageing. Lastly, upon the completion of the 9-month ageing period, flexural strength returned to a similar value to that obtained for the original dry specimens. Competing ageing-induced effects were thus considered resulting in different gradients in flexural strength retention. A similar loss in flexural strength was detected, upon full immersion at 23 °C and 50 °C. At 50 °C, the strength loss for W 3030/1273 was less significant than that of SE 3030/1260. This further validates the resilience of W 3030/1273 to mechanical degradation at elevated temperatures and despite absorbing larger levels of moisture.

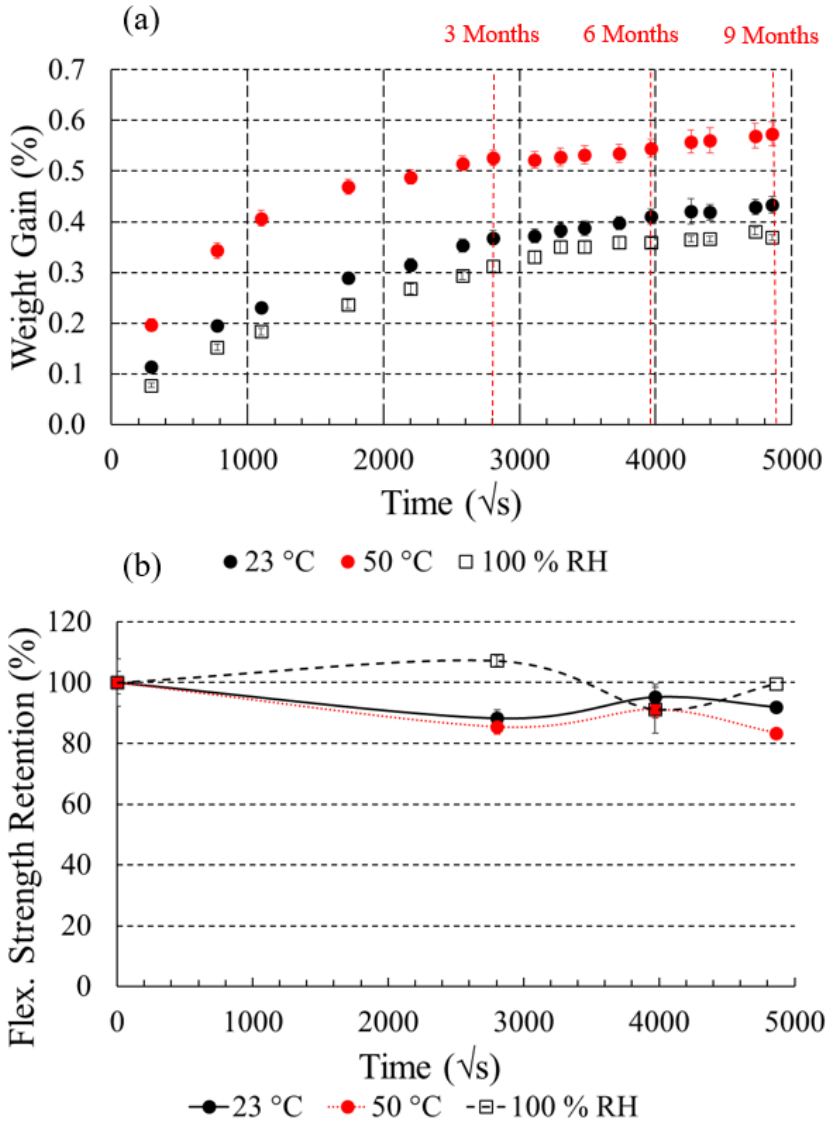

Figure 5-22: *(a) Weight gain vs ageing time plot for 3-point bending, W 3030/1273 composite specimens at different ageing conditions. The red gridlines indicate the ageing period in "months". (b) Flexural strength retention vs ageing time plot for 3-point bending, W 3030/1273 composite specimens at different ageing conditions.*

The average Young's modulus of the W 3030/1273 composite in its un-aged state was experimentally obtained to be 38.2 GPa. This value is only approximately 5 % lower than the Young's modulus value obtained for SE 3030/1260, whereas the ILSS and flexural strength of W 3030/1273 were around 25 % lower than those observed for its counterpart. Furthermore, according to Polynt, the flexural moduli of DION 1273 and DION 1260 were 2 GPa and 3.4 GPa, respectively. This clearly shows the contribution of the HiPertex W 3030 fibre to the stiffness properties of W 3030/1273. A Young's modulus retention vs ageing time plot is presented in *Figure 5-23*. It can be seen that Young's modulus remains relatively constant throughout the ageing period, especially when accounting for the 95 % error bars featured. Such results were similar to ones obtained for SE 3030/1260 and suggest that the reinforcement was least affected by ageing, in both composites.

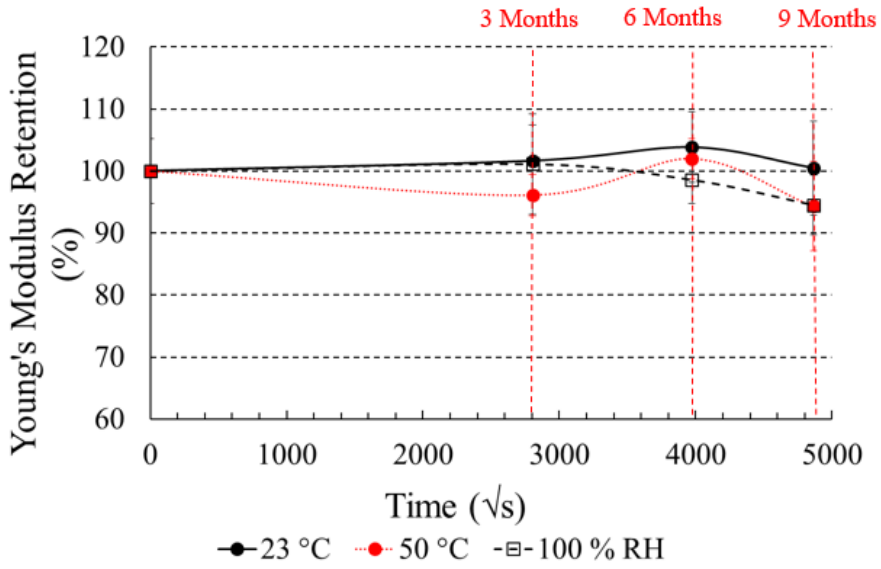

Figure 5-23: *Young's modulus retention vs ageing time plot for 3-point bending, W 3030/1273 composite specimens at different ageing conditions.*

Given the more effective mechanical properties retention against ageing for W 3030/1273 and that DION 1273 was found to be a more hydrophilic matrix, it can be accepted that W 3030/1273 had a more adequately "tailored" interface. Essentially, this is the inverse effect featured in the SE 3030/1260 laminate, which comprises of a less hydrophilic matrix, but an interface more susceptible to moisture attack. As entailed in the DION 1273 datasheet, DION 1273 is a vinyl ester matrix designed to provide enhanced adhesion. Further validation are the microbond test results presented in *Chapter 4*, which showed that W 3030/1273 indeed yields a higher IFSS than SE 3030/1273. Moreover, SEM results also presented in *Chapter 4* showed

an adequately bonded droplet for W 3030/1273, whereas cracking around the droplet meniscus was seen for SE 3030/1260. It is also possible that on a laminate scale such micro-cracks are present at the fibre/matrix bonds of SE 3030/1260, making it more susceptible to mechanical degradation under the influence of moisture and elevated temperature.

The effect of the reinforcing fibre should not be ignored, since HiPertex (W 3030) is designed to provide superior fibre properties to Advantex (SE 3030) [184]. The contribution of fibre properties was clear in the Young's modulus of the two systems, which were found to be close in magnitude, despite DION 1273 possessing a lower stiffness than DION 1260. This is a reasonable observation considering the rule of mixtures in the longitudinal direction, and the higher tensile modulus of HiPertex than that of Advantex [184]. According to SBS tests conducted by Peters et al [192] on an EP-based FRP made using the same matrix but using either HiPertex or Advantex, there was no significant variation in the output ILSS. No variation in ILSS was also shown for EP-based laminates made of either SE 2020 or W 2020 as a function of ageing in hydrothermal environments, whereas notable ILSS reductions were featured for an EP-based FRP reinforced with SE 1500 glass fibres [191]. On the other hand, a slightly higher flexural strength (10 %) was measured for EP-based FRPs made with HiPertex glass fibre, when compared to ones of the same matrix, made with Advantex, as a function of ageing in seawater, as per Boisseau et al [193]. It is noteworthy that FRP flexural properties are indeed sensitive to the properties of the fibre and the resulting fibre/matrix interface. Fibres that possess a high tensile strength allow for a more efficient stress transfer capability from the fibre to the matrix and can increase the flexural strength of the FRP [194,195]. However, all aforementioned results have been reported on EP-based laminates, and as previously discussed in *Chapter 4* interfacial properties between an EP system and a VE system may vary significantly. This is due to VE-compatible sizings being notably different from EP-compatible sizings. These may react differently with the glass formulation and subsequently with the matrix. Hence, although it was determined that DION 1273 can provide a more effective stress transfer capability to the interface, no definitive answers can be provided regarding interfacial properties in a bulk VE composite when switching from Advantex to HiPertex (or inversely).

5.2.4. Composite: Dynamic Mechanical Analysis (DMA)

DMA Characterisation of Moisture-aged SE 3030/1260 Composite Laminate

Weight gain of DMA bars and Tg vs ageing time plots are shown in *Figure 5-24*. The water uptake behaviour was found to be close to Fickian at all conditions. Increased moisture gain

was attained at all conditions when compared to the 80 x 80 mm specimens. At 50 °C and particularly at 23 °C, large error bars were featured. Composites were tested for their Tg in their "wet" state after 3 and 6 months of ageing, while ageing for 9 months was not allowed, due to lack of available material. In a similar fashion to SBS specimens, DMA specimens were adversely affected by direct contact with the water medium resulting in excess sealant removal.

Firstly, the Tg of the laminate was only higher by 3 °C than that of the neat matrix. Thus, the addition of the reinforcement did not have a huge influence on composite Tg. Generally, fibres do contribute to a Tg increase, but this is not always the case, since Tg is known to be a matrix-dominated property [196,197]. In fact, in certain cases, the addition of reinforcing fibres to the matrix has been found to cause a slight Tg decrease [33,34]. A common reason for this has been found to be incomplete wetting of the fibres by the matrix [198] or plasticisation of the matrix induced by the diffusion of fibre sizing components into the matrix [197].

Overall, it was observed that Tg depression was not dramatic at any ageing conditions, especially accounting for the 95 % error bars featured. At all ageing conditions, the largest part of Tg was reduced after 3 months of ageing. The greatest Tg decrease was seen at 50 °C after 3 months of ageing, but part of the lost Tg was regained after 6 months of ageing. Tg fluctuations as a function of ageing have been reported in numerous studies, reflecting the complexity of ageing-induced degradation mechanisms [22,33,34,199]. At 23 °C and 100 % RH, a gradual Tg decrease was observed with increased ageing time. At the latter conditions, the initial largest Tg depression was followed by a smaller decrease of only 1 – 2 °C, recorded after 6 months of ageing. Although composites were less susceptible to Tg depression than the neat matrix, similar trends can be identified in both cases within the ageing period of 6 months.

Overall, under the range of conditions studied, Tg change was minor and was greatest only at 50 °C. Moreover, as featured in neat matrix DMA measurements, most moisture-induced Tg reduction was also attributed to plasticisation since Tg depression was apparent for wet specimens but was fully restored upon re-drying the specimens. It is thus probable that similar behaviour would be exhibited by the composite if it was re-dried. It can hence be concluded that the Tg trend as a function of ageing is not in correlation with the loss of mechanical properties. On one hand, this validates the hypothesis that ageing-induced mechanical degradation discussed in the previous section is not matrix-dominated, but could be owed to probable weakening of the interface. On the other hand, in this work, composites exhibited a high fibre content and thus it can be assumed that the matrix is in fact bound to the interface. In any case, the thermal properties of the composite do not necessarily reflect its mechanical properties, and thus deviation in their trends vs ageing might be expected. For instance,

localised damage, such as cracking and delamination may have a different effect on the mechanical and thermal properties of the system. Allred [170] has reported an interesting observation on the Tg of moisture-aged (at 150 °C) Kevlar/EP composites with varying void content. The author found that composites with a higher void content showed a higher Tg, which he attributed to the presence of free water in the material pores that had not yet diffused to the matrix to affect the Tg. In the meantime, composites with a higher void content underwent a greater flexural strength depression as a function of ageing time than those with a lower void content.

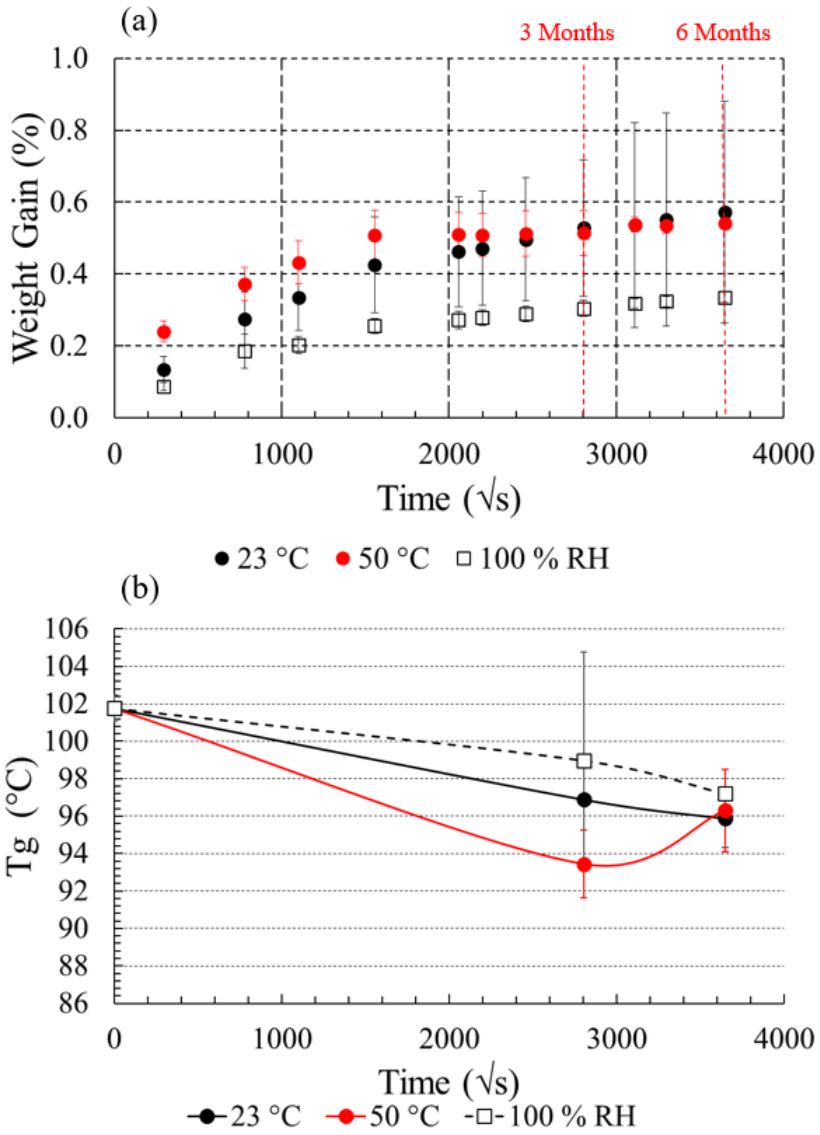

Figure 5-24: *(a) Weight gain vs ageing time plot for DMA-suitable, SE 3030/1260 composite at different ageing conditions. The red gridlines indicate the ageing period in "months". (b) Tg vs ageing time plot for DMA-suitable, SE 3030/1260 composite at different ageing conditions.*

DMA Characterisation of Moisture-aged W 3030/1273 Composite Laminate

Weight gain of DMA bars and Tg vs ageing time plots are shown in *Figure 5-25*. Specimens were tested for their "Tg" in their wet state. The weight gain behaviour was similar to that obtained from the 80 x 80 mm specimens; matrix relaxation reflected by an increasing weight gain as a function of ageing was discerned. Nonetheless, a slightly higher moisture gain was obtained.

The addition of fibres in the matrix increased Tg significantly. A Tg of 90 °C was detected for the un-aged composite laminate, whereas a Tg of 77 °C was found for the un-aged matrix. This is an indication of a strong, highly cross-linked chemical bond between the fibre and the matrix. This was not the case for the SE 3030/1260, which is another sign of greater interfacial properties of W 3030/1273 when compared to its counterpart.

In spite of the Tg increase offered by the addition of the fibres to the matrix, Tg was significantly reduced as a function of ageing. Tg depression upon ageing was higher for W 3030/1273 than that of SE 3030/1260. Since Tg is a material property highly influenced by the chemistry of the matrix, such a change was expected, as also DION 1260 has been identified to be less hydrophilic than DION 1273. Based on the assumption that Tg is a matrix-dominated property, Tg depression for W 3030/1273 may be attributed to the plasticisation of the matrix. Please note that chemical changes could not be confirmed, since specimens were tested in their wet state. Besides, Tg depression does not necessarily imply reversible degradation [61]. A validation of this was the variation between wet (reduced Tg) and re-dried (regained Tg) DMA measurements for the neat DION 1260.

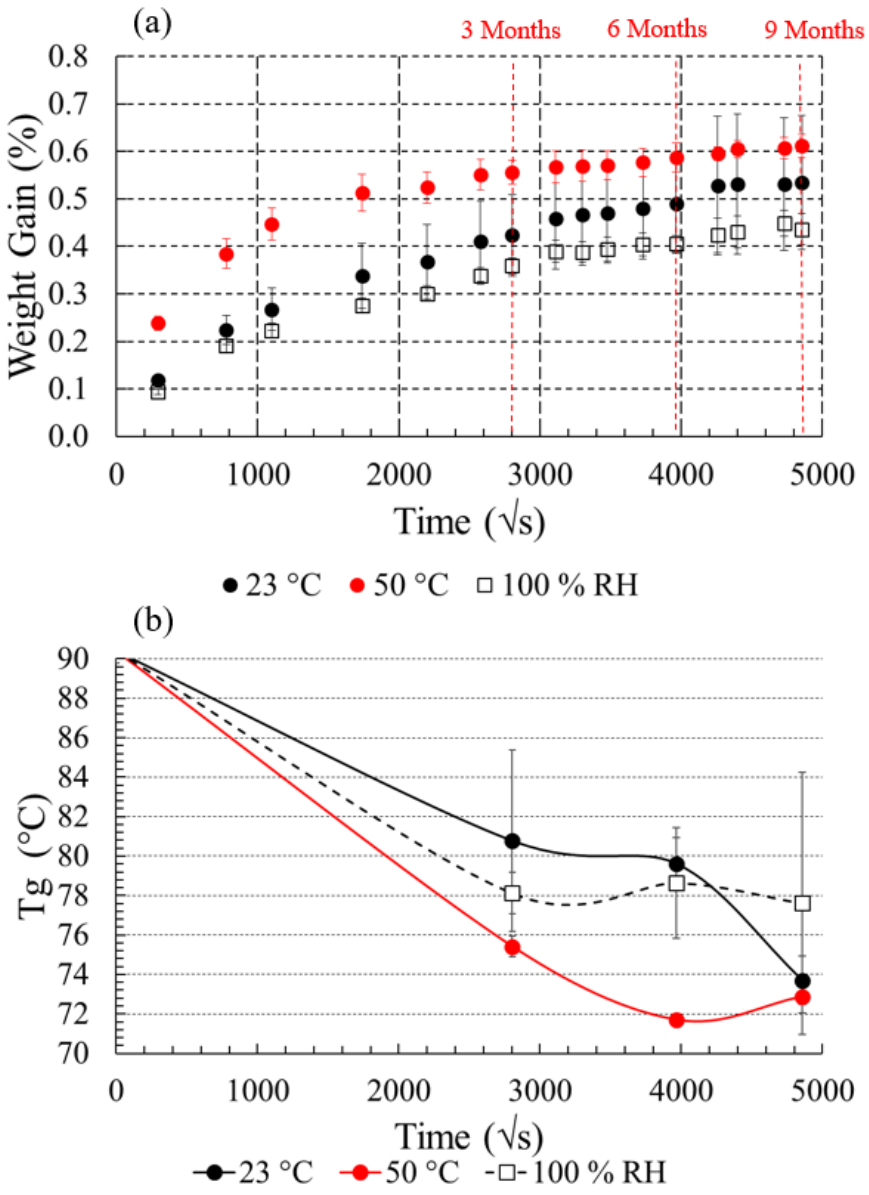

Figure 5-25: *(a) Weight gain vs ageing time plot for DMA-suitable, W 3030/1273 composite at different ageing conditions. The red gridlines indicate the ageing period in "months". (b) Tg vs ageing time plot for DMA-suitable, W 3030/1273 composite at different ageing conditions.*

5.3. CONCLUDING REMARKS

In conclusion, this study enabled a comparison between two vinyl ester matrices and their composites;

- DION 1260 – "baseline" VE and DION 1273 – "experimental" VE matrices under wet environments. A comparison between different curing conditions for DION 1260 was also allowed.

- SE 3030/1260 – “baseline” laminate and W 3030/1273 – “experimental” laminate.

Generally, the DION 1260 matrix was found to be less hydrophilic than DION 1273. Overall, 23 °C and 100 % RH had a similar effect on both matrices and were found to be milder than 50 °C resulting in a lower moisture gain and less pronounced degradation.

50 °C was used as a means of accelerating ageing. However, the degradation mechanisms activated by the elevated temperature in combination with direct water immersion were irreversible in most cases. Chemical degradation in the forms of hydrolysis, leaching and secondary cross-linking was induced by the elevated temperature environment, which was not always apparent in RT conditioning. It is possible that such effects may be evident when ageing composites in humid environments at “normal”, outside temperatures in the long term or in warmer climates. However, this remains in question.

This study further validated that oxygen intrusion in the polymerising vinyl ester medium and styrene loss can alter the chemistry of the polymer. Different uptake kinetics were exhibited by DION 1260 open mould specimens, which were characterised by a higher moisture gain and a more anomalous water uptake behaviour. On the other hand, the effect of a higher cure temperature of 100 °C did not have a great effect on the uptake kinetics of the DION 1260, provided it was cured in a sealed mould.

For adequately cured DION 1260, DMA measurements showed Tg depression for specimens tested in their wet state. However, Tg was fully recovered upon re-drying the specimens, and most of the reduction was attributed to plasticisation. For re-dried specimens, there was a hint suggesting secondary cross-linking, primarily for elevated temperature conditioning. DMA indicated plasticisation of DION 1260 open mould specimens aged at 23 °C, suggested by broadening of the loss modulus shoulder, which was also shifted at lower temperature values. On the other hand, depression of the loss modulus shoulder was evident in DION 1260 open mould specimens aged at 50 °C, indicative of secondary cross-linking of the lower Tg, presumably styrene-rich phase of vinyl ester. Secondary cross-linking was also indicated for re-dried DION 1273 “Polynt Standard”, denoted by a notable Tg increase.

Mechanical testing results obtained from the two composite systems in wet environments contradicted the behaviour of the matrix. Despite W 3030/1273 exhibiting a more hydrophilic matrix constituent than SE 3030/1260, it was found to be more resilient in hydrothermal environments and after long-term ageing. The more hydrophilic nature of DION 1273 over DION 1260 was confirmed by both gravimetric and DMA results. Given the former observation, the resilience of W 3030/1273 to mechanical degradation can be attributed to a more “adequately” tailored interface primarily offered by the matrix. It is yet unclear whether

the glass formulation (HiPertex vs Advantex) has an effect on adhesion. ILSS retention of EP-based FRPs of the same matrix but with a reinforcement of the same sizing and different glass formulation (HiPertex vs Advantex) was reported to be similar for the two systems [191,192]. However, the chemistry of the interface may be significantly different when changing from an EP system to a VE system. The stiffness of the two composites, indicated by Young's modulus was similar for both systems and was not hugely affected by ageing. Since Young's modulus was measured in the direction of the fibre, the property was fibre-driven, and hence the influence of the stiffness properties of HiPertex vs Advantex was clearly reflected in the two composites. Varying moisture content was found across specimens of the same laminate thickness but of a different length and width. The effect was more prominent in SE 3030/1260 than in W 3030/1273. This was attributed to excess sealant decomposition, amplified interfacial weakening allowing moisture wicking and possible varying void content, when compared to W 3030/1273. Void content measurements on SE 3030/1260 suggested a void content increase for aged specimens, which was fairly similar upon ageing at any of the employed conditions. As presented in the literature review, a potential void content increase can significantly affect the mechanical properties of FRPs. The extent that voids affected mechanical performance remains unclear and further experimentation would be desirable.

It was found that the Tg of SE 3030/1260 in its un-aged state was only higher by 2 °C than that of neat DION 1260, whereas the Tg of W 3030/1273 was higher by 23 °C than that of neat DION 1273. Although a definitive answer cannot be provided on what may be causing such a huge Tg increase when adding W 3030 to DION 1273, it can be presumed that this an interfacial effect. It is possible that certain chemical reactions take place between the glass, the sizing and in turn the matrix, which result in an increase in thermal properties. Anyhow, the above observation confirmed that DION 1273 can provide superior composite properties when used as a composite constituent.

A Tg retention characterisation as a function of ageing time was conducted for both composites. Tg vs ageing trends were found to be in disagreement with mechanical property retention upon ageing for the two laminates. A small Tg decrease was discerned for SE 3030/1260 as a function of ageing time. Tg decrease was similar at all ageing conditions, but it appeared to be slightly lower after 3 months at 50 °C, before it was increased again after 6 months of ageing to a level similar obtained at RT ageing. Competing ageing effects were thus considered, but the majority of degradation can be attributed to plasticisation of the matrix, also knowing that Tg measurements were conducted in the "wet" state of the specimens. Please note that a similar trend was obtained for the "wet" Tg of neat DION 1260, but Tg depression

was reversed upon re-drying the matrix. W 3030/1273 composites underwent a greater Tg depression vs ageing than SE 3030/1260. This depression was attributed to similar reasons to the ones discussed above. On one hand, considering that the Tg of the matrix was regained upon re-drying and the fact that Tg is primarily a matrix-dominated property, the attribution of Tg depression to matrix plasticisation is a reasonable approach. This would also be in line with the observation that DION 1273 is more hydrophilic than DION 1260, but possesses a stronger and more ageing resilient interface. On the other hand, one should consider that when referring to composite laminates with such a high fibre weight fraction, as in this the case, the matrix is essentially bound to the interface. A definitive answer on what may be causing such contrasting trends in the two composites cannot be provided, but we should consider that the thermal properties of a composite may not always fully reflect its mechanical performance. Besides this, it is possible that if the composite was fully re-dried it would re-gain Tg, as was the case with the neat matrix.

CHAPTER 6: THE MOISTURE UPTAKE OF GLASS FIBRE/VINYL ESTER MICRO-DROPLETS AND ITS DIRECT TRANSLATION INTO THE MICRO-MECHANICAL PERFORMANCE OF THE SYSTEM

The main objective of this chapter is to investigate how environmental ageing can affect the glass fibre thermoset matrix interface. Although the main focus is vinyl ester, an epoxy system is employed for comparison. In bulk composites, it is common to correlate the moisture content of the composite with the retention of its mechanical properties. However, macro-mechanical (or meso-mechanical) testing usually fails to provide direct information on the integrity of the composite interface as a function of durability in wet environments. In this work, the stress transfer capability at the interface was evaluated by means of the microbond test, as a measure of interfacial shear strength (IFSS) and as a function of environmental history. The greatest challenge of this work was to create a correlation between the absorbed moisture in a matrix micro-droplet and its direct effect on the micro-mechanical properties of the system. The approach for this would involve monitoring the weight gain of a microbond droplet in a wet environment. However, a gravimetric analysis of microbond droplets upon moisture absorption was deemed impractical, due to their particularly low mass (being in the nanoscale range), removal of excess surface water from the sample before weighing, and the mass of water evaporating from the sample during the measurement process. These result in weight variations much greater than the accuracy of the measurement required. Previously, it was shown that microbond droplets can exhibit a similar surface-to-volume ratio to thin films used throughout this study. Thus, experimental thin film models along with basic mathematical diffusion models have been used to estimate moisture uptake of microbond droplets. FTIR and DMA were conducted on aged vinyl ester films to assess the effects of ageing on vinyl esters on a microscale. SEM was also employed to study the structure and morphology changes in microbond droplets and embedded fibres.

6.1. EXPERIMENTAL

6.1.1. Materials

Matrix

Two vinyl ester resins and one epoxy resin were used for the analysis. All matrix details are entailed in *Table 6-1*. Vinyl ester was the main focus of this study. Both the DION 1260 (commercial, “baseline”) and the DION 1273 (experimental) vinyl ester resins were used. A

bisphenol-A DGEBA epoxy resin (DER 332) was used to allow comparison between the micromechanical performance of epoxy and vinyl ester as a function of environmental ageing.

Designation	Resin Type	Curing Agent	Cure	Post-cure	Resin : Curing Agent, wt %	Resin/Curing Agent Supplier
VE - 1260	Vinyl ester, bisphenol epoxy-based	BC-21 UN 3103 Organic peroxide type C initiator	24 h at RT, inert N_2	24 h at 60 °C, 3 h at 80 °C, 1 h at 100 °C	97.5 : 2.5	Polynt/United Initiators GmbH
VE - 1273	Vinyl ester, MMA, styrene-based		24 h at RT, inert N_2	24 h at 60 °C, 3 h at 80 °C, 1 h at 100 °C	97.5 : 2.5	
DER™ 332	Bisphenol-A DGEBA	TETA technical grade 60%	2 h at 60 °C, 1 h at 120 °C	N/A	85.7 : 14.3	Merck

Table 6-1: *Matrix, curing agent and cure cycle details.*

Fibres

Two vinyl ester-compatible and one epoxy-compatible glass fibres were used for the analysis. All fibres details are entailed in *Table 6-2*. DION 1260 was applied on the SE 3030 fibre and DION 1273 was applied on the W 3030 fibre. This selection was carried out according to the material combination selection for DACOMAT laminates. SE 3030/1260 was considered as the "baseline" system both for DACOMAT and this study. The SE 2020 fibre was combined with the DER 332 epoxy system for an interfacial comparison as a function of environmental ageing.

Designation	Compatibility	Average Measured Fibre Diameter (μm)	Density tex (gr/km)	Supplier
Advantex® SE 3030	Vinyl ester, polyester, epoxy	19	1200	3B
HiPer-tex™ W 3030	Vinyl ester, polyester, epoxy	19	1200	3B
SE 2020	Epoxy	19.3	2400	3B

Table 6-2: *Fibres used and compatibility.*

6.1.2. Ageing and Thin Film Gravimetric Analysis Details

The purpose of an ageing study was to provide insight into the environmental durability of the glass fibre/vinyl ester interface and to allow comparison between different material systems under wet environments. The same ageing conditions employed in bulk composites laminates were used throughout this chapter. The selected conditions were full immersion in DI water at 23 °C and 50 °C. The condition of 100 % RH at RT was only employed for certain specimens, such as films.

A primary objective of this study was to establish a relationship between the moisture uptake of a microbond droplet and its effect on the micro-mechanical performance of the interface. However, moisture quantification in microbond droplets was impractical, due to their small size (being in the nanoscale range). Therefore, DION 1260 and DION 1273 film models of a similar surface-to-volume ratio as microbond droplets were used. All films used in the gravimetric analyses exhibited a thickness in the range of $0.10 \leq t \leq 0.18$ mm. These refer to "standard" cure vinyl ester films introduced in *Chapter* 3. A set of DION 1260 films manufactured at the early stages of this project was used for a preliminary FTIR analysis. This set of films was produced by applying multiple resin layers on a flat, rectangular silicone rubber substrate by the means of a seam roller. The resin was left at RT for 0.5 h to gel and become viscous prior to use to facilitate the manufacturing process. The resulting films exhibited a thickness close to 0.25 mm and were cured under the "standard" cure cycle. These were found to exhibit slightly inferior thermal properties to "standard" cure films and have thus been used only for a small part of this work.

All films upon removal from the nylon substrate were cut into square specimens 25 x 25 mm and were dried under vacuum for 48 h prior to ageing to ensure removal of ambient moisture. The gravimetric analysis on thin films was carried out by removing the specimens from the exposure medium, drying them with a paper towel and weighing them at an analytical balance. The weight measurement was taken 60 s after the specimen had been removed from the exposure medium. Weight gain and diffusivity calculations were carried out using *Equations 2-4* and *2-7*, respectively, assuming 1-D Fickian diffusion. In certain cases, precise diffusivity calculations were found to be a challenge, due to the fast saturation of the films, and may be an approximation. Film specimens were re-dried upon ageing to examine the likelihood of hydrolysis. Thin films were re-dried at 40 °C (< Tg of films) in a convection oven for 48 h, followed by at least 48 h in a dry desiccator at RT and an approximate RH of 10 %. A re-drying temperature well below the Tg of films was selected to prevent weight loss (through

oxidation) during the re-drying cycle. Simple diffusion models have been used to study what may be happening in an infinite parallel-sided, flat slab polymer films and polymer micro-droplet specimens, using *Equations 6-1* and *6-2*, respectively [200].

$$\frac{M(t)}{M_m} = 1 - \frac{8}{\pi^2}\sum_{i=0}^{n}\infty \frac{1}{(2n+1)}\exp[-(2n+1)^2(\frac{D\pi^2 t}{h^2})]$$

6-1

$$\frac{M(t)}{M_m} = 1 - \frac{6}{\pi^2}\sum_{i=1}^{n}\infty \frac{1}{n^2}\exp[-\frac{Dn^2\pi^2 t}{h^2}]$$

6-2

where: $M(t)$ is the time-dependent water uptake of the polymer, M_m is the final equilibrium attained by the polymer, D is the diffusivity coefficient of the polymer and h is the thickness of the flat slab/radius of the spherical particle. Diffusion trends suggested by mathematical models have been compared to experimental results obtained by real-life film models of micro-droplets. The gravimetric analysis was coupled with DMA and FTIR results to provide an in-depth understanding of moisture-induced degradation.

6.1.3. Fourier-transform Infrared Spectroscopy (FTIR)

FTIR analyses were performed for the coupling of gravimetric measurements and the assessment of ageing-induced chemical changes in the polymer structure. The analysis was only conducted on DION 1260 films. DION 1273 films were not analysed since their unknown (confidential) polymer network introduced a high level of complexity in the analysis, which could lead to false interpretations. Both a diamond ATR interface and a 45° specular reflectance were used. The equipment used and the testing procedure for the ATR interface are the same as the one entailed in section *3.1.5.* All spectra were averaged and normalised using Origin software. Spectragryph software was used for peak identification and quantitative analysis.

Diamond ATR was used both in an attempt to quantify moisture and to assess chemical changes, upon ageing and re-drying the specimens. Analysis was performed in the 650 cm^{-1} to 4000 cm^{-1} range with a spectral resolution of 8 cm^{-1} and 64 scans per specimen. Films were aged for a period of 336 h when they were re-dried. The analysis was not conducted on all employed specimens, but a representative specimen range was used. The spectral region of the hydroxyl group at 3100 - 3600 cm^{-1} was used for the evaluation of moisture content. The

vibration of aromatic compounds C=C at 1510 cm^{-1} remained unchanged during ageing and was used as internal standard. The fractional absorbed water calculation was carried out using the following *Equation 6-3*, derived by Fick's law, based on the principle of Beer-Lambert law whereby the intensity is proportional to the concentration of species, i.e. moisture in this case [155].

$$\frac{\Delta w_t}{W_0} = \frac{\frac{A_{t\ 3100-3600}}{A_{0\ 1510}} - \frac{A_{0\ 3100-3600}}{A_{0\ 1510}}}{\frac{A_{0,5215}}{A_{0,4623}}}$$

6-3

where subscripts "0" and "t" denote un-aged and aged polymer, respectively.

Hydrolytic changes in vinyl ester films were examined upon ageing for 336 h and after the specimens had been re-dried. A representative specimen range of the aged films was used for the analysis. The hydrolysis indices suggested by Visco et al [32] for the evaluation of hydrolytic changes in vinyl ester and polyester matrices were used. The spectral regions of C-O ester stretching vibration at 1230 cm^{-1} to 1280 cm^{-1}, ester carbonyl C=O at 1725 cm^{-1} and the C–O stretching vibration of alcohol at 1040 cm^{-1} were used. The C-H vinyl ester backbone at 830 cm^{-1}, which remained stable prior to and after ageing was used as internal standard. All hydrolysis matrices were presented in the literature review section *2.5.5.* of this work.

At the early stages of this project, a 45° specular reflectance interface was used for the coupling of gravimetric measurements of DION 1260 films. These refer to the films consisting of multiple resin layers, manufactured as entailed in the previous section. Recorded results are preliminary. 45° specular reflectance is a non-destructive interface and allowed multiple measurements of the same specimens at different ageing intervals. It can also provide a higher penetration depth than the most commonly used diamond-ATR interface which can only provide information on a surface level of the polymer. A thin and lightweight stainless steel plate was placed on top of the thin film to strengthen the IR signal by reflecting and transmitting it back to the specimen. This was required due to the partial transparency of the specimen, which can cause the light exerted on the interface to dissipate. Spectra were run with background scans between each run at 64 scans and 8 cm^{-1} resolution resulting in a spectral acquisition time of under 30 seconds. All measurements were taken from the centre point of the films and all spectra were averaged and normalised using Origin software per batch/ageing condition. The spectral region of 3584 cm^{-1} – 3700 cm^{-1} (O-H group) was used whereby a peak area increase was observed as a function of ageing. The spectral region at

2000 cm $^{-1}$ - 2090 cm $^{-1}$, which remained unchanged during ageing, was used as internal standard. The fractional absorbed water calculation was carried out using *Equation 6-3*, derived from Fick's law (and based on the principles of the Beer-Lambert law) [155].

6.1.4. Thin Film Ageing & DMA

"Standard" cure DION 1260 and DION 1273 film specimens were tested in a film tension configuration upon being aged for 336 h and subsequently re-dried. The thickness of the tested films ranged from 0.1 mm to 0.18 mm. All DMA test parameters used for this thickness range are entailed in *3.1.4.*

6.1.5. Microbond Test & Ageing

The microbond test sample preparation and procedure are described in *4.1.2*. The stainless steel rig presented in *4.1.2.* was utilised to allow the conditioning of micro-composites in wet environments. Micro-composites were adhered to stainless steel washers, which were positioned on the rig. Aged microbond specimens were tested both in their "wet" and "re-dried" states. "Wet" microbond specimens were removed from the conditioning medium 0.5 h prior to testing. Upon removal paper towels were used to dry off moisture found on the stainless steel rig, nonetheless avoiding interaction with the specimens. Specimens were kept in an ambient environment for the duration of testing of approximately 1 – 2 hours. Note that no major data scatter was observed due to probable moisture loss between the first and last test specimen. "Re-dried" specimens were re-dried in a dry desiccator (≈ 10 % RH) for at least 24 h prior to testing. Re-drying the specimens enabled the examination of the reversibility of the ageing effect.

6.1.6. Scanning Electron Microscopy (SEM)

Scanning Electron Microscopy (SEM) was used to examine the morphology and structure of aged DION 1260 and DION 1273 microbond droplets bonded on SE 3030 and W 3030 glass fibres, respectively. The ageing conditions explored were full immersion at 23 °C and 50 °C. Micro-composites were examined both in their wet state and upon re-drying in a dry desiccator of 10 % RH at RT for at least 24 h. The ageing intervals employed were 24 h and 312 h at 23 °C, and 24 h and 96 h at 50 °C. All experimental details regarding the use of SEM are described in section *4.1.3.*

6.2. RESULTS AND DISCUSSION

As previously discussed, a gravimetric analysis of microbond droplets was not feasible due to their particularly low mass. This can be further justified by attempting to actually approximate the mass of a microbond droplet. The estimation was conducted on DION 1260 microbond droplets by employing their droplet length and diameter to calculate their volume, in accordance with the hypothesis that their shape is close to that of an ellipsoid. Assuming no scaling effects, the weight of the polymer droplet was estimated by using the cured DION 1260 density value of 1.127 g/cm^3, provided by Polynt. The contribution of the glass fibre embedded in the microbond droplet was subtracted from the calculation. The polymer droplet length was plotted against their resulting approximate mass range in *Figure 6-1*, for a representative set of SE 3030/1260 in their un-aged state.

It can be observed that the mass of the majority of droplets is less than or close to 1 µg. The measurement of a droplet mass with an accuracy better than 1 ng would thus be required for a typical gravimetrical analysis.

The estimation of moisture absorption in a microbond droplet was carried out by using experimental thin film models exhibiting a thickness equivalent to that of a droplet (≈ 0.15 mm). Basic mathematical diffusion models, which obeyed *Equations 6-1* and *6-2* were also employed to estimate diffusion in microscopic vinyl ester films and spheres, respectively.

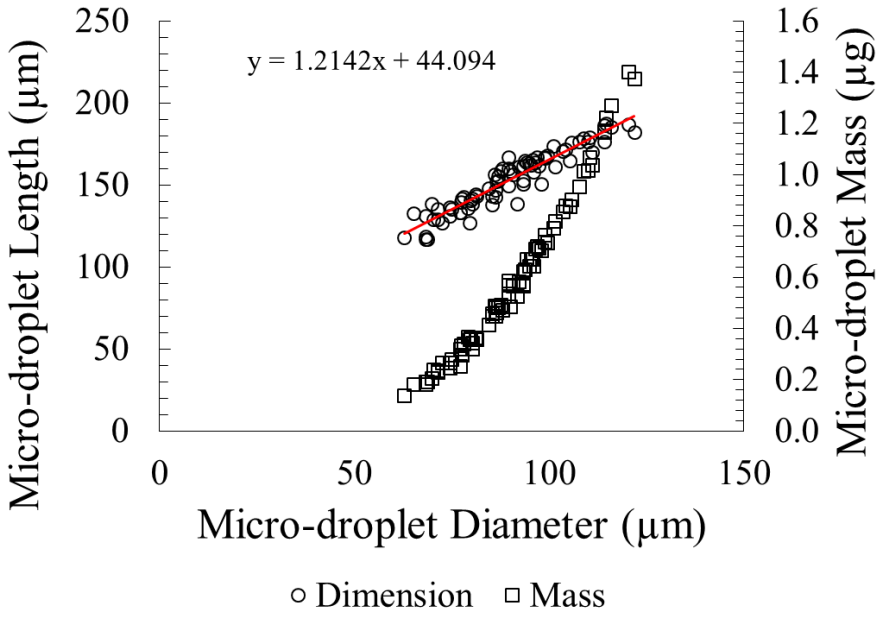

Figure 6-1: *Micro-droplet dimension (length : diameter) of a typical range of DION 1260 microbond droplets on SE 3030 fibre in their un-aged state vs their approximated mass.*

6.2.1. Gravimetric Analysis

Moisture Uptake Kinetics of DION 1260 Vinyl Ester on a Microscale

A weight vs ageing time plot of "standard" cure films at different ageing conditions up to a total ageing time of 336 h is shown in *Figure 6-2*. 95 % error bars were included at all ageing conditions. All diffusivity and moisture gain values of the films obtained after conditioning at all three conditions are shown in *Table 6-3*. In certain cases, equilibrium times and moisture levels were unclear, and hence in such cases obtained diffusivities are an approximation. In a similar fashion to bulk "Polynt Standard" DION 1260 (*Figure 5-4*), one main trend is featured. The curves at 23 °C and 100 % RH exhibited similar uptake patterns and moisture gains, notably lower than that achieved at 50 °C. Direct exposure to DI water at 23 °C resulted in a slightly higher moisture gain than at 100 % RH. At both 23 °C and 100 % RH conditions and the beginning of the ageing period, a Fickian-like pattern was attained, and equilibrium appears to be reached between 24 h and 48 h (≈ 125 - 295 √s, respectively). Small weight fluctuations were exhibited by the films thereafter, which may be an indication of competing moisture-induced effects, including moisture uptake and plasticisation, and (or) even irreversible degradation, such as hydrolysis and leaching. A rapid and more abrupt weight gain increase was featured at 50 °C. Films seemed to have reached equilibrium within the first 2 – 5 hours of exposure with strong weight fluctuations observed beyond that point and throughout the whole period of conditioning.

Re-drying the specimens resulted in a weight loss between approximately 0.2 % and 0.5 % for films aged both at 23 °C and 100 % RH. This was an indication of hydrolytic degradation through leaching. A maximum weight loss of 0.95 % was observed for films aged at 50 °C. Although this implies that the actual weight gain of the film in the water was more than 2 %, this is not an absurd observation considering that DION 1260 open mould specimens reached a weight gain up to 2.6 % at 50 °C (presented in *Chapter 5*). Besides, please note that "standard" cure films and open mould samples showed a similar chemistry when analysed by FTIR in *Chapter 3, Figure 3-7*. However, varying weight loss values were noted throughout the employed specimen range, while some of the films could not be fully re-dried, noting mass values higher than the ones recorded prior to ageing. This was the case even when films were stored in a dry desiccator (10 % RH) for over 8 weeks. This was in accordance with the observation of Han and Drzal [134], who reported that the difficulty of re-drying the matrix may be due to water molecules trapped within the micro-cavities and capillaries of the polymer network indicating chemical ageing. Varying weight loss values across the employed

specimen range denoted varying ageing effects on films. This may be due to scalability effects when producing microscopic vinyl ester specimens, such as varying styrene loss between films, which may influence the uptake kinetics of vinyl esters [44], as well as varying thicknesses and voids, such as air gaps across the matrix. The chemical integrity of the films was further checked through FTIR and DMA, presented in the following chapters of this work.

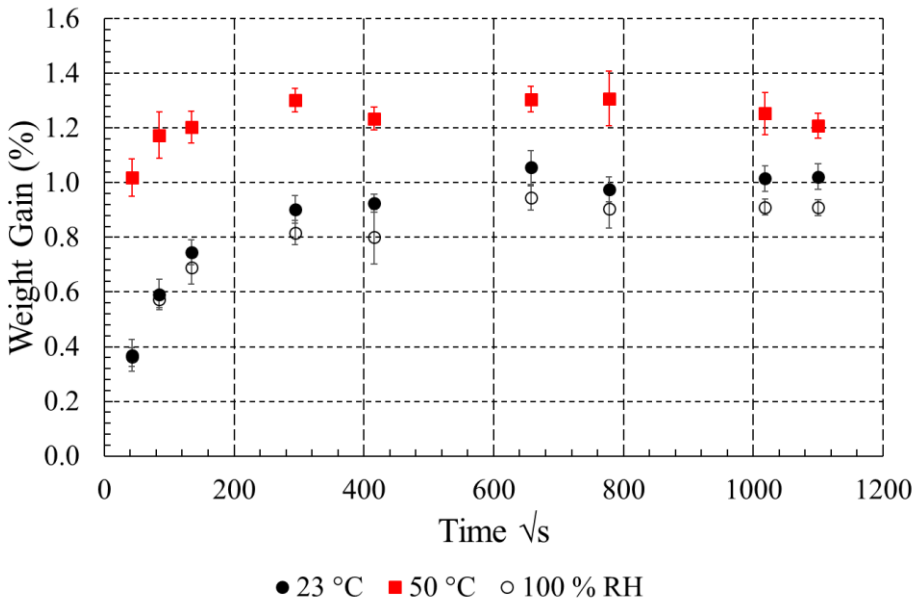

Figure 6-2: *Weight gain vs ageing time plot for "standard" cure DION 1260 films of an average thickness of 0.13 mm at different ageing conditions.*

Condition	Thickness (mm)	Equilibrium - Weight Gain (%)	Diffusivity x 10^{-6} (mm^2/s)
23 °C	0.13	0.91	0.19
50 °C	0.13	1.2	1.3
100 % RH	0.13	0.81	0.14

Table 6-3: *Weight gain at equilibrium and diffusivity of "standard" cure DION 1260 films at different ageing conditions.*

It can be seen that the weight gain values of the films at all ageing conditions (*Table 6-3*) are slightly different from the ones attained by the bulk "Polynt Standard" but are very close to those of "UoS Op. Mould – 100 °C" specimens – *Table 5-2*. On that basis using *Equation 6-1*, assuming 1-D Fickian diffusion and using the saturation and diffusivity values of the bulk specimens, a predicted weight gain of the thin films (t = 0.13 mm) was calculated. These values

are compared with the experimental data obtained on thin films in *Figure 6-3*. It can be seen that when modelling with respect to "Polynt Standard", there are significant differences in the format of the curves (and the moisture gain levels), especially at 50 °C. The main resemblance can be found at 23 °C at the beginning of the moisture uptake process. However, when modelling with respect to the "UoS Op. Mould – 100 °C", the prediction is significantly closer to the experimental values. As aforementioned, the produced FTIR signal of bulk DION 1260 open mould specimens was also closer to that of "standard" cure films, as presented in *Chapter 3, Figure 3-7*, due to excessive styrene loss and interaction of the pre-polymer mix with ambient oxygen. This refers to the FTIR comparison of the two specimens in their un-aged state and is not part of the work conducted in this chapter.

A reasonable question would be whether the uptake kinetics of a thin film can compare to those of a microbond droplet. A DION 1260 microbond droplet captured at 200x magnification is featured in *Figure 6-4*. The marked dotted lines allow a comparison between the thickness of a film and the equivalent diameter of a sphere. It is apparent that between the latter two, a sphere model resembles a microbond droplet better when considering the available analytical solutions to the 1-D Fickian diffusion equation. Thus by using *Equation 6-2* and the saturation and diffusion values of the "UoS Op. Mould – 100 °C", the model of a 0.13 mm diameter sphere has been compared to the experimentally obtained weight gain of 0.13 mm films in *Figure 6-4*. The plot is focused on the early stages of moisture uptake and shows that the sphere model may be capable of reaching saturation faster than a thin film. At 50 °C, equilibrium was attained within 0.5 h for the sphere model, as opposed to 2 – 5 h for the film. In fact, it can be seen that the sphere model has reached around 70 % of its maximum moisture gain within 3 minutes. At 23 °C, equilibrium was attained within less than 1 h for the sphere model, as opposed to 24 – 48 h for the film. A sphere of 0.13 mm diameter appears to exhibit a lower volume than a microbond droplet, while a thin film has been estimated to exhibit a similar volume to a microbond droplet, but a notably larger surface area and an entirely different geometry. In reality, whereby 1-D diffusion may not be apparent, such geometry changes can significantly affect the uptake kinetics of the matrix. Therefore, it can be assumed that the predicted saturation times of a sphere and the experimentally obtained saturation times of a film may resemble the minimum and maximum saturation times of a microbond droplet, respectively.

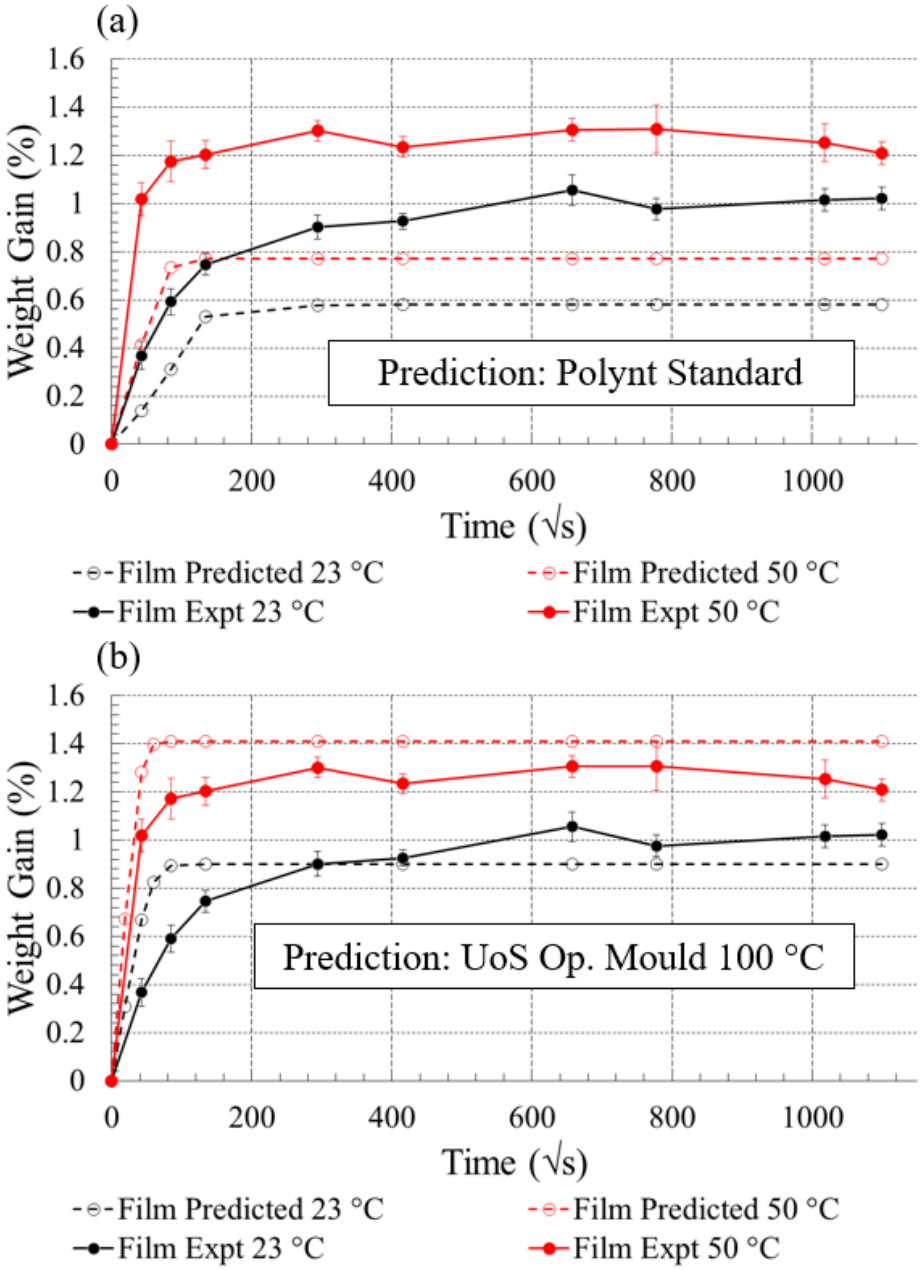

Figure 6-3: *(a) Weight gain vs ageing time plot for 0.13 mm thin film prediction using diffusivity and saturation values of "Polynt Standard" vs experimental measurements on 0.13 mm film (b) Weight gain vs ageing time plot for 0.13 mm thin film prediction using diffusivity and saturation values of "UoS Op. Mould – 100 °C" vs experimental measurements on 0.13 mm film.*

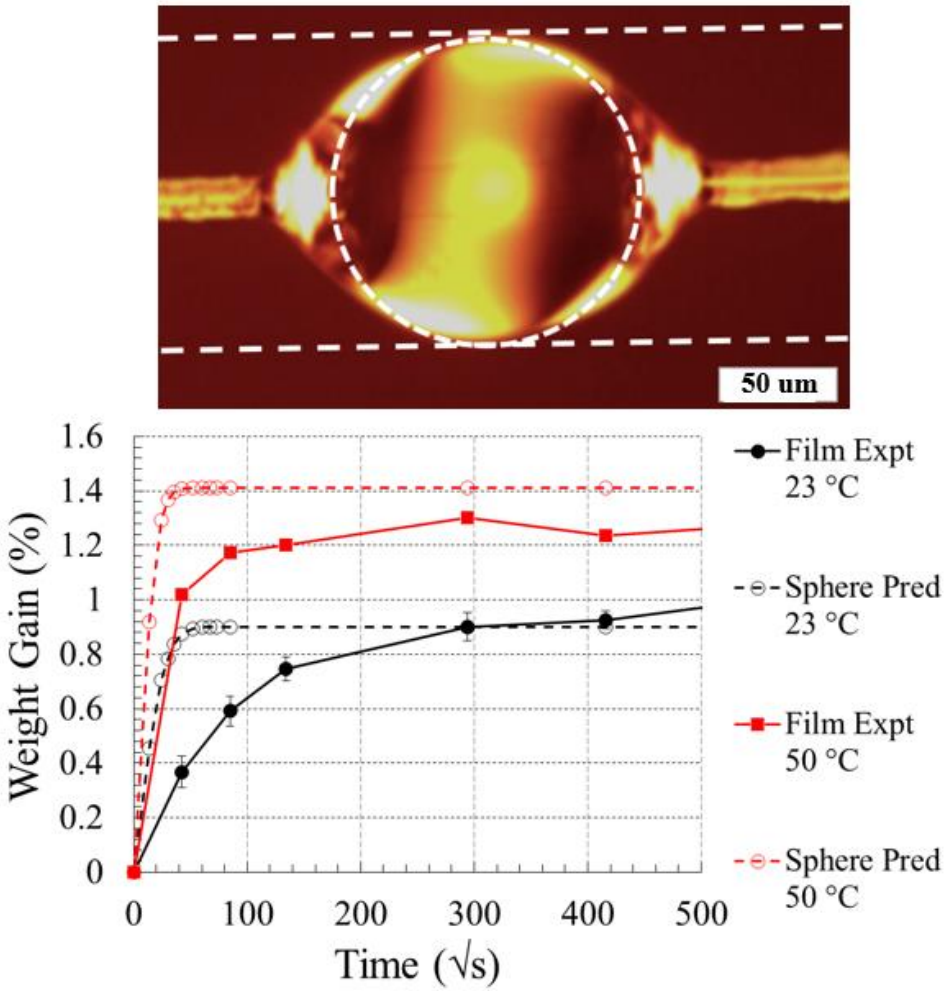

Figure 6-4: *(a) Comparison of thin film and sphere as models for micro-droplet diffusion (b) Weight gain vs ageing time plot for 0.13 mm diameter DION 1260 "UoS Op. Mould – 100 °C" sphere prediction vs experimental measurements on 0.13 mm film.*

Moisture Uptake Kinetics of DION 1273 Vinyl Ester on a Microscale

A weight vs ageing time plot of "standard" cure films at different ageing conditions and up to a total ageing period of 336 h is shown in *Figure 6-5*. 95 % error bars were included at all ageing conditions. All diffusivity and moisture gain values of the films at all three conditions are shown in *Table 6-4*. In all cases, equilibrium times and moisture levels were unclear and hence obtained diffusivities are an approximation and were determined assuming 1-D Fickian diffusion. A continuously increasing weight gain pattern was observed for the largest part of moisture uptake at all conditions, in a similar fashion to the bulk DION 1273 "Polynt Standard" specimens – *Figure 5-8*. A possible reason for this is matrix relaxation governing the sorption process. Matrix relaxation is essentially the moisture-induced plasticisation of the matrix and can be marked by a Tg decrease as a function of moisture content [166]. Yu et al

[138] has reported matrix relaxation due to matrix expansion (i.e. swelling) of vinyl ester, especially at high temperatures. At 50 °C and 100 % RH the initial weight increase reached a maximum (after 120 h ≈ 655 √s and 168 h ≈ 775 √s, respectively) and was then followed by a subsequent weight drop, indicative of matrix leaching. This was not the case for films aged at 23 °C, which nonetheless featured weight fluctuations, primarily evident after 120 h (≈ 655 √s) of ageing. These can be attributed to moisture-induced degradation processes, such as matrix swelling and leaching acting in combination. None of the aged DION 1273 films could be fully re-dried, even when following the evelated temperature re-drying schedule films were stored in a dry dessicator for over 8 weeks. The difficulty of re-drying moisture-aged thermoset polymer has been previsouly associated with chemical ageing [134].

By using *Equation 6-2* and the saturation and diffusion values of DION 1273 "Polynt Standard", the model of a 0.13 mm diameter sphere has been compared to the experimentally obtained weight gain of 0.13 mm films in *Figure 6-6*. It can be seen that saturation is reached rapidly by sphere models in less than 0.5 h at 50 °C and just over 0.5 h at 23 °C. However, provided that there is no direct property transferability between the bulk DION 1273 "Polynt Standard" and the DION 1273 microscopic specimens, it can be assumed that saturation will occur even faster (reduced styrene and oxygen inhibition for films).

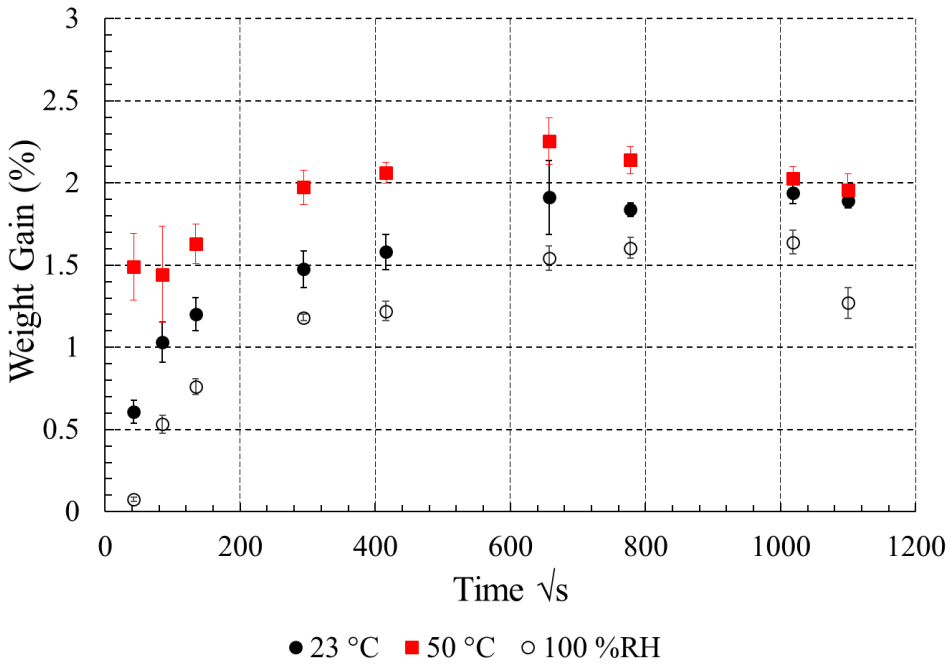

Figure 6-5: *Weight gain vs ageing time plot for "standard" cure DION 1273 films of an average thickness of 0.13 mm at different ageing conditions.*

Condition	Thickness (µm)	Equilibrium Weight Gain (%)	Diffusivity x 10^{-6} (mm^2/s)
23 °C	0.13	1.6	0.22
50 °C	0.13	1.5	1.6
100 % RH	0.13	1.2	0.13

Table 6-4: *Weight gain at equilibrium and diffusivity of "standard" cure DION 1273 films at different ageing conditions.*

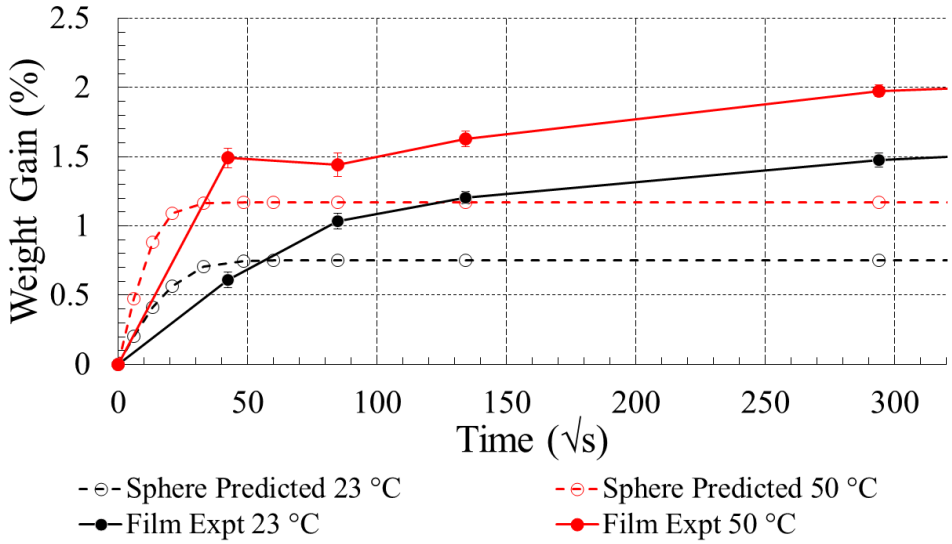

Figure 6-6: *Weight gain vs ageing time plot for 0.13 mm diameter DION 1273 "Polynt Standard" sphere prediction vs experimental measurements on 0.13 mm film.*

6.2.2. Fourier-transform Infrared Spectroscopy (FTIR)

DION 1260 Vinyl Ester on a Microscale – Moisture Uptake and FTIR

Output results of the fractional absorbed water vs ageing time of "standard" cure DION 1260 films, as measured by ATR-FTIR are plotted in *Figure 6-7*. It can be seen that only a few data points were close in magnitude to the ones obtained by the gravimetric analysis, such as the ones recorded at 288 h (≈1020 √s) at 50 °C and some at 100 % RH. This was attributed to the particularly small penetration depth of the ATR-FTIR interface (maximum 4 µm) and thus its ability to only provide information on the outside layer of the films. It is very likely that these surface layers dry out upon wiping the outer surface of the films prior to measurement.

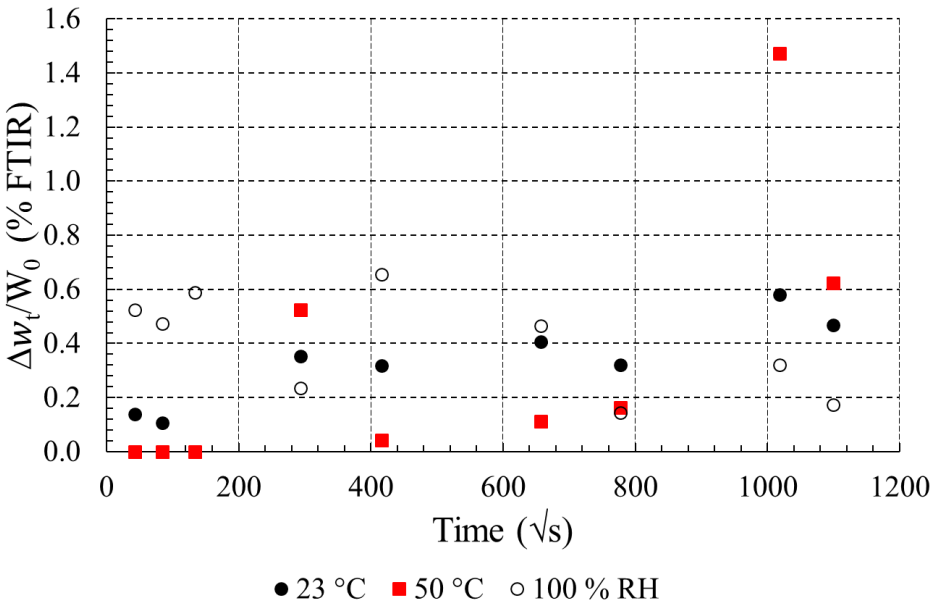

Figure 6-7: *Fractional absorbed moisture vs ageing time at different ageing conditions, as obtained by ATR-FTIR.*

More encouraging results were recorded when the 45° specular reflectance FTIR interface was used for a quantitative moisture sorption analysis. Weight gain and fractional absorbed moisture values measured by FTIR are plotted in *Figure 6-8* as a function of ageing time at the conditions of 23 °C and 50 °C. FTIR values were determined by using *Equation 6-3* derived from Fick's law (based on the principles of Beer-Lambert law) to monitor the spectral changes in the 3584 cm^{-1} – 3700 cm^{-1} region (O-H group). Featured results were recorded on poorer quality films, manufactured by applying multiple resin layers on a silicone rubber substrate by the means of a seam roller. These results were generated prior to optimising the film manufacturing process, at the early stages of the project, and thus gravimetric results may vary slightly from the ones presented in the previous section.

Good correlation between gravimetric and FTIR results was shown regarding the weight gain patterns as a function of ageing at both 23 °C and 50 °C. At 23 °C, the fractional absorbed moisture measured by FTIR showed excellent agreement and a similar magnitude to the gravimetric values. Such results demonstrate a great improvement of the quantitative analysis when using a 45° specular reflectance over ATR. The former exhibits a higher penetration depth and allowed scanning through the structure of the polymer, whereas the latter was only capable of obtaining information on its outer layer. To this author's best knowledge, no literature is available on the quantification of moisture in polymer using specular reflectance. However, at 50 °C, although there is agreement regarding the moisture uptake pattern between

FTIR and gravimetric results, poorer agreement was exhibited in the magnitude of the recorded values, when compared to the ones obtained at 23 °C.

Variations between the moisture content obtained by the 45° specular reflectance FTIR interface and the gravimetric results are generally expected. This is due to *Equation 6-3* obeying the Beer-Lambert law, whih can account for absorption but not scatter apparent in specular reflectance methods. Besides, vinyl ester films are fairly transparent, but upon ageing, especially at elevated temperature, strong discolouration and opaqueness were induced, which may have led to erroneous results [201,202]. Thus a multi-variate analysis and accurate modelling would be required to precisely evaluate the moisture content in vinyl ester films.

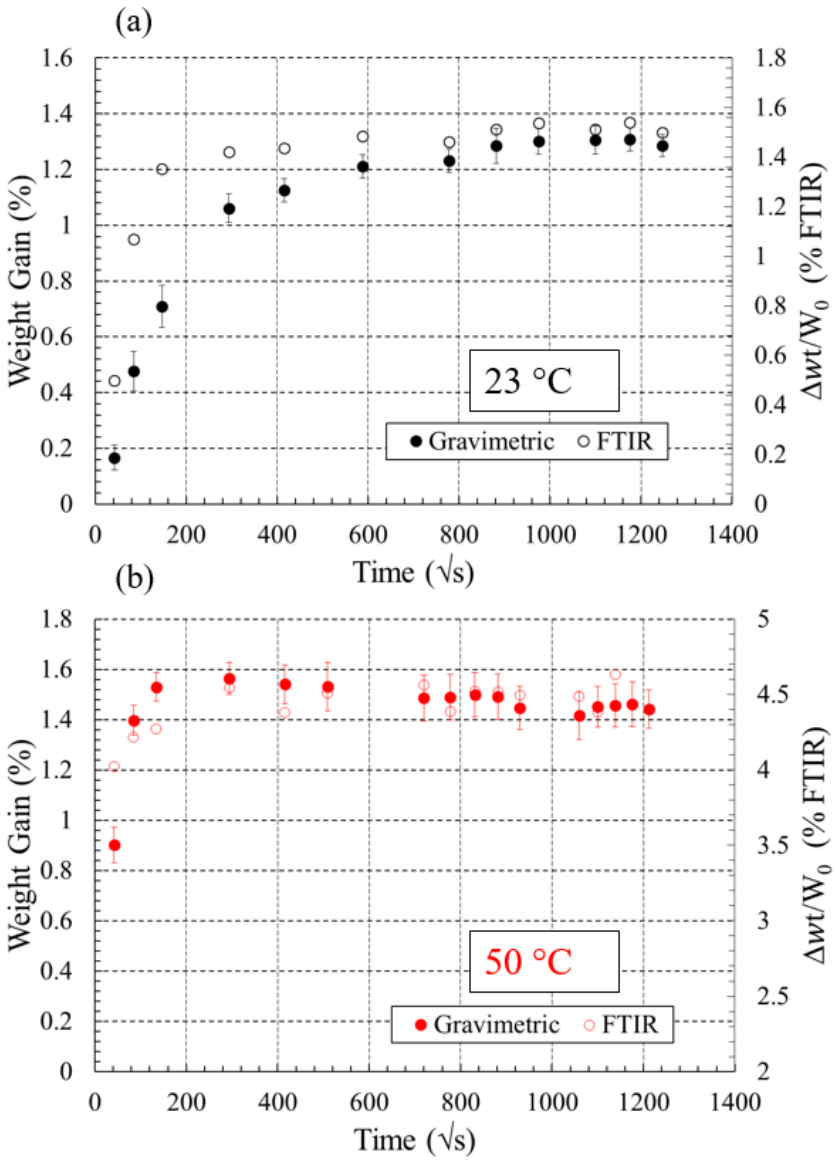

Figure 6-8: *Experimentally obtained weight gain and FTIR obtained fractional moisture absorption values at (a) 23 °C and (b) 50 °C.*

A quantitative analysis using the hydrolysis matrices presented by Visco et al [32] is presented in *Table 6-5*. Hydrolytic changes were confirmed after ageing at all employed conditions. Reductions in the spectral regions of 1230 cm^{-1} to 1280 cm^{-1} - $HI_{COester}$ and 1725 cm^{-1} - $HI_{C=Oester}$ were confirmed. According to Visco et al [32], these suggest bond rupture due to the hydrolytic degradation resulting in the depletion of the ester bond signals concentration. Despite the resulting index values after ageing being only slightly lower than those recorded for the un-aged films, the depletion was consistent throughout all ageing conditions, while a minimum of 6 scans were conducted at each condition allowing for a valid statistical analysis. An increase after ageing at 50 °C was featured in the spectral region of 1040 cm^{-1} - $HI_{COalcohol}$, which was an indication of further hydrolytic degradation at that ageing condition [32]. No changes were featured between the un-aged films and those aged at 23 °C and 100 % RH in 1040 cm^{-1}. Despite the indication of chemical changes provided by FTIR, it should be kept in mind that ATR can only provide information on a surface level and thus coupling with further experiments is usually required to understand the leaching reaction in more depth. In this case, these results are a validation of the hydrolysis suggested by the gravimetric analysis.

A quantitative analysis could not be carried out for DION 1273 films, due to the uncertainty involved in the assignment of spectral bands. DION 1273 consists of a complex polymer network of various monomers, and thus the use of the spectral bands employed in the analysis of conventional vinyl esters may lead to inaccuracies or false interpretations.

Condition	Treatment	$HI_{COester}$	$HI_{C=Oester}$	$HI_{COalcohol}$
23 °C	Un-aged	1.18	0.48	0.33
	Aged	1.17	0.45	0.33
50 °C	Un-aged	1.182	0.49	0.33
	Aged	1.18	0.47	0.34
100 % RH	Un-aged	1.17	0.46	0.31
	Aged	1.15	0.43	0.31

Table 6-5: *Quantitative analysis of hydrolytic changes in DION 1260 vinyl ester films.*

6.2.3. Dynamic Mechanical Analysis (DMA)

Relative Tg (%) data for aged (336 h) and re-dried "standard" cure DION 1260 and DION 1273 films are tabulated in *Table 6-6*, as recorded by DMA. Tg values were obtained from the main onset of the storage modulus vs time curve, presented on a logarithmic scale. Note that the first, small storage modulus onset, which was suggestive of a diphasic material, also reflected in a loss modulus shoulder was not considered in *Table 6-6*. The Tg of un-aged DION 1260 and DION 1273 was 107 °C and 87 °C, respectively.

	Relative Tg (%)		
	23 °C	**50 °C**	**100 % RH**
DION 1260	-1.87	1.04	-1.87
DION 1273	-0.5	7.83	-0.31

Table 6-6: *Relative Tg (%) of vinyl ester films after ageing for 336 h following re-drying*

DMA Characterisation of Moisture-aged DION 1260 Vinyl Ester on a Microscale

A storage and loss modulus thermal curve comparison of DION 1260 "standard" cure films aged at different conditions and subsequently re-dried is illustrated in *Figure 6-9*. As shown in *Table 6-6*, the relative Tg (%) in DION 1260 films obtained from the main storage modulus onset was minor at all ageing conditions. Nevertheless, a small Tg decrease was seen for films aged at 23 °C and 100 % RH, whereas a small Tg increase was recorded after ageing at 50 °C. No major changes were recorded in the Tg obtained from the main loss modulus peak after ageing at any of the three conditions. However, the most profound changes can be located in the loss modulus shoulder format upon ageing.

After ageing at 50 °C, the first transition is the storage modulus prior to the main onset became less apparent. There is a slight suggestion that this was also the case for the loss modulus shoulder, which appears to be flatter after ageing at 50 °C. These along with the featured increase in the main storage modulus onset were indications that secondary cross-linking had started to take place.

The Tg decrease (storage modulus onset) featured after ageing at 23 °C and 100 % RH was considered to be minor. However, at 23 °C the loss modulus shoulder appeared to be slightly more pronounced when compared to that of the un-aged film, suggesting moisture-induced phase separation. Phase separation was more clearly manifested after ageing at 100 % RH, and reflected in the appearance of two distinct loss modulus peaks. It was uncertain what degradation effect(s) may have caused the phase separation in the polymer. Thus both plasticising and hydrolytic effects were considered. It is likely that upon long-term ageing at 23 °C, the direct contact with water introduced post-curing which may counteract phase separation, and thus the featured shoulder was not as apparent as the one seen at 100 % RH.

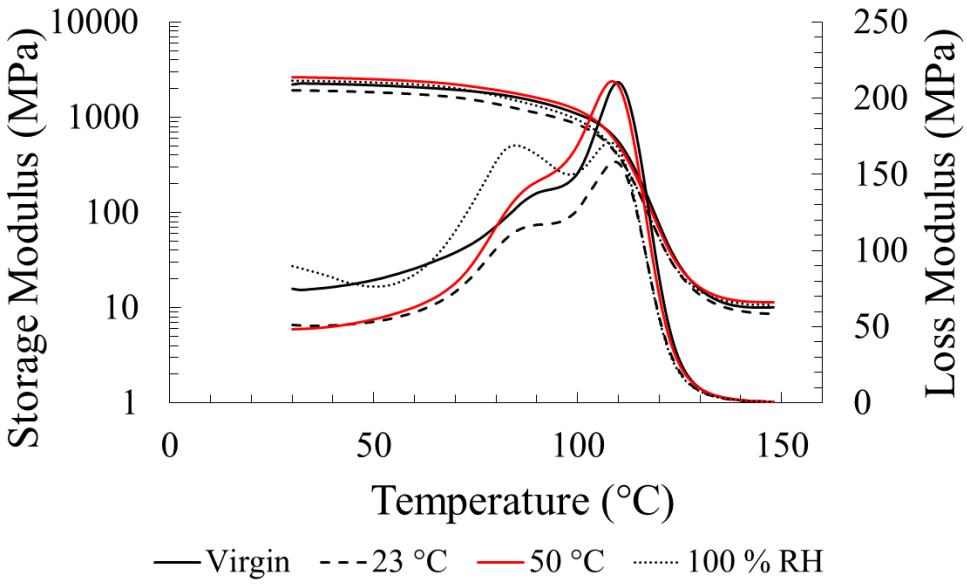

Figure 6-9: *DMA thermal curves for re-dried "standard" cure DION 1260 films after ageing for 336 h at different conditions.*

DMA Characterisation of Moisture-aged DION 1273 Vinyl Ester on a Microscale

A storage and loss modulus thermal curve comparison of DION 1273 "standard" cure films aged at different conditions and subsequently re-dried is featured in *Figure 6-10*. As shown in *Table 6-6*, ageing at 23 °C and 100 % RH did not affect the onset of the storage modulus of the material significantly. However, upon the observation of the loss modulus peak shifting to slightly lower temperatures after ageing at 23 °C and 100 % RH, it can be concluded that there may have been a minor Tg depression in the material. In addition, broadening of the loss modulus peak was evident after ageing at any of the three conditions, which was indicative of phase separation beginning to take place. Loss modulus broadening was more significant after ageing at 50 °C featuring a hint of a dual transition appearance at 77 °C and 89 °C. Moreover,

as shown in *Table 6-6*, a Tg increase was obtained by the onset of the storage modulus, which shows that the polymer has possibly undergone anti-plasticisation. Besides, a large magnitude increase was featured in loss modulus, indicating a ductile material, induced by plasticisation/swelling. Taking into account the above observations for the polymer film aged at 50 °C, it is possible that competing ageing effects took place; hydrolysis and post-curing, followed by plasticisation resulting in phase separation and softening. However, it is noteworthy that this result has not been repeated and relies on a single DMA run, thus further experimentation would be fruitful.

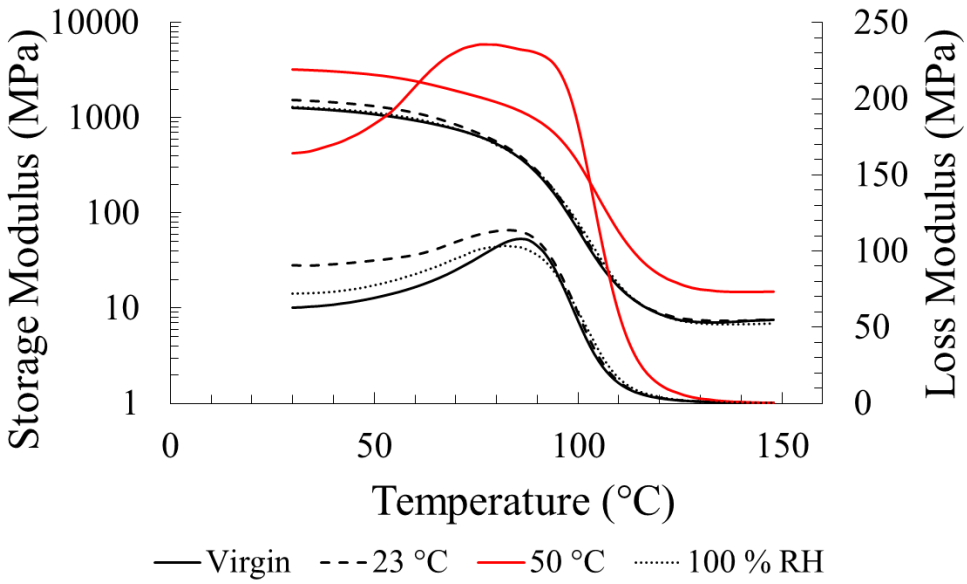

Figure 6-10: *DMA thermal curves for re-dried "standard" cure DION 1273 films after ageing for 336 h at different conditions.*

6.2.4. Micro-mechanical Testing: Microbond Test

Microbond Test Characterisation of Moisture-aged SE 3030/1260 Micro-composites

IFSS retention vs ageing time plots for "wet" and "re-dried" SE 3030/1260 single fibre micro-composites aged at 23 °C and 50 °C are illustrated in *Figure 6-11* and *Figure 6-12*, respectively. 95 % error bars are featured in all cases. The apparent IFSS value of un-aged, pristine single SE 3030/1260 was determined to be 36.9 MPa.

Upon ageing at 23 °C for 24 h, a slight IFSS increase was featured, which nonetheless was very close to the dry value. Further conditioning led to a steady IFSS decline up to 264 h, followed by a subsequent, abrupt drop. At 312 h, numerous debonds and varying low IFSS resulted in data scatter, as demonstrated by the large featured error bar. IFSS of re-dried micro-

composites more or less tracked the wet specimens, given the error bars. An indication of recovery of a small portion of reduced IFSS was given after 264 h of ageing. However, the majority of degradation was found to be irreversible.

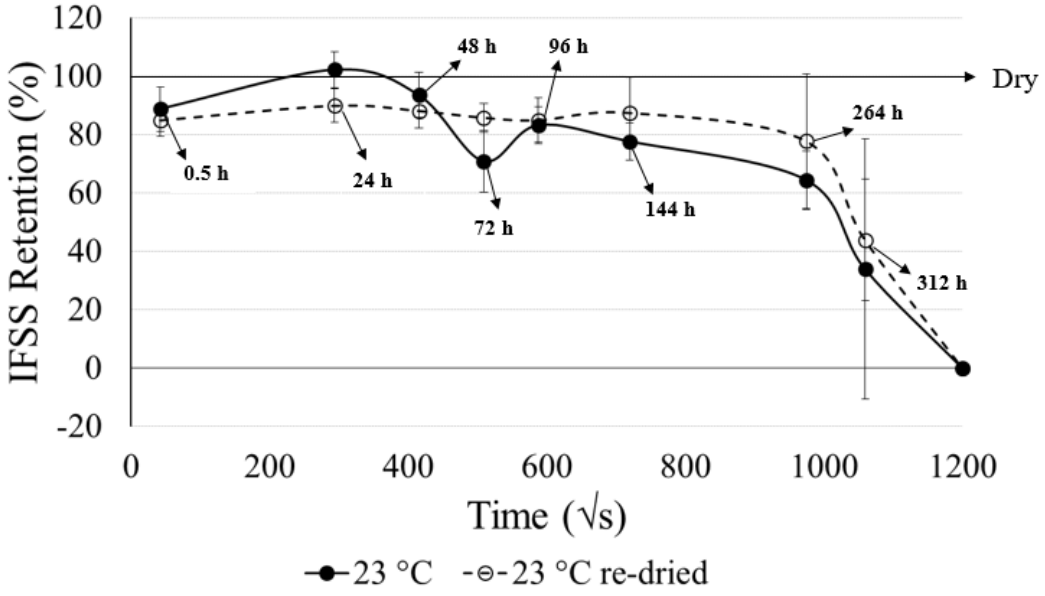

Figure 6-11: *IFSS retention vs ageing time plot for "wet" and "re-dried" SE 3030/1260 single fibre micro-composites aged at 23 °C.*

Immersion at 50 °C was proven to be a notably more aggressive environment for SE 3030/1260 micro-composites. This was manifested by an immediate IFSS decrease of 35 % after 0.5 h of conditioning, which remained relatively stable between 25 % and 35 % up to 72 h. A subsequent steep decrease of almost 70 % was observed after 96 h when interfacial adhesion was significantly compromised. At that interval, numerous debonds and scatter in data were recorded resulting in a high error bar, in a similar fashion to 23 °C and 312 h. The IFSS was found to be unmeasurable when further conditioning was employed. Apparent IFSS of re-dried specimens followed the pattern of the IFSS of wet specimens to a great degree. Encouraging but rather slight indications of IFSS recovery were shown in most cases, considering the featured error bars. It can thus be concluded that moisture attack at 50 °C was primarily irreversible, but some degree of swelling and plasticisation may have been introduced, especially after 96 h of conditioning, which was no longer apparent upon re-drying.

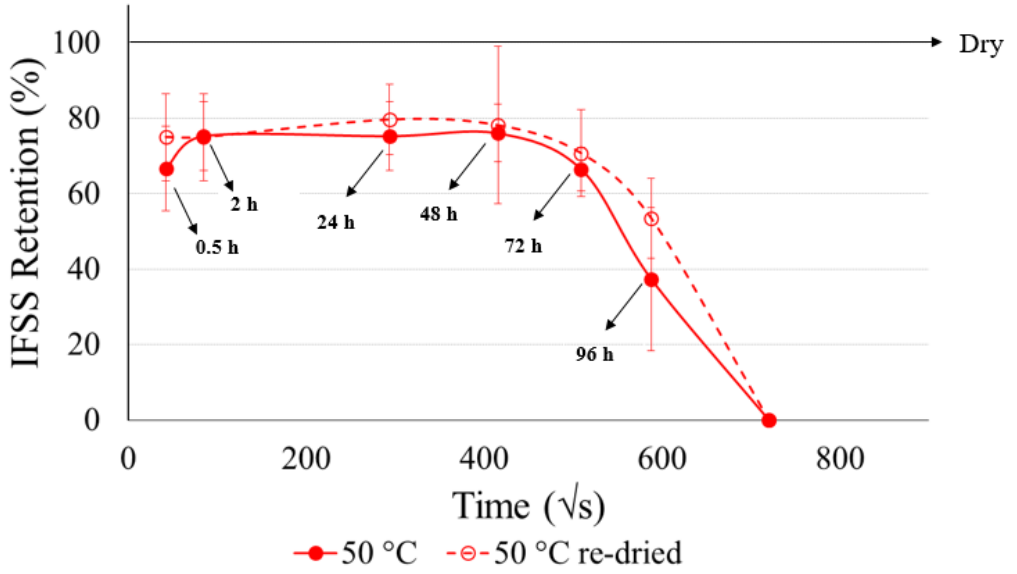

Figure 6-12: *IFSS retention vs ageing time plot for "wet" and "re-dried" SE 3030/1260 single fibre micro-composites aged at 50 °C.*

Microbond Test Characterisation of Moisture-aged Aged W 3030/1273 Micro-composites

An IFSS retention vs ageing time plot for "wet" and "re-dried" W 3030/1273 single fibre micro-composites aged at 23 °C and 50 °C is presented in *Figure 6-13*. 95 % error bars are featured in all cases. The apparent IFSS value of un-aged, pristine single W 3030/1273 was determined to be 43.4 MPa, close to 20 % higher than that recorded for the SE 3030/1260 system.

For microbond specimens aged by water immersion at 23 °C, a maximum ageing period of 312 h was employed, which is the point when the adhesion of SE 3030/1260 was significantly compromised. Wet specimens aged at 23 °C noted a gradual IFSS decline throughout this ageing period. W 3030/1273 specimens showed great resilience to short-term ageing, with only around 5.5 % of IFSS being lost within the first 24 h of ageing. Approximately 20 % of IFSS was lost after 96 h of ageing when IFSS plateaued for the remaining ageing period. Re-drying the specimens more or less tracked the values of the wet specimens. The only exception was short-term ageing at 2 h when re-drying resulted in IFSS to return to the un-aged IFSS value. Therefore, it can be deduced that moisture-induced IFSS reduction may be reversed upon short-term ageing, but it is final after 24 h of ageing.

As expected, ageing at 50 °C, amplified the level of degradation and increased the IFSS loss. An immediate IFSS decrease of almost 15 % was observed within the first 2 h of ageing and

a gradual decline followed. A further 5 % reduction was recorded upon 24 h of ageing, and a loss of around 35 % was observed after ageing for 96 h. Please note at that time interval SE 3030/1260 specimens had undergone an adhesion loss of over 60 % including numerous debonds. Re-drying the specimens showed that IFSS could not be recovered upon short-term and (or) long-term ageing. An indication of recovering a notable portion of lost IFSS was seen after 24 h of ageing. This may be attributed to the probable presence of post-curing effects, which became apparent upon extracting entrapped moisture from the specimens. However, the error bars of "wet" and "re-dried" data points at 24 h overlapped, and thus the latter statement is not definitive. Nevertheless, similar trends have been identified in the literature in bulk vinyl ester-based composites, which showed enhanced mechanical properties upon long-term ageing and after these had been compromised upon short-term ageing [6].

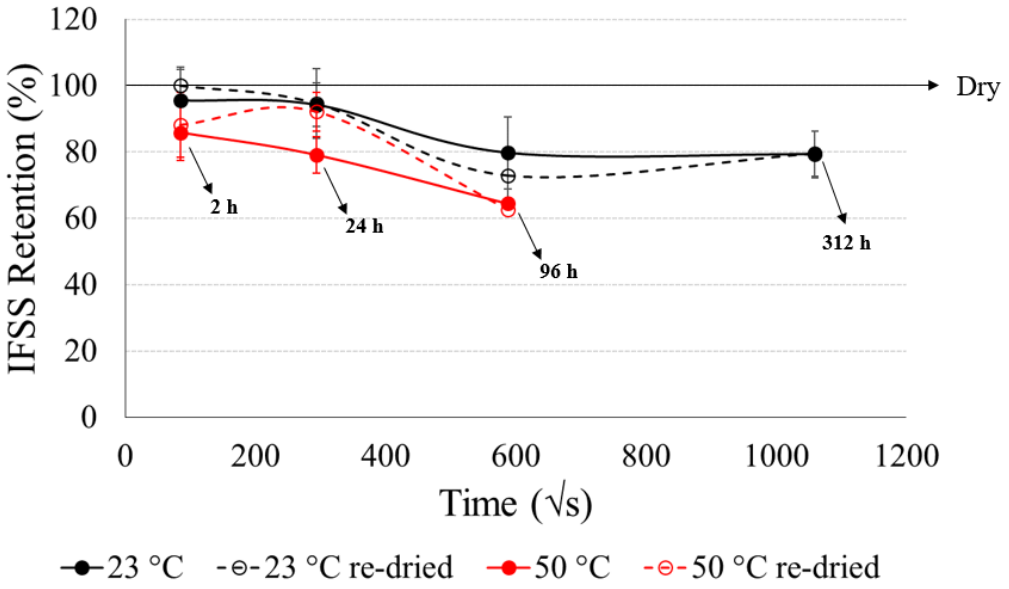

Figure 6-13: *IFSS retention vs ageing time plot for "wet" and "re-dried" W 3030/1273 single fibre micro-composites aged at 23 °C and 50 °C.*

Generally, W 3030/1273 exhibited a notably stronger and more hydrothermally stable interface than SE 3030/1260, which was also further validation of the mechanical testing results obtained in bulk specimens. This was despite the neat DION 1273 matrix being more susceptible to moisture attack than DION 1260 both on the microscale and macroscale. This was also in spite of W 3030/1273 possessing lower macro-mechanical properties in its dry state, when compared to its countepart. However, when the fibre/matrix interface was directly characterised by means of micro-mechanical testing, it was shown that W 3030/1273

possessed the highest adhesion. As shown in *Chapter 3*, when SE 3030 was used with DION 1273, or W 3030 with DION 1260, IFSS remained at 37 and 35 MPa, respectively. As previously discussed, the contribution of the HiPertex fibre to IFSS, which possesses superior properties over Advantex is unclear. Thus, it is likely that DION 1273 has been tailored to offer strong interfacial adhesion, although it possesses inferior material properties to commercial vinyl esters when used in its neat, unreinforced form. These results highlight the importance of the fibre/matrix interface in the hydrothermal durability of the resin, as well as the importance of conducting durability and interface tests as part of material selection for infrastructure applications.

Microbond Test Characterisation of Moisture-aged SE 2020/DER 332 Micro-composites

An IFSS retention vs ageing time plot for "wet" and "re-dried" SE 3030/DER 332 (TETA) single fibre micro-composites aged at 23 °C and 50 °C is featured in *Figure 6-14*. 95 % error bars are included in all cases. The apparent IFSS value of un-aged,SE 2020/DER 332 micro-composites was determined to be 31.7 MPa. This was lower than IFSS obtained for glass fibre/vinyl ester systems, but also surprisingly lower than results obtained by different operators when specimens were manufactured on card instead (fibre fixing adhesive: CA glue) of steel washers (fibre fixing adhesive: Araldite EP) [55]. Nevertheless, measurements and output IFSS remained consistent throughout the ageing study. Reasons behind a varying IFSS output especially when different fibre fixing adhesives, substrates or operators are involved have been found to be rather complex. However, the microbond test has still been deemed useful in characterising interfaces of different treatments [55,72–74,78–80,182]. The purpose of this study was to compare the hydrothermal durability of glass fibre/epoxy and glass fibre/vinyl ester interfaces.

Generally, IFSS was found to be particularly stable as a function of different ageing times, both when immersed in DI water at 23 °C and 50 °C. Re-dried IFSS values were close to the ones obtained from wet specimens. A slight indication of secondary cross-linking was observed upon long-term ageing for 312 h at 23 °C, following re-drying, but the resulting IFSS remained close to that recorded for un-aged specimens.

Literature reports suggest that vinyl ester films of 0.23 – 0.26 mm thickness were more hydrophobic than their epoxy counterpart [36]. In addition, bulk VE-based FRPs were found to be more hydrophobic than EP-based FRPs regarding mechanical property retention [123]. A comparison between the moisture uptake kinetics of vinyl ester and epoxy films was not conducted in this study, due to challenges faced in epoxy film manufacturing. Although

literature results do not refer to micro-mechanical testing, they suggest that vinyl ester can overall be more hydrophobic than epoxy. Presumably, this could translate into vinyl ester systems retaining interfacial adhesion to a greater level than their epoxy counterpart as a function of ageing. Nevertheless, results obtained through the microbond test suggest that the examined epoxy system was capable of retaining IFSS more effectively than the employed vinyl ester systems. However, one shall consider the following; DER 332 (TETA) has been found to exhibit a Tg of 123 °C, significantly higher than that of the VEs under investigation, DER 332 (TETA) has been found to exhibit a superior interface compared to other EP systems and finally, DER 332 (TETA) micro-droplets do not undergo major curing agent vaporisation, as opposed to other commercially available EPs [55]. On the other hand, severe curing issues were presented throughout this work regarding DION 1260 and DION 1273 micro-droplet cure. All the above parameters are valid reasons why GF/VE IFSS was more severely affected by ageing than the IFSS of GF/EP. This was also an indication that bulk to microscale material property transferability of an EP system can be carried out more effectively than vinyl ester. It is nevertheless a possibility that if another GF/EP system was employed, different trends might have been obtained. These results were therefore deemed preliminary. For a more accurate comparison between GF/VE and GF/EP, it would be useful to employ a wider range of GFs and matrices. EP matrix films models would also be useful for the estimation of the moisture uptake of EP micro-droplets allowing a correlation to IFSS retention as a function of ageing.

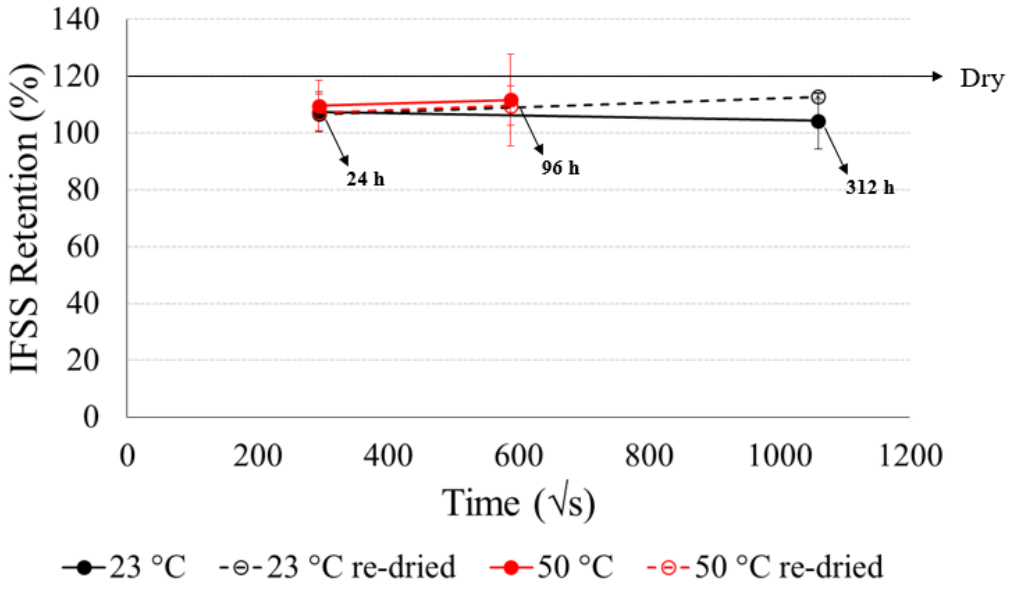

Figure 6-14: *IFSS retention vs ageing time plot for "wet" and "re-dried" SE 2020/DER 332 single fibre micro-composites aged at 23 °C and 50 °C.*

6.2.5. Scanning Electron Microscopy (SEM)

SEM of Moisture-aged SE 3030/1260 Micro-composites

Un-aged DION 1260 micro-droplets exhibited a featureless surface, but some cracking around the meniscus was distinguished in certain droplets, as shown in *Figure 6-15*. This appears to be surface-level cracking, but was amplified with ageing and became apparent in most droplets, especially when ageing time increased. Such cracks may introduce an easier route for water to penetrate directly to the fibre-matrix interface and may in turn affect the resultant debonding load-displacement curve during a microbond test. SEM was conducted on micro-droplets in both "wet" and "re-dried" states, but no major difference was shown between them. This was another indication that irreversible degradation was induced by ageing.

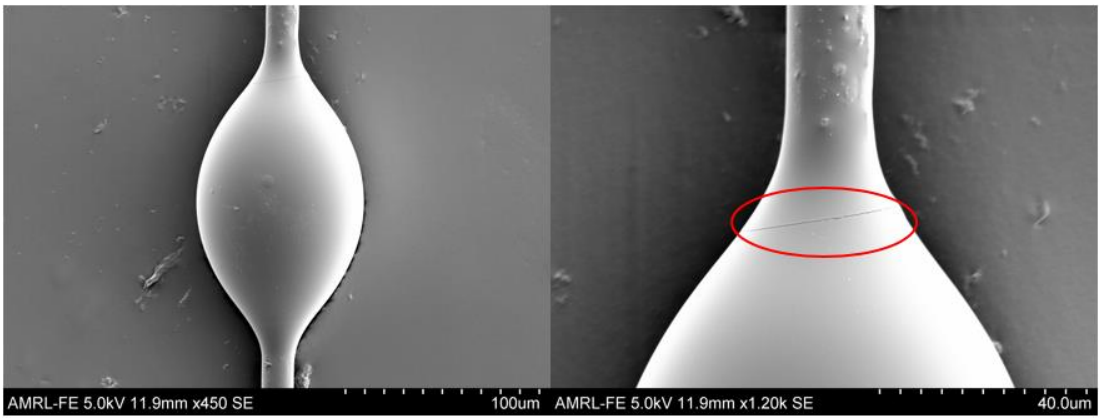

Figure 6-15: *Un-aged DION 1260 microbond droplets on SE 3030 fibre.*

DION 1260 microbond droplets on SE 3030 fibre after ageing by full immersion in DI water at 23 °C are presented in *Figure 6-16*. The major form of degradation identified for micro-droplets aged at 23 °C for 24 h was the appearance of mild surface blistering. This was a probable indication of the vinyl ester two-phase structure being made visible upon ageing. Slight cracking around the droplet meniscus was also seen for some micro-droplets. Similar but more amplified degradation was seen after 312 h of ageing at 23 °C. This was an indication of wicking and water penetration along the interface, which can weaken the fibre/matrix, result in debonding and compromise micro-mechanical performance. The evolution of degradation was variant throughout the examined set of droplets, with numerous debonds apparent. This observation is further validation for the varying IFSS at the latter condition and the produced data scatter.

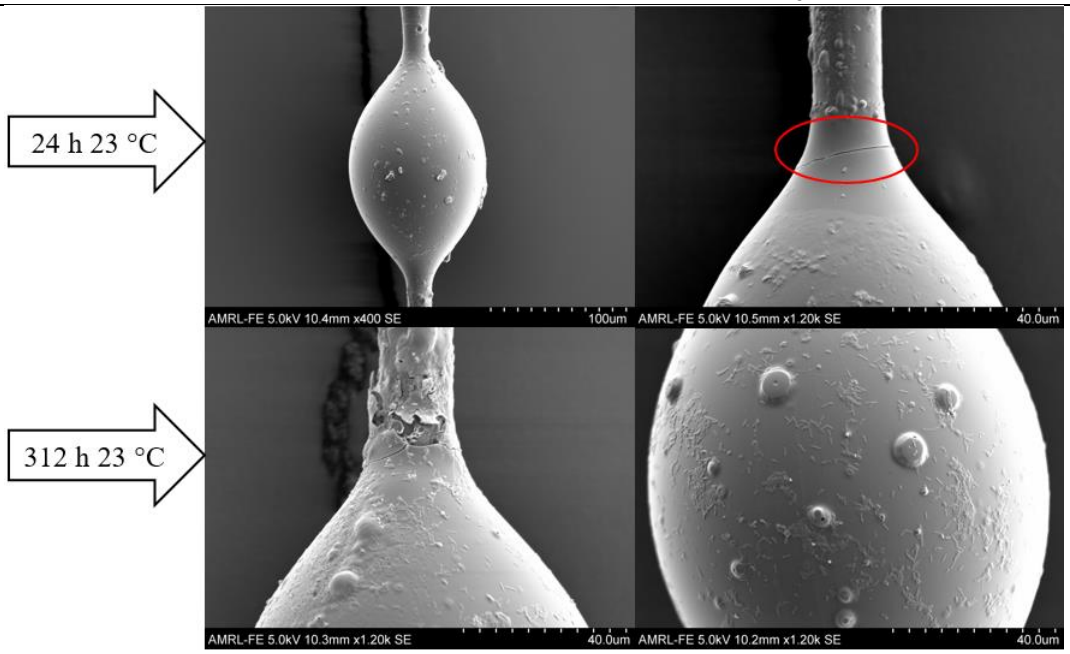

Figure 6-16: *DION 1260 microbond droplets on SE 3030 fibre after ageing by full immersion in DI water at 23 °C.*

DION 1260 microbond droplets on SE 3030 fibre after ageing by full immersion in DI water at 50 °C are shown in *Figure 6-17*. Moisture attack was accelerated and was more pronounced at 50 °C, but produced effects similar to the ones detected at 23 °C. Degradation types included cracking around the meniscus, leaching, and blistering and pitting (micro-cavity formation), which resulted in a clearer appearance of a two-phase structure. As expected, degradation was less distinct upon short-term ageing and became more prominent after 96 h of ageing. At this stage, cracking around the micro-droplet meniscus became more apparent, indicative of reduced interfacial adhesion. The droplet featured on the bottom RHS of *Figure 6-17* shows substantial damage induced by hydrothermal ageing. Ageing has resulted in the formation of disk-shaped blisters throughout the surface of the droplet. There are traces of some of these being removed through leaching, while others appear to be in the process of being removed. Preferential swelling of one phase may have caused sufficient stress to remove these disks. Alternatively, water penetration at the phase boundary may be the catalyst which drives the disk debonding process. In any case, the use of water immersion to reveal this interesting microstructure in VE microdroplets invites further investigation.

Upon the observation of the SEM images recorded for droplets after the ageing time at which these were debonded from the fibres, it can be concluded that a possible reason for debonding was the cracking around the meniscus. Upon ageing, cracking was notably amplified, and it may have potentially resulted in weaker interfacial adhesion or even debonding. Leaching and

pitting may also be responsible for creating voids along the droplet surface and in turn resulting in excess moisture ingress.

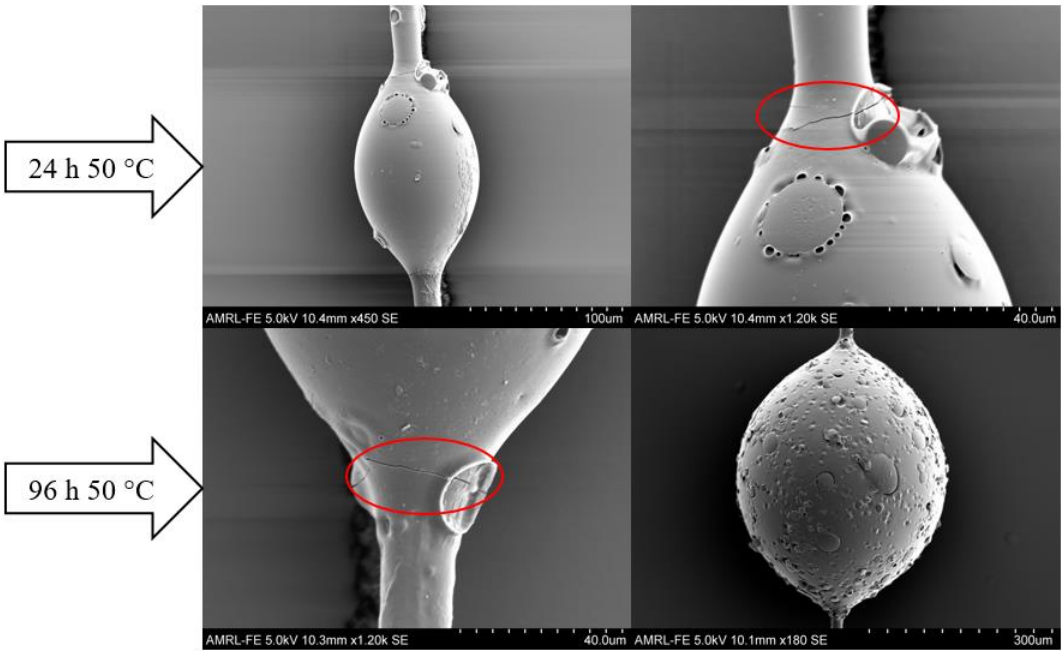

Figure 6-17: *DION 1260 microbond droplets on SE 3030 fibre after ageing by full immersion in DI water at 50 °C.*

SEM of Moisture-aged W 3030/1273 Micro-composites

An un-aged DION 1273 microbond droplet on a W 3030 fibre is shown in *Figure 6-18*. The majority of un-aged DION 1273 droplets showed a featureless surface. As opposed to their counterpart, un-aged W 3030/1273 droplets showed good bonding and no cracking around the meniscus. However, some of the droplets featured small micro-cavities, which appear to exist on a surface level, such as the one shown on the RHS of *Figure 6-18*.

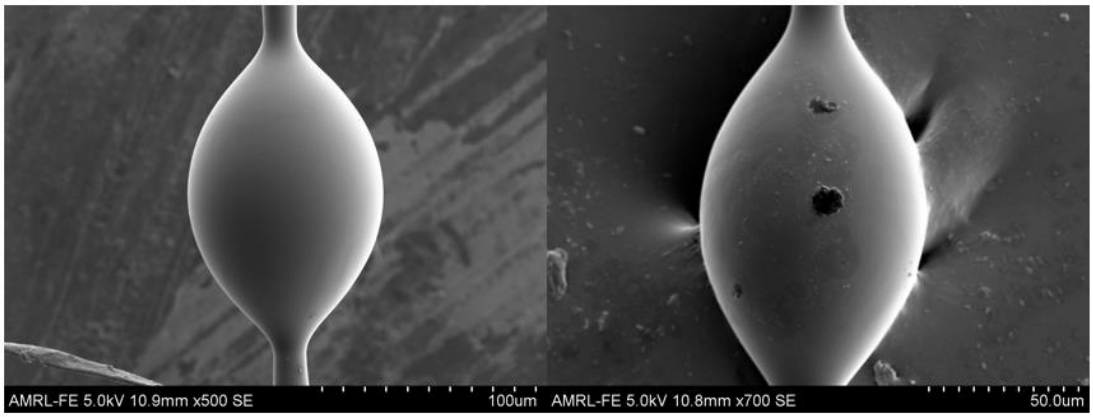

Figure 6-18: *Un-aged DION 1273 microbond droplets on W 3030 fibre.*

SEM imaging of DION 1273 microbond droplets on W 3030 fibre after ageing by full immersion in DI water at 23 °C is presented in *Figure 6-19*. The main degradation types featured in DION 1273 droplets aged at 23 °C were morphology changes, including blistering and pitting, and further evolution of the already existent micro-cavities as a function of conditioning time. However, overall the degree of degradation appears to be notably lower than the one observed in DION 1260 droplets. A close-up at 24 h 23 °C shows further development of a micro-cavity and the formation of small blisters around it. Enlarged micro-cavities may allow excessive moisture ingress until interfacial adhesion will eventually be compromised. Long-term ageing at 23 °C seemed to have increased the concentration of blisters/grains across the surface of the droplets. Nevertheless, it is noteworthy that as opposed to DION 1260, no meniscus cracking was evident in any of the examined droplets. This was an indication that this micro-composite had greater potential in retaining interfacial adhesion as a function of their immersion period at 23 °C when compared to SE 3030/1260.

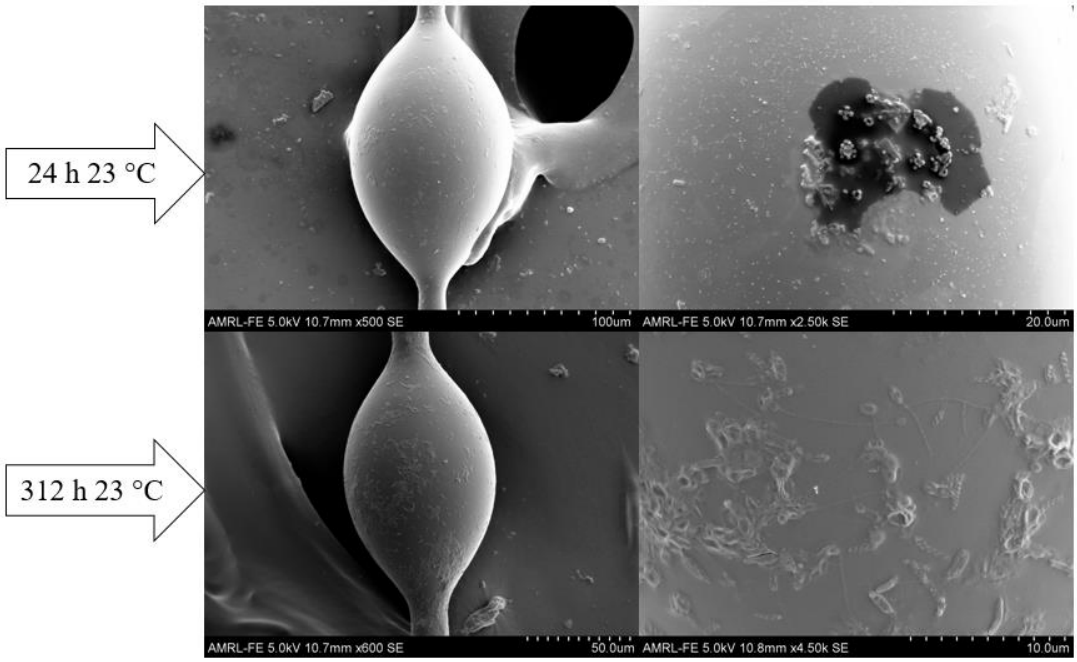

Figure 6-19: *DION 1273 microbond droplets on W 3030 fibre after ageing by full immersion in DI water at 23 °C.*

DION 1273 microbond droplets on W 3030 fibre after ageing by full immersion in DI water at 50 °C are depicted in *Figure 6-20*. Surface-level cracking was discernible around the droplet meniscus even after short-term ageing at 50 °C. Such degradation was only evident after ageing at elevated temperature and did not occur when micro-composites were aged at 23 °C. The development of micro-cavities was also further amplified at 50 °C when compared to 23 °C, as shown in the images. Cracking and micro-cavity development may explain the higher

IFSS loss noted at 50 °C. It is probable that ageing for longer periods would result in similar degradation apparent in the SE 3030/1260 system, such as wicking along the interface and through the formed cracks, and in turn debonding. Small blisters/grains were also featured along the main surface of the droplets, in a similar fashion to those aged at 23 °C. These may be a degradation type characteristic of the DION 1273 matrix aged in wet environments.

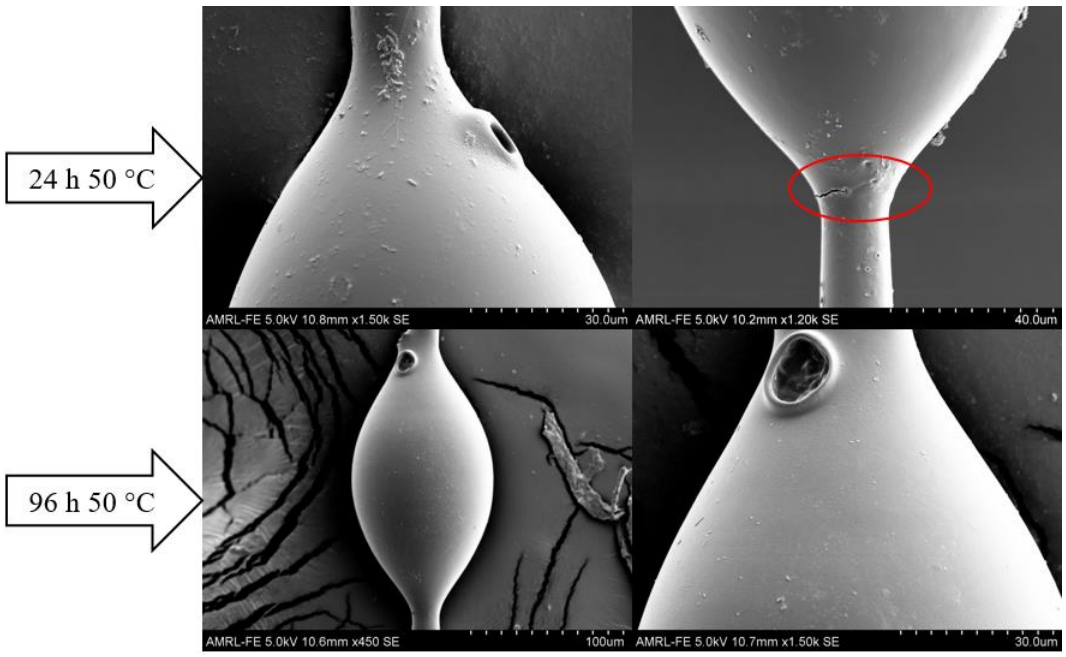

Figure 6-20: *DION 1273 microbond droplets on W 3030 fibre after ageing by full immersion in DI water at 50 °C.*

6.3. CONCLUDING REMARKS

This study allowed an estimation of the moisture content of vinyl ester micro-droplets bonded on glass fibre and enabled an assessment of its direct effect on the micro-mechanical performance of the system. The micro-mechanical performance of SE 3030/1260 and W 3030/1273 after full immersion in DI water at 23°C and 50 °C were characterised by means of the microbond test. Real-life matrix film models were used to estimate the water absorbed by microbond droplets. Simple mathematical diffusivity prediction models in spheres were also employed since spheres resemble the geometry of micro-droplets more closely than films do. In fact, given the ellipsoidal shape of micro-droplets, it was deduced that the saturation times of a mathematically modelled sphere and an actual matrix film are an estimation of the minimum and maximum that a micro-droplet may achieve, respectively.

In conclusion, experimentally obtained results on “standard” cure DION 1260 films suggested similar uptake patterns and (estimated) diffusivities at 23 °C and 100 % RH. Immersion at 50

°C was proven to be a more aggressive ageing environment resulting in immediate saturation and a higher moisture content. Re-drying experiments suggested that all specimens underwent chemical ageing after being conditioned for 336 h. The saturation and diffusivity values of bulk specimens were used to predict the weight gain vs time for film models. These were plotted against experimentally obtained results from actual thin films and, it was shown that the absorption curves, as well as the total moisture gain at equilibrium of films, were closer to that of "UoS" Op. Mould 100 °C" than that of "Polynt Standard". This was in good agreement with the FTIR analysis entailed in *3.2.1.*, and was due to the interaction of the pre-polymer mix with oxygen, and styrene loss. It was concluded that DION 1260 microbond droplets would reach saturation between 0.75 hours and 48 hours at 23 °C and between 3 minutes and 5 hours at 50 °C.

Experimentally obtained results on "standard" cure DION 1273 films suggested that matrix relaxation dominated sorption. This was indicated by an increasing weight gain as a function of ageing time at all conditions. At 50 °C and 100 % RH, a weight decrease was discerned after the weight had reached a maximum. This was indicative of leaching. On the other hand, at 23 °C, the weight gain maximum was followed by weight fluctuations throughout the remaining ageing period. None of the aged films could be fully re-dried, indicative of chemical ageing. Similar diffusivities to DION 1260 were estimated, but a higher maximum moisture content was attained, confirming the hydrophilic nature of DION 1273 over DION 1260 on both macroscale and microscale.

ATR-FTIR was not capable of evaluating the fractional absorbed moisture in vinyl ester films, since it could only provide information on the outer layer of the matrix, which dried out before the measurement. A 45° specular reflectance interface was nevertheless utilised, which produced useful quantitative data on moisture sorption at 23 °C. Moisture gain measured by FTIR for films vinyl ester aged at 50 °C resulted in higher values than those obtained gravimetrically. Generally, the use of specular reflectance FTIR is restricted by the lack of spectral libraries. However, this data remains encouraging and may form a basis for future research; the implementation of accurate modelling could potentially be used to precisely evaluate moisture content in thin polymer films. ATR-FTIR and the hydrolysis matrices presented by Visco et al [32] were also used in providing information on the condition of the outer layer of films. Hydrolysis of vinyl ester films was suggested following the analysis after ageing at all three ageing conditions, and was found to be more severe at 50 °C.

DMA of aged and re-dried DION 1260 films showed that although ageing at 50 °C can lead to post-curing through anti-plasticisation, room temperature ageing may lead to Tg reduction

and phase separation. The DMA thermal curve obtained on DION 1273 films after ageing at 50 °C manifested the action of completing ageing effects, such as anti-plasticisation and subsequent plasticisation. However, the latter result required further validation. For DION 1273 films conditioned at 23 °C and 100 % RH, DMA indicated a small Tg decrease, while broadening of the loss modulus curve indicated that phase separation could have begun to take place.

Despite neat DION 1273 being more susceptible to moisture attack than DION 1260, W 3030/1273 was found to have a stronger and a more hydrothermally durable interface than SE 3030/1260. IFSS vs ageing results were further validation to bulk composite mechanical testing results suggesting a more a more ageing resilient W 3030/1273 interface than its SE 3030/1260 counterpart. It is also noteworthy that W 3030/1273 measured a higher IFSS than SE 3030/1260 when un-aged. However, it can be concluded that the DION 1273 matrix has also been tailored to provide a stronger interface than the commercial DION 1260, despite the former possessing inferior properties to the latter, as a neat matrix outside a composite system. This is further indicated by studying the micro-mechanical test results of SE 3030/1273 (IFSS = 37.4 MPa) and W 3030/1260 (IFSS = 35.2 MPa). Even when DION 1260 is used on W 3030, which possess superior proeprties to SE 3030, it does not reach the IFSS level obtained by W 3030/1273 (IFSS = 43.4 MPa). It is still uncertain whether the variation in glass formulation affects interfacial adhesion and how. The reaction of silane and coupling agent can be different on each glass formulation with the glass surface and in turn the matrix producing a unique interface.

Interestingly both SE 3030/1260 and W 3030/1273 retained satisfactory levels of IFSS even upon the saturation of the matrix droplets, as these were indicated by the gravimetric analysis. Debonding was observed for SE 3030/1260 after 312 h and 96 h of ageing at 23 °C and 50 °C, respectively. At these timescales, W 3030/1273 had only lost 20 % and almost 40 % of its IFSS, respectively. Micromechanical property reduction was found to be primarily irreversible for both systems. The epoxy system SE 2020/DER 332 was found to be consistently stable throughout the entire ageing period at both 23 °C and 50 °C, retaining its IFSS fully.

Lastly, SEM confirmed that SE 3030/1260 was more susceptible to hydrolytic degradation than W 3030/1273, mainly after long-term ageing at 23 °C, and even after short-term ageing at 50 °C. Degradation was amplified with an increase in ageing time and (or) temperature in both systems. However, the rate of degradation was significantly higher in the SE 3030/1260 when compared to W 3030/1273. The main types of degradation identified through SEM for SE 3030/1260 were; cracking around the meniscus (also apparent in some dry specimens, but

increased with ageing), leaching, blistering and pitting resulting in the appearance of what seems to be a two-phase structure, and interfacial debonding. Degradation in W 3030/1273 appeared in the forms of micro-cavity formation (apparent in un-aged specimens but intensified with ageing) mild blistering and grain formation around the droplet surface, and finally cracking around the meniscus after elevated temperature ageing.

CHAPTER 7: SUMMARY OF CONCLUSIONS AND FUTURE WORK RECOMMENDATIONS

7.1. SUMMARY OF CONCLUSIONS

Investigation Of The Effects Of Scale And Cure Environment On Physical And Chemical Properties Of The Vinyl Ester Resin – Chapter 3

A large part of this thesis was aimed at providing an assessment of the durability of composite laminates through the understanding of the changes in the micro-mechanical performance of the employed composite system, assessed by the microbond test. This required a thorough investigation of the transferability of the cure kinetics of vinyl ester resin from a bulk composite (macroscale) constituent to a micro-composite (microscale) constituent, which was presented in *Chapter 3*. Two DACOMAT resins were used; the commercially available DION 1260 and the experimental DION 1273. The majority of experimental results were presented on the former, while a preliminary analysis was allowed for the latter, due to its more complex polymer network. The characterisation was conducted on thin film models, which exhibited a similar surface-to-volume ratio to microbond droplets, through thermal analyses (DSC and DMA) and FTIR.

DSC allowed a Tg comparison as a function of scale, while DMA provided insight into the thermal behaviour of the matrix. For DION 1260, a dual Tg was featured in thin film specimens consisting of a low-temperature transition and a higher-temperature transition. The Tg level was found to be dependent on film thickness; Tg was lower for lower thickness films. This dual transition was not apparent in bulk specimens and was an indication of incomplete curing. A thin film study as a function of styrene content confirmed literature trends on macroscale VE matrices suggesting a slightly higher Tg and crosslink density for low styrene VE specimens. The higher the styrene content of the films was, the less pronounced the low-temperature Tg was, which remained nevertheless evident. A DMA study as a function of scale revealed that the appearance of the first low-temperature transition was characteristic of specimens that had been exposed to ambient oxygen at any stage of their cure. The longer the exposure was, the more pronounced the transition appeared to be. Both bulk matrix plates and thin films cured fully under the influence of oxygen featured a clear double peak (transition) in the loss modulus curve. Curing and post-curing films in an N_2 environment resulted in a single transition at a higher temperature, while an increase in P-C temperature along with the implementation of an N_2 P-C environment increased Tg further. It was thus concluded that the exposure of DION 1260 films to atmospheric conditions, even during the post-cure phase,

accompanied by styrene loss, reduced copolymerisation of styrene and vinyl ester monomers, and was the driver of the lower temperature transition that can be found in thermal analysis data. Regarding the deconvolution of the diphasic DION 1260 vinyl ester network in thin films, it was concluded that the lower temperature Tg could be attributed to the styrene-rich phase of the matrix, given the excess monomer evaporation and knowing that the cross-link density of the styrene-rich phase is lower than that of the vinyl ester phase.

The conduction of both cure and post-cure phases along with a higher P-C temperature was found to also increase the Tg of DION 1273 films. These, however, exhibited a different microscale behaviour from DION 1260; their Tg was indeed decreased when compared to that obtained in thick specimens, but they featured only one transition, which was found to be loosely dependent on film thickness.

An FTIR analysis suggested styrene evaporation and oxidation of the ester groups in VE films of both matrices in the study. A degree of conversion quantitative analysis was attempted for both matrices. For DION 1260, such an analysis was hindered by a surprising increase in the VE and styrene C=C, due to oxidation. A preliminary quantification of the degree of cure in thin films vs bulk specimens was provided for DION 1273. On a qualitative basis, FTIR confirmed thermal analysis results suggesting a lower degree of cure for specimens affected by oxygen and styrene loss in both matrices.

The Interface of Glass Fibre/Vinyl Ester And The Influence Of The Fibre Fixing Adhesive In Single Fibre Microbond Specimens – Chapter 4

In *Chapter 4*, the characterisation of the GF/VE interface in its un-aged state through the microbond test was presented. This investigation also involved the examination of the interaction of the cyanoacrylate adhesive often used in the microbond test to “fix” single fibre micro-composites on a mounting card, with glass fibre sizing. A novel observation was presented.

Firstly, by conducting basic mathematical surface-to-volume calculations for VE films and microbond droplets, it was indeed confirmed that the thickness of the thin films investigated in this study was more or less equivalent to the embedded length of a microbond droplet. Close correlation between the degree of cure of these was suggested by FTIR. According to ACG findings reported by Thomason et al [182], micro-droplet curing could not be achieved in a styrene environment as previously suggested by Laurikainen [68]. However, enhanced interfacial adhesion can be achieved by preventing oxygen interaction with the pre-polymer mix. Furthermore, it was unexpectedly discovered that the type of adhesive used for the

mounting of different glass fibre vinyl ester microbond specimens can have a huge influence on the IFSS results obtained. A series of experiments were conducted suggesting that there are probable reactions of CA vapour with glass fibres of vinyl ester-compatible sizings and (or) when vinyl ester matrix is used on other sized fibres. The effect was owed to the contamination of the glass fibre surface with CA glue vapour, which reacted with certain sizing components and (or) affected the cure kinetics of matrix droplets. When the CA adhesive was substituted with an EP adhesive the IFSS of glass fibre vinyl ester was approximately doubled.

An interfacial comparison between SE 3030 and W 3030 glass fibres (Advantex vs HiPertex, respectively) with DION 1260 and DION 1273 resins was enabled via the microbond test. No major variation was obtained between the IFSS of DION 1260 on either glass fibre substrates. The highest IFSS was attained by the W 3030/1273 system. SEM images on SE 3030/1260 and W 3030/1273 revealed cracking in the meniscus of the former, whereas a stronger interfacial bond was apparent for the latter. The effect of using Advantex vs HiPertex in IFSS remained unclear. Nevertheless, the main reason for a higher IFSS of W 3030/1273 over SE 3030/1260 was attributed to the DION 1273 matrix being designed to offer increased adhesion, despite possessing inferior properties to DION 1260 in its neat form. It was lastly suggested that the meniscus cracking detected in SE 3030/1260 micro-composites may be a promoter of the debonding process during the microbond test, and may consequently reduce the required debonding force, and in turn resulting IFSS.

The Influence Of Moisture Ageing on Glass/Fibre Vinyl Ester Laminates – Chapter 5

In *Chapter 5*, a macroscale characterisation of the water uptake kinetics, mechanical and thermal properties of SE 3030/1260 and W 3030/1273 VE FRPs and their matrix constituents DION 1260 and DION 1273 as a function of environmental history was enabled. All specimens were aged at 23 ° C and 50 °C by full immersion in DI water, and at 100 % RH at RT.

DION 1260 matrix was found to be less hydrophilic than DION 1273. Overall, 23 °C and 100 % RH had a similar effect for both matrices and were found to be milder than 50 °C, resulting in a lower moisture gain and less pronounced degradation. The degradation mechanisms promoted by the accelerated, 50 °C ageing environment were overall more exaggerated and often irreversible when compared to those apparent at RT ageing, and were thus deemed unrealistic for a real-life composite. However, this remains in question.

Ageing of a bulk open mould DION 1260 cured under the influence of oxygen showed a more hydrophilic and a more anomalous water uptake than an adequately cured specimen. DMA on

neat DION 1260 specimens indicated plasticisation during ageing, which was nonetheless reversed upon extracting the moisture out of the specimens. Anti-plasticisation effects were nevertheless considered, indicated by the discolouration of specimens and small Tg decreases, with the effect being more pronounced after elevated temperature ageing. Secondary cross-linking was also indicated for aged and re-dried DION 1273, denoted by notable increases in Tg. In addition, DMA was conducted on aged DION 1260 specimens cured in an open mould under the influence of oxygen; plasticisation was indicated for specimens aged at 23 °C, suggested by broadening of the loss modulus shoulder, characteristic of oxygen-inhibited DION 1260 specimens, which was also shifted at lower temperature values. On the other hand, depression of the loss modulus shoulder was detected for specimens aged at 50 °C, indicative of secondary cross-linking of the lower Tg phase of the matrix.

Despite W 3030/1273 exhibiting a more hydrophilic matrix constituent than SE 3030/1260, it was found to retain its mechanical properties more effectively than its counterpart in hydrothermal environments and after long-term ageing. The majority of mechanical degradation was attributed to interfacial failures. The resilience of W 3030/1273 to mechanical degradation can be attributed to a more "adequately" tailored interface primarily offered by the matrix. It is yet unclear whether the glass formulation (HiPertex vs Advantex) had an effect on adhesion. The stiffness of the two composites, indicated by Young's modulus (measured in the direction of the fibre) was similar for both systems and was not hugely affected by ageing, indicative of the resilience of the reinforcement in wet environments. Varying moisture content was found across specimens of the same laminate thickness but of different length and width. This was attributed to excess sealant decomposition, amplified interfacial weakening allowing moisture wicking and possible varying void content. Void content measurements on SE 3030/1260 suggested a void content increase for aged specimens, which was fairly similar upon ageing at any of the employed conditions. It is possible that an increase in void content contributed to mechanical property reductions in the material, but obtained mechanical property retention trends suggested that mechanical properties were primarily influenced by the severity of the ageing environment. Nevertheless, the effect of void content in the composite invites further investigation.

The Tg of W 3030/1273 was found to be notably higher than that of the matrix, which confirmed that DION 1273 can provide great performance when used as a composite constituent. Tg retention vs ageing trends were found to be in disagreement with mechanical property retention vs ageing trends for the two laminates; greater Tg depression was found for W 3030/1273 as a function of ageing time when compared to SE 3030/1260. These results

were attributed to the plasticisation of the matrix of the two composites. The higher Tg depression featured by W 3030/1273 was attributed to the more hydrophilic nature of DION 1273 when compared to DION 1260.

The Moisture Uptake of Glass Fibre/Vinyl Ester Micro-droplets And Its Direct Translation Into The Micro-mechanical Performance Of The System – Chapter 6

An interfacial assessment of the composite systems used in *Chapter 5* as a function of ageing was presented in *Chapter 6*, which also involved the comparison of GF/VE with an EP micro-composite system. This study allowed an estimation of the moisture content of vinyl ester micro-droplets bonded on glass fibre and enabled an assessment of its direct effect on the micro-mechanical performance of the system. The micro-mechanical performance of SE 3030/1260 and W 3030/1273 after full immersion in DI water at 23°C and 50 °C were characterised by means of the microbond test. Real-life matrix film models were used to estimate the water absorbed by microbond droplets. Simple mathematical diffusivity prediction models in spheres were also employed since spheres resemble the geometry of micro-droplets more closely than films do. In fact, given the ellipsoidal shape of micro-droplets, it was deduced that the saturation times of a mathematically modelled sphere and an actual matrix film are an estimation of the minimum and maximum that a micro-droplet may achieve, respectively.

Both physical and chemical ageing took place in films of both matrices. DION 1273 showed a higher moisture uptake and was thus more hydrophilic than DION 1260. Immediate saturation and amplified degradation were nonetheless apparent for both matrices upon immersion at 50 °C. The use of diffusion prediction models in films showed that films exhibit more similar uptake kinetics to bulk open mould specimens, which have been impaired by excess styrene loss and interaction with oxygen during polymerisation. It was concluded that DION 1260 micro-droplets may reach saturation between 0.75 hours and 48 hours at 23 °C and between 3 minutes and 5 hours at 50 °C. No clear equilibrium was reached for DION 1273 films but the use of diffusion models suggested that equilibrium may be reached at around 0.5 h or less at both 23 °C and 50 °C. Re-drying experiments suggested that all specimens underwent chemical ageing after being conditioned for 336 h.

ATR-FTIR was not capable of evaluating the fractional absorbed moisture in vinyl ester films, since it could only provide information on the outer layer of the matrix, which dried out before the measurement. However, a novel FTIR quantitative analysis on moisture sorption evaluation in thin VE films was carried out by using a specular reflectance interface. Excellent

agreement was shown between specular reflectance measurements and gravimetric results for films aged at 23 °C, but higher values were shown by FTIR for films aged at 50 °C. This work may form a basis for future research involving the implementation of accurate modelling which would be able to precisely measure moisture content in thin polymer films. ATR-FTIR was further utilised for the evaluation of hydrolysis in aged DION 1260 films; hydrolysis was indeed confirmed after RT ageing and was found to be more severe after ageing at 50 °C. DMA of aged VE films suggested the action of competing ageing effects, while ageing-induced phase separation (appearance of a dual Tg) was also indicated for both matrices.

Despite neat DION 1273 being more susceptible to moisture attack than DION 1260 on the microscale, W 3030/1273 was found to have a stronger and a more hydrothermally durable interface than SE 3030/1260. This observation was deduced from the microbond test results as a function of ageing showing higher IFSS retention of W 3030/1273 than SE 3030/1260. Such results were also in agreement with mechanical property retention trends obtained on bulk composites, which suggested that ageing promoted interfacial weakening, and was higher for SE 3030/1260 than for W 3030/1273. Nonetheless, interestingly, both SE 3030/1260 and W 3030/1273 micro-composites retained satisfactory levels of IFSS even upon the saturation of the matrix droplets, as indicated by the gravimetric analysis.

Lastly, SEM confirmed that SE 3030/1260 was more susceptible to hydrolytic degradation than W 3030/1273, mainly after long-term ageing at 23 °C, and even after short-term ageing at 50 °C. The main types of degradation identified through SEM for SE 3030/1260 were; cracking around the meniscus (also apparent in some dry specimens, but increased with ageing), leaching, blistering and pitting resulting in the appearance of what seems to be a two-phase structure, and interfacial debonding. It is likely that debonding was promoted by the cracking apparent in the meniscus of the droplets, which can function as a passageway for water ingress to the interface and may affect the resultant load-displacement curve during a microbond test. Degradation in W 3030/1273 appeared in the forms of micro-cavity formation (apparent in un-aged specimens but intensified with ageing), mild blistering and grain formation around the droplet surface. Cracking around the meniscus after elevated temperature ageing was also detected, which may have been responsible for the higher IFSS reduction measured for micro-composites conditioned at 50 °C.

7.2. FUTURE WORK RECOMMENDATIONS

In *Chapter 3*, the effect of oxygen inhibition during the curing of both microscopic and macroscopic VE specimens was investigated. An FTIR quantitative analysis for microscopic

DION 1260 films and DION 1260 bulk plates cured in open moulds was deemed infeasible since unexpected increases in the C=C of VE and styrene monomer were discovered. These were higher than the C=C of VE and styrene of the unreacted resin, due to oxidation, although they were expected to be depleted with cure. That was the case even for films fully cured under N_2. The effect was found to take place early in the film manufacturing process when the resin was applied onto the substrate and was subsequently degassed. This was an interesting observation, which certainly allows for further investigation. It may be fruitful to monitor precisely at which stage oxygen diffusion starts to impair the properties of the resin. Furthermore, film manufacturing could be attempted in a glove box to restrict oxygen interaction with the polymerising medium, or freeze-thaw cycles could be used, as previously proposed by Albertin et al [47]. In addition, although the films used in this study were found to exhibit a similar surface-to-volume ratio to micro-droplets, and FTIR on large micro-droplets (embedded length ≈ 400 μm) produced a similar signal to that of the films, the direct characterisation of micro-droplets by FTIR was impractical. This work may thus be expanded by using more suitable equipment, such as FTIR microscopy for the assessment of the cure kinetics directly on microbond droplets of an embedded length of 100 – 180 μm.

Moreover, Nouranian et al [48] suggested that VEs cured under the influence of oxygen present an oxygen-affected top layer, which possesses different properties from the rest of the material. It would be thus interesting to attempt and remove the top layer of oxygen-affected specimens, followed by the conduction of appropriate thermal analysis and FTIR to evaluate potential variations in their thermal behaviour and chemistry, respectively. Such an experiment may be more constructive for bulk specimens and based on the assumption that oxygen has only diffused onto their top surface and not their inner structure. Regarding film specimens, it is likely that oxygen is capable of diffusing through their thickness, due to their high surface-to-volume ratio, as also confirmed by scouting experiments carried out during this work.

Lastly, FTIR results presented on the DION 1273 were deemed preliminary due to the complexity of the matrix network and hence further work may be conducted on the topic. Oxygen-affected specimens exhibited notable increases in several spectral regions, the components of which could not be identified. Hence, a thorough search of spectral libraries would be required, and knowledge of the exact polymer composition of the resin would be useful. Other spectroscopic technqiues, such as nuclear magnetic resonance spectroscopy, mass spectroscopy and gas chromatography–mass spectrometry could also be potentially utilised.

In *Chapter 4*, the interaction of CA adhesive vapour, used to "fix" glass fibre microbond specimens on card, with VE-compatible glass fibre sizing and vinyl ester resins was studied. The resulting effect was found to severely affect IFSS. Further analysis may be carried out by using spectroscopic techniques, such as FTIR on affected glass fibre to evaluate the nature of interactions between CA vapour and micro-composites. The exposure of glass fibres to CA vapour before their use in microbond specimens may be attempted. Moreover, this work may be scaled up to composite laminates. For instance, a mechanical property characterisation of laminates containing VE-compatible sizings previously exposed to CA vapour may be performed.

In *Chapter 5*, the mechanical properties of VE-based composites as a function of their environmental history were monitored. The reduction in mechanical properties was primarily attributed to the moisture-induced weakening of the fibre/matrix interface. It was suggested that DION 1273 can provide a more efficient stress transfer capability at the interface than DION 1260, despite the former being more hydrophilic than the latter, when in their neat form. A more in-depth understanding of the behaviour of the matrices in wet environments, and in turn their performance as matrix constituents, would benefit from a mechanical property assessment as a function of ageing at similar conditions employed for the composites. In addition, SEM could be utilised for the examination of composites aged at different conditions, and for different time intervals, and subsequently fractured upon mechanical testing. This may reveal information on the development of degradation at the interface, such as cracking, which was identified in SEM of micro-composites and was deemed responsible for lower IFSS.

Further experimentation regarding the effect of voids on hydrothermal aged VE composites is also required. Some of the specimens were impaired during mechanical testing resulting in particularly high void contents. A similar composite to SE 3030/1260 was used for baseline, un-aged void content measurements. Therefore, SE 3030/1260 shall be used for a more precise comparison, while the work could also be expanded to the W 3030/1273 system. Other testing techniques may also be used for void content identification and quantification, such as nuclear magnetic resonance spectroscopy or non-destructive testing (NDT), i.e. ultrasound.

In *Chapter 6*, FTIR was used to monitor moisture uptake and hydrolytic changes in thin films. The former was deemed infeasible when using an ATR interface, as it offers a particularly low penetration depth, and films dried out prior to the analysis. Encouraging data was nonetheless provided by a 45° specular reflectance interface. However, it was concluded that the scatter apparent in specular reflectance methods (which are not accounted for by the Beer-Lambert law), along with the resulting opaqueness of vinyl ester films upon ageing could lead to

erroneous results. Such data would require further manipulation, such as accurate modelling to evaluate moisture in polymer films adequately. An example is the Beer-Lambert law parametric model proposed by Aiken et al [202] on dyed fabrics using specular reflectance spectroscopy.

Microbond test results on an epoxy-compatible fibre with an epoxy matrix as a function of ageing were presented, and comparison with VE systems was allowed. However, there was no insight into the moisture uptake kinetics of EP droplets or films, as was the case with VE. EP film fabrication was attempted but was not developed further due to the inability to remove EP films from the nylon substrate. Different film fabrication techniques may be attempted, such as spin coating and (or) the use of different substrates.

Furthermore, in *Chapter 3*, it was shown that curing microscopic scale specimens of vinyl esters in an N_2 atmosphere for both cure and post-cure phases, and increasing the P-C temperature at 150 °C resulted in a significantly higher Tg than that achieved when "standard" cure was employed. It would be thus fruitful to enable an IFSS comparison between "standard" cure and "Full N_2 150 °C" cure microbond specimens for both DION 1260 and DION 1273 resin systems. A subsequent, complementary ageing study of films and microbond specimens of "Full N_2 150 °C" would also be beneficial.

Finally, ageing in milder, more realistic conditions for both bulk laminates and microbond composites may be useful. Bulk laminate behaviour showed a similar hydrothermal response of the composite to the ageing conditions of 23 °C and 100 % RH. Furthermore, the microbond test was deemed useful in evaluating the performance of micro-composites, of which their counterpart was tested on a bulk scale. However, a micro-mechanical characterisation at the condition of 100 % RH was not enabled but would be desirable.

REFERENCES

[1] Thomason JL. The interface region in glass fibre-reinforced epoxy resin composites: 2. Water absorption, voids and the interface. Composites 1995;26:477–85.

[2] Sethi S, Ray BC. Environmental effects on fibre reinforced polymeric composites: Evolving reasons and remarks on interfacial strength and stability. Adv Colloid Interface Sci 2015;217:43–67.

[3] Maxwell AS, Broughton WR. Survey of Long-Term Durability Testing of Composites , Adhesives and Polymers 2017:1–8, 12.

[4] Pandey G, Kareliya C, Hinkley J, Singh RP. Interfacial Micromechanics and Effect of Moisture on Fluorinated Epoxy Carbon Fiber Composites. Polym Compos 2011:1961–9.

[5] Zhong Y, Zhou J. Study of thermal and hygrothermal behaviors of glass/vinyl ester composites. J Reinf Plast Compos 1999;18:1619–29.

[6] Karbhari VM, S. Zhang. E-Glass/Vinylester Composites in Aqueous Environments – I: Experimental Results. Appl Compos Mater 2003;10:19–48.

[7] Schumacher A, Pulido MDG. Introduction: Fiber reinforced polymer (FRP) composites. Struct Eng Int J Int Assoc Bridg Struct Eng 2010;20:362.

[8] Jones RM. Introduction to Composite Materials. Mech Compos Mater 2018:1–53.

[9] Thomason JL. The interface region in glass fibre-reinforced epoxy resin composites: 1. Sample preparation, void content and interfacial strength. Composites 1995;26:467.

[10] Pascault JP, Williams RJJ. Overview of thermosets: Present and future. 2nd ed. Elsevier Ltd; 2018.

[11] Lubin G. Handbook of Composites. Van Nostrand Reinhold Company Inc.; 1982.

[12] Thomason JL. Glass fibre sizing: A review. Compos Part A Appl Sci Manuf 2019;127.

[13] Krauklis A. Environmental Aging of Constituent Materials in Fibre-Reinforced Polymer Composites. NTNU Norwegian University of Science and Technology; 2019.

[14] Krishnan P. Evaluation and methods of interfacial properties in fiber-reinforced composites. Mech. Phys. Test. Biocomposites, Fibre-Reinforced Compos. Hybrid Compos. 1st ed., Elsevier Ltd; 2019, p. 343–85.

[15] Jesson DA, Watts JF. The interface and interphase in polymer matrix composites: Effect on mechanical properties and methods for identification. Polym Rev 2012;52:321–54.

[16] Ray BC. Temperature effect during humid ageing on interfaces of glass and carbon fibers reinforced epoxy composites. J Colloid Interface Sci 2006;298:111–7.

[17] Stone MA, Fink BK, Bogetti TA, Gillespie JW. Thermo-chemical response of vinyl-ester resin. Polym Eng Sci 2000;40:2489–97.

[18] Boinard E, Pethrick RA, Dalzel-Job J, Macfarlane CJ. Influence of resin chemistry on water uptake and environmental ageing in glass fibre reinforced composites-polyester and vinyl ester laminates. J Mater Sci 2000;35:1931–7.

[19] Chauhan SR, Kumar A, Singh I. Sliding friction and wear behaviour of vinylester and its composites under dry and water lubricated sliding conditions. Mater Des 2010;31:2745–51.

[20] Cook WD, Simon GP, Burchill PJ, Lau M, Fitch TJ. Curing kinetics and thermal properties of vinyl ester resins. J Appl Polym Sci 1997;64:769–81.

[21] Zhang J, Richardson MOW. Micro-heterogeneity of urethane vinylester resin networks. Polymer 2000;41:6843–9.

[22] Chu W, Karbhari VM. Effect of Water Sorption on Performance of Pultruded E-Glass/Vinylester Composites. J Mater Civ Eng 2005;17:63–71.

[23] Karbhari VM, Rivera J, Zhang J. Low-temperature hygrothermal degradation of ambient cured E-glass/vinylester composites. J Appl Polym Sci 2002;86:2255–60.

[24] Scott TF, Cook WD, Forsythe JS. Kinetics and network structure of thermally cured vinyl ester resins. Eur Polym J 2002;38:705–16.

[25] Ziaee S, Palmese GR. Effects of Temperature on Cure Kinetics and Mechanical Properties of Vinyl–Ester Resins. J Polym Sci Part B Polym Phys 1999;37:725–44.

[26] Li P, Yu Y, Yang X. Effects of initiators on the cure kinetics and mechanical properties of vinyl ester resins. J Appl Polym Sci 2008;109:2539–45.

[27] Brill RP, Palmese GR. Investigation of vinyl-ester - styrene bulk copolymerization cure kinetics using fourier transform infrared spectroscopy. J Appl Polym Sci 2000;76:1572–82.

[28] Moad G SD. The chemistry of free radical polymerization. Second Ful. Elsevier; 1995.

[29] Sobrinho LL, Da Costa MF, Bastian FL. The Effects of Water Absorption on an Ester Vinyl Resin System The Effects of Water Absorption on an Ester Vinyl Resin System. Mater Res 2009;12:353–61.

[30] Dannenberg H, Jr WRH. Detrrmination of Cure and Analysis of Cured Epoxy Resins. Anal Chem 1956;28:86–90.

[31] Gillham JK. The TBA torsion pendulum : A technique for characterizing the cure and properties of thermosetting systems. Polym Int 1997;44:262–76.

[32] Visco AM, Brancato V, Campo N. Degradation effects in polyester and vinyl ester resins induced by accelerated aging in seawater. J Compos Mater 2012;46:2025–40.

[33] Karbhari VM, Wang Q. Multi-frequency dynamic mechanical thermal analysis of moisture uptake in E-glass/vinylester composites. Compos Part B Eng 2004;35:299–304.

[34] Ghorbel I, Valentin D. Hydrothermal Effects on the Physico-Chemical Properties of Pure and Glass Fiber Reinforced Polyester and Vinylester Resins. Polym Compos 1993;14:324–34.

[35] Garay AC, Paese LT, Souza JA, Amico SC. Studies on thermal and viscoelastic properties of vinyl ester resin and its composites with glass fiber. Rev Mater 2015;20:64–71.

[36] Chin JW, Nguyen T, Aouadi K. Sorption and Diffusion of Water, Salt Water, and Concrete Pore Solution in Composite Matrices. J Appl Polym Sci 1998;71:483–92.

[37] Alateyah AI, Dhakal HN, Zhang ZY. Water Absorption Behavior, Mechanical and Thermal Properties of Vinyl Ester Matrix Nanocomposites Based on Layered Silicate. Polym - Plast Technol Eng 2014;53:327–43.

[38] Ray D, Sarkar BK, Das S, Rana AK. Dynamic mechanical and thermal analysis of vinylester-resin-matrix composites reinforced with untreated and alkali-treated jute fibres. Compos Sci Technol 2002;62:911–7.

[39] Fraga AN, Alvarez VA, Vazquez A. Relationship Between Dynamic Mechanical Properties and Water Absorption of Unsaturated Polyester and Vinyl Ester Glass Fiber Composites. J Compos Mater 2003;37:1553–74.

[40] Mousa A, Karger-Kocsis J. Cure characteristics of a vinyl ester resin as assessed by FTIR and DSC techniques. Polym Polym Compos 2000;8:455–60.

[41] Matyjaszewski K, Davis TP. Handbook of Radical Polymerization. 2nd ed. John Wiley & Sons; 2003.

[42] Xu L, Drzal LT. Improvement of adhesion between vinylester resin and carbon fibers. ICCM-13 Conf. Proc., 2001, p. 1–10.

[43] Sultania M, Yadaw SB, Rai JSP, Srivastava D. Laminates based on vinyl ester resin and glass fabric: A study on the thermal, mechanical and morphological characteristics. Mater Sci Eng A 2010;527:4560–70.

[44] Hammami A, Al-Ghuilani N. Durability and environmental degradation of glass-vinylester composites. Polym Compos 2004;25:609–16.

[45] Bénéthuilière T, Duchet-Rumeau J, Dubost E, Peyre C, Gérard JF. Vinylester / glass fiber interface: Still a key component for designing new styrene-free SMC composite materials. Compos Sci Technol 2020;190:108037.

[46] Hernández E, Marcovich NE, Mosiewicki MA. Integrating ricinoleic acid derivates to thermoset polymers with tunable properties. Polym Int 2021;70:1298–308.

[47] Albertin L, Stenzel MH, Barner-Kowollik C, Foster LJR, Davis TP. Solvent and oxygen effects on the free radical polymerization of 6-O-vinyladipoyl-D-glucopyranose. Polymer 2005;46:2831–5.

[48] Nouranian S, Lee J, Torres GW, Lacy TE, Toghiani H, Pittman CU. Effects of Moulding condition and curing atmosphere on the flexural properties of vinyl ester. Polym Polym Compos 2013;21:61–4.

[49] Rao V, Herrera-Franco P, Ozzello AD, Drzal LT. A Direct Comparison of the Fragmentation Test and the Microbond Pull-out Test for Determining the Interfacial Shear Strength. J Adhes 1991;34:65–77.

[50] Graciani E, Mantič V, París F, Varna J. Fiber-matrix debonding in composite materials: Axial loading. Model Damage, Fatigue Fail Compos Mater 2015:117–41.

[51] Sørensen BF. Micromechanical model of the single fiber fragmentation test. Mech Mater 2017;104:38–48.

[52] Kelly A, Tyson WR. Tensile properties of fibre-reinforced metals: Copper/tungsten

and copper/molybdenum. J Mech Phys Solids 1965;13.

[53] Zinck P, Wagner HD, Salmon L, Gerard JF. Are microcomposites realistic models of the fibre/matrix interface? I. Micromechanical modelling. Polymer 2001;42:5401–13.

[54] Zhandarov S, Mäder E. Analysis of a pull-out test with real specimen geometry. Part I: Matrix droplet in the shape of a spherical segment. J Adhes Sci Technol 2013;27:430–65.

[55] Bryce D. Investigation of a micromechanical measurement methodology for assessing the influence of processing variables and fibre sizing on interphase in composites for wind turbine applications. Univeristy of Stratchlyde, 2021.

[56] Piggott MR, Xiong Y. Direct observation of debonding in fiber pull-out specimens. ASTM Spec Tech Publ 1996;1290:84–91.

[57] Tripathi D, Jones FR. Single fibre fragmentation test for assessing adhesion in fibre reinforced composites. J Mater Sci 1998;33:1–16.

[58] Feih S, Wonsyld K, Minzari D, Westermann P, Lilholt H. Testing procedure for the single fiber fragmentation test. Risoe Natl Lab 2004:1–30.

[59] Schultheisz CR, Mcdonough WG, Schutte CL, Macturk KS, Schultheisz R. Effect of Moisture on E-Glass / Epoxy Interfacial and Fiber Strengths. Compos Mater Test Des 1997;13:257–86.

[60] Hunston D, McDonough W, Holmes G, Parnas R. Test Protocol for Single-Fiber Fragmentation Test. Int Round Robin 2000:1–9.

[61] Bian XS, Ambrosio L, Kenny JM, Nicolais L, Dibenedetto AT. Effect of water absorption on the behavior of E-glass fiber/nylon-6 composites. Polym Compos 1991;12:333–7.

[62] Awal A, Cescutti G, Ghosh SB, Müssig J. Interfacial studies of natural fibre/polypropylene composites using single fibre fragmentation test (SFFT). Compos Part A Appl Sci Manuf 2011;42:50–6.

[63] Mahato B, Babarinde VO, Abaimov SG, Lomov S V., Akhatov I. Interface strength of glass fibers in polypropylene: Dependence on the cooling rate and the degree of crystallinity. Polym Compos 2020;41:1310–22.

[64] Favre JP, Jacques D. Stress transfer by shear in carbon fibre model composites - Part 1

Results of single-fibre fragmentation tests with thermosetting resins. J Mater Sci 1990;25:1373–80.

[65] Dai SR, Piggott MR. The strengths of carbon and kevlar fibres as a function of their lengths. Compos Sci Technol 1993;49:81–7.

[66] Nairn JA, Liu YC, Galiotis C. Analysis of stress transfer from the matrix to the fiber through an imperfect interface: Application to Raman data and the single-fiber fragmentation test. ASTM Spec Tech Publ 1996;1290:47–66.

[67] Miller B, Muri P, Rebenfeld L. A microbond method for determination of the shear strength of a fiber/resin interface. Compos Sci Technol 1987;28:17–32.

[68] Laurikainen P. Characterization of the ageing of glass fibre-reinforced polymers. Tampere University of Technology, 2017.

[69] Yang L, Thomason JL. Development and application of micromechanical techniques for characterising interfacial shear strength in fibre-thermoplastic composites. Polym Test 2012;31:895–903.

[70] Herrera-Franco PJ, Rao V, Drzal LT, Chiang MYM. Bond strength measurement in composites-Analysis of experimental techniques. Compos Eng 1992;2:31–45.

[71] Sockalingam S, Nilakantan G. Fiber-matrix interface characterization through the microbond test: A review. Int J Aeronaut Sp Sci 2012;13:282–95.

[72] Day RJ, Cauich Rodrigez J V. Investigation of the micromechanics of the microbond test. Compos Sci Technol 1998;58:907–14.

[73] Chou CT, Gaur U, Miller B. The effect of microvise gap width on microbond pull-out test results. Compos Sci Technol 1994;51:111–6.

[74] Herrera-Franco PJ, Drzal LT. Comparison of methods for the measurement of fibre/matrix adhesion in composites. Composites 1992;23:2–26.

[75] Penn LS, Lee SM. Interpretation of experimental results in the single pull-out filament test. J Compos Technol Res 1989;11:23–30.

[76] Miller B, Gaur U, Hirt DE. Measurement and mechanical aspects of the microbond pull-out technique for obtaining fiber/resin interfacial shear strength. Compos Sci Technol 1991;42:207–19.

[77] Laurikainen P, Kakkonen M, von Essen M, Tanhuanpää O, Kallio P, Sarlin E.

Identification and compensation of error sources in the microbond test utilising a reliable high-throughput device. Compos Part A Appl Sci Manuf 2020;137:105988.

[78] Cranmer DC, Deshmukh UV, Coyle TW. Comparison of Methods for Determining Fiber/Matrix Interface Frictional Stresses in Ceramic Matrix Composite. ASTM Spec Tech Publ 1990;STP:124–35.

[79] Schultheisz CR, Schutte CL, McDonough WG, Macturk KS, McAuliffe M, Kondagunta S, et al. Effect of temperature and fiber coating on the strength of E-glass fibers and the E-glass/epoxy interface for single-fiber fragmentation samples immersed in water. ASTM Spec Tech Publ 1996;1290:103–31.

[80] Wagner HD, Gallis HE, Wiesel E. Study of the interface in Kevlar 49-epoxy composites by means of microbond and fragmentation tests: effects of materials and testing variables. J Mater Sci 1993;28:2238–44.

[81] Järvelä P, Laitinen KW, Purola J, Törmälä P. The three-fibre method for measuring glass fibre to resin bond strength. Int J Adhes Adhes 1983;3:141–7.

[82] Chen EJH, Young JC. The microdebonding testing system: A method of quantifying adhesion in real composites. Compos Sci Technol 1991;42:189–206.

[83] Mandell JF, Chen JH, McGarry FJ. A microdebonding test for in situ assessment of fibre/matrix bond strength in composite materials. Int J Adhes Adhes 1980;1:40–4.

[84] Desaeger M, Verpoest I. On the use of the micro-indentation test technique to measure the interfacial shear strength of fibre-reinforced polymer composites. Compos Sci Technol 1993;48:215–26.

[85] Godara A, Gorbatikh L, Kalinka G, Warrier A, Rochez O, Mezzo L, et al. Interfacial shear strength of a glass fiber/epoxy bonding in composites modified with carbon nanotubes. Compos Sci Technol 2010;70:1346–52.

[86] Medinam C, Molina-Aldareguía JM, González C, Melendrez MF, Flores P, Llorca J. Comparison of push-in and push-out tests for measuring interfacial shear strength in nano-reinforced composite materials. J Compos Mater 2016;50:1651–9.

[87] Chandra N, Ghonem H. Interfacial mechanics of push-out tests: Theory and experiments. Compos Part A Appl Sci Manuf 2001;32:575–84.

[88] Mandell JF, Grande DH, Tsiang TH, McGarry FJ. Modified Microdebonding Test for Direct in Situ Fiber/Matrix Bond Strength Determination in Fiber Composites. ASTM

Spec Tech Publ 1986:87–108.

[89] Larson BK, Drzal LT. Glass fibre sizing/matrix interphase formation in liquid composite moulding: effects on fibre/matrix adhesion and mechanical properties. Composites 1994;25:711–21.

[90] Jenkins PG, Bryce D, Xypolias G, Thomason JL. Micro-mechanical investigation of glass fibre/resin interface failure in mode i and mode II. IOP Conf Ser Mater Sci Eng 2020;942.

[91] Drzal LT, Madhukar M. Fibre-matrix adhesion and its relationship to composite mechanical properties. J Mater Sci 1993;28:569–610.

[92] Zinck P, Wagner HD, Salmon L, Gerard JF. Are microcomposites realistic models of the fibre/matrix interface? II. Physico-chemical approach. Polymer 2001;42:6641–50.

[93] Yang L, Thomason JL, Zhu W. The influence of thermo-oxidative degradation on the measured interface strength of glass fibre-polypropylene. Compos Part A Appl Sci Manuf 2011;42:1293–300.

[94] Thomason JL, Yang L. Temperature dependence of the interfacial shear strength in glass reinforced polypropylene and epoxy composites. ICCM Int Conf Compos Mater 2013;2013-July:3308–16.

[95] Thomason JL, Yang L. Temperature dependence of the interfacial shear strength in glass-fibre epoxy composites. Compos Sci Technol 2014;96:7–12.

[96] Petersen HN, F. Minty R, Thomason JL, Yang L, Kusano Y, Brøndsted P, et al. The amine:epoxide ratio at the interface of a glass fibre/epoxy matrix system and its influence on the interfacial shear strength. Compos Interfaces 2019;26:493–505.

[97] Minty RF, Yang L, Thomason JL. The influence of hardener-to-epoxy ratio on the interfacial strength in glass fibre reinforced epoxy composites. Compos Part A Appl Sci Manuf 2018;112:64–70.

[98] Bryce D, Thomason J, Yang L. Micromechanical and spectroscopic characterisation of the curing performance of epoxy resins in the microbond test. IOP Conf Ser Mater Sci Eng 2020;942.

[99] Ozzelo A, Grummon DS, Drzal LT, Kalantar J, Loh I-H, Moody RA. Materials Resarch Society Symposium Interfaces Between Polymers, Metals, and Ceramics Proceedings. Mater Res Soc Symp Proc 1989;153:217–22.

[100] Laurikainen P, Jokinen J, Lindgren M, Kallio P, Kanerva M, Oreski G, et al. High throughput mechanical micro-scale characterization of composites and the utilization of the results in finite element analysis. Proc 18th Eur Conf Compos Mater 2018:24–8.

[101] Liao YT, Tung IC. Properties of carbon fibre-polymer interfaces. J Mater Sci Lett 1991;10:272–5.

[102] Zinck P, Gérard JF. Thermo-hydrolytic resistance of polyepoxide-glass fibres interfaces by the microbond test. Compos Sci Technol 2008;68:2028–33.

[103] Haaksma RA, Cehelnik MJ. A Critical Evaluation of the Use of the Microbond Method for Determination of Composite Interfacial Properties. MRS Proc 1989;170.

[104] Ash JT, Kjerengtroen L, Cross WM, Kellar JJ. Estimation of the true interfacial shear strength for composite materials with the microbond test. ASME Int Mech Eng Congr Expo Proc 2013;1:1–10.

[105] Yang L, Thomason JL. Interface strength in glass fibre-polypropylene measured using the fibre pull-out and microbond methods. Compos Part A Appl Sci Manuf 2010;41:1077–83.

[106] Dirand X, Hilaire B, Soulier JP, Nardin M. Interfacial shear strength in glass-fiber/vinylester-resin composites. Compos Sci Technol 1996;56:533–9.

[107] Mak M, Lowe A, Jar B, Stachurski Z, Fitzgerald J. Improvements to the microdroplet single fibre composite test. J Mater Sci Lett 1998;17:645–7.

[108] Charlier Q, Lortie F, Gérard JF. Interfacial adhesion in glass-fiber thermoplastic composites processed from acrylic reactive systems, a multi-scale experimental analysis. Int J Adhes Adhes 2020;98.

[109] Biro DA, Pleizier G, Deslandes Y. Application of the microbond technique: Effects of hygrothermal exposure on carbon-fiber/epoxy interfaces. Compos Sci Technol 1993;46:293–301.

[110] Galiotis C. Interfacial studies on model composites by laser Raman spectroscopy. Compos Sci Technol 1991;42:125–50.

[111] Piggott MR. Failure processes in the fibre-polymer interphase. Compos Sci Technol 1991;42:57–76.

[112] Pitkethly MJ, Favre JP, Gaur U, Jakubowski J, Mudrich SF, Caldwell DL, et al. A round-robin programme on interfacial test methods. Compos Sci Technol 1993;48:205–14.

[113] ASTM D2344/D2344M - 16. Standard Test Method for Short-Beam Strength of Polymer Matrix Composite Materials and Their Laminates. Am Stand Test Methods 2016:1–8.

[114] Bai SL, Djafari V, Andréani M, François D. In situ study of short-beam shear tests for composite materials. Compos Sci Technol 1995;55:343–8.

[115] Rosselli F, Santare MH. Comparison of the short beam shear (SBS) and interlaminar shear device (ISD) tests. Compos Part A 1997;28A:587–94.

[116] ASTM D 7264. Standard Test Method for Flexural Properties of Polymer Matrix Composite Materials. Am Stand Test Methods 2015:1–11.

[117] Weitsman YJ. Fluid Effects in Polymers and Polymeric Composites. Springer New York; 2012.

[118] Rod Martin. Ageing of Composites. 1st ed. Elsevier Science; 2008.

[119] ASTM D5229/D5229M − 14ε1. Standard Test Method for Moisture Absorption Properties and Equilibrium Conditioning of Polymer Matrix Composite Materials. Am Stand Test Methods 2014:1–13.

[120] Shen C-H, Springer GS. Moisture Absorption and Desorption of. J Compos Mater 1976;10:2–20.

[121] Nestle NFEI, Kimmich R. Concentration-dependent diffusion coefficients and sorption isotherms. Application to ion exchange processes as an example. J Phys Chem 1996;100:12569–73.

[122] Suh DW, Ku MK, Nam J Do, Kim BS, Yoon SC. Equilibrium water uptake of epoxy/carbon fiber composites in hygrothermal environmental conditions. J Compos Mater 2001;35:264–78.

[123] Narasimha Murthy HN, Sreejith M, Krishna M, Sharma SC, Sheshadri TS. Seawater durability of epoxy/vinyl ester reinforced with glass/carbon composites. J Reinf Plast Compos 2010;29:1491–9.

[124] ASTM D570-98. Standard Test Method for Water Absorption of Plastics ASTM D570-

98. Am Stand Test Methods 1999:1–4.

[125] Alam P, Robert C, Ó Brádaigh CM. Tidal turbine blade composites - A review on the effects of hygrothermal aging on the properties of CFRP. Compos Part B Eng 2018;149:248–59.

[126] Sarlin E, Sironen R, Pärnänen T, Lindgren M, Kanerva M, Vuorinen J. The effect of matrix type on ageing of thick vinyl ester glass-fibre-reinforced laminates. Compos Struct 2017;168:840–50.

[127] Ray BC. Effects of crosshead velocity and sub-zero temperature on mechanical behaviour of hygrothermally conditioned glass fibre reinforced epoxy composites. Mater Sci Eng A 2004;379:39–44.

[128] Apicella A, Migliaresi C, Nicodemo L, Nicolais L, Iaccarino L, Roccotelli S. Water sorption and mechanical properties of a glass-reinforced polyester resin. Composites 1982;13:406–10.

[129] Mouzakis DE, Zoga H, Galiotis C. Accelerated environmental ageing study of polyester/glass fiber reinforced composites (GFRPCs). Compos Part B Eng 2008;39:467–75.

[130] Gautier L, Mortaigne B, Bellenger V, Verdu J. Osmotic cracking in unsaturated polyester matrices under humid environment. J Appl Polym Sci 2001;79:2517–26.

[131] Bao LR, Yee AF. Effect of temperature on moisture absorption in a bismaleimide resin and its carbon fiber composites. Polymer 2002;43:3987–97.

[132] Roy R, Sarkar BK, Bose NR. Effects of moisture on the mechanical properties of glass fibre reinforced vinylester resin composites. Bull Mater Sci 2001;24:87–94.

[133] Eslami S, Honarbakhsh-raouf A, Eslami S. Effects of moisture absorption on degradation of E-glass fiber reinforced Vinyl Ester composite pipes and modelling of transient moisture diffusion using finite element analysis. Corros Sci 2015;90:168–75.

[134] Han SO, Drzal LT. Water absorption effects on hydrophilic polymer matrix of carboxyl functionalized glucose resin and epoxy resin. Eur Polym J 2003;39:1791–9.

[135] Zhou JM, Lucas JP. Hygrothermal effects of epoxy resin. Part I: the nature of water in epoxy. Polymer 1999;40:5505–12.

[136] Zhou J, Lucas JP. Hygrothermal effects of epoxy resin. Part II: Variations of glass

transition temperature. Polymer 1999;40:5513–22.

[137] Zafar A, Bertocco F, Schjødt-Thomsen J, Rauhe JC. Investigation of the long term effects of moisture on carbon fibre and epoxy matrix composites. Compos Sci Technol 2012;72:656–66.

[138] Yin X, Liu Y, Miao Y, Xian G. Water absorption, hydrothermal expansion, and thermomechanical properties of a vinylester resin for fiber-reinforced polymer composites subjected to water or alkaline solution immersion. Polymers (Basel) 2019;11.

[139] Karbhari VM, Member A, Pope G. impact and Flexure Properties of Glass/Vinyl Ester Composites in Cold Regions. J Cold Reg Eng 1994;8:1–20.

[140] Buck E, Lischer D, Nemat-Naser S. The durability of E-glass/Vinyl Ester Composite Materials subjected to environmental conditioning and sustained loading. J Compos Mater 1998;32:874–92.

[141] McBagonluri, Garcia K, Hayes M, Verghese KNE, Lesko JJ. Characteristics of fatigue and combined environments on durability performance of glass/vinylester composites for infrastructure. Int J Fatigue 2000;22:53.

[142] Yu Y, Yang X, Wang L, Liu H. Hygrothermal aging on pultruded carbon fiber/vinyl ester resin composite for sucker rod application. J Reinf Plast Compos 2006;25:149–60.

[143] Fragassa C. Rate of water absorption in polyester and vinyl ester matrices. NauTech 2016:39–43.

[144] Jain A, Rana KB, Tripathi B. Hygrothermal Ageing Effect on Glass Fiber Composites: a Review. Int J Adv Reseacrh Sci Eng 2018;07:599–610.

[145] Krauklis AE, Echtermeyer AT. Long-Term Dissolution of Glass Fibers in Water Described by Dissolving Cylinder Zero-Order Kinetic Model: Mass Loss and Radius Reduction. Open Chem 2018;16:1189–99.

[146] Maxwell AS, Broughton WR, Dean G, Sims GD. Review of accelerated ageing methods and lifetime prediction technique for polymeric materials. NPL Rep DEPC MPR 016 2005:1–84.

[147] Gautier L, Mortaigne B, Bellenger V. Interface damage study of hydrothermally aged glass-fibre-reinforced polyester composites. Compos Sci Technol 1999;59:2329–37.

[148] Yu B, Jiang Z, Yang J. Long-term moisture effects on the interfacial shear strength between surface treated carbon fiber and epoxy matrix. Compos Part A Appl Sci Manuf 2015;78:311–7.

[149] Hara T, Katogi H, Takemura K. Effect of Water Absorption and Resin Particle on Interfacial Shear Strength of CF/MAPP. Adv Mater Res 2015;1110:23–6.

[150] Kootsookos A, Mouritz AP. Seawater durability of glass- and carbon-polymer composites. Compos Sci Technol 2004;64:1503–11.

[151] Chin JW, Aouadi K, Haight MR, Hughes WL, Nguyen T. Effects of water, salt solution and simulated concrete pore solution on the properties of composite matrix resins used in civil engineering applications. Polym Compos 2001;22:282–97.

[152] Cotugno S, Larobina D, Mensitieri G, Musto P, Ragosta G. A novel spectroscopic approach to investigate transport processes in polymers: The case of water-epoxy system. Polymer 2001;42:6431–8.

[153] McClelland A, Bulat E, Bernier B, Murphy EL. Specular Reflection FTIR: A Non-Contact Method for Analyzing Coatings on Photographs and Other Cultural Materials. J Am Inst Conserv 2020;59:123–36.

[154] Technologies A. Training manual for operating Agilent Technologies 4100 Exo Scan FTIR (Fourier transform infrared spectrometer). n.d.

[155] González MG, Cabanelas JC, Baselga J. Applications of FTIR on Epoxy Resins – Identification, Monitoring the Curing Process, Phase Separation and Water Uptake 2012:261–84.

[156] Wu P, Siesler HW. Water diffusion into epoxy resin: A 2D correlation ATR-FTIR investigation. Chem Phys Lett 2003;374:74–8.

[157] Antoon MK, Starkey KM, Koenig JL. Applications of Fourier Transform Infrared Spectroscopy to Quality Control of the Epoxy Matrix. Bull Seismol Soc Am 1979:541–52.

[158] Jana S, Zhong WH. FTIR study of ageing epoxy resin reinforced by reactive graphitic nanofibers. J Appl Polym Sci 2007;106:3555–63.

[159] Sharma N, Surendra Kumar M, Ray BC. Study of the effect of hygrothermal ageing on glass/epoxy micro-composites by FTIR-imaging and alternating DSC techniques. J Reinf Plast Compos 2008;27:1625–34.

[160] González-Benito J. The nature of the structural gradient in epoxy curing at a glass fiber/epoxy matrix interface using FTIR imaging. J Colloid Interface Sci 2003;267:326–32.

[161] Mehdikhani M, Gorbatikh L, Verpoest I, Lomov S V. Voids in fiber-reinforced polymer composites: A review on their formation, characteristics, and effects on mechanical performance. J Compos Mater 2019;53:1579–669.

[162] Gagani AI, Echtermeyer AT. Influence of delaminations on fluid diffusion in multidirectional composite laminates – Theory and experiments. Int J Solids Struct 2018;158:232–42.

[163] Greenhalgh ES. Delamination-dominated failures in polymer composites. Fail. Anal. Fractography Polym. Compos., Woodhead Publishing Limited; 2009, p. 164–237.

[164] Harper BD, Staab GH, Chen RS. A Note on the Effects of Voids Upon the Hygral and Mechanical Properties of AS4/3502 Graphite/Epoxy. J Compos Mater 1987;21:280–9.

[165] ASTM D2734-94. Standard Test Methods for Void Content of Reinforced Plastics 1. Am Stand Test Methods 2016:1–4.

[166] Choi HS, Ahn KJ, Nam JD, Chun HJ. Hygroscopic aspects of epoxy/carbon fiber composite laminates in aircraft environments. Compos Part A Appl Sci Manuf 2001;32:709–20.

[167] Woo M, Piggott MR. Water Absorption of Resins and Composites: Iv. Water Transport in Fiber Reinforced Plastics. J Compos Technol Res 1988;10:20–4.

[168] Youssef Z, Jacquemin F, Gloaguen D, Guilln R. Hygro-elastic internal stresses in porous composite materials: A multi-scale analysis. J Reinf Plast Compos 2007;26:1865–80.

[169] Costa ML, Rezende MC, De Almeida SFM. Strength of hygrothermally conditioned polymer composites with voids. J Compos Mater 2005;39:1943–61.

[170] Allred RE. The Effect of Temperature and Moisture Content on the Flexural Response of Kevlar/Epoxy Laminates: Part I. [0/90] Filament Orientation*. J Compos Mater 1981;15:100–16.

[171] Zhang AY, Li DH, Zhang DX, Lu HB, Xiao HY, Jia J. Qualitative separation of the effect of voids on the static mechanical properties of hygrothermally conditioned carbon/epoxy composites. Express Polym Lett 2011;5:708–16.

[172] Almeida M De, Santacreu DM. Environmental Effects in Composite Laminates with Voids. Polym Polym Compos 1995;3:193–204.

[173] ASTM D5023-15. Standard Test Method for Plastics: Dynamic Mechanical Properties: In Flexure (Three-Point Bending). 2015.

[174] ASTM D5026−15. Standard Test Method for Plastics : Dynamic Mechanical Properties : In Tension. 2015.

[175] ASTM D7028-07. Standard Test Method for Glass Transition Temperature (DMA Tg) of Polymer Matrix Composites by Dynamic Mechanical Analysis (DMA). 2015.

[176] Hoyle CE. An Overview of Oxygen Inhibition in Photocuring Charles. Tech. Conf. Proceedings-UV EB Technol. Expo Conf., 2004, p. 892–9.

[177] Rueggeberg FA, Margeson DH. The Effect of Oxygen Inhibition on an Unfilled/Filled Composite System. J Dent Res 1990;69:1652–8.

[178] Scott TF, Cook WD, Forsythe JS, Bowman CN, Berchtold KA. FTIR and ESR spectroscopic studies of the photopolymerization of vinyl ester resins. Macromolecules 2003;36:6066–74.

[179] Arrieta JS, Richaud E, Fayolle B, Nizeyimana F. Thermal oxidation of vinyl ester and unsaturated polyester resins. Polym Degrad Stab 2016;129:142–55.

[180] Namouchi F, Smaoui H, Fourati N, Zerrouki C, Guermazi H, Bonnet JJ. Investigation on electrical properties of thermally aged PMMA by combined use of FTIR and impedance spectroscopies. J Alloys Compd 2009;469:197–202.

[181] Bryce D, Yang L, Thomason JL. An investigation of fibre sizing on the interfacial strength of glass-fibre epoxy composites. ECCM 2018 - 18th Eur Conf Compos Mater 2020:24–8.

[182] Thomason JL, Jenkins PG, Xypolias G. Microbond testing of the interface in glass fibre vinylester composites. Compos Interfaces 2021;00:695–709.

[183] Wargacki SP, Lewis LA, Dadmun MD. Understanding the chemistry of the development of latent fingerprints by superglue fuming. J Forensic Sci 2007;52:1057–62.

[184] 3B-Fibreglass. 3B solutions for wind energy the winds of change. n.d.

[185] Chung DDL. Polymer-Matrix Composites: Structure and Processing. Second Edi.

Elsevier Inc.; 2017.

[186] Weast RC. Handbook of Chemistry and Physics 53rd Edition. 1972.

[187] Visco AM, Campo N, Cianciafara P. Comparison of seawater absorption properties of thermoset resins based composites. Compos Part A Appl Sci Manuf 2011;42:123–30.

[188] N'Diaye M, Pascaretti-Grizon F, Massin P, Baslé MF, Chappard D. Water absorption of poly(methyl methacrylate) measured by vertical interference microscopy. Langmuir 2012;28:11609–14.

[189] Krauklis AE, Karl CW, Rocha IBCM, Burlakovs J, Ozola-Davidane R, Gagani AI, et al. Modelling of Environmental Ageing of Polymers and Polymer Composites—Modular and Multiscale Methods. Polymers (Basel) 2022;14.

[190] Bowles KJ, Frimpong S. Void Effects on the Interlaminar Shear Strength of Unidirectional Graphite-Fiber-Reinforced Composites. J Compos Mater 1992;26:1487–509.

[191] Peters L. Properties, Influence of Glass Fibre Sizing and Storage Conditions on Composite Properties. Durab. Compos. a Mar. Environ. 2, vol. 245. 1st ed., Springer Cham; 2018, p. 19–31.

[192] Peters L, Adolphs G, Bech JI, Brøndsted P, S OC, Battice B. HiPer-tex WindStrand : A new generation of high performance reinforcement n.d.

[193] Boisseau A, Davies P, Thiebaud F. Sea water ageing of composites for ocean energy conversion systems: Influence of glass fibre type on static behaviour. Appl Compos Mater 2012;19:459–73.

[194] Caixeta RV, Guiraldo RD, Berger SB, Kaneshima EN, Júnior ÉMF, Drumond AC, et al. Influence of glass-fiber reinforcement on the flexural strength of different resin composites. Appl Adhes Sci 2015;3:4–9.

[195] Nugroho G, Budiyantoro C. Optimization of Fiber Factors on Flexural Properties for Carbon Fiber Reinforced Polypropylene 2022:1–12.

[196] Kumar DS, Shukla MJ, Mahato KK, Rathore DK, Prusty RK, Ray BC. Effect of post-curing on thermal and mechanical behavior of GFRP composites. IOP Conf Ser Mater Sci Eng 2015;75.

[197] Rebenfeld L, Desio GP, Wu JC. Effects of fibers on the glass transition temperature of

polyphenylene sulfide composites. J Appl Polym Sci 1991;42:801–5.

[198] Trey SM, Kristofer Gamstedt E, Mäder E, Jönsson S, Johansson M. Glass fiber reinforced high glass transition temperature thiol-ene networks. Compos Part A Appl Sci Manuf 2011;42:1800–8.

[199] Sousa JM, Garrido M, Correia JR, Cabral-Fonseca S. Hygrothermal ageing of pultruded GFRP profiles: Comparative study of unsaturated polyester and vinyl ester resin matrices. Compos Part A Appl Sci Manuf 2021;140:106193.

[200] Crank J. Mathematics of Diffusion. 2nd ed. Oxford: Clarendon Press; 1975.

[201] Andor. Andor - An Oxford Instruments Company: Absorption / Transmission / Reflection Spectroscopy n.d.

[202] Aiken D, Ramsey S, Mayo T, Lambrakos SG, Peak J. Beer-Lambert-Law Parametric Model of Reflectance Spectra for Dyed Fabrics. Washington, DC 20375-5320: Naval Research Laboratory Report; 2016.